High-resolution Palaeoenvironmental Information from Southeast Australian Speleothems

by

Jolyon Michael Desmarchelier BSc (Hons)

A thesis submitted in fulfilment of the requirements for the degree of Doctor of Philosophy

December, 1999

School of Geography and Environmental Studies

University of Tasmania

Hobart

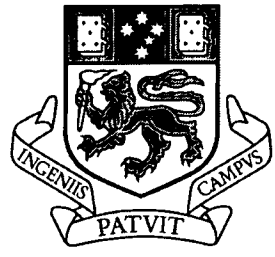

UNIVERSITY OF TASMANIA

Declaration

This thesis contains no material which has been accepted for the award of any other degreee or diploma in any tertiary institution. To the best of my knowledge and belief this thesis contains no material previously published or written by others except where due reference is made in the text.

(Jol Desmarchelier)

Statement of Previous Publications

Parts of the material presented in this thesis were published as:

Desmarchelier, J.M. and Goede, A. 1996 High resolution stable isotope analysis of a Tasmanian speleothem. *Papers and Proceedings of the Royal Society of Tasmania*, 130, 7-13.

Desmarchelier, J.M., Goede, A., Ayliffe, L.K., McCulloch, M.T. and Moriarty, K. 2000 Stable isotope record and its palaeoenvironmental interpretation for a late Middle Pleistocene speleothem from Victoria Fossil Cave, Naracoorte, South Australia. *Quaternary Science Reviews*, 19, 763-774.

Statement of Authority of Access

This thesis may be made available for loan and limited copying in accordance with the *Copyright Act 1968*.

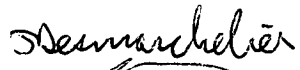 16/6/2000

(J.M. Desmarchelier)

Abstract

Speleothems, chemical cave deposits such as soda-straw stalactites, stalagmites and flowstones, have great potential as archives of high-resolution terrestrial palaeoenvironmental change at both short and long term temporal scales. In this study temporal control is achieved using various high precision radiometric techniques such as TIMS $^{230}Th/^{234}U$ dating, AMS radiocarbon dating, and ^{210}Pb excess dating, the latter two methods used to investigate contemporary speleothem material. An additional method adopted only with certain samples, but showing considerable promise, is autocorrelation of annual variations in speleothem minor element concentrations. 43 new TIMS $^{230}Th/^{234}U$ speleothem age estimates from several karst areas in Tasmania are presented as a cumulative frequency distribution and are compared with some previously published and unpublished speleothem data from southeast Australian continent. The distribution of ages allows some comments to be made on past environmental conditions and their effect on speleothem growth in southeastern Australia.

Laser ablation inductively coupled plasma mass spectrometry (LA-ICP-MS) has been used to investigate minor element variations along the whole growth axis of several speleothems. Some soda-straw stalactites are found to contain quasi-periodical variations in their minor element composition, in some cases it is in phase with surface ridges, *ie* annual banding, sometimes visible on the surface. Measurements of the surface ridging using dendrochronological equipment allow a temporal framework to be developed and comparisons to be made between this chronology and one established using the annual cyclicity of certain minor elements. The chronologies agree very closely, indicating that soda-straw stalactites can potentially provide annually resolved records. Measurements of the minor element and stable isotope composition of flowstone material have been taken in order to provide records of palaeoenvironmental change in areas not previously studied in southeastern Australia using speleothems as an information source. Temporal control is provided by a suite of TIMS $^{230}Th/^{234}U$ age estimates.

Acknowledgements

This thesis is dedicated to the loving memory of my father, Michael. I miss him greatly.

I am extremely grateful to Dr Albert Goede for his supervision, patience, and encouragement over the past few years. I also thank him for his continuing support after his retirement and for proof reading the thesis. I thank Dr Manuel Nunez for adopting me as his student and for the fruitful discussions and suggestions he has made over the past year.

Many thanks to Professor Malcolm McCulloch for the invitation to work at the Research School of Earth Sciences at the Australian National University. A major part of the work was conducted there and I am sincerely grateful for his support.

I thank John Hellstrom for the assistance and advice given with the ICP-MS and TIMS dating analyses. The thesis also benefited from the many discussions we had on life, the universe and everything. I also "thank" him for demonstrating that working through the night is extremely productive and free of distractions. I would also like to express my gratitude to Graham Mortimer, Linda Ayliffe, Dan Sinclair, Pyramo Marianelli, Les Kinsley, and Gael Watson for their invaluable advice and technical assistance while I was in Canberra. A special thanks to Graham for his patience and understanding while I was in his laboratory and to Dan for "firing up" the ICP-MS occasionally.

A special thank you is extended to Dr Andy Baker (University of Exeter but now at the University of Newcastle-upon-Tyne) for providing enouragement and fruitful e-mail discussions during the course of the project.

This project would not have been possible without the support and permission to collect speleothem samples by Mr Ian Houshold (Tasmanian National Parks and Wildlife Service), Dr Kevin Kiernan Forestry Tasmania), and Mr Andy Spate (New South Wales National Parks and Wildlife Service).

A big thank you to the Kerry Bridle for allowing me to use her beloved computer over the last six months, and to Mike Harlow for resurrecting said beloved computer after an unexpected power cut. A thousand thank-you's to Sapphire McMullen-Fisher for typing in pages and pages of references. I also thank the students of the various floors I choose to inhabit for their understanding and patience as I strove to destress by babbling away. Thanks to Mona Loofs for bullying people into bringing cakes on Wednesday thus providing a suitable incentive for retired staff to show up.

I would like to thank Jay Wellington for her patience and understanding over the last year.

Finally, I would like to thank my mother, Gill, for all of the support and understanding over the last nine years. I am deeply indebted to her.

Table of Contents

Chapter 1
Introduction

"The farther backward you can look the farther forward you are likely to see"

Winston Churchill

1.1. Why Study Past Climate?

In recent years there has been a tremendous growth of interest in global climate cycles particularly those of the last 2.4 million years, a period referred to as the Quaternary, and of their apparent hemispheric synchronicity (Bender *et al.*, 1994; Bard *et al.*, 1997). This interest reflects increasing global governmental concern regarding future climatic change, due to anthropogenic influence on the Earth's climate system, and the likely impacts on future generations. There is a certain degree of optimism that researchers will be able to predict future climate changes using Global Climate Models (GCM) with data from studies of various proxy records such as lake and marine cores, ice cores, tree rings, and speleothems.

In order to accurately predict future global climate changes we must first understand what has happened to the Earth's climate in the past. As scientific interest grows so too does our understanding of both the external and internal processes driving climate change as well as the scales at which they operate. During the Quaternary period, global climate has been dominated by a series of glacial/interglacial cycles but our understanding of the mechanisms forcing these cycles is limited (Hays *et al.*, 1976; Martinson *et al.*, 1987; Winograd *et al.*, 1992). Currently research is focussed on investigating and determining temporal relationships, the magnitude, and the global extent of key individual events within the Quaternary, for example the Younger Dryas, Last Glacial Maximum, and Little Ice Age, so that the GCM models which attempt to explain climate change can be tested.

High-resolution studies of marine and ice cores have highlighted the dynamic and abrupt nature of the Earth's climate system (Dansgaard *et al.*, 1993; Taylor *et al.*, 1993; Adams *et al.*, 1999). Recent investigations of terrestrial sequences such as loess and lake sediment cores also support the dynamism and brusqueness of the global climate system (Ding *et al.*, 1995; Kershaw *et al.*, 1991). A common problem with all of these studies is the accuracy of their temporal frameworks as many of them rely on radiocarbon dating, palaeomagnetism, or on tuning the record to the oxygen isotope stage (OIS) chronology. The chronology of a deposit

has the potential to create considerable controversy, for example the Devils Hole calcite (Winograd *et al.*, 1992 and associated papers) or the Lake George sediment core in Australia (Singh and Geissler, 1985).

In terrestrial situations there are many sources of data on Quaternary climate change. However, apart from ice cores there are very few temporally continuous proxy records like those found in marine cores. Ice cores provide high-resolution palaeoclimate records spanning tens of thousands of years with the majority of cores taken from the polar ice sheets in Antarctica and Greenland. A major source of continental palaeoenvironmental information comes from the analysis of variations in the quantity and type of pollen found in sediment cores taken from lakes. The main problem with these deposits is the reliability of the chronologies, which are usually based on radiocarbon dating and modelling of the sedimentation rate, and their relatively low sampling resolution. Other sources of terrestrial palaeoenvironmental information include loess stratigraphy (Kukla, 1987) and uplifted marine terrace sequences, *eg* Huon Peninsula (Aharon and Chappell, 1986), however their usefulness is limited as they lack sufficient temporal resolution.

Speleothems have considerable potential to provide reliable high-resolution terrestrial palaeoenvironmental records for the last 600 ka against which other terrestrial and marine records can be compared. Although speleothems have made relatively few significant contributions to the study of Quaternary climate they still have much unrealised potential (Hellstrom, 1998). Notable studies using speleothems as a data source include the constraint of sea-level changes by Li *et al.* (1989) and Richards *et al.* (1994) and the investigation of climate change in NW Europe using the growth frequency distribution through time (Baker *et al.*, 1993a). The potential for speleothems to provide high-quality terrestrial records was demonstrated by the Devils Hole record (Winograd *et al.*, 1992). Most palaeoenvironmental information from speleothems is gleaned from the analysis of the stable carbon and oxygen isotope composition of the carbonate. Some research effort is being directed to the minor element and organic acid content of speleothems, both of which have recently been shown to have annual resolution (Baker *et al.*, 1993b; Roberts *et al.*, 1998) illustrating the potential resolution possible. A significant advantage of speleothems is the ability to precisely constrain the growth of these chemical deposits with radiometric ages back to approximately 500 ka, particularly as they do not suffer from bioturbation or compaction effects and with prudent sampling, will be free from any post-depositional changes. The ability to resolve the temporal framework of speleothems at high resolution enables investigation of the rate of past global climatic changes and how quickly they influence the surface and cave environments. This information is critical to our understanding of global environmental change particularly in relation to modelling future climate change scenarios and how we might respond to them. Although it is speculative to suggest that climate change led directly to humans dominating the earth, it is not too presumptuous to suggest that this dominance could be curtailed by a dramatic change in climate.

1.2. Thesis Aims

The main aims of this thesis are:

(1) To investigate the age distribution of speleothems in Tasmania and how it relates to past global climate changes.

(2) To compare stable isotope profiles of stalagmites with overlapping ages from different karst areas in order to investigate regional differences in past climate.

(3) To examine the minor element composition of soda-straw stalactites as a proxy record for recent climate.

(4) To investigate the minor element composition of speleothems using continuous scanning and discrete ablation techniques.

1.3. Thesis Outline

Chapter 2 introduces the reader to some important background information on the nature of speleothems including the factors influencing speleothem deposition, the types of speleothems used for palaeoenvironmental research, the kind of information acquired from speleothems, and the main methods of age determination that are applied to speleothems. Chapter 3 discusses the regional setting, giving the reader some background information on the study areas, mechanisms and evidence for past climate changes, and sample descriptions.

Chapter 4 describes the methods of age determination used in this study including a new method using autocorrelation together with the more conventional radiometric methods such as uranium series and radiocarbon dating. The results of four different age determination techniques are presented.

Chapter 5 discusses the minor element composition of speleothems, an area of rapidly growing research. It includes some background information on the factors influencing the incorporation of minor elements into speleothem calcite, and the analytical techniques used in the study. The results from the analysis of several different types of speleothems are presented and the most significant results discussed.

Chapter 6 discusses the stable isotope composition of speleothems on which most palaeoenvironmental reconstructions rely. The chapter examines the factors influencing the carbon and oxygen isotope composition of speleothems and their interpretation. The results of multiple stable isotope analyses of samples taken from the longitudinal profile of three different speleothems are presented and compared with several other palaeoenvironmental proxies.

Chapter 7 presents a brief discussion of the results and the final conclusions. It also suggests avenues for further research.

Chapter 2

The Nature of Speleothems

2.1. Introduction

Most caves are at near constant temperature (Gascoyne, 1992) and, when invaded by percolating solutions carrying various ions in solution, form an excellent environment for the deposition of minerals sometimes resulting in spectacular crystal formations (White, 1976). A speleothem is a secondary mineral deposit formed in caves (Moore, 1952), the term refers to the morphology of the mineral and not to its composition.

Since only calcite speleothems are used for palaeoenvironmental analysis, discussion will focus on calcite, one of three polymorphs of calcium carbonate ($CaCO_3$) and the one most commonly found in caves. Calcite is deposited in various forms, most commonly as dripstone and flowstone speleothem types, for example stalactites, stalagmites, flowstone, draperies, columns, *etc.* but also as less common speleothem types, for example pearls, rafts, rims, rimstone dams, *etc.* (Hill and Forti, 1997).

The aim of this chapter is to give some background information on speleothems and the physical processes that influence them. A brief account on the range of chemical deposits in caves is given together with a history of speleothem study. Dissolution and precipitation processes affecting speleothem deposition are discussed, as well as the specific types used for palaeoenvironmental studies. The chapter finishes with a review of the techniques used to obtain palaeoenvironmental information from speleothems.

2.2. Chemical Deposits in Caves

Approximately 250 different cave minerals are known. Cave minerals are defined as secondary minerals and are derived by a physio-chemical chemical reaction from a primary mineral in bedrock or detritus and deposited due to suitable environmental conditions within a cave (Hill and Forti, 1997). The most widely used classification scheme is by chemical class, for example arsenates, borates, carbonates, halides, nitrates, oxides and hydroxides, organic minerals, phosphates, silicates, sulphates, sulphides, and vanadates (Hill and Forti, 1997).

The great majority of cave minerals are are rare and only found where certain environmental and geological conditions exist, in some cases the conditions causing mineral formation may be unique. Calcite is by far the most common cave mineral, followed in decreasing significance by aragonite, gypsum, other carbonates and hydrated carbonates, sulphates, halides, nitrates

and phosphates, silica and silicates, manganese and hydrated iron oxides, and ore associated minerals (Ford and Williams, 1989).

2.3. Carbonate Dissolution and Precipitation

2.3.1. Dissolution of Host Limestone

Karst landscapes develop in limestone bedrock due to the dissolution of calcium carbonate by carbonic acid. This is produced when rainfall absorbs carbon dioxide from the air and soil atmosphere which readily dissolves in water to give carbonic acid:

Equation 2.1

$$CO_2^g + H_2O \rightarrow H_2CO_3$$

Biological activity in the soil, microbial decomposition of organic matter and root respiration, provides the bulk of carbon dioxide in the acidification of percolation water (Figure 2.1). The dissolution of calcium carbonate is determined by the following reversible reaction equation:

Equation 2.2

$$CO_2^g + H_2O + CaCO_3 \rightarrow Ca^{2+} + 2HCO_3^-$$

The kinetics of dissolution and precipitation of calcium carbonate from thin water films can occur under both open and closed system conditions and is controlled by three main mechanisms which act independently but any one can determine the overall rate of dissolution (Buhmann and Dreybrodt, 1985a):

(1) the kinetics of dissolution at the phase boundary between the $CaCO_3$-H_2O-CO_2 system and the limestone;

(2) the kinetics of the conversion of CO_2 to carbonic acid (H_2CO_3); and

(3) mass transport of the dissolved ions by diffusion from and to the phase boundaries.

2.3.2. Dissolution of Calcium Carbonate

Buhmann and Dreybrodt (1985a, 1985b) developed a model to predict calcite dissolution rates in both open and closed systems, deducing that the dissolution rate is determined by the volume (V) of water to surface area (A) of the reacting mineral:

Equation 2.3

$$R = \frac{V}{A} \cdot \frac{d[CO_2]}{dt}$$

where $[CO_2]$ is the concentration of CO_2, and R is the flux of Ca^{2+} from the mineral surface, which depends on the chemical composition of the solution. R (mole cm^{-2} s^{-1}) can be resolved using the PWP equation (Plummer *et al.*, 1978):

Equation 2.4

$$R = \kappa_1[H^+] + \kappa_2[H_2CO_3] + \kappa_3 - \kappa_4[Ca^{2+}][HCO_3^-]$$

where κ_1, κ_2, and κ_3 are temperature dependent rate constants, and κ_4 is the expression for back reaction and is approximated by standard rate equations for calcite precipitation.

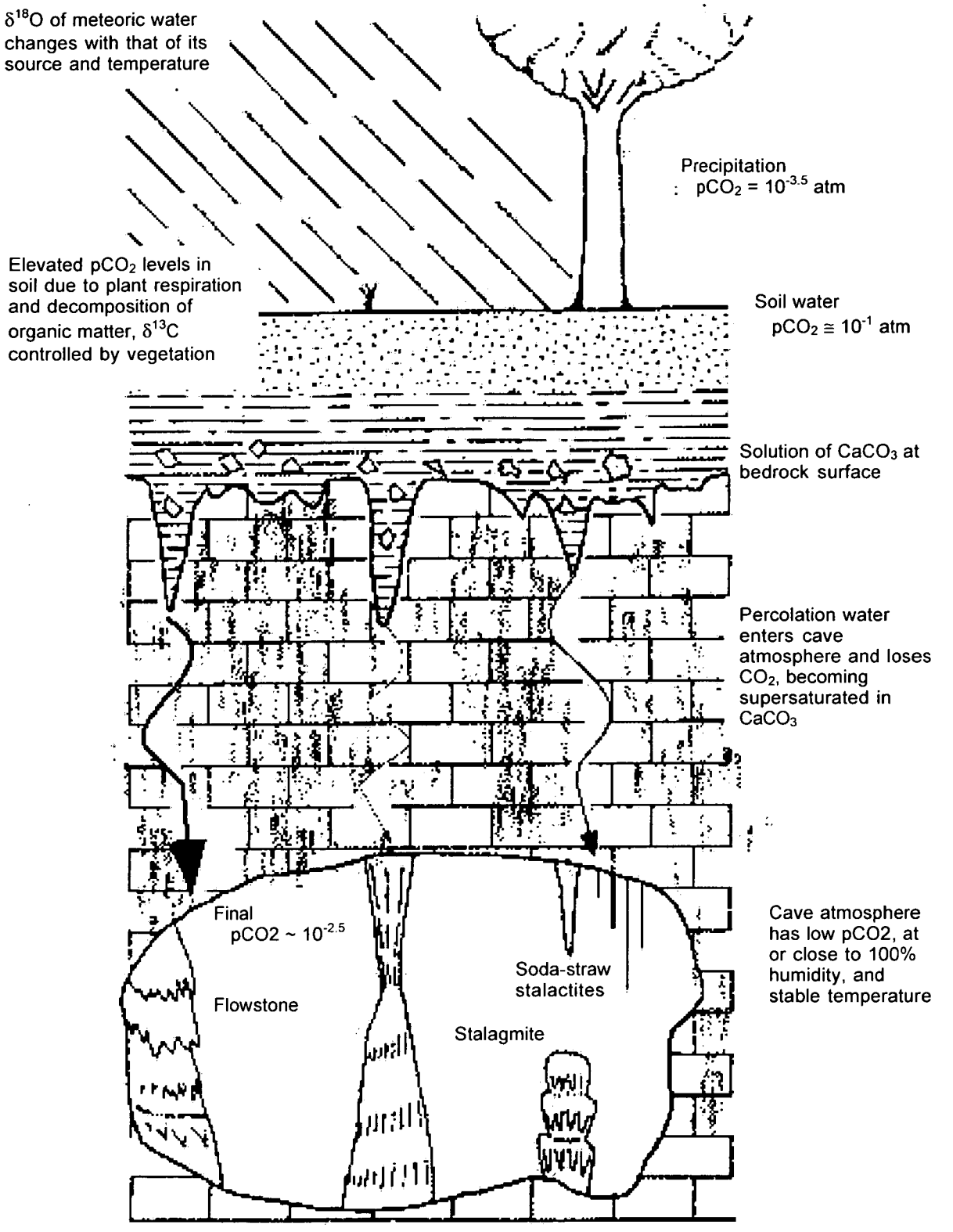

Figure 2.1. Diagram illustrating the processes influencing the formation of speleothems. Environmental conditions on the surface influence the seepage water chemistry which in turn govern the variations of stable isotope and minor element composition of speleothems (Adapted from Holland *et al.*, 1964; Hellstrom, 1998).

These equations (page 5) demonstrate that CO_2 conversion limits the dissolution rate, where the V/A ratios are small, but as the volume of water increases the limiting influence of CO_2 decreases considerably until dissolution is inhibited when CO_2 approaches equilibrium with the water (Dreybrodt *et al.*, 1996). This theoretical model agrees fairly closely with experimental data for V/A ratios in the range from 0.0002 cm to 0.1 cm (Dreybrodt and Buhmann, 1991, Dreybrodt *et al.*, 1996).

2.3.3. Precipitation of Calcium Carbonate

When a carbonate saturated solution reaches an air filled cavity, deposition of $CaCO_3$ occurs by one or more of three processes acting individually or in combination (Hill and Forti, 1997):

(1) carbon dioxide diffusion (common);

(2) evaporation (minor); and

(3) common ion effect/incongruent dissolution (rare).

Diffusion of CO_2 from solution, due to pressure differences between the host solution and the cavity air pressure, is by far the most common mechanism of $CaCO_3$ deposition in caves in humid environments (Figure 2.1). As percolation water moves through the soil, a high CO_2 partial pressure is imparted to the water by soil processes. This pressure can be up to 250 times normal atmospheric pressure. When the water enters a cave, which may have a CO_2 pressure much lower than that of the overlying soil, CO_2 is lost until the CO_2 pressure of the percolation water attains equilibrium with the CO_2 pressure of cave atmosphere. Degassing of CO_2 from solution occurs and causes it to become supersaturated and $CaCO_3$ is deposited:

Equation 2.5

$$Ca^{2+} + 2HCO_3^- \rightarrow CaCO_3 + CO_2^g + H_2O$$

It is important to note that the majority of studies on limestone dissolution and calcite precipitation have been conducted under laboratory conditions. They do not take into account the many possible interferences that occur in natural environments, for example those caused by minor elements and dissolved organic complexes. Some studies have attempted to address the problem of minor elements by using solutions containing varying concentrations of a particular element (*eg.* Katz *et al.*, 1993, Mucci and Morse, 1983, Reddy and Wang, 1980). Lebron and Suarez (1998) have investigated the kinetics and precipitation mechanisms of calcite by varying the partial pressures of carbon dioxide and the concentrations of dissolved organic carbon in saturated solutions of calcium carbonate.

2.4. History of Speleothem Study

Recorded investigations of cave deposits are believed to have begun in the first century AD when it was postulated by scholars that speleothems formed by the petrification of seepage water. By the 17th century several theories about the formation of speleothems began to merge into one that explained speleothem formation by the solidification of some material carried in the water. It was not until 1812 that investigations using the "new" science of

chemistry revealed the role of limestone and carbonic acid in the formation of calcite speleothems, despite this several other theories explaining speleothem formation were still propounded. Shaw (1992) and Shaw (1997) contain reviews on the history of cave science and speleothem formation prior to 1900.

Prior to the 20th century, palaeoenvironmental inferences from speleothems were isolated and discussion centred mainly on the effects of changes in the surface vegetation, of air circulation within the cave, and on speleothem growth rate. In the 19th century attention was focussed on the growth rate of speleothems as a means of assessing the antiquity of the earth. However, despite much investigation, the only conclusion reached was that speleothem growth rates were highly variable (Shaw, 1992). The first measurement of long-term speleothem growth rates was by Broecker *et al.* (1960) using conventional radiocarbon dating. Their study showed that a stalagmite had grown at 60 microns per year, on average, over a 1,400-year period. Radiocarbon dating has been used ever since by researchers to estimate ages and growth rates of speleothems but a major problem with the method, is incorporation of an unknown amount of ancient carbon derived from the carbonate bedrock.

A more reliable method of dating speleothem calcite was tried initially by Rosholt and Antal (1962) using the $^{230}Th/^{234}U$ method but the attempt had limited success due to the impure nature of the speleothem material that was being analysed. A more thorough investigation of the technique by Duplessy *et al.* (1970) yielded the first successful uranium-series ages by alpha spectrometry using speleothem material. The development of thermal ionisation mass spectrometry (TIMS) to directly measure the concentrations of uranium and thorium isotopes has resulted in a significant reduction in sample size and in analytical errors in comparison with the conventional alpha-spectrometric method (Edwards *et al.*, 1987).

Hendy and Wilson (1968) were one of the first (Galimov *et al.*, 1965) to use the stable isotope ratios of oxygen and carbon in speleothems as a proxy for past terrestrial climate. Many researchers have since followed a similar path but temperature estimates are still of a semi-quantitative nature and, until a method of analysing the isotopic composition of fluid inclusions trapped within the speleothem calcite is perfected, fully quantitative temperature histories will remain elusive. However, recent work by Rowe *et al.* (1998) suggests that a breakthrough in the development of fluid inclusion extraction methodology is very close and that fully quantitative temperature records may soon be produced from speleothems.

2.5. Types of Speleothems

Secondary mineral deposits formed in caves are called speleothems, "spelaion" = cave and "thema" = deposit (Moore, 1952). Hill and Forti (1997) use a classification system, divided into types, sub-types, and varieties, based primarily on morphology and secondly on the origin and crystallography of the speleothem. They describe over 38 different speleothem types and numerous sub-types and varieties. The type morphology is essentially controlled by eight different hydrologic mechanisms, dripping, flowing, pool, geyser, capillary, condensation,

aerosol, and phreatic water, which may act independently or in combination. For example, dripping types include stalactites and stalagmites, capillary types include coralloids and frostwork, aerosol types include sinter crusts, and phreatic water types include cave clouds and spar crystals. Sub-types are speleothems that are structurally similar to types but differ sufficiently in origin to produce a morphology with additional structural elements. For example, cave cones are a sub-type of cave rafts because they consist of piles of sunken cave rafts piled up into cones on the floor of a cave pool (Hill and Forti, 1997).

The following discussion focuses on the three main types of speleothem used in palaeoenvironmental studies: soda-straw stalactites, stalagmites, and flowstone.

2.5.1. Soda-straw Stalactites

The name of these cave decorations comes from their remarkable resemblance to drinking straws. Their defining morphology is that they hang from the roof of a cave, are usually hollow, tubular in shape, with a diameter of approximately 5 mm, and vary from a few millimetres up to 6 m in length. Water flows down through the central channel of the soda-straw stalactite with deposition occurring at the tip-water interface but a minor amount of deposition also occurs along the inner surface. In some cases deposition occurs mainly within the soda-straw stalactite with $CaCO_3$ filling in some of the tube or even the entire void. Growth rates of soda-straw stalactites vary enormously with estimations and observations ranging from a few microns per year up to several millimetres per year. Radiometric dating of soda-straw stalactites in order to estimate growth rate has been attempted using radiocarbon (Broecker *et al.*, 1960), the $^{230}Th/^{234}U$ method (Gascoyne and Nelson, 1983) and more recently by excess ^{210}Pb dating (Baskaran and Iliffe, 1993; Tanahara *et al.*, 1998).

2.5.2. Stalagmites

Stalagmites are mineral deposits which rise from the floor of a cave as a result of water dripping directly from the roof or from stalactites (Ford and Williams, 1989). Stalagmites attain a wide variety of size, shapes and forms [see Hill and Forti (1997) for a comprehensive account] but generally their diameter is larger than the stalactite above and they usually have rounded tops. Many factors such as the amount of solution, distance of drip fall, evaporation, and solution chemistry influence the size and shape of stalagmite morphology (Hill and Forti, 1997).

Most palaeoclimatic studies using stalagmites as a data source have used the uniform diameter type as they are assumed to grow continuously over long time periods and the long term growth rate often remains relatively constant. This appears to be a valid assumption but Hellstrom (1998) suggests that as stalagmites are predominantly fed by a single drip source they are very sensitive to microscale changes in the paths of the percolation waters, which could cause discontinuous growth independent of any variations in external climate. A solution would be to sample a number of stalagmites from the same cave and, using radiometric dating techniques, analyse those that have overlapping records (for example see Dorale *et al.*, 1998). But this approach faces several ethical and conservation problems.

The internal structure of uniform diameter stalagmites consists of cuspate layers or caps and the equilibrium diameter, D, of these stalagmites can be specified by the following relation:

Equation 2.6

$$D = 2\sqrt{\frac{CoQ}{\pi Z}}$$

where Co equals the amount of $CaCO_3$ in solution available for deposition; Q equals the flow rate of the solution; and Z equals the vertical rate of growth. The minimum diameter is approximately 30 mm and any increase in diameter is broadly proportional to Q (Ford and Williams, 1989). Observation of uniform diameter stalagmites indicates that the flow rate is not constant and Q may be more appropriately identified as the most probable or modal value of the flow (Goede, pers. comm.).

2.5.3. Flowstone

According to Hill and Forti (1997), flowstones are one of the most common forms in caves. They consist of a planar deposit covering the cave floor/wall, reminiscent of a frozen "river" of calcium carbonate. In most cases deposition of subaerial flowstone occurs where thin films of water flow over an area of cave floor. The origin of water can either be from a single source or from multiple sources. Deposition occurs predominantly as fine layers, sometimes interbedded with detritus and other minerals [see Hill and Forti (1997) for a broader description of flowstone types].

There are very few published palaeoenvironmental records that specifically use flowstones as an information source (see Hellstrom *et al.*, 1998). This is partly due to the relative ease of recovering stalagmite samples from caves and partly due to the fact that for stalagmites there is an accepted method for testing that deposition occurred under conditions of oxygen isotope equilibrium. A major advantage that flowstones have as a source of palaeoclimatic information is that they are often fed by several independent sources of seepage water and therefore more likely to grow continuously over long periods of time (Hellstrom, 1998).

2.5.4. Crystallography of Calcite Speleothems

An understanding of the processes operating at the solid-solution interface may be important in understanding the minor element composition of speleothem calcite. Precipitation of calcite can occur by one of two mechanisms, homogeneous or heterogeneous nucleation. The predominant formation process of crystals in natural waters is through heterogeneous nucleation, aided by dissolved ions and organic acids acting as catalysts. Crystals are seeded by nuclei, usually microscopic particulate matter which is common as "dust rain" in caves, but inorganic crystals, skeletal particles, sand, and biological surfaces also serve as suitable substrates (Stumm *et al.*, 1992). Crystal growth occurs by ions, molecules, and ion pairs diffusing into the adsorption layer where they are adsorbed directly at "steps", "kinks", and other lattice defects. The "step and kink" model of crystal growth assumes that atoms and molecules in crystals are ordered into layers. At the solid surface steps, two sided, and kinks, three sided, are the preferred sites for precipitation (Ford and Williams, 1989).

Nucleation points are important for the continuing growth of individual crystals but it does not necessarily guarantee their survival given the variability in the orientation of the nuclei and adsorption surfaces. Interface roughness also has a bearing on nucleation success as a rougher substrate would tend to collect/trap more particulate matter (Gonzalez *et al.*, 1992). The initial crystal form dictates the final form of the crystal, which grows by repetition in three dimensions, the crystal faces (limiting surfaces) depend on the shape of the initial structural unit. The environmental conditions under which the crystal is growing also influence the crystal morphology and these include factors such as temperature, pressure, conductivity, nature of the solution, flow direction, availability of space for free growth, and convection streams (Hill and Forti, 1997).

As noted by Roberts (1998), recent work by Paquette and Reeder (1990; 1995) has highlighted the role of crystal surface microtopography in governing minor element partitioning. The results indicate that the minor element composition of time-equivalent regions precipitated from the same solution may in fact vary significantly between adjacent crystal sectors and within the crystal sectors themselves, this was termed "sector zoning" (Reeder and Grams, 1987) and "intrasectoral zoning" (Paquette and Reeder, 1990), respectively. The zoning clearly indicates the importance of surface-structural controls on the incorporation of minor elements during crystal growth (Paquette and Reeder, 1995). The authors note that empirical partition coefficients are wholly dependent on the configuration of available adsorption sites, since these have been shown to vary over both the surface of the crystal and with growth conditions, the partition coefficients are unlikely to represent equilibrium ones and will therefore have a significant effect on any calculations derived from them. Roberts (1998) points out that the research by various workers on the microtopographical controls on minor element partitioning into calcite highlights the limitations of using equilibrium partition coefficients in natural settings.

2.5.5. Cave Climatology

Environmental factors influencing the climate of a cave include temperature, relative humidity, air flow, and the carbon dioxide content of the air, all are controlled by the regional climate on the surface. The near constant temperature of most caves is directly related to the surface mean annual temperature (Yonge *et al.*, 1985), in some cases to within approximately ± 1°C (Goede *et al.*, 1982). Variable cave temperatures are mainly related to factors such as the presence of flowing water in the cave, the size and number of cave entrances, the extent of the cave system, the altitudinal extent of the cave system, and differences in the geothermal gradient (Bögli, 1980; Ford and Williams, 1989).

Relative humidity is generally high (>90%) in caves located in humid climates and low in caves located in semi-arid to arid climates (<90%) but no definitive classification can be provided as great within cave variations can occur. Deposition of minerals is strongly influenced by relative humidity. Since evaporation occurs at low humidity, sulfate, halide, and nitrate minerals are deposited At high humidity, carbonates are deposited by carbon dioxide loss, however carbonates can also be deposited by evaporation (Hill and Forti, 1997). Seasonal variations in

relative humidity strongly influenced the carbonate mineralogy of a late Holocene stalagmite from Botswana. In the winter months low humidity resulted in aragonite being deposited and in summer high humidity resulted in calcite deposition (Railsback *et al.*, 1994).

Airflow also has a strong influence on cave climatology. Air movement in a cave is influenced by exogenous and endogenous factors, acting independently or in combination, including differences between the cave and surface air pressure, differences between the cave and surface temperature, the number of cave entrances, the presence of flowing water, the dimensions of cave passages, and the distance from the surface. The carbon dioxide content of air within a cave can influence the deposition of minerals and speleothems (Cabrol and Coudray, 1982). Where air flow is negligible or non-existent the cave atmosphere may become stratified according to the density of the gases present, but where significant airflow exists, carbon dioxide concentrations are generally higher where water enters the cave. Condensation-corrosion can occur if high levels of carbon dioxide are present in water condensing on the limestone bedrock or on the surfaces of speleothems (Hill and Forti, 1997).

2.6. Speleothems as Palaeoenvironmental Recorders

Palaeoenvironmental interpretations using speleothems as an information source are based on variations in speleothem growth rates, the frequency distribution of speleothem growth in time, variations in speleothem mineralogy, analyses of stable oxygen and carbon isotope ratios, luminescence microbanding, minor element variations, the organic content of speleothems, and speleothem colour. Most speleothem research has focused on the interpretation of stable isotopes but in recent years a growing amount of research has been done on minor elements and how their variations relate to environmental parameters. Luminescence microbanding of speleothems is currently being investigated for its potential usefulness as a palaeoenvironmental information source as well as a dating tool.

2.6.1. Variation in Growth Rates

Speleothem growth rate is a potentially important palaeoenvironmental signal as the chemical kinetics of growth are dependent on several variables which can be determined by climate and vegetation changes (Baker *et al.*, 1998b). Early attempts to investigate speleothem growth rates were crude and consisted marking the growth surfaces in some way, for example using the soot from a candle, or noting the growth on human-made structures.

Recent attempts at measuring speleothem growth rates have relied on selecting samples with a known age, for example speleothems from abandoned mines (Baker, 1993) or railway tunnels (Genty *et al.*, 1996), or by using recently developed high precision dating techniques (Baker *et al.*, 1993b; Roberts *et al.*, 1998). These samples have been shown to have annual laminations enabling comparisons to be made between measurements of the growth lamina and other high resolution climatic records and predicted growth rates. Baker *et al.* (1998b) used annually laminated speleothems to compare theoretically predicted rates with measured rates in order to investigate which variables controlled or contributed to growth. The results

indicate that speleothem growth rate is sensitive to variations in Ca ion concentration and water supply, confirming that the Dreybrodt model (Buhmann and Dreybrodt, 1985a, 1985b; Dreybrodt and Buhmann, 1991), used for predicting speleothem growth, adequately predicts actual growth rates under present day conditions in the caves used in this study.

2.6.2. Speleothem Growth Frequency Variations Through Time

Several studies have used the growth frequency of secondary calcite deposits through time as an indicator of past climate change (Baker *et al.*, 1993a; Gordon *et al.*, 1989; Ayliffe *et al.*, 1998). Calcite deposition in caves is dependent, to a large extent, on the degassing of groundwaters which have elevated carbon dioxide concentrations. This raised level of carbon dioxide is a result of water passing through the soil atmosphere, where high carbon dioxide partial pressures are generated by microbiological processes and root respiration. Warm conditions are associated with high soil respiration rates and CO_2 production (Dörr and Münnich, 1989) and, therefore, the higher probability of speleothem growth. In regions affected by ice sheets, where ice is situated over a cave or the area is influenced by permafrost, conditions will prevent or inhibit speleothem growth altogether (Baker *et al.*, 1993a). Regions which are not influenced by ice sheets may instead be limited either by a lack of surplus water inhibiting speleothem growth, or regional temperatures may have a greater role in determining soil CO_2 production and ultimately speleothem growth (Ayliffe *et al.*, 1998).

Good correlations have been found between marine oxygen isotope stratigraphy, pollen records, and insolation changes and the record of speleothem growth frequency in northwest Europe (Baker *et al.*, 1993a; Gordon *et al.*, 1989). In the southeastern region of South Australia the speleothem growth frequency record indicates that greater effective precipitation occurs during stadials and cool interstadials, thus providing ideal conditions for speleothem growth. Interglacials and glacial maxima inhibit speleothem growth as it appears that there is insufficient water available for speleothem growth (Ayliffe *et al.*, 1998).

2.6.3. Variations in Mineralogy

The majority of secondary mineral deposits in caves are carbonates. In most situations the precipitation of carbonates occurs by carbon dioxide degassing and the resulting mineralogy of the deposit is either aragonite or calcite, or a combination of the two. For example, Railsback *et al.* (1994) analysed a stalagmite from Botswana with alternating layers of calcite and aragonite. Each calcite/aragonite pair, referred to by the authors as composite layers, represents one year and approximately 1,500 were counted. The model presented to explain the composite layers suggests that the main control is the highly seasonal nature of the precipitation and the quantity of water reaching the stalagmite.

In some situations, usually in semi-arid and arid regions, evaporation is the dominant mode of deposition and secondary mineral deposits consist mainly of sulphates and halides. A good example of this occurs in caves on the Nullarbor Plain, Australia where a progressive drying out of the regional climate has occurred during the Pleistocene which is reflected in the mineralogy of the speleothems. Goede *et al.* (1990a) used alpha spectrometic $^{230}Th/^{234}U$ dating to

distinguish several different mineralogical phases of speleothem deposition in the Nullarbor caves. The analyses indicate that no significant calcite deposition has occurred in approximately the last 400,000 years and that gypsum and halite have been deposited sometime since thus indicating an extended period of aridity.

Genty and Quinif (1996) used variations in the character of annual calcite layers in several modern stalagmites from four caves and a sealed tunnel to investigate what environmental conditions controlled their deposition. The layers consist of white-porous calcite (WPC) and dark-compact calcite (DPC) lamina, measured using a microscope and digital image processing. The lamina thickness is best explained by the high seasonality of the water excess, which has been calculated using the Thornthwaite equation based on monthly records of temperature and precipitation.

2.6.4. Stable Isotope Ratios

The majority of palaeoenvironmental reconstructions using speleothems as a data source rely on the analysis of the stable isotopes of oxygen and carbon (Goede *et al.*, 1990b; Harmon *et al.*, 1978; Thompson *et al.*, 1974). The isotope variations are usually expressed as parts per mil relative to a standard, the PeeDee Belemnite standard in the case of carbonates (Craig, 1957):

Equation 2.7

$$\delta^{18}O = \left[\frac{\left(\delta^{18}O/\delta^{16}O\right)_{sample} - \left(\delta^{18}O/\delta^{16}O\right)_{PDB}}{\left(\delta^{18}O/\delta^{16}O\right)_{PDB}} \right] \times 1000$$

Equation 2.8

$$\delta^{13}C = \left[\frac{\left(\delta^{13}C/\delta^{12}C\right)_{sample} - \left(\delta^{13}C/\delta^{12}C\right)_{PDB}}{\left(\delta^{13}C/\delta^{12}C\right)_{PDB}} \right] \times 1000$$

Oxygen isotope fractionation occurs between the speleothem calcite and the drip-water from which it forms. The degree of fractionation is sensitive to temperature and, under ideal conditions of constant oxygen isotope composition of the dripwater, records cave temperature changes in the calcite at a rate of -0.24 ‰°C^{-1} (Hendy, 1971). Unfortunately conditions considered "ideal" are rarely attained as the isotopic composition of the dripwater changes over time. Palaeotemperature calculations based on the degree of fractionation can be used only if the oxygen isotope composition of the dripwater can be estimated and so far no reliable method has been developed (but see Dennis *et al.*, 1996).

Carbon isotope variations are interpreted mainly in relation to changes in the composition of vegetation through time (Brook *et al.*, 1990; Dorale *et al.*, 1992; Talma and Vogel, 1992) but several authors have pointed out problems with this (Baker *et al.*, 1997b; Goede, 1994). As carbon is present only as a minor constituent in cave seepage water, it is susceptible to fractionation at all stages of transport from the soil right through to incorporation in speleothem calcite (Hendy, 1971). Therefore, while it can be relatively easy to predict the carbon isotope composition of soil CO_2 for any given vegetation type and environmental conditions (Bird *et al.*,

1996; Cerling *et al.*, 1989; Dulinski and Rozanski, 1990), predicting the carbon isotope composition of speleothems derived from this soil CO_2 is in many cases not possible (Baker *et al.*, 1997b). A more detailed discussion on stable isotopes is given in Chapter 6.

2.6.5. Minor Elements

Carbonate minerals, precipitated from solution, contain minor elements whose concentrations are governed by the composition of the parent solution and the conditions under which the carbonate was precipitated (Roberts, 1997). The minor element composition of speleothems is "largely unexplored" according to Gascoyne (1992) but studies by Gascoyne (1983), Goede and Vogel (1991), and Goede (1994) are early attempts to relate palaeoenvironmental conditions to minor element fluctuations in speleothems. Recent attempts to investigate the minor element composition of speleothems have used microprobe analytical techniques at very high resolution (Hellstrom, 1998; Roberts *et al.*, 1998) and have lead to the discovery of annual variations in the content of magnesium, strontium, and barium. A more detailed review of the minor element composition of speleothems is given in Chapter 5.

2.6.6. Colour

In its pure form, and as a primary mineral, calcite is colourless. As a secondary mineral calcite is found in a range of colours from translucent, white, yellow through to dark brown or black. Various ionic species and organic acids, present in the parent water, substitute for Ca^{2+} or are included in the crystal structure. Prior to any analytical work, speleothem colour was attributed to specific elements, for example blue and green colours due to copper, brown and black due to iron or manganese oxide pigments, and yellow, orange, and brown colours due to hydrated iron oxide stains (White, 1981). Measurements of the minor/trace element and organic acid content of coloured speleothems disproves these simplistic observations, for example, Gascoyne (1977) analysed a number of speleothems and showed that there was no correlation between colour and the amount of iron present.

A study by White (1981) used reflectance spectroscopy and chemical composition to investigate speleothem colour. The results suggest that some of the transition elements and Fe^{2+}, Ni^{2+} and Cu^{2+}, act as colourants by replacing Ca^{2+} in the crystal structure (Table 2.1). The ions of these elements are able to produce colour because they have only partially filled outer electron shells which allows some light energy to be absorbed and some to be reflected thus giving the sensation of colour (Battey, 1981). For example, the d-shell of the Zn^{2+} ion is full and since there are no empty states to which electrons can be activated by light it can not serve as a colouring ion (White, 1981).

Colour may also be influenced by pigmentation, that is the presence of impurities within the speleothem. The oxides and oxyhydroxides of iron, mainly haematite and goethite, and organic acids, probably humic and fulvic acids, act as pigments in calcite and are responsible for the commonly seen yellow, tan, orange, and brown speleothem colours. White (1981) was able to distinguish which pigments were responsible for colour by their spectral signatures, for

example 850 to 950 nm for the iron oxides whereas organic acids have a rising absorption "edge" in the red end of the spectrum.

Table 2.1 Qualitative chemical analyses of some coloured speleothems by White (1981). In all the samples analysed by White (1981) the following elements were not detected B, Be, Mo, Y, Cr, Ni, V, Ti, Co, Zr, and La (Source: White, 1981).

	Colour	Minor Elements (0.02-2 %)	Trace Elements (< 0.02 %)	Not Detected
Stalactite	Yellow	Mg	Si, Al, Yb, Sr	Mn, Ba
Calcite Flowstone	Green	Zn, Cu	Mg, Al, Sr	Si, Mn, Al, Yb, Ba
Aragonite Flowstone	Green	Zn, Cu, Sr	Mg, Si, Ba	Mn, Al, Yb
Aragonite	Blue	Mg, Sr	Si, Al, Yb, Ba	Mn

2.6.7. Organic Content

Humic and fulvic acids are products of organic matter breakdown and are introduced into the cave environment by percolation waters. Gascoyne (1977) has suggested that organic compounds such as humic and fulvic acids were responsible for the common yellow-tan-brown speleothem colours present in caves, this hypothesis was supported by White (1981) using reflectance spectroscopy. Samples with organic compounds present have most light absorbed in the blue wavelengths and significantly less light absorbed in the red wavelengths, thus a typical reflectance spectrum for a sample containing organic acids has a characteristic rising absorption edge. The yellow to tan to brown colours are due to the absorption edge moving further into the red and near infra-red wavelengths and the slope of the absorption edge becoming less steep (White, 1981; 1997). Much recent research has focused on the luminescence, produced by organic acids when calcite is exposed to ultraviolet light, and its potential as a palaeoclimate proxy.

2.6.8. Luminescence Microbanding

A recent development in attempts to reconstruct palaeoenvironmental conditions from speleothems is the use of luminescence microbanding. The luminescence phenomenon in speleothems is thought to be caused by humic and fulvic acids trapped within the calcite lattice during precipitation. When exposed to ultra-violet light some speleothems display a blue-green luminescence (White and Brennan, 1989), the luminescence is believed to be due to the excitation of the organic acids present in the speleothem calcite. The concentrations of organic acids are thought to vary in response to changes in the activity and rate of decomposition of surface vegetation (Baker *et al.*, 1993; Shopov *et al.*, 1994).

Luminescence is not present in all speleothems, for example only 5 out of the 43 samples examined by Baker *et al.* (1993b) exhibited banding, but those that have it sometimes display

microscale banded patterns parallel to the growth layers. Thus our understanding of the nature of and the processes that control speleothem luminescence is still limited but several investigations are in progress (Baker and Barnes, 1998; Baker *et al.*, 1998a; Baker *et al.*, 1999c).

2.7. Age Determination of Speleothems

Reliable, precise and accurate dating is of fundamental importance to palaeoenvironmental studies as without it, it would be impossible to match proxy records from different sources and assess the rate of past environmental change. For example, Richards *et al.* (1994) used the mass spectrometric $^{230}Th/^{234}U$ technique to date submerged speleothems from Blue Holes in the Bahamas to constrain maximum glacial sea levels. Without precise age estimates it would not have been possible to examine the several thousand year difference between the speleothem and coral ages (Bard *et al.*, 1996) that record the Flandrian transgression. The discrepancy is attributed to a regional increase in aridity causing a reduction in groundwater recharge and ultimately the cessation of speleothem growth a few thousand years prior to flooding of the cave by rising sea levels.

Most dating techniques applicable to the study of speleothems use radioactive isotopes. They measure either the rate of radioactive decay (radiometric dating) or the accumulation of damage to the crystal lattice caused by radiation (radiogenic methods). Incremental methods rely on the counting of regular cycles to discriminate time, for example the annual rings in trees or coral, or the annual layers of lake sediments (varves). Chemical methods rely on the gradual breakdown of either inorganic or organic substances that can be time related, for example weathering rinds of dolerite have been used to date Quaternary glacial deposits (Kiernan, 1990). Table 2.2 lists the techniques used to date speleothems and their approximate temporal ranges.

2.7.1. Radiometric Methods

Radiometric techniques rely on the time-dependent decay/growth of parent and daughter nuclides as they restore equilibrium in the isotope series. The following three techniques have been used in this study and are discussed in detail in Chapter 4.

2.7.1.1. Uranium-series Dating

The uranium decay series provides several geochronometers capable of measuring time from several years up to several million years thus filling an important gap between radiocarbon and potassium-argon dating (Faure, 1986). The disequilibrium methods have proved the most useful in dating various materials used in studying events in the Pleistocene. The most common technique applied to speleothems exploiting the parent-daughter disequilibrium is the $^{230}Th/^{234}U$ method. This method has used by many researchers to date speleothems, for example Edwards and Gallup (1993), Gascoyne *et al.* (1979), Li *et al.* (1989), and Richards *et al.* (1994), and reviews and methods are presented in Gascoyne (1985), and Ivanovich and Harmon (1982; 1992).

2.7.1.2. Excess ^{210}Pb

The decay chain of ^{238}U contains the ^{210}Pb isotope, a solid with a half-life of 22.26 years. This provides it a maximum age range of some two hundred years and making it useful tool for investigating late Holocene environmental history and recent anthropogenic impacts on the environment. ^{210}Pb excess dating is therefore a useful technique for establishing the ages of recently deposited sediments such as marine, lake, and ice cores as well as speleothems (Tanahara *et al.*, 1998).

2.7.1.3. Radiocarbon

One of the most common methods used to investigate late Quaternary palaeoenvironmental history is radiocarbon dating. It can be applied to a great range of materials such as peat, bone, wood, shells, marine and lacustrine sediments, and palaeosols. Radiocarbon dating is sometimes also applied to speleothems (Broecker *et al.*, 1960; Hendy and Wilson, 1968; Pazdur *et al.*, 1996) but its accuracy is low because while most of the carbon is derived from biological activity in overlying soils there is a variable amount of "dead" carbon contributed by the parent limestone (Genty and Massault, 1997), something that is highly variable both temporally and spatially.

Table 2.2 Table showing the methods used to date speleothems together with an indication of their temporal range, their frequency of application to speleothems, and an indication of their accuracy.

Method	Name	Temporal Range (Years)	Application to Speleothems	Accuracy
Radiometric	Uranium/Thorium			
	Alpha spectrometry	10,000 → 350,000	common	***
	Mass Spectrometry $^{230}Th/^{234}U$	0 → 500,000	common	*****
	$^{231}Pa/^{235}U$	5,000 → 150,000	rare	*****
	$^{234}U/^{238}U$	10,000 → 1,500,000	rare	*
	Pb-210	0 → 200	increasing	***
	Radiocarbon	0 → 40,000	common	*
Radiogenic				
	Thermoluminescence	10,000 → 1,000,000	rare	*
	Electron Spin Resonance	2,000 → 1,000,000	rare	*
Isochron				
	Palaeomagnetism	0 → ?	rare	**
Incremental				
	Luminescence microbanding	0 → ?	increasing	***
Chemical				
	Amino Acid Racemisation	0 → 500,000	rare	*

2.7.2. Radiogenic Methods

2.7.2.1. Thermoluminescence (TL)

TL has rarely been applied to speleothems because it is a complex and time consuming method which sometimes yields anomalous results (Debenham, 1983). Geyh and Schleicher (1990) point out that calcites of the same age can yield results that deviate from each other by up to 200 percent. Where TL ages have been compared to uranium-series ages the correlations are sometimes excellent and sometimes poor (Ford and Williams, 1989).

2.7.2.2. Electron Spin Resonance (ESR)

Motoji Ikeya (1975) pioneered the method of dating speleothem calcite using the ESR technique. The technique itself has undergone considerable development and refinement (Ikeya, 1988). Its application to speleothems has not been restricted to dating (Goede and Hitchman, 1984; Goede *et al.*, 1990b) but variations in one of the spectral peaks (h_3) have also been found to be related to variations in the concentrations of some minor elements in speleothems bearing some relationship to palaeoenvironmental change (Goede, 1991; 1998).

2.7.3. Isochron Methods

2.7.3.1. Palaeomagnetism

Palaeomagnetism relies on the preservation of the orientation of magnetic particles to record fluctuations in the Earth's magnetic field. Cave sediments and speleothems have long been recognised as recorders of remnant magnetism which may be either detrital or chemical in nature (Latham *et al.*, 1979). As stalagmites and flowstones usually have a relatively simple stratigraphy, *i.e.* growth layers decrease in age towards the top, and they usually have a relatively slow growth rate, the past geomagnetic field variation must be recorded continuously in the sequence of growth layers as long as growth has been continuous (Latham *et al.*, 1982; Inokuchi *et al.*, 1981).

However, as noted by Latham *et al.* (1979; 1982; 1986) the disadvantages of using speleothems is firstly that the remnant intensities are often low, frequently too low to provide useful records, and secondly in finding suitable specimens to allow multiple sampling of a single time horizon. A major drawback of the technique is that it only allows the identification of event horizons such as magnetic reversals or excursions that have already been dated by other methods.

2.7.4. Chemical Methods

2.7.4.1. Amino Acid Racemisation (AAR)

Dating speleothems by AAR was attempted by Lauritzen *et al.* (1994) with conventional uranium-series dating providing an independent chronological control thereby effectively calibrating the AAR measurements. The AAR technique has some potential to allow dating beyond the range of uranium-series dating.

2.7.5. Incremental Methods

2.7.5.1. Luminescence Microbanding

Baker *et al.* (1993) have shown that luminescent banding present in speleothems is annual by using high precision mass spectrometric U-series dating. A feature of the bands used in this study is that they consist of pairs of high and low luminescence layers that are thought to reflect seasonal variations in organic acid formation. This study demonstrates that in some cases luminescence microbanding can be used as a powerful chronological tool. Roberts *et al.* (1997) used luminescence banding in a 2.4 mm section of stalagmite to establish a chronology and also investigate annual minor element variations and luminescence. TIMS $^{230}Th/^{234}U$ dating was used to establish and independently check the chronology.

2.8. Advantages and Disadvantages of Studying Speleothems

The growth record of secondary calcite deposits offers great potential as a proxy record of past regional climate change (see Table 2.3). When calcite precipitates onto the growing surface of a speleothem the minor element and stable isotope composition will reflect environmental conditions on the surface at the time of calcite deposition. The crystalline nature of speleothems ensures that they remain a closed system unlike marine, lake, and ice cores which are subject to temporal blurring through bioturbation and diffusion, respectively. The application of precise radiometric dating methods allows precise temporal assignment for the last 500,000 years and also allows comparisons with other proxy records. Temporal resolution is potentially very high and is dependent on speleothem growth rate which can vary from 20 to 50 mm ka^{-1}, but rates of up to 600 mm ka^{-1} have been recorded.

Speleothems do have great potential as palaeoenvironmental proxies but more research is required into the processes controlling their minor element and stable isotope compositions. Prior to percolation water entering a cave it has been subject to a number of environmental influences which may filter or significantly influence the environmental signal. Some of these aspects have been highlighted by Smart *et al.* (1996) in a critical review of speleothem research. They suggest that the use of individual speleothems for palaeoenvironmental interpretations is fraught with difficulty, subject to essentially random site specific controls which may filter or moderate the signal. But the need for duplication and reproducibility conflicts with the strict conservation ethic demanded by recreational cavers.

Table 2.3 Potential palaeoenvironmental indicators based on speleothems.

Indicator	Potential palaeoclimatic significance
Growth frequency	LOW: cool, decreased effective precipitation or arid conditions HIGH: warm, increased effective precipitation, surface vegetated conditions
Internal stratigraphy (*eg* growth hiatus, colour change, *etc*)	possible sudden climate change
$\delta^{18}O$ variation	change in the ^{18}O of water and/or temperature of deposition
$\delta^{13}C$ variation	change in the ^{13}C of source and/or calcite precipitation process
Variation of δD in fluid inclusions	change in ^{2}H of water due to varying climate
Pollen content	indicates surface vegetation type
Organic content	indicates vegetation activity
Variation of minor element content	indicates change in water composition and/or temperature of deposition, investigations at an early stage may also indicate derivation from an exogenic source such as dust, sea-salt, and smoke

Chapter 3
Regional Setting

3.1. Introduction

In southern Australia the late Tertiary was a period of marked dryness, lower temperatures, and increasing seasonality compared with the warm and humid climates of the early- and mid-Tertiary (Jackson, 1999). The drying out of the continent was also accompanied by a change in the seasonal distribution of precipitation from a pattern of dominantly summer to winter precipitation receipts (Bowler, 1982). During the Pleistocene there have been repetitive cycles of glacial/interglacial climate oscillations influencing the Australia's climate system together with significant changes in moisture availability. The glacial/interglacial cycles have had major impacts on global climate particularly in areas which presently experience cool temperate climates.

This chapter introduces the reader to the factors influencing environmental change both in a contemporary and antecedent context, and at a regional and global scale. No attempt will be made to cover all aspects relating to palaeoenvironmental change as the literature is extensive and beyond the scope of the thesis. A review of current and past environmental conditions will be given for the Australian region including details of studies outside this region where deemed relevant.

3.2. Climate in the Australian Region

The climate of the Southern Hemisphere is governed by an asymmetrical distribution of land and sea, the minor amount of land, and the extremely cold polar region (Markgraf *et al.*, 1992). A steep pole-equator temperature gradient results in much more vigorous activity of the general circulation systems, the circum-polar lows with easterly wind flow, the Westerly Wind Belt (WWB), the Sub-Tropical High pressure (STH) systems, and the tropical easterlies (Pittock *et al.*, 1978). Seasonal changes in the extent of Antarctic sea ice have a significant effect on the mean latitudinal position of the STH and WWB, shifting by up to 10° and resulting in strong seasonal precipitation variations in the southern parts of the continents (Markgraf *et al.*, 1992).

3.2.1. Present Day Climate

The Australian continent stretches from latitude 10°S to 42°S and longitude 115°E to 155°E, and is bounded by the Indian, Pacific, and Southern Oceans. It has a variety of climate

regimes ranging from tropical monsoonal in the north, arid in central Australia, to westerly maritime in the far south. Past changes in the positions of major atmospheric and oceanic boundaries have had a significant impact on the climate of the region.

3.2.1.1. Atmosphere

The present climate of southeastern Australia is dominated by the STH, and a broad band of westerly winds, the Roaring Forties (Dodson, 1998). The high pressure systems move in an east-west direction, their mean latitude migrating seasonally from 37-38°S in summer to 29-32°S in winter (McTainsh, 1989). The prevailing westerly circulation, expanding and contracting seasonally with the STH and extent of Antarctic sea ice, affects southeast Australia throughout the year but is far more vigorous in the cooler half of the year (Derbyshire, 1971). The STH is furthest south in February, with a mean latitudinal track of approximately 40°S, when the westerlies that influence southern Australia are at their lowest ebb and when northern Australia is most affected by the northwest monsoon. In August, the STH moves to its most northerly track at approximately 30°S and the westerlies influence most of the southern part of the continent.

In the north, the South East Tradewinds (SET) replace the monsoon with cooler, drier air. In summer, tropical cyclones form in the Arafura, Coral, and Timor Seas and the Gulf of Carpentaria. They cross the coast and move inland, bringing large amounts of precipitation to northern Australia. Sometimes they move south along the coast as rain bearing depressions, bringing heavy falls as far south as Tasmania (Colhoun, 1991).

The southern part of the continent generally experiences mild to hot, dry summers and cool to mild, wet winters but the west coast of Tasmania experiences precipitation throughout the year. A steep west to east precipitation gradient presently exists in Tasmania, from approximately 3,500 mm in the West Coast Range down to 500 mm in the interior basins of the Midlands (Figure 3.1.c). The high relief of the west coast and Central Plateau intercepts most of the moisture, although the Ben Lomond plateau in the northeast has precipitation in the 1,500 to 2,000 mm range. The persistence of the precipitation gradient is evidenced by a gradient in relict glacial landforms, reflecting a change in ice accumulation, and therefore a reduction in the intensity of glacial activity, from west to east (Davies, 1967). Currently no permanent ice exists anywhere on the mountainous areas of Australia as the snowline lies some 300 m above the highest peaks (Colhoun and Peterson, 1986).

On the Australian mainland the distribution of precipitation (Figure 3.1a and b) is mostly affected by onshore winds, topography, and distance from the coast. In the southeast mainland, precipitation ranges from 250 to 500 mm in sub-humid areas such as west of the Australian Alps, western Victoria, and South Australia, and between 800 to 1,500 mm in humid areas such as the Australian Alps, other high ranges, and the coastal river valleys (Gentilli, 1986; Nanson *et al.*, 1992). Regional rainfall is influenced by the mean position of the subtropical high pressure belt which shifts on a seasonal as well as a longer-term basis (Pittock, 1975; Pittock, 1978).

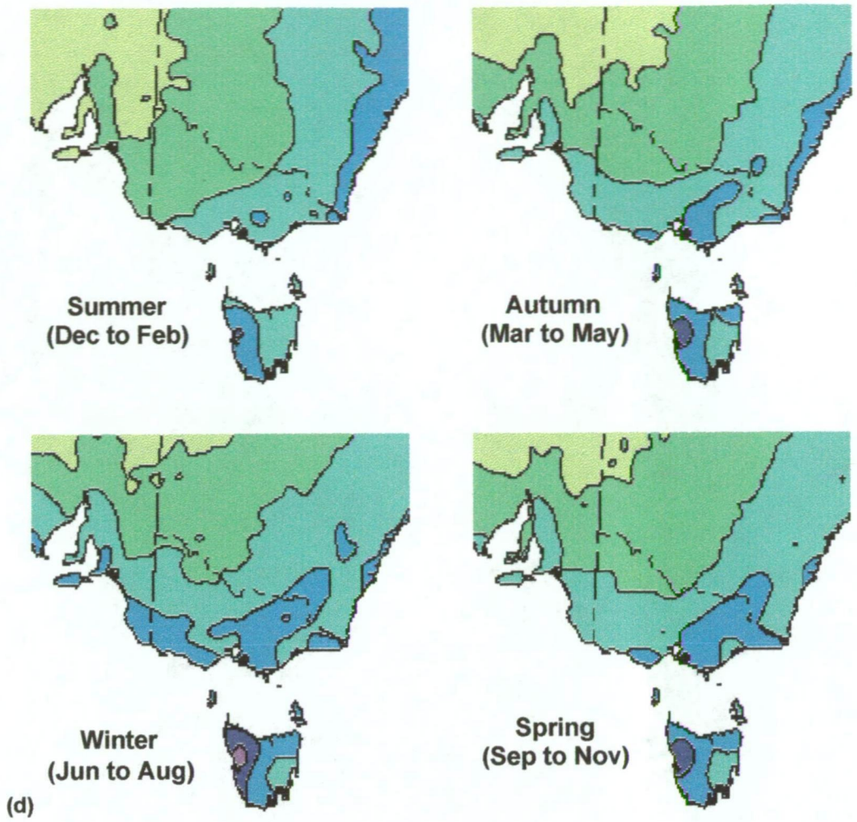

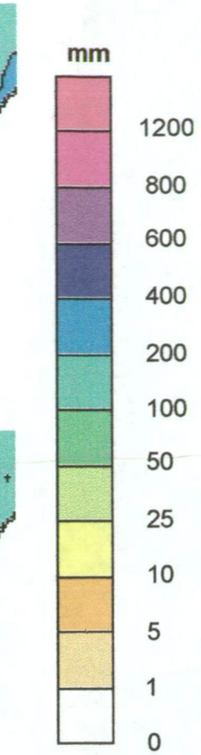

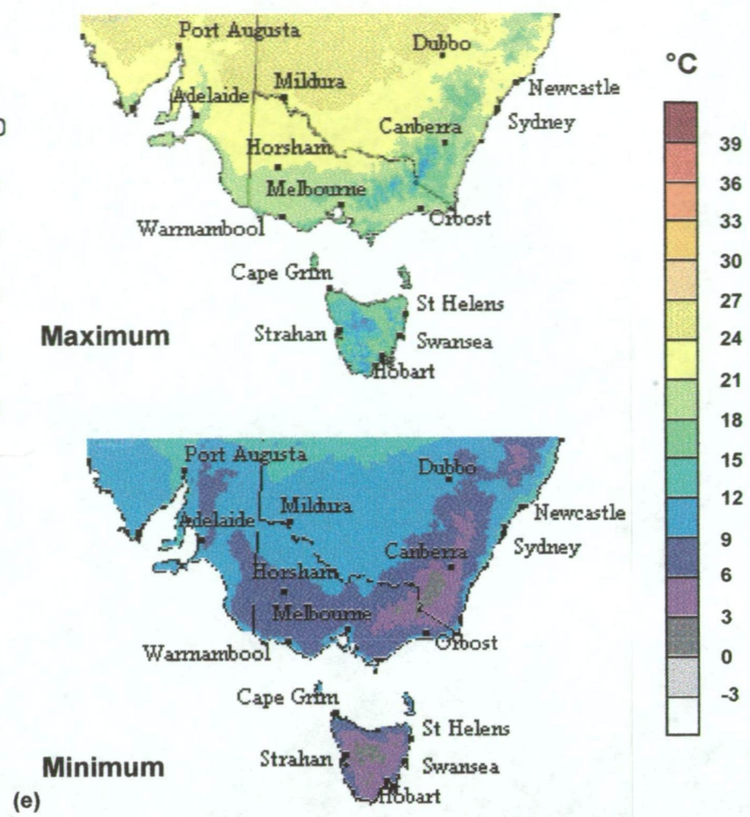

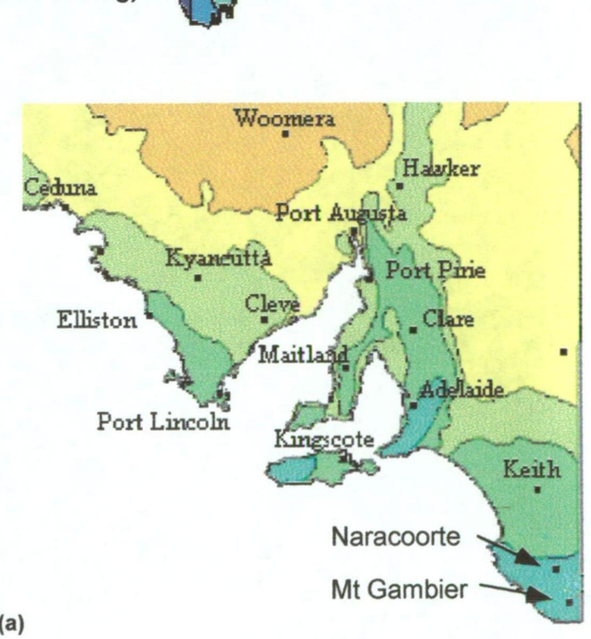

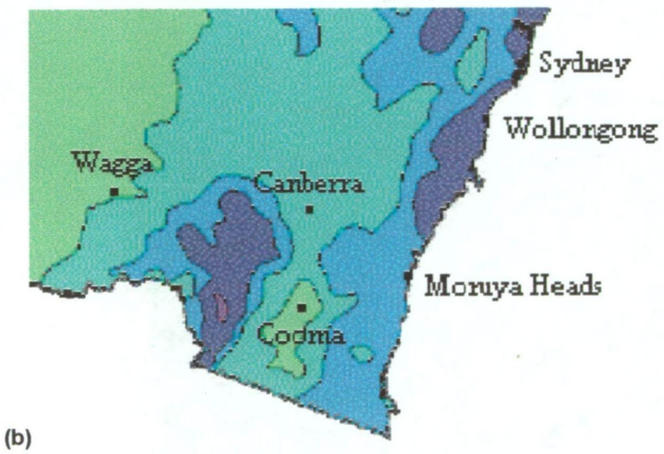

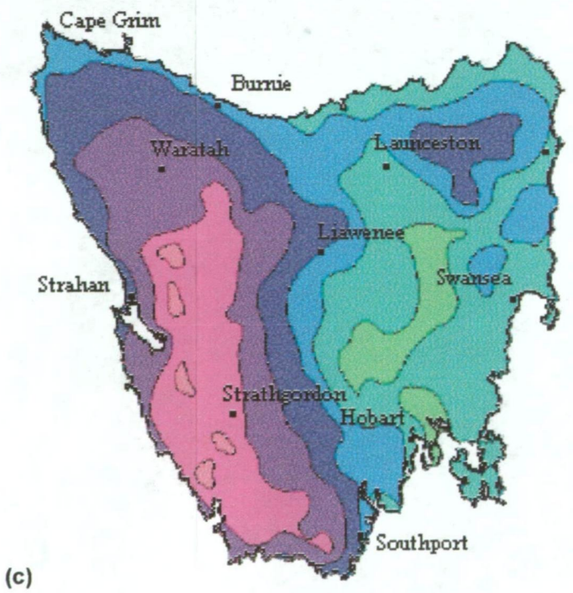

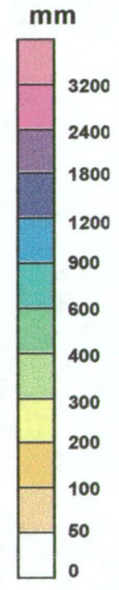

Figure 3.1. Temperature and precipitation maps for southeastern Australia. The lower maps, (a) to (c), are mean annual precipitation for southern South Australia, southeastern New South Wales, and Tasmania, respectively. The seasonal distribution of precipitation for southeastern Australia is shown in (d). The mean annual minimum and maximum temperature for southeastern Australia are shown in (e). (Figures adapted from maps provided by the National Climate Centre, Bureau of Meteorology, Commonwealth of Australia, 1999. http://www.bom.gov.au/)

3.2.1.2. *Ocean Currents*

Seasonal changes in the extent of Antarctic sea ice strongly influence the southern part of the Australian continent, the sea ice limits vary from approximately 65°S in summer to 60°S in winter. The boundaries of major ocean features are also affected by the seasonal fluctuation in sea ice extent including the Polar Front (PF) or Antarctic Convergence, which has an average position of approximately 55°S, and the Sub-Tropical Convergence Zone (STCZ), between 36° and 45°S.

The east coast of Australia is influenced by the warm East Australian Current (EAC), a series of disjointed gyres with an anticlockwise motion and flowing in a southerly direction as far as Tasmania (McGowran *et al.*, 1997). The warm water forming the EAC originates from the westerly flowing South Equatorial Current (SEC) via the Coral Sea. The western and southern continental coasts are influenced by the cool, south to north/west to east flowing West Australian Current (WAC). These coasts are also affected by the warm, north to south flowing Leeuwin Current (LC), which is fed by the warm, low-salinity SEC via the Indonesian Throughflow (Colhoun, 1991; McGowran *et al.*, 1997).

The position of the STCZ is the most important feature influencing the present and past climates of the southern latitudes between 30° and 45°. Generally the STCZ is located at around latitude 40°S (Figure 3.2) but it can be forced to deviate to the south at times due to the influence of currents flowing north to south along the coasts of the southern continents. There is evidence to suggest minor changes in the mean latitudinal position of the STCZ and the West Wind Drift (WWD) during the Quaternary resulting in the shutting down of the LC (McGowran *et al.*, 1997) and a strengthening/weakening of the EAC (Nees, 1997) when the ITCZ moves north during cool climate phases.

3.2.2. Palaeoclimate

3.2.2.1. *Evidence for Palaeoenvironmental Changes*

Throughout Australia there is ample evidence to suggest major fluctuations in regional climate in response to past realignments of major synoptic and ocean current systems (Derbyshire, 1971; Okada and Wells, 1997). During the Last Glaciation the Australian continent was influenced by a much drier and windier climatic regime due to the northward movement of the STH and the WWB. The resultant compression of the synoptic systems, effectively forced by a significant expansion in the extent of sea ice, induced a significant increase in the meridional pressure gradient. This resulted in a major increase in average wind speeds, enough to induce significant dune and dust mobilisation (McTainsh, 1989).

The land surface area of the Australian continent also grew in size due to an estimated 120 m drop in sea level at the Last Glacial Maximum resulting from significant expansion of global ice volume, therefore increased continentality is to be expected during glacial periods. Significant responses from several geomorphic systems including cold climate, desert, and fluvial landforms resulted from the progressive amelioration of climate during the Last Glacial. The Penultimate Glaciation is characterised by subdued moraines and lightly weathered drifts lying

several kilometres beyond the limits of the fresher and sharper features of the Last Glacial. However, the actual extent of the Penultimate Glacial is not particularly well documented or dated in the Southern Hemisphere (Clapperton, 1990).

Additional evidence for climate fluctuations comes from aeolian, fluvial, and lacustral sediments. Dunefields occupy approximately 40 percent of the Australian land area (*eg.* Simpson dunefield), several large lakes with vast catchment areas (*eg.* Lake Eyre basin) are found in the arid interior, and there are several rivers (*eg.* Darling and Murray Rivers) that span the continent. These systems have reacted to past climate changes and the fluctuations are faithfully recorded in various sediment sequences. For example, age frequency histograms of aeolian, fluvial, and lacustral sediment dates indicate periods of enhanced aeolian and fluvial activity associated with changes in regional moisture availability. These variations are coupled to global fluctuations in climate and sea level (Nanson *et al.*, 1992).

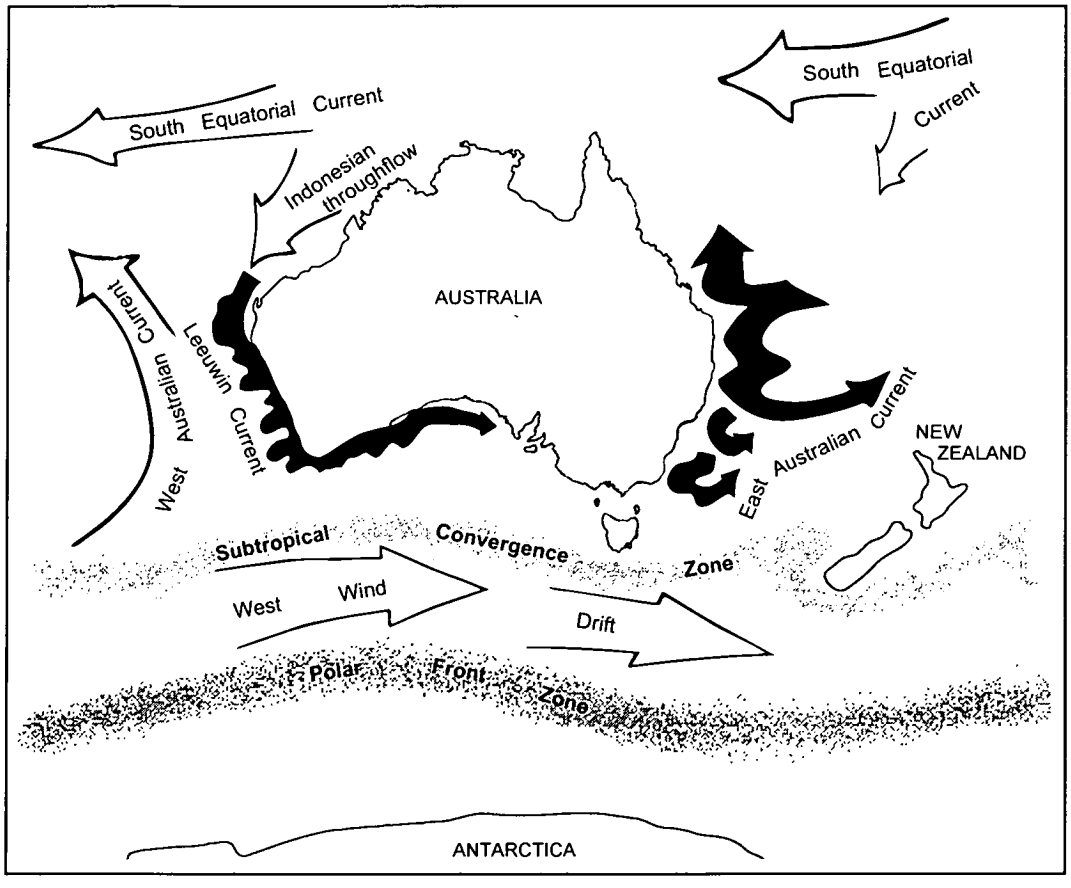

Figure 3.2. Location of main ocean current systems influencing the Australian region. The East Australian and Leeuwin Currents are warm flows sourced from the warm, low salinity South Equatorial Current. These currents play significant roles in causing episodic warm and wet conditions in Southern Australia. The Leeuwin current shuts down when the West Wind Drift and Subtropical Convergence move north during cooler periods (McGowran *et al.*, 1997). (Figure adapted from McGowran *et al.*, 1997)

Unlike New Zealand, which has experienced widespread vulcanism throughout the Quaternary, Australian chronologies do not have temporally discrete and spatially extensive tephras within their Quaternary sediment sequences. While tephrochronolgy provides a very powerful and independent means of dating sediment sequences in New Zealand (Lowe and Newnham, 1999), most chronologies from Australian sediments rely on radiocarbon and luminescence dating.

Advances in dating techniques, such as optically stimulated luminescence (OSL), accelerator mass spectrometry (AMS), and exposure dating (*ie* ^{10}Be, ^{36}Cl) allow more precise determinations of age using significantly smaller samples therefore producing better temporal control and higher quality chronologies. For example, the OSL technique can use a single grain of quartz to make an age estimate thereby avoiding contamination from material of different ages (*eg* Roberts, R. *et al.*, 1998), a problem with some studies relying on thermoluminescence age estimates (*eg* Fullagar *et al.*, 1996). Many radiocarbon dates on important Australian sequences and material are currently being revised using AMS radiocarbon dating in conjunction with refined chemical extraction methods (Bird *et al.*, 1999). Tim Barrows (RSES, ANU, Canberra) is presently using ^{10}Be and ^{36}Cl dating to date moraine sequences in the highlands of Australia in order to better understand their glacial history.

A plethora of marine sediment cores from the oceans and seas bounding Australia provide a wealth of palaeoenvironmental information including variations in sea surface temperatures (Linsley, 1996), and productivity (Nees, 1997), displacement of currents (McGowran *et al.*, 1997), ice volume changes (Labeyrie *et al.*, 1996), continental dust records (Hesse, 1994), terrestrial vegetation fluctuations (Heusser and Van de Geer, 1994; Harle, 1997), *etc.* The general findings, from several cores in the region, is that during glacial-interglacial cycles significant relocations occur of major oceanographic features such as the Tasman Front, the Subtropical Convergence, the East Australian Current (Nees, 1997). There also appears to be an on/off switching of the Leeuwin Current (McGowran *et al.*, 1997). Records of ice volume changes, and thus the record of past glacial-interglacial cycles, are recorded by changes in the oxygen isotope composition of various species of marine organisms, for example planktonic and benthic foraminifera. These observations are supported by a remarkable record from the Huon Peninsula, Papua New Guinea, of sea-level fuctuations from tectonically uplifted coral terraces (Chappell and Shackleton, 1986).

3.2.2.2. Late Quaternary Climate in Southeast Australia

In Australia, periods of wetter conditions occurred between 270 to 220 ka years ago (OIS 7), between 110 to 80 ka (OIS 5), and between 55 and 30 ka (OIS 3). Drier conditions occurred between approximately 200 and 130 ka (OIS 6) between 75 and 55 ka (OIS 4), and between 25 to 15 ka (OIS 2) (Wasson, 1986; Nanson *et al.*, 1992). A common problem with many studies is the lack of rigid temporal control, a reflection of the sparsity of sites and quality of the material available for dating.

Although the paucity and poor temporal fixing of most proxy records from Australia precludes making any unequivocal conclusions about past circulation patterns and the timing of their influence, some careful postulating using various assumptions has spawned a reasonably

detailed palaeoenvironmental history of the Australian continent as it responds to global climatic changes (Derbyshire, 1972; Markgraf *et al.*, 1992). Chappell (1991) noted that, in some cases, low-quality chronologies lead to conflicting interpretations or inconsistencies between sites. Despite this, the weight of evidence clearly supports phases of wetting and drying, and cooling and warming in Australia. The use of speleothems, which can be accurately and precisely dated by independent means, will provide additional evidence for the timing and occurrence of past periods of fluctuating moisture availability and temperature.

Evidence of several periods of glacial activity during the Quaternary in Tasmania comes from widespread moraine and till deposits, block streams, scree deposits, and cirques. Individual events can be distinguished by the degree of weathering of dolerite clasts contained within till and glacial outwash deposits but also with radiocarbon dates of organic material and charcoal. Recent work by Augustinus *et al.* (1999) used uranium/thorium dating of ferricrete bands within glacigenic sediments to estimate the ages of glacial advances in Tasmania. On the highlands of the southeastern Australian mainland no firm evidence has been found for multiple glaciations. In the last glacial episode some mainland mountains had limited cirque and short valley glaciation. Ice cover was limited to approximately 32 km^2 on the Snowy Mountains (Galloway, 1963).

In Tasmania ice caps were developed on the West Coast Range (Margaret Glaciation), Central Plateau (St Clair and Rowallan Glaciations, south and north respectively), and on the Ben Lomond plateau (Cirque Glaciation), with an areal extent of around 2,000 km^2 (Derbyshire, 1972). An older and more extensive glaciation, in the order of five to ten times larger in some areas, is evident from till and moraine deposits that encompass deposits of the Last Glaciation (Colhoun and Hannan, 1990). The Penultimate Glaciation has significant deposits on the West Coast (Henty/Comstock Glaciation), Central Plateau (Butlers Gorge and Arm Glaciations, south and north respectively), and on Ben Lomond (Plateau Glaciation). Deposits from the Penultimate Glaciation have soil profiles approximately 1.5 m thick and dolerite clast weathering rinds between 2 and 20 mm thick. In comparison, the Last Glaciation has soil profiles less than 0.5 m thick and weathering rinds less than 1.5 mm on average (Kiernan, 1983; Colhoun and Peterson, 1986).

3.3. Mechanisms and Evidence for Long-term Climatic Fluctuations

Various theories have been put forward to explain the abundance of evidence for "catastrophic" environmental changes on Earth's landscape. The evolution of geology as a discipline came at a time of intellectual revolution evoking considerable debate in the mid- to late-18th century concerning the origin of humans and the environment they live in. At that time the Earth was thought to have been divinely created and the idea of a biblical "flood" used to explain many aspects of the contemporary landscape. This creationist view is still held today by some religous groups. As our knowledge and understanding of the Earth increases so to does the evidence against creationist theories.

The following discussion focuses on the now widely accepted astronomical theory and its influence on Earth's environmental history, and the evidence for past changes. For a brief synopsis on alternate theories of environmental change, Bell and Walker (1992) and Goudie (1992) are suggested.

3.3.1. Orbital Forcing and Autovariation

Until recently the available records of environmental change were temporally fragmented and it was not until ocean cores were investigated that the true cyclical nature and scale of climate change became clear and theories to explain it universally credible. Hays *et al.* (1976) have demonstrated that fluctuations in Earth's orbital parameters are reflected in the oxygen isotope record from the deep oceans. Prior to this, evidence of past environments has come from a variety of sources including historical records and investigations of terrestrial deposits and landforms (Bell and Walker, 1992). However, the majority of these studies are mere snapshots and do not indicate the true cyclical nature of long-term environmental changes. It is also very difficult to find consensus among Quaternary scientists on a universal theory to explain the causes of past global environmental change. Some early attempts at explaining climate fluctuations included the idea that variations in the Earth's orbit may act as a trigger, but this was generally disregarded due to the lack of evidence.

3.3.1.1. Causes of Long-Term Climate Changes

The astronomical theory was first proposed by Aldéman in 1842 and was further elaborated by James Croll (Imbrie and Imbrie, 1979). Milutin Milankovitch was the first to provide testable predictions about the geological record of climate by producing radiation curves for high northern latitudes based on changes in the Earth's orbital parameters, namely precession, obliquity, and eccentricity, that enabled him to predict the number of glacial episodes and their timing during the last 650,000 years (Imbrie and Imbrie, 1979).

The eccentricity of the Earth's orbit has a period of approximately 100,000 years, obliquity of the ecliptic around 43,000 years, and precession of the equinoxes at 23,000 and a minor one at about 19,000 years (Bell and Walker, 1992). At the time of publication (Milankovitch, 1927) the fragmentary nature of the available evidence did not strongly support the hypothesis and it was not until long-term records were gleaned from ocean cores that it gained widespread support. Hays *et al.* (1976) have clearly demonstrated that the astronomical frequencies are present in the isotopic record of the deep ocean.

Recent work has revealed that the magnitude of the 100,000-year palaeoclimatic cycle expected on theoretical grounds is not in agreement with the available geological evidence. Some doubt exists as to our current understanding of internal and external climate feedbacks and how they have operated in the past (Broecker, 1992; Winograd *et al.*, 1988; Imbrie *et al.*, 1993b). Liu and Chao (1998) investigated orbital variations and palaeoclimatic cycles using wavelet time-frequency spectrum analysis. They found that a signal-noise resonance effect could explain the obliquity period variations and that "flickers" within cycles were due to amplitude variations of the obliquity and precession.

It is now generally accepted that the variability of insolation receipts on higher latitudes of the continental landmasses in the Northern Hemisphere exerts considerable influence over global temperature, albedo, and sea-level. In the Southern Hemisphere the ocean to land ratio is about four to one, the ratio in the Northern Hemisphere is almost equal. However, the effects of orbital variations on insolation alone are not sufficient to explain the large temperature fluctuations in the Quaternary. Other mechanisms must be amplifying or modulating their influence, so called positive and negative feedbacks (*ie* autovariation) such as albedo, greenhouse gases, ocean currents, *etc*. For example, a lowering of radiant energy on the surface leads to cooling of landmasses which results in increased snow and ice cover and therefore elevated surface albedo, this provides a positive feedback increasing the likelihood of ice accumulation.

3.3.1.2. Causes of Shorter Term Climate Variation

While the Milankovitch theory goes a long way to explaining some of the major features of Pleistocene climatic fluctuations it seems unable to account for small- to medium-term changes, particularly in the Holocene (Goudie, 1992). Using wavelet time-frequency spectral analysis of orbital variations and geological records, Liu and Chao (1998) have suggested that these climate "flickers" are induced by the amplitude variation of obliquity and precession. It is also likely that these shorter-term changes are responses to complex interactions between positive and negative feedbacks in the climate system and perhaps are only partially modulated by the long-term insolation variations. For example, the amount of carbon dioxide in the Earth's atmosphere influences the strength of the atmosphere's greenhouse effect. Natural variations in the concentration of carbon dioxide occur because of changes in global mean temperature. When average global temperatures are warmer there is a net movement of carbon dioxide from the oceans into the atmosphere but cooler temperatures reverse this process thereby lowering the concentration of carbon dioxide in the atmosphere.

Another example of an autovariation variable are volcanic eruptions, which can cause short-term cooling of the Earth's climate. Some of these eruptions can release large amounts of material into the stratosphere that effectively block the receipt of solar radiation by the Earth's surface therefore providing an additional negative feedback when climate is in a cooling phase or as a positive feedback by decreasing albedo for a short time during climate amelioration. However, the exact nature of its influence is still a matter of debate due to an apparent correlation between cool phases and increased vulcanism (Goudie, 1992).

3.3.1.3. Abrupt Climate Changes

Recent studies of marine cores from the North Atlantic have identified relatively short but sudden periods of climatic instability called Heinrich events (Heinrich, 1988), they are also found in ice-cores as Dansgaard-Oeschger events (Bond *et al.*, 1993). In marine-cores these sudden events have been shown to relate to large inputs of ice and meltwater from Northern Hemisphere ice-sheets causing a marked reduction in the salinity of surface waters and temporarily bringing to a halt the thermohaline circulation in the Norwegian-Greenland Sea that provides a major constituent of the North Atlantic Deep Water (NADW) ultimately affecting climate, both regionally and globally (Broecker and Denton, 1990; Rasmussen *et al.*, 1997).

The causes of abrupt climatic events are not completely understood but most explanations refer to the inherent instability of large ice masses, a contemporary example is the Ross Ice Sheet in Antarctica.

3.3.2. Evidence for Long-term Palaeoenvironmental Change

Evidence to support long-term cyclicity of climate comes mainly from investigation of marine-core records, some of which extend well back into the Tertiary, but also from ice-core (Vostok and GRIP) and loess records (Guo *et al.*, 1996), which can encompass several glacial-interglacial cycles. Most palaeoenvironmental evidence comes from the Northern Hemisphere due to the small number of marine and terrestrial records analysed so far from the Southern Hemisphere. The majority of temporally long palaeoenvironmental records provides supporting evidence for the Milankovitch orbital forcing theory and supports an apparent synchronicity of climate change between the Northern and Southern Hemispheres, the comparison of the Vostok and GRIP ice-cores is a classic example (Bender *et al.*, 1994). However, most of the available records are not particularly well dated because currently there are no methods available to independently verify their chronologies. As Hellstrom (1998) suggests, most records are "tuned" to known orbital variations assuming that they are directly responsible for the isotopic variations recorded in the cores (Martinson *et al.*, 1987) but it is apparent that this is a circular argument.

Very few independently dated, extensive climate records exist and some do not fully support the orbital forcing theory, the Devils Hole calcite is a good example (Winograd *et al.*, 1992). It has a very good independent chronology (Ludwig *et al.*, 1992) which spans several glacial-interglacial cycles but it does not appear to support the premise of orbital theory, although this is somewhat controversial (Imbrie *et al.*, 1993a; Crowley, 1994). The Devils Hole record indicates that speleothems have the potential to provide long-term records of climate change that are of a high quality and being independently dated, they may provide important evidence on the timing of key climatic events between the hemispheres.

A popular paradigm to explain the apparent synchroneity between Northern and Southern Hemisphere palaeoclimate change is the "conveyor belt" theory (Charles *et al.*, 1996). Changes in the high northern latitudes are propagated globally through the varying flux of the North Atlantic Deep Water (NADW). Various marine and ice core records indicate that during glacial times the North Atlantic conveyor is disrupted resulting in an alternate mode of operation and a major reorganisation of ocean circulation (Broecker and Denton, 1989).

Currently there are few terrestrial records in the Southern Hemisphere that support global palaeoclimate synchronicity although Hellstrom *et al.* (1998) and Goede *et al.* (1996) are exceptions by demonstrating the existence of the Younger Dryas Stade in the Southern Hemisphere. Investigating the timing of key global climate events, such as the Younger Dryas and the Last Glacial Maximum, also enables examination of synchroneity between the hemispheres but such research requires rigorous and precise dating. The application of the $^{230}Th/^{234}U$ technique to speleothems, described in detail in Chapter 4, can provide accurate and precise age estimates allowing rigorous testing of the conveyor belt theory.

3.4. Sample Descriptions and Location Data

A number of speleothems were collected from several karst localities in Tasmania with permission from the National Parks and Wildlife Service (NPWS) and Forestry Tasmania (ForTas). Figure 3.3 shows the locations of the karst areas used in this study and Table 3.1. gives sample details. Karst area descriptions given below are taken from the Australian Karst Index (Matthews, 1985). Samples were also taken from the Naracoorte Caves, southeast South Australia and the Yarrangobilly Caves, southern New South Wales.

3.4.1. Tasmanian Karst

The karst areas described below were selected as study sites because a significant amount of work has already been accomplished (for example Goede and Harmon., 1982; Goede *et al.*, 1986; Goede *et al.*, 1998). Apart from the soda-straw stalactites no "live" speleothem samples were collected and most were either "recycled" from Dr Albert Goede's collection, or were found displaced or already in a broken state and collected under the supervision of Mr Ian Houshold (NPWS). Two samples, CTH-1 and PB-1, were contributed by Dr Kevin Kiernan (ForTas).

3.4.1.1. Mole Creek Karst

This karst area of approximately 150 km^2 is located in northern Tasmania between 41°30'S, 146°10'E and 41°35'S, 146°30'E and is west of Deloraine and close to the township of Mole Creek (Figure 3.3d). The area is between approximately 200 and 600 metres above present sea-level and has extensive cave development in strongly folded Ordovician limestone of the Gordon Group (Burrett and Goede, 1987). Speleothems were collected with permission from several caves in the Mole Creek karst including Baldocks Cave (BC), Croesus Cave (CC), King Solomons Cave (KS), Little Trimmer Cave (LT), Marakoopa Cave (MC), My Cave (MYC), and Wet Cave (WC).

The area has a cool, moist climate with a mean annual temperature of approximately 10.5°C and mean annual precipitation of around 1,100 mm with a pronounced winter maximum. The preceding figures are calculated using the two nearest climate stations Sheffield (41°23'S, 146°20'E; 280 m a.s.l.) and Deloraine (41°32'S, 146°42'E; 250 m a.s.l.) with mean annual temperatures of 11.0 °C and 10.3°C respectively, and mean annual precipitation receipts of 1,181.9 mm and 961.7 mm respectively (Bureau of Meteorology, 1999). The natural vegetation consists of wet sclerophyll (*Eucalypt*) forest, some areas of which in the past have been subject to forest management practices. Recently areas of the Mole Creek Karst containing significant features have been declared a National Park, although this does not necessarily ensure their protection given the nature of karst hydrology. Much of the Mole Creek and surrounding areas have been cleared of forest and are now open pasture.

3.4.1.2. Junee-Florentine Valley Karst and Risbys Basin Karst

The Junee-Florentine Valley (JF) karst area is located northwest of the Maydena township and west of Mt Field National Park between 42°30'S, 146°25'E and 42°50'S, 146°35'E (Figure 3.3d). The area is between approximately 300 and 800 metres above sea-level and has extensive cave development in Ordovician limestone. Several stalagmites and soda-straw

stalactites have been collected with permission from Frankcombes Cave (FC) and several soda-straw stalactites have also been collected from Burning Down the House Cave (BDTH). The Risbys Basin (RB) karst area is located south of the Maydena township at approximately 42°46'S, 146°35'E. It has limited cave development in Ordovician limestone. Several soda-straw stalactites were collected with permission from Risbys Basin Cave (RB).

The area has a humid temperate climate with a mean annual temperature of approximately 10.5°C and mean annual precipitation of around 1,500 mm. The nearest climate stations are Maydena (42°46'S, 146°36'E; 270 m a.s.l.) and Butlers Gorge (42°17'S, 146°16'E; 666 m a.s.l.) with mean annual temperatures of 10.7 °C and 7.6°C respectively, and mean annual precipitation receipts of 1,214.5 mm and 1,684.7 mm respectively (Bureau of Meteorology, 1999). Vegetation in the Florentine Valley consists of a mixture of temperate rainforest, dominated by *Nothofagus cunninhamii* and *Atherosperma moschota*, and wet eucalypt forest consisting of mixed forest, in which *Eucalyptus* species dominate with rainforest species as understorey, and wet sclerophyll forest, in which there are no rainforest elements present in the subordinate forest layers (Gilbert, 1958; Kirkpatrick, 1991). Much of the area is subject to forest management practices (Eberhard, 1994; Eberhard, 1996).

3.4.2. Naracoorte Karst, South Australia

The Naracoorte area is part of the south-east karst province of South Australia, a coastal plain of low relief with many karst features (Marker, 1975; Grimes, 1984) and caves (Figure 3.3c). Speleothem SC-S11, used in this study, was collected from Spring Chamber in Victoria Fossil Cave near Naracoorte at latitude 36°58'S, longitude 140°45'E, at an elevation between 70 and 80 meters above present mean sea level. The regional karst rock is a flat lying, soft, porous marine limestone of Oligocene-Miocene age (Gambier Limestone) and is locally overlain by Pliocene sands (Parilla Sand) and by calcarenite dune limestones of the Pleistocene Bridgewater Formation. The Naracoorte caves are located under the East Naracoorte dune, which currently consists of a discontinuous capping of Plio- Pleistocene calcarenites and sands. The phreatic cave systems, developed in the underlying Gambier Limestone, have formed since the early Pliocene.

The climate is sub-humid Mediterranean with a steep regional rainfall gradient from south to north (Penney, 1983). Mean annual precipitation at Naracoorte is between 550 and 600 mm. Low summer rain is due mainly to convectional activity while heavier winter rain is attributed to frontal activity. There is a marked moisture deficit during the summer months and slow cave drips are likely to derive their water supply from winter rain. The mean annual temperature recorded at Naracoorte (36°59'S, 140°29'E) is 14.4 °C, significantly lower than the 16.8 °C recorded in Spring Chamber of Victoria Fossil Cave.

The natural vegetation of the East Naracoorte Range consists of *Eucalyptus* woodland with an open understorey. Only small patches remain as most of the land has been cleared to make way for improved pasture, *Pinus radiata* plantations and vineyards.

3.4.3. Yarrangobilly Karst, New South Wales

The Yarrangobilly Limestone, a Late Silurian limestone member (Wyborn *et al.*, 1990), is located in the Kosciuszko National Park, between 35°38'S and 35°44'S, 148°27'E and 148°29'E, on the western slopes of Yarrangobilly Mountain (1,628 m). The caves used in this study are located in the southern most section of the Yarrangobilly Limestone, within the Yarrangobilly River valley at an altitude of approximately 300 to 600 m above sea level (see Figure 3.3b). The samples used in this study were collected from Jersey Cave by Mr Andy Spate, NSW National Parks and Wildlife Service (Scientific Licence #A2215).

The area has a cool, moist climate with a mean annual temperature of approximately 12°C and mean annual precipitation of around 1,000 mm. The preceding figures are calculated using the several nearby meteorological stations, mean annual temperature and precipitation is given in Table 3.2. (Bureau of Meteorology, 1999).

The Yarangobilly Limestone block, approximately 1.5 kilometres wide and 14 kilometres long, lies within the Great Dividing Range, a range of mountains and hills running parallel to the eastern coast of Australia extending from the Brindabella Range (ACT) through the Snowy Mountains, New South Wales and the Victorian Alps, Victoria to the highland areas of south eastern Tasmania, a latitudinal extent of approximately 15°. The north-south alignment of the range interrupts the moisture-laden Roaring Forties, bringing significantly more rain and snow to the western escarpment than to the lower rain-shadowed areas to the east.

The higher areas of the Range have a much cooler and moister climate than the rest of the continent, precipitation is high throughout the year. Glaciation was not extensive in the Australian Alps and is not known in Victoria. Cirques and moraines are only found at the highest elevations of the Snowy Mountains on the south east facing slopes. Periglacial features such as terracing, soil movement, shattered boulders and boulder fields are much more extensive than glacial features in the Australian Alps (Costin *et al.*, 1979).

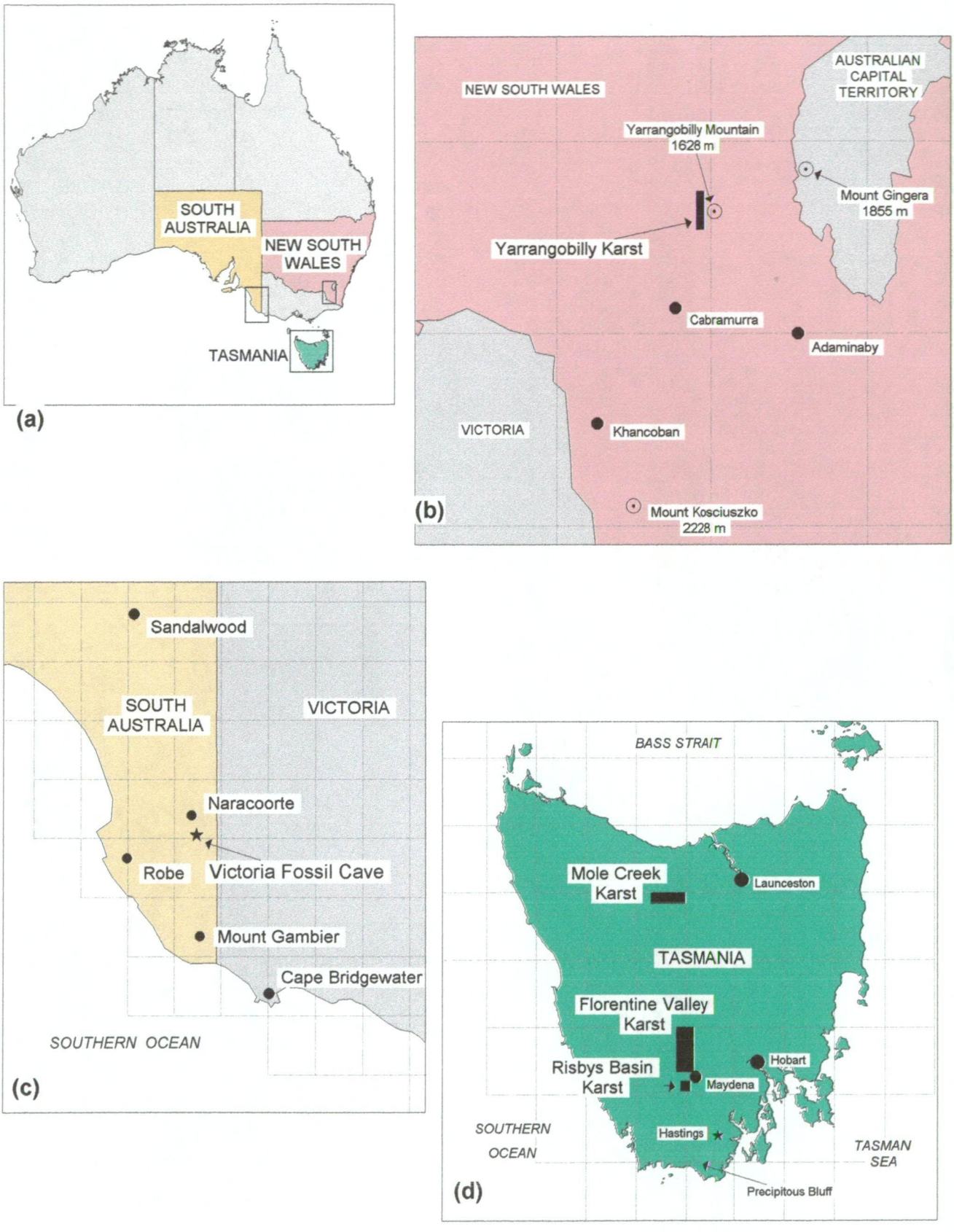

Figure 3.3. Map (a) illustrates the location of the study areas in Australia. Maps (b) to (d) show the karst locations in New South Wales, South Australia, and Tasmania, respectively.

Table 3.1. **Details of stalagmite (st) and flowstone (fl) samples used in this study. Cave names, the first two letters in the sample number, are given elsewhere. Figures in the $^{238}U/^{232}Th$ column are results from solution introduction ICP-MS (Chapter 5) used to determine uranium concentrations and to aid in selecting samples for $^{230}Th/^{234}U$ TIMS dating (Chapter 4).**
Karst areas key: FV = Florentine Valley, IB = Ida Bay-Hastings, MC = Mole Creek, Tasmania; NC = Naracoorte, South Australia; YB = Yarrangobilly, New South Wales.

Sample #	Karst Area	Type	Height (mm)	$^{238}U/^{232}Th$	U (nmol g^{-1})
BDTH-F1aa	FV	fl	130	8.92	0.028
BDTH-F1bb	FV	fl	70	5.77	0.039
BDTH-F1cc	FV	fl	100	4.21	0.020
FC-S3	FV	st	150	95.55	0.346
FC-S4	FV	st	28	34.15	0.076
BQ-S1	IB	st	143	24.01	0.210
IB-S1	IB	st	350	40.55	0.117
BC-S1a	MC	st	421	17.14	0.072
BC-S1b	MC	st	487	4.65	0.112
BC-S1c	MC	st	228	11.86	0.079
BC-S2	MC	st	260	106.05	0.278
BC-S3	MC	st	120	19.14	0.108
BC-S4	MC	st	226	33.41	0.051
BC-S5	MC	st	287	1.83	0.049
CTH-S1	MC	st	1030	-	-
KK	MC	st	1070	-	-
KS-F1	MC	fl	200	24.48	0.052
KS-F2	MC	fl	58	0.90	0.044
KS-S1	MC	st	452	-	-
KS-S2	MC	st	488	1.44	0.016
KS-S3	MC	st	235	1.28	0.045
KS-S4	MC	st	229	0.96	0.020
LT	MC	st	1965	-	-
MKC-S1	MC	st	190	28.09	0.077
MKC-S2	MC	st	288	65.52	0.061
WC-S1	MC	st	208	34.49	0.716
WC-S2	MC	st	20	-	-
WC-S3	MC	st	213	989.28	1.320
WC-S4	MC	st	50	-	-
WC-S5	MC	st	142	74.17	0.402
WC-S6	MC	st	146	454.90	1.615
WC-S7	MC	st	92	206.37	0.638
SC-S11	NC	st	545	-	-
JC-F1aa	YB	fl	138	36.78	0.051
JC-F1bb	YB	fl	100	152.29	0.125
JC-F2	YB	fl	100	36.18	0.010
JC-F4	YB	fl	49	37.64	0.085

Table 3.2. Climate averages for several meteorological stations close to the Yarrangobilly karst. Data provided by Bureau of Meteorology (1999).

Station Name	Latitude	Longitude	Altitude (m)	Mean Annual Temperature (°C)	Mean Annual Precipitation (mm)
Khancoban	36° 14'	148° 8'	337.0	13.8	1,001.7
Cabramurra	35° 56'	148° 23'	1,475.0	7.7	1,710.3
Tumbarumba PO	35° 47'	148° 1'	645.0	11.5	986.9
Kiandra Chalet	35° 53'	148° 30'	1,395.0	6.8	1,563.6

3.5. Summary

In Australia a number of glacial-interglacial cycles during the Late Quaternary had significant impacts on the environment with conditions very much different from that of the present time. Compared with many other regions Australia has limited material with which to investigate past environmental changes. As demonstrated in the previous chapter speleothems have great potential as palaeoenvironmental recorders and have provided reliable information on past conditions on other continents. Karst areas are widespread in Australia and thus provide an important information source. Speleothems from various caves in three karst areas located in southeastern Australia have been selected in order to try to investigate the extent of this change.

Chapter 4
Speleothem Age Determination

4.1. Introduction

Of fundamental importance to any palaeoenvironmental study is the ability to correlate key climatic events between spatially variable, fragmentary and discontinuous deposits, something that can only be achieved by dating individual sites using very precise dating techniques (Smart, 1991). For example, Dorale *et al.* (1998) applied high-precision $^{230}Th/^{234}U$ dating to the $\delta^{13}C$ and $\delta^{18}O$ profiles of 4 separate stalagmites in order to investigate mid-continental climate change. The precise dating established that all of the stalagmites overlapped in age. Cross-correlation between individual stalagmites and other proxy records was possible because the dating was of a high enough quality and resolution. Thus the ability to precisely date and cross-correlate speleothem material with other proxy records potentially makes it a very important source of proxy records for both regional and global Quaternary palaeoenvironmental studies.

This chapter focuses on the three methods of age determination used in this study namely ^{230}Th-^{234}U uranium-series, excess Pb-210, and radiocarbon dating.

4.2. Mass Spectrometric Uranium Series Dating

This section gives some background information on the method and then details the methodology used. The speleothem dating work was done while a visitor at the Research School of Earth Sciences (RSES), Australian National University (ANU), Canberra under the supervision of Professor Malcolm McCulloch. A successful outcome would not have occurred without his ardent and unqualified support.

4.2.1. Background

The radioactive decay of the parent isotopes uranium and thorium occurs by the spontaneous emission of either an alpha particle or a beta particle, together with several different wavelengths of gamma rays. Uranium series dating encompasses a range of techniques which exploit the decay products, or daughters, of the parent isotopes ^{238}U and ^{235}U. The following discussion will focus on the ^{230}Th-^{234}U technique, a method which has been applied to a wide range of materials including speleothems (Li *et al.*, 1989, Richards *et al.*, 1994), travertine (Schwarcz, 1980), coral (Chappell, 1996), bone (Ayliffe and Veeh, 1988), teeth, (Grun *et al.*, 1999), and lacustrine sediments (Szabo and Butzer, 1979).

Speleothems are an ideal material for the application of the ^{230}Th-^{234}U method as samples comprising non-porous, macrocrystalline calcite can be considered a closed system. The range of the method is from approximately 1 ka to 350 ka for conventional alpha-spectrometry and from around 50 years to 600 ka for thermal ionisation mass spectrometry (TIMS).

Alpha-spectrometry relies on the passive counting of alpha particle emissions from each decaying nuclide. A complex chemical extraction procedure is required to separate them from the surrounding matrix and from other isotopes with overlapping spectra (Gascoyne *et al.*, 1978). Errors are estimated by taking the standard deviation of the number of counts using the formula:

Equation 4.1

$$\sigma = \left(\sqrt{m}/m\right) * 100$$

where m is the number of counts, for each isotope 10,000 counts are required to give a 1σ error of ± 1 percent (Smart, 1991). Counting periods can be extended over a considerable length of time given that over a counting period of one week only one in 5×10^6 ^{230}Th atoms will have been counted (Roberts, 1998). It is therefore essential that the chemical yields obtained are as high as possible and that the uranium concentrations of the detritus free sample are greater than 0.05 ppm (Gascoyne *et al.*, 1978).

The development of TIMS allows the direct counting of individual atoms and has revolutionised palaeoenvironmental research through the tremendous improvement in the precision of age estimates, with errors reduced to 0.1 percent. Additionally, much smaller sample sizes are used when applying the TIMS technique and that allows more samples to be dated, thus boosting temporal resolution, but also reduces time averaging as large samples integrate significant time slices, inevitable when the alpha-spectrometric method is used to date speleothem calcite with low uranium concentrations.

4.2.2. Uranium Geochemistry

The main source of uranium and thorium is the weathering of crustal rocks, the antiquity of which ensures that the rocks are in secular radioactive equilibrium with respect to uranium and thorium, that is, that the $^{230}Th/^{234}U$ and $^{234}U/^{238}U$ ratios are equal to one. At low temperatures the behaviour of uranium and thorium in the +4 valency/oxidation state is one of near chemical immobility in near-surface environments (Gascoyne, 1982). However, uranium is readily oxidised from the +4 to the +6 valency state:

Equation 4.2.

$$U^{4+} + 2H_2O \rightarrow UO_2^{2+} + 4H^+ + 2e^-$$

The uranyl ion may undergo further complexing depending on the pH and the presence of inorganic and organic ions. Uranium is transported in groundwater, in concentrations from 0.1 to 3 ppb, as a uranyl complex, with either carbonate, sulphate, or dissolved organic species, as long as it remains in the hexavalent state. Thorium on the other hand is almost completely absent from groundwater due to its very low solubility and scavenging by clay minerals and other sediments (Langmuir and Herman, 1980; Gascoyne and Schwarcz, 1982). Calcite is precipitated by degassing of carbon dioxide from groundwater, saturated with respect to

calcium carbonate. Uranium, along with many other dissolved minor constituents, is deposited and the ^{238}U and ^{234}U isotopes are fractionated.

When the calcite is precipitated secular equilibrium is disturbed and disequilibrium between the parent and daughter nuclides results. By measuring the degree to which the system has returned to a state of secular equilibrium an estimate can be made of the timing of the depositional event, assuming that the system has remained closed and that no thorium was present at the time of deposition (Ivanovich, 1982). The age of a sample is determined using an iterative calculation because one of the decay systems has an unknown degree of disequilibrium. The time, *t*, of a speleothem sample is given by its $^{230}Th/^{234}U$ ratio by the relationship (Schwarcz, 1986):

Equation 4.3.

$$\left[{}^{230}\mathrm{Th}/{}_{234}\mathrm{U}\right]_{act} = \left[{}^{238}\mathrm{U}/{}_{234}\mathrm{U}\right]_{act}\left(1 - e^{-\lambda_{230}t}\right) + \lambda_{230}/\lambda_{230} - \lambda_{234} \times \left(1 - \left[{}^{238}\mathrm{U}/{}_{234}\mathrm{U}\right]_{act}\right)\left(1 - e^{-(\lambda_{230} - \lambda_{234})t}\right)$$

where the decay constants λ_{234} and λ_{230} are the reciprocals of the half lives of ^{234}U (108,750 ± 850 years) and ^{230}Th (352,740 ± 710 years), respectively, and "act" denotes the activity ratio (Edwards *et al.*, 1986). The selection of samples consisting of non-porous, macrocrystalline calcite with no evidence of post-depositional alteration usually satisfies the assumption of a closed system.

At the time of deposition speleothem calcite is essentially free of thorium except where it occurs due to significant detrital contamination, or other impurities present in the speleothem calcite, the extent of which can be gauged from the presence of non-radiogenic ^{232}Th (Schwarcz, 1986). Detrital contamination can be detected by measuring the $^{230}Th/^{232}Th$ activity ratio, a ratio less than 20 (Schwarcz, 1980), or for TIMS dates, less than 100 (Li *et al.*, 1989) indicates significant detrital contamination. There have been various attempts to correct for detrital contamination based on isochron methods (Bischoff and Fitzpatrick, 1991) and assumed isotope ratios (Dorale *et al.*, 1992) but these have had limited success and are at best only crude estimations. A more robust and practical method is to avoid the analysis of visibly "dirty" speleothem calcite.

Chen *et al.* (1998) used U-Th-Pa dating techniques to investigate non-concordant carbonate materials, *ie.* those that have behaved as open systems, in order to evaluate the use of models/concordia plots in a similar manner to U-Pb dating methods. The models aid in assessing what effects diagenetic processes have had on the uranium-series isotopic ratios in materials that have behaved as open systems, in some cases they allow the true age to be determined or at least better constrained.

The precision of dating is highly dependent on the accuracy of measuring the $^{230}Th/^{238}U$ activity ratio. In the chemical extraction procedure it is possible that the uranium and thorium isotopes will fractionate relative to one another in an unpredictable way. A known amount of spike, consisting of ^{233}U and ^{229}Th, two isotopes not found in nature, is added to samples during

dissolution. Any fractionation of the natural isotopes during the chemical extraction procedure or mass spectrometry can be accounted for by measurement relative to the artificial isotopes, therefore the absolute and relative concentrations in the speleothem sample can be resolved. In some laboratories a double spike mixture is added but the chemical procedure employed at RSES and described in Section 4.2.4 uses a single spike.

4.2.3. Applications of Uranium-series Dating to Speleothems

The majority of speleothem studies to date have used conventional alpha-spectrometry (α–S) to estimate the ages of samples (Goede and Harmon, 1983; Harmon *et al.*, 1981;) Thompson *et al.*, 1976). The main problem has been the lack of precision, traditionally the ages are quoted to 1σ meaning that there is only a 68 % probability that the age is within the quoted limits, and consequently there has been a lack of temporal resolution (Winograd *et al.*, 1992). The advent of high-quality mass spectrometric (MS) analysis has seen a significant improvement in the precision of dating, ages which are now quoted to 2σ , *ie.* a 95% confidence interval. Baker *et al.* (1993b) used high precision $^{230}Th/^{234}U$ TIMS dating to demonstrate that the luminescent microbanding present in a stalagmite (SU-80-11) from Traligill, Scotland was annual. Other studies have used stable isotope analyses (Dorale *et al.*, 1992; Dorale *et al.*, 1998), minor element analyses (Roberts *et al.*, 1998), and luminescence intensity variations with high temporal resolution (Shopov *et al.*, 1994; Baker *et al.*, 1998a; 1999c) to investigate palaeoenvironmental change with MS uranium-series dating providing precise chronological control.

Another application of high precision $^{230}Th/^{234}U$ MS dating to speleothems is the analysis of submerged speleothems (Richards *et al.*, 1994) in order to investigate sea-level change. Since speleothem growth in this situation only occurs in subaerial conditions it provides an upper limit for the maximum elevation of past sea-levels. Richards *et al.* (1994) have analysed a number of speleothems from submerged caves in the Bahamas, an area tectonically stable and well suited to investigating sea level changes. Results indicate good agreement between sea-level records obtained using coral terraces (Aharon and Chappell, 1986) and those estimated by dating submerged speleothems.

As speleothem growth is dependent on a constant supply of seepage water and soil CO_2, a change in the surface environment to cold and dry conditions or extreme aridity will inhibit speleothem growth. Conversely warm and humid conditions are ideal for speleothem growth. Several studies have used the speleothem growth frequency distribution to investigate past climate change using both α–S and MS dates (Atkinson *et al.*, 1978; Ayliffe *et al.*, 1998; Baker *et al.*, 1993a; Gordon *et al.*, 1989; Hennig *et al.*, 1983). The results of the studies show good agreement with other palaeoenvironmental records such as marine and ice cores although in some regions a continuous record is not obtained because growth is inhibited in interglacials, warm interglacials, and glacial maxima (Ayliffe *et al.*, 1998).

Subaqueous calcite crust from Devils Hole, Nevada was dated by 47 high precision $^{230}Th/^{234}U$ TIMS analyses, demonstrating that it grew from approximately 560,000 to 60,000 years. To

date this is the longest continuous speleothem record as it spans several glacial-interglacial cycles. However, its palaeoenvironmental interpretation and the implications for our understanding of the mechanisms forcing climate change is subject to some debate (Winograd *et al.*, 1992).

4.2.4. $^{230}Th/^{234}U$ Analytical Procedure

Age estimates are determined by isotope dilution thermal ionisation mass spectrometry (TIMS) uranium series (^{238}U-^{234}U-^{230}Th) dating. The weight of sample used for analysis is dependent on the uranium concentration and typical sample weights vary from approximately 1 up to 5 grams. Uranium concentrations were determined using solution introduction ICP-MS, discussed in Chapter 5. Samples were cut using a diamond saw and trimmed along prominent growth layers with a small dental grinding wheel. The subsamples are cleaned in an ultrasonic bath in alternate solutions of Milli-Q water and AR grade acetone. To avoid interference in the chemical procedure from any organic complexes present in the speleothem matrix, the samples are combusted in an oven at 800°C for 4 hours.

Samples are dissolved by the stepwise addition of concentrated HNO_3 in acid cleaned teflon beakers, once dissolution is complete a measured amount of mixed ^{233}U-^{229}Th spike is added to the solution. A few drops of H_2O_2 are added to ensure any residual organic compounds are destroyed. The sample-spike mixture is refluxed overnight to ensure the complete equilibration of the sample with the U and Th isotopes. Although co-precipitation with $Fe(OH)_2$ removes the majority of U and Th isotopes from the Ca^{2+}, the co-precipitation step is often repeated. The U and Th isotopes are separated with HCl acid in a column containing an anion exchange resin.

Samples are loaded onto single (Th) and double (U) zone refined rhenium filaments and the U and Th isotope ratios measured on a multicollector TIMS (Finnigan MAT 261). Aspects of uranium mass spectrometry and spike calibration are given in Stirling *et al.* (1995).

4.2.5. Age Calculation

This study follows the example of Hellstrom (1998) in its treatment and calculation of errors, and acknowledgment is given to the stimulating discussions and helpful advice he has provided. A spreadsheet is used to calculate ages using the ion and activity ratio output from the MAT 261, the software of which corrects for mass fractionation according to the spike isotope ratios. Equation 4.3 is used to calculate ages iteratively and errors are calculated using two different methods, error propagation and Monte Carlo simulation. Hellstrom (1998) notes that while some authors have treated age errors with great care (Edwards *et al.*, 1987; Ludwig *et al.*, 1992) others fail to mention how their age errors were calculated and in some cases whether they are quoted to 1σ or 2σ (Atkinson *et al.*, 1978; Bar-Matthews *et al.*, 1996; Falguères *et al.*, 1992; Ford *et al.*, 1993). In this study all ages are quoted to 2σ, the 95 % level.

In conventional error propagation there are two assumptions, that the percentage error is small and that the probability distribution is symmetrical around the mean. In a uranium series age

estimate where the percentage error is very small, the error can be considered to be symmetrical about that age. Three components are associated with uranium-series errors:

(1) systematic error is reproducible inaccuracy introduced by machine idiosyncrasies, calibration, or from uncertainty in the value of known decay constants;

(2) error derived from uncertainty in the measurement of the isotopic ratios for any given sample; and

(3) potential error resulting from failures in the assumptions of the method, such as inclusion of ^{230}Th in the sample at the time of formation, or post-depositional alteration of the speleothem.

In this study, as in the study by Hellstrom (1998), systematic errors are not propagated as they will reduce the precision of the ages unnecessarily. Stirling *et al.* (1995) noted that systematic error associated with the uranium isotope decay constants is small, and for an age of approximately 100,000 years it will contribute less than 1,000 years to the total age error if propagated. Errors associated with possible failures of the assumptions implicit in the method are also ignored as they are very difficult to quantify. No attempt has been made to correct ages for detrital ^{230}Th contamination.

Recently Chen et al. (1998) has investigated the use of TIMS $^{231}Pa/^{235}U$ measurements to check the concordance of $^{230}Th/^{234}U$ ages. Materials that were not concordant were investigated using concordia diagrams in a similar manner to U-Pb dating. For materials such as carbonates where the initial concentration of ^{238}U can vary between 0.1 ppm and 3 ppm, the models describe the variation of $\delta^{234}U$, episodic U loss or gain, continuous U loss or gain, and continuous ^{234}U, ^{230}Th, and ^{231}Pa loss or gain. These models have the potential of allowing estimates of ages for materials that have behaved as open systems, thus the third error component may be more thoroughly investigated in order to provide a more precise age estimate.

4.2.6. Error Calculation

Age error estimates are calculated using two methods, error propagation and Monte Carlo simulation. All TIMS dates in this study are reported to the 2σ (95 %) level. Calculated ages with near symmetrical errors will produce no discernible differences between results based on error propagation or Monte Carlo simulation. For ages over 100,000 years or with large percentage errors, error propagation inflates the lower error and underestimates the upper error, relative to the errors calculated by Monte Carlo simulation (Hellstrom, 1998). Error propagation calculates error estimates from the counting statistics reported by the MAT 261 mass spectrometer, which are determined from the measurement of the uranium isotope activity ratios within a sample.

Monte Carlo simulation calculates an error where error propagation or calculation by other means is impractical. Each input variable to the age equation is randomised, the uranium isotope decay constants are assumed to be constant, such that after enough iterations its mean and standard deviation correspond to its reported value and reported error respectively. In the spreadsheet developed by Hellstrom (1998) the age equation is calculated a thousand

times using the randomised input and the distribution of the resulting ages reflects the true precision of the date (Hellstrom, 1998).

4.3. Excess ^{210}Pb Dating

This work was supported by Gary Hancock (CSIRO) and a grant to Dr Albert Goede from the Australian Institute of Nuclear Science and Engineering (AINSE) in 1997. Samples have been analysed at the Environmental Division, Australian Nuclear Science and Technology Organisation (ANSTO), Lucas Heights, NSW, under the supervision of Dr Henk Heijnis.

4.3.1. Background

Very few chemical cave deposits have been precisely dated with radiometric methods that span the last one thousand years, a period which offers the best opportunity to corroborate or calibrate speleothem records with recent climate variations or instrumental records. Dating speleothem material less than 1,000 years old by the ^{230}Th/^{234}U method is difficult due to the extremely low concentrations of ^{230}Th, the signal is sometimes not more than that of the machine background and therefore very difficult to measure accurately. Whitehead *et al.* (1999) suggest that the difficulty may also be due to the incorporation of ^{231}Pa and ^{230}Th with uranium into the speleothem calcite, contrary to the most basic assumption for the U-series dating technique that no daughter radionuclides are precipitated with the parent U isotopes. The excess ^{210}Pb method lends itself to dating young speleothem material and several studies have borne this out.

The decay of uranium and thorium produces isotopes of radium, of particular interest is ^{226}Ra ($t_{1/2}$ = 1,622 years) which decays to an inert gas ^{222}Rn ($t_{1/2}$ = 3.8 days) from the ^{238}U decay series (Dickin, 1995). This gas diffuses into the atmosphere from the cryosphere and is distributed globally eventually decaying to ^{210}Pb ($t_{1/2}$ = 22.3 years) through a series of short-lived daughter isotopes (Faure, 1985). The change in phase disturbs the initial secular equilibrium between ^{222}Rn and ^{226}Ra and a new secular equilibrium is established between ^{222}Rn and its decay products, ^{210}Pb becoming the predominant radionuclide. When ^{210}Pb is incorporated into sediments it is referred to as unsupported or excess ^{210}Pb (Baskaran and Illiffe, 1993; Gale *et al.*, 1995).

The ^{210}Pb excess method allows dating of very recent sediments, with a maximum age limit of approximately 200 years, such as snow (Crozaz *et al.*, 1964), marine sediments (Koide *et al.*, 1972), and lake sediments (Gale *et al.*, 1995). However, recent studies by Santschi *et al.* (1983) and Benoit and Hemond (1991) have illustrated several problems with the method when used to date some sediments. The main difficulty relates to ^{210}Pb remobilisation and redistribution by pore-water diffusion (Dickin, 1995). An apparently ideal application of the excess ^{210}Pb method is to date very young speleothem material as it can be considered a closed system once precipitation has occurred.

4.3.2. Previous Applications of Excess ^{210}Pb Dating to Speleothems

Baskaran and Illiffe (1993) used the excess ^{210}Pb technique to determine the growth rates of a conical stalactite, a lateral growth rate of 0.028 mm yr^{-1} corresponding to a mass growth rate of 78 mg yr^{-1}, and a soda-straw stalactite, longitudinal growth rate of 1.1 mm yr^{-1} corresponding to a mass growth rate of 149 mg y^{-1}. The study showed that speleothems may contain high concentrations of excess ^{210}Pb and that the ^{210}Pb excess can be successfully exploited to obtain ages and growth rates for speleothem material that has grown in the last two hundred years. Baskaran and Krishnamurthy (1993) measured the $\delta^{13}C$ profiles of several speleothem types to investigate the variations in atmospheric CO_2 concentration using the excess ^{210}Pb method for chronological control.

Tanahara (1998) has used excess ^{210}Pb dating to investigate the growth rate of two soda straw stalactites from a cave in southern Okinawa Island, Japan. In this study an attempt has been made to address the problem of contamination by "fresh" ^{210}Pb plating-out onto the outer and inner surfaces over the growth period of the straw. The outer surface can be contaminated by the adsorption of "fresh" ^{210}Pb from the parent isotope ^{222}Rn in the cave air. The inner surface can be contaminated by cave seepage water containing high levels of the parent isotope ^{222}Rn trickling down the inside of the straw stalactite. An improvement to the procedure is to rinse the surfaces with a dilute acid first prior to the chemical extraction or measurement procedure, something that was apparently not done in the study by Baskaran and Illiffe (1993).

4.3.3. Excess ^{210}Pb Dating Analytical Procedure

No preliminary treatments were applied in this study. In hindsight a preliminary treatment such as that suggested by Tanahara *et al.* (1998) to eliminate surface contamination should have been applied. It was not used as analysis preceded publication of the Tanahara *et al.* (1998) study.

Several soda-straw stalactites were selected from various caves in Tasmania. Details are given in Table 4.1. Preliminary analyses indicate that ^{210}Pb content is high enough to be analysed and that some variability in the level of ^{210}Pb activity exists between cave locations. Samples were carefully broken into sections approximately 20 mm long and then weighed. ^{210}Pb levels were sufficiently high to measure gamma emissions using a Compton Suppression gamma detector. Some measurements were performed at the Environmental Division, Australian Nuclear Science and Technology Organisation (ANSTO), Lucas Heights, NSW, and some analyses were done by Dr Gary Hancock at the Division of Water Resources, CSIRO, Canberra.

As no certified calcite standard is currently available, the introduction of an unknown systematic error is possible, activities of the samples were determined against the IAEA-308 Mixed Seaweed standard which has a nominal ^{210}Pb activity of 73 Bq kg^{-1} as at 1-Jan-1988. The results are therefore semi-quantitative as the results may contain an unknown systematic error, however, it will not affect the calculation of a growth rate as the slope of the regression line is used.

Table 4.1. Details of soda-straw stalactites used in excess ^{210}Pb and ^{14}C dating. Details are also given for several samples which had laser ablation ICP-MS (Chapter 6) analysis applied to them.

Name	Length (mm)	Cave and Location	Analysis
BDTH-SS1	290	Burning Down the House, Florentine Valley	^{210}Pb + ^{14}C, ANSTO ICP-MS, ANU
BDTH-SS3	110	Burning Down the House, Florentine Valley	ICP-MS, ANU
BDTH-SS5	135	Burning Down the House, Florentine Valley	^{210}Pb + ^{14}C, ANSTO ICP-MS, ANU
BDTH-SS6	85	Burning Down the House, Florentine Valley	ICP-MS, ANU
FC-SS1	300	Frankcombe Cave, Florentine Valley	^{210}Pb, CSIRO
FC-SS5	151	Frankcombe Cave, Florentine Valley	ICP-MS, ANU
RB-SS1	1,020	Risbys Basin Cave, Risbys Basin	^{210}Pb, CSIRO
RB-SS4	270	Risbys Basin Cave, Risbys Basin	^{210}Pb + ^{14}C, ANSTO
RB-SS5	290	Risbys Basin Cave, Risbys Basin	^{210}Pb + ^{14}C, ANSTO

4.4. Radiocarbon Dating

This work was done as part of an AINSE grant (AINSIE 97/075R) given to Dr Albert Goede in 1997, all samples were measured at the ANTARES Mass Spectrometry facility, Physics Division, ANSTO, Lucas Heights, NSW, by Dr E.M. Lawson.

4.4.1. Background

Carbon has two stable isotopes (^{12}C and ^{13}C) and a radioactive one (^{14}C). Radiocarbon ($t_{1/2}$ = 5,730 ± 40 years) is produced continuously in the upper atmosphere by cosmic radiation bombardment of atmospheric nitrogen (^{14}N). The ^{14}C atoms are rapidly oxidised to form carbon dioxide (CO_2) which is taken up by the Earth's physical and biological processes (Dickin, 1995). A dynamic equilibrium exists between the biosphere and carbon dioxide but when an organism dies a closed system is created and the concentration of ^{14}C will decline exponentially (Pilcher, 1991). The $^{14}C/^{12}C$ ratio is measured by conventional β-particle counting methods or by accelerator mass spectrometry (AMS).

Conventional radiocarbon dating requires the conversion of the sample into a gas or liquid and the number of β-particles are counted, the age limit of this technique is about 30,000 years. The development of AMS allows direct measurement of the isotopes therefore enabling more precise calculation of the $^{14}C/^{12}C$ ratio and a reduction in age errors, theoretically the limit of this technique is approximately 60,000 years. Sample contamination from "younger" or "older" carbon is the biggest problem with this method, for example, contamination by as little as one

percent modern carbon will give an apparent age of 37,000 years BP for material that may in reality be very much older. Chemical extraction procedures are becoming more sophisticated in order to deal with this problem.

The fluctuation of ^{14}C production due to variations in cosmic ray influx is also a potential source of error, a problem that can only be resolved by using special calibration curves (*eg* Bard *et al.*, 1990; Stuiver and Reimer, 1993). The above description does not describe several complexities associated with application of the technique to specific materials, the reader is referred to Bradley (1985) or Pilcher (1991) for a more extensive account of the method (or several WWW sites such as http://c14.sci.waikato.ac.nz/webinfo/). The following discussion will focus on radiocarbon dating speleothems.

4.4.2. Previous Applications of Radiocarbon Dating to Speleothems

The radiocarbon method has been used to date speleothems since the 1960's. Broecker *et al.* (1960) used the method to investigate speleothem growth layers to see if they were annual. Application of the method to speleothems is not straightforward because there are multiple sources of carbon or "mixing effects" (Hendy, 1970) which influence measurement of the radioactive nuclide. There are two principal sources of carbon in speleothems, the first is from carbon dioxide generated in the soil above the cave, and the second from carbon derived from dissolution of the host limestone (Genty and Massault, 1997).

The precipitation of calcium carbonate to form speleothems is dependent on the supply of CO_2 which contains ^{14}C contributed both from the atmosphere and from soil processes, specifically the decomposition of soil organic matter (SOM) and plant root respiration. Genty *et al.* (1998) and Genty and Massault (1999) have described a model for carbon infiltration in the karst system incorporating several influences on the final carbon content of speleothems including soil and epikarst CO_2 formation, soil CO_2 dissolution and bicarbonate formation, limestone dissolution, mixing effects, and $CaCO_3$ precipitation in the cave (Figure 4.1).

Some workers have tried to address the problem of carbon derived from limestone, termed the "reservoir effect", by estimating the percentage of "dead" carbon to be approximately 15 percen. Recent studies by Genty and Massault (1997) have confirmed that 15 ± 5 percent, a dilution factor of 0.85 ± 0.5, is an acceptable value for estimating the dead carbon proportion (DCP). Genty and Massault (1997) have listed the methods used by different speleothem workers to estimate the DCP including measurement of the ^{14}C activity of active stalagmites, by age-distance interpolation, by analysis of the pollen contained in the speleothem, or by comparison with uranium series ages.

4.4.3. Analytical Procedure

All samples and targets were prepared and analysed by Dr E.M. Lawson, Physics Division, ANSTO, Lucas Heights, NSW using the ANTARES tandem accelerator mass spectrometer (AMS) facility.

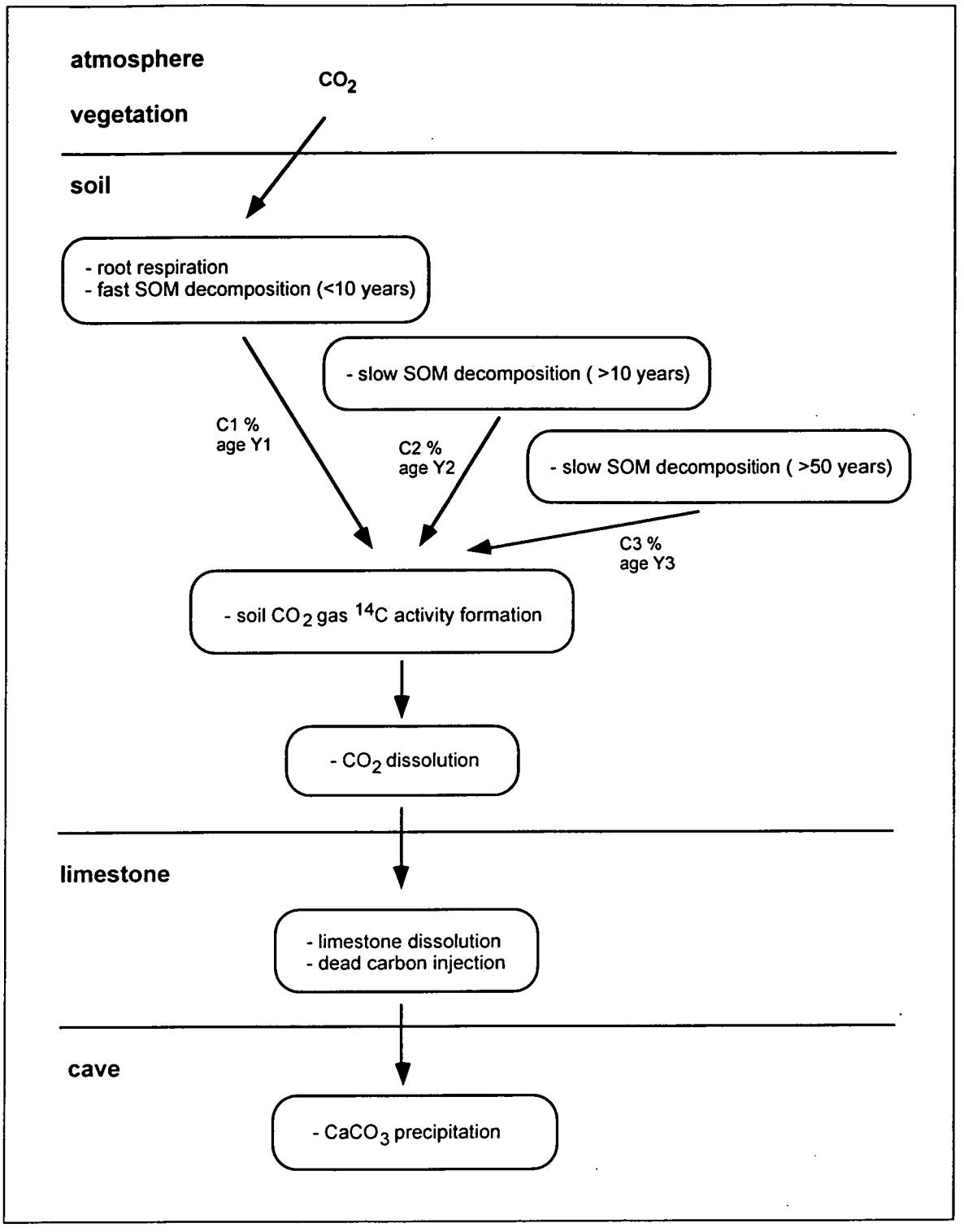

Figure 4.1. **Model illustrating carbon infiltration into karst systems with three soil organic matter (SOM) components and the controls on the final ^{14}C and carbon content of speleothems (adapted from Genty and Massault, 1999).**

4.5. Results and Discussion

4.5.1. Age Frequency Histogram of Uranium Series Analyses

Table 4.2 gives the analytical details for each of the stalagmite samples examined in this study. The frequency distribution of 37 new Tasmanian speleothem ages is presented in Figure 4.2(a). Histogram is produced by summing the individual age distributions for each of the age estimates, the width of of the age distributions is a gaussian function of the 2σ errors. Samples with small errors have narrow age distributions and larger errors have broader age distributions (Ayliffe *et al.*, 1998). Also plotted are several other palaeoenvironmental proxy records including the South Australian speleothem data from Ayliffe *et al.* (1998), a number of alpha-spectrometric speleothem dates from Tasmania (Goede and Harmon, 1983), and several marine core sequences.

Figure 4.2(b) and Figure 4.2(c) show the Tasmanian speleothem age distribution at 0 to 200 ka and 0 to 50 ka, respectively. The Tasmanian TIMS ages are predominantly less than 130 ka old with a few greater than 200 ka, possibly reflecting a sampling bias. However, there are several observations that can be made about the frequency distribution of the Tasmanian TIMS ages and those from Naracoorte (Ayliffe *et al.*, 1998).

Beyond approximately 120 ka years ago age frequency data for Tasmania is sparse, however, the few dates available, *ie* prior to 150 ka, do overlap with the Naracoorte data but the small number of older dates from Tasmania prevents any meaningful comparisons. There are no speleothems aged between 150 ka and 125 ka in the 37 analyses presented by this author suggesting either a genuine climatic event during this period or a possible sampling bias.

From 125 ka years ago to the present, speleothem deposition is more abundant. The distribution of ages provides meaningful insights into past climatic conditions affecting southeastern Australia. The data suggests that conditions in Tasmania were conducive to speleothem growth throughout this period except during the LGM with no speleothem age determinations falling between approximately 22 and 19 ka years.

Table 4.2. Analytical details for all sample analysed. Sample details are given in Table 3.1.

Sample	^{238}U (nm/g)	± ^{238}U (nm/g)	^{230}Th (nm/g)	$\frac{^{230}Th}{^{238}U}$ (Act)	± $\frac{^{230}Th}{^{238}U}$ (Act)	$\frac{^{234}Th}{^{238}U}$ (Act)	$\frac{^{230}Th}{^{232}Th}$ (Act)	Age (years)	± 2_ error
BC-S1(C) (Base)	0.5625	0.00064	2.50E-06	0.2631	0.05331	1.9067	4	15962	3446
BC-S1A (Top)	0.2466	0.00021	3.06E-07	0.0736	0.00383	1.5551	3	5257	281
BC-S2 (Base)	1.5291	0.02166	8.38E-06	0.3247	0.02435	2.0325	18	18661	1506
BC-S2 (Top)	2.3271	0.02425	7.22E-06	0.1839	0.00305	1.7102	34	12277	217
BC-S3 (Top)	0.3760	0.00023	3.68E-07	0.0580	0.01000	1.5529	5	4132	725
BC-S4 (Base)	0.3332	0.00030	2.51E-06	0.4466	0.06451	1.3123	1	44443	7797
BC-S4 (Top)	0.1414	0.00048	2.84E-07	0.1192	0.00303	1.4524	4	9275	254
BC-S5 (Base)	0.2703	0.00017	6.77E-07	0.1485	0.00942	1.5132	2	11174	742
BC-S5 (Top)	0.3470	0.00026	8.64E-07	0.1476	0.01338	1.4991	1	11208	1065
BQ-S1 (Base)	0.5000	0.00190	7.87E-06	0.9326	0.03420	1.1564	96	166991	14024
BQ-S1 (Top)	0.8012	0.00244	1.25E-05	0.9255	0.00840	1.1971	416	150686	3038
CTH (Base)	0.6978	0.03117	2.90E-06	0.2463	0.01275	3.1674	12	8727	468
CTH-Top	0.5783	0.00083	1.10E-06	0.1132	0.00337	2.9067	117	4302	131
FC-S3 (Base)	1.2802	0.00080	1.19E-06	0.0552	0.00264	1.6732	17	3448	178
FC-S3 (Top)	2.1007	0.00240	1.20E-07	0.0034	0.00097	1.7060	1	224	32
FC-S5 (Base)	0.1243	0.00027	1.18E-06	0.5630	0.11169	1.3412	23	57672	14726
FC-S5 (U-4) Top	0.0945	0.00004	6.90E-07	0.4348	0.00652	1.6680	16	30653	674
IB-S1 (Base)	0.3961	0.00030	2.04E-06	0.3057	0.00948	3.2696	7	10560	341
IB-S1 (Top)	0.2734	0.00021	1.29E-06	0.2801	0.01949	3.3030	74	9542	687
KS-F1 (Top)	0.1506	0.00070	2.54E-06	1.0006	0.04434	1.0379	38	331307	94261
LT (Top)	7.3362	0.01596	1.69E-04	1.3633	0.00968	2.3975	27849	83073	834
LT (Base)	1.0084	0.00080	1.99E-05	1.1700	0.01044	1.8527	1226	98551	1346
MC-S1 (Base)	0.3239	0.00018	7.29E-06	1.3348	0.00552	1.8509	521	121474	1889
MC-S1 (BelowH)	0.3171	0.00026	7.45E-06	1.3925	0.00750	1.9095	98	119979	676
MC-S1 (AboveH)	0.2779	0.00030	7.11E-06	1.5164	0.00627	2.2820	100	104401	740
MC-S1 (Top)	0.3656	0.00034	7.53E-06	1.2206	0.00475	2.3474	134	73654	1349
MC-S2 (Base)	0.2781	0.00025	5.06E-06	1.0776	0.00959	1.5175	183	121901	1274
MC-S2 (Top)	0.2423	0.00025	4.24E-06	1.0362	0.00575	1.4759	113	120117	1349
PB (Top)	0.2664	0.00037	4.89E-06	1.0881	0.01966	1.2159	99	211674	10991
WC-S3 (Base)	5.8009	0.00277	3.99E-05	0.4078	0.00277	1.9476	1111	25071	189
WC-S3 (Top)	4.8103	0.00336	3.36E-05	0.4139	0.00468	1.9857	231	24938	312
WC-S5 (Base)	0.8956	0.00192	1.08E-05	0.7175	0.02262	1.8724	14	50457	1953
WC-S5 (Top)	1.2550	0.00127	1.20E-05	0.5646	0.00801	1.9012	336	37234	616
WC-S6 (Base)	5.3613	0.00362	3.40E-05	0.3761	0.01508	1.9291	36	23183	1019
WC-S6 (Top)	5.6133	0.00338	4.01E-05	0.4236	0.00670	1.9643	20	25899	455
WC-S7 (Base)	3.1366	0.01020	3.90E-05	0.7369	0.00440	1.8163	443	54225	412
WC-S7 (Top)	0.7034	0.00344	7.06E-06	0.5951	0.02176	1.7716	20	43135	1901

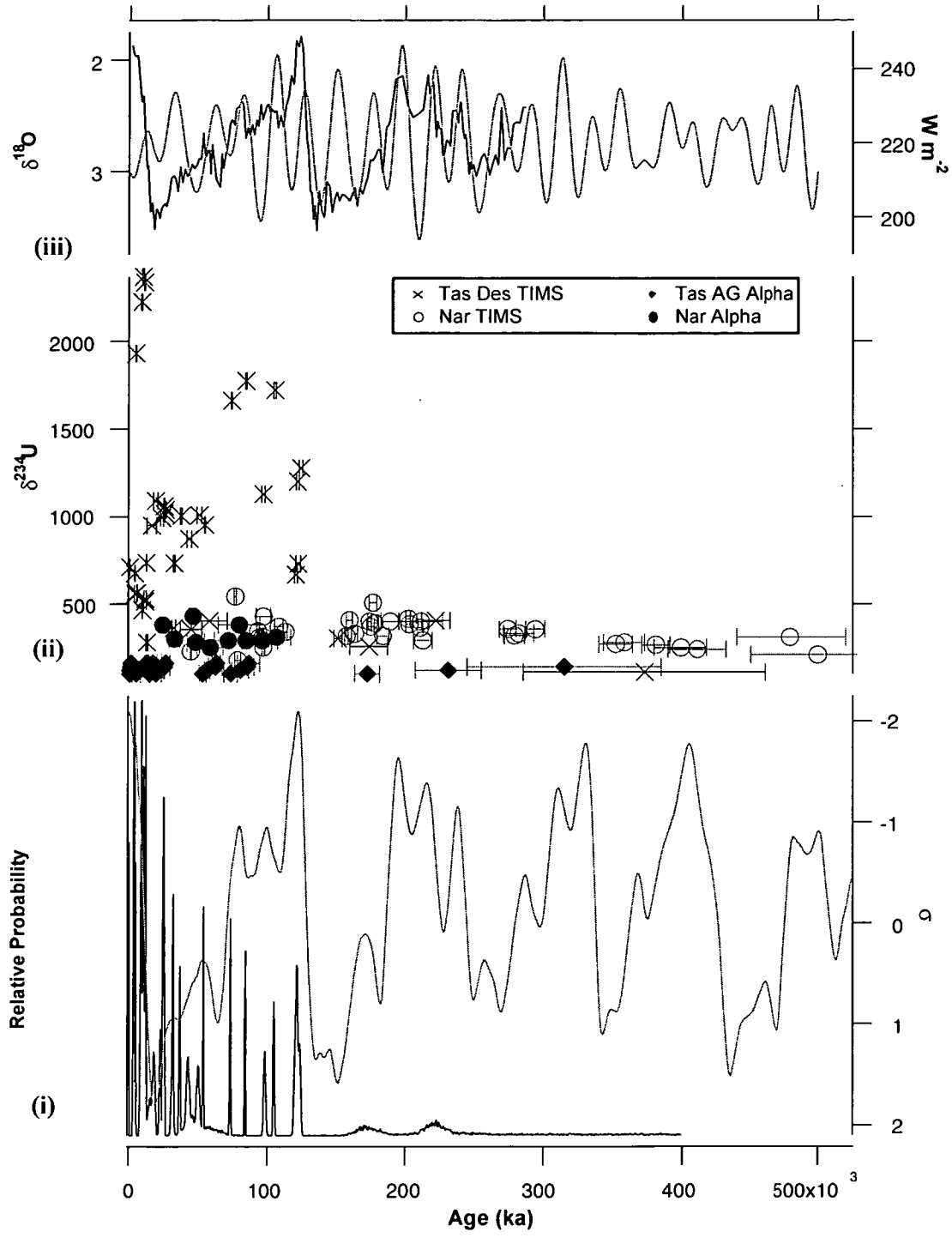

Figure 4.2(a). **(i) Left axis plots a histogram (black line) of 37 new Tasmanian speleothem ages compiled by summing individual age distributions; calculated as a by-product of the age error calculation method (Section 4.2.6.) For a more detailed description of the histogram method see Ayliffe *et al.* (1998). Also plotted for comparison purposes is the SPECMAP record (right axis, grey line). Bottom axis is common to all graphs and covers the last 500 ka.**

(ii) $\delta^{234}U(o)$ data for Tasmanian (crosses) and Naraccorte (open circles; Ayliffe *et al.*, 1998) TIMS dates together with Tasmanian (filled diamonds; Goede, 1998) and Naracoorte (filled circles; Ayliffe *et al.*, 1998) α-spectrometric age estimates. Errors shown are 2σ except for the Tasmanian α-spectrometric age estimates.

(iii) Left axis plots the RC11-120 (Martinson *et al.*, 1987) foramanifera $\delta^{18}O$ record (black line) and the right axis plots the 30°S December insolation record (grey line; Berger and Loutre, 1991).

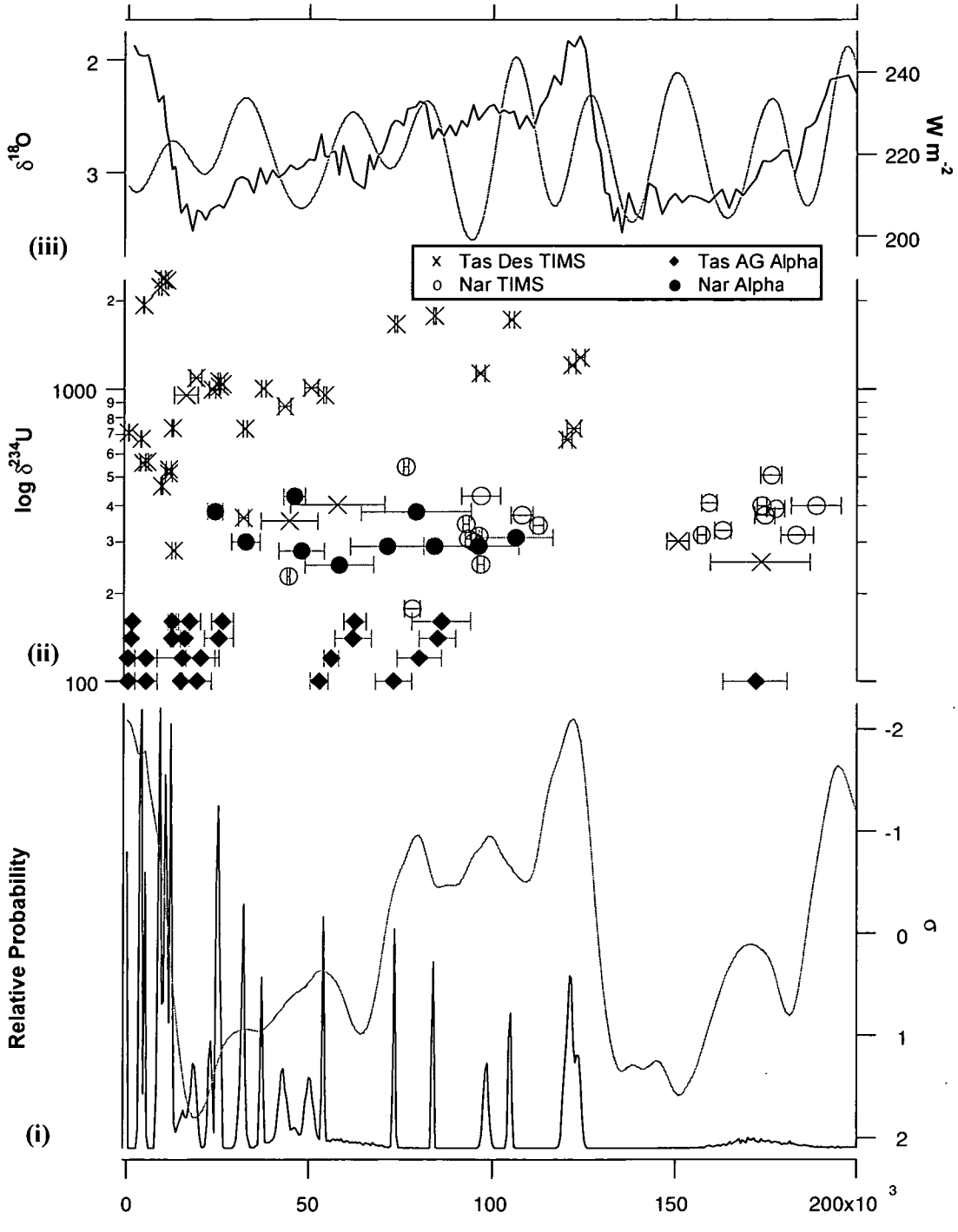

Figure 4.2(b). (i) Left axis plots a histogram (black line) of 37 new Tasmanian speleothem ages compiled by summing individual age distributions; calculated as a by-product of the age error calculation method (Section 4.2.6.) For a more detailed description of the histogram method see Ayliffe *et al.* (1998). Also plotted for comparison purposes is the SPECMAP record (right axis, grey line). Bottom axis is common to all graphs and covers the last 200 ka.
(ii) $\delta^{234}U$(o) data for Tasmanian (crosses) and Naraccorte (open circles; Ayliffe *et al.*, 1998) TIMS dates together with Tasmanian (filled diamonds; Goede, 1998) and Naracoorte (filled circles; Ayliffe *et al.*, 1998) α-spectrometric age estimates. Errors shown are 2σ except for the Tasmanian α-spectrometric age estimates.
(iii) Left axis plots the RC11-120 (Martinson *et al.*, 1987) foramanifera $\delta^{18}O$ record (black line) and the right axis plots the 30°S December insolation record (grey line; Berger and Loutre, 1991).

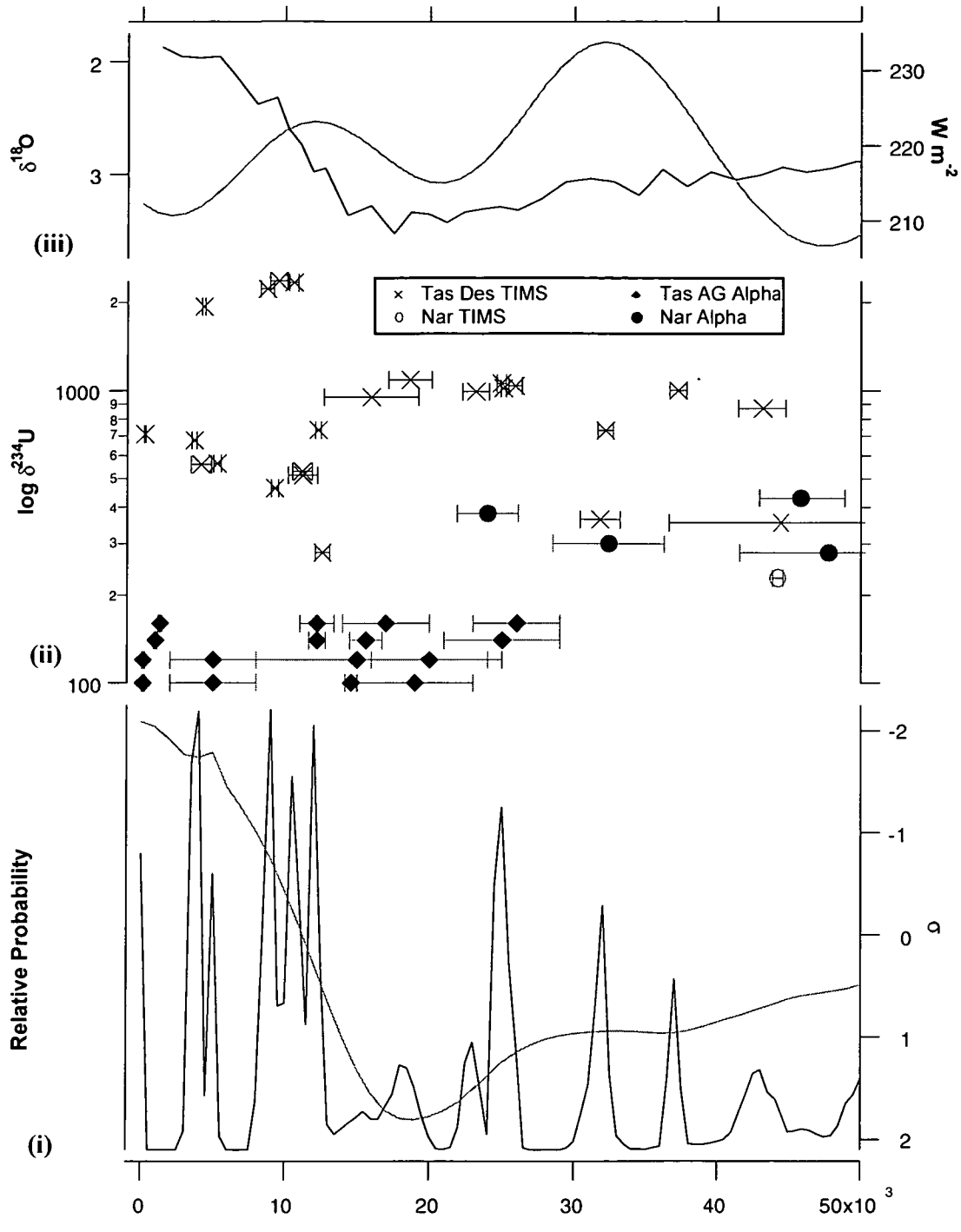

Figure 4.2(c). (i) Left axis plots a histogram (black line) of 37 new Tasmanian speleothem ages compiled by summing individual age distributions; calculated as a by-product of the age error calculation method (Section 4.2.6.) For a more detailed description of the histogram method see Ayliffe *et al.* (1998). Also plotted for comparison purposes is the SPECMAP record (right axis, grey line). Bottom axis is common to all graphs and covers the last 50 ka.
(ii) $\delta^{234}U$(o) data for Tasmanian (crosses) and Naraccorte (open circles; Ayliffe *et al.*, 1998) TIMS dates together with Tasmanian (filled diamonds; Goede, 1998) and Naracoorte (filled circles; Ayliffe *et al.*, 1998) α-spectrometric age estimates. Errors shown are 2σ except for the Tasmanian α-spectrometric age estimates.
(iii) Left axis plots the RC11-120 (Martinson *et al.*, 1987) foramanifera $\delta^{18}O$ record (black line) and the right axis plots the 30°S December insolation record (grey line; Berger and Loutre, 1991).

4.5.2. Age Frequency Histogram Discussion

While it is possible to investigate climate change at relatively high resolution using cumulative probability plots a weakness of the method is the implicit assumption that speleothems of random age are sampled. As noted by Hellstrom (1998) there is an obvious bias towards younger ages apparent in all such records, presumably reflecting progressive burial or removal of older speleothems by cave processes. For example, the alteration of the flow path of water feeding a stalagmite or some other less obvious factors are also biasing sample selection. A better method of palaeoenvironmental investigation using cumulative speleothem growth frequency may be the mass dating of the prominent hiatuses present in many speleothems, that is, dating the time of cessation and resumption of speleothem growth on a regional basis, and "stacking" the results. This method may give a clearer and less biased picture of regional palaeonvironments and global climate change. There are problems with this as cessation is often associated with detrital contamination.

Many caves in Tasmania seem to be in a cycle of excavation of detrital sediments. The alluvial and colluvial fills have been deposited at a time of greater sediment availability probably and have probably buried older speleothem material. More work is required to establish the temporal relationships between phases of clastic sedimentation and speleothem deposition. The factors discussed above may help to explain the apparent young age bias of the Tasmanian growth frequency histogram but at this stage that cannot be confirmed. It is expected that, with the gradual expansion of the number of Tasmanian and Australian speleothem dates, this deficiency will be more satisfactorily explained. However, some observations and comments will be made on the present data set.

In Tasmania, the extent and timing of the Last Glacial (LG) is fairly well determined, however the timing of previous glaciations cannot be so tightly constrained (Hannan and Colhoun, 1987). The lack of speleothem age between approximately 150 ka and 125 ka suggests that there was either an extended period of moisture deficiency and lower temperatures, inhibiting CO_2 production and halting speleothem growth, or that glacial ice covered the area. The extensive Penultimate Glacial (PG) glaciation in Tasmania was characterised by its severity with ice limits almost everywhere well beyond those of the Last Glacial Maximum (LGM). The severity of the climate during the Penultimate Glacial Maximum (PGM) is also supported by the Devils Hole record and marine records from the North Pacific and Atlantic Oceans, all of which indicate that subpolar oceanic fronts were up to 5° further south than during the LG (Crowley, 1994). Although some Tasmanian karst areas were covered by glacial ice during the PG there is no field evidence that this was the case in any of the areas where speleothems were collected for this study.

Insolation values at 45°S had two minima at 150 ka (592 W m^{-2}) and 127 ka (586 W m^{-2}) and a peak at 138 ka (642 W m^{-2}) during stage 6 (Berger and Loutre, 1991). The Chinese (Xifeng Loess, Kukla, 1987) and New Zealand (Marton event, Pillans, 1988; 1991) loess records also support an extended period of severe and arid climate during this time. It is difficult to comment on the activity of dunes in Australia during the PG as very few dates are available for this time period (Wasson, 1986) but since climatic conditions would have been similar to the

LG, it has been argued that dune activity was similar to the LG. Oxygen and strontium isotope measurements of samples from a *Porites* coral from the Huon Peninsula, Papua New Guinea indicate that a substantial cooling of approximately 6°C (± 2°C) occurred in the equatorial oceans during the PG (McCulloch *et al.*, 1999), a figure also supported by analysis of the ODP Site 769 marine core from the Sulu Sea (Linsley and Dunbar, 1994; Linsley, 1996).

In contrast an abundance of speleothem age estimates exists in the period from approximately 125 ka to present with only minor breaks in deposition suggesting less severe conditions than during the PG. No speleothem growth occurred in the LGM period, approximately 22 to 19 ka, supporting the idea that moisture availability and temperature reached their lowest values at this time, thus inhibiting speleothem growth. This period also corresponds to a peak, at 22 ka, of approximately 625 W m^{-2} in total insolation at 45°S with higher summer and lower winter solar input (Berger and Loutre, 1991). No speleothem growth has been detected throughout the whole of the LGM and PG intervals.

Periods of greater moisture availability in southeastern Australia are supported by abundant speleothem growth, particularly in the last 50 ka. However there are significant differences between the speleothem data of Ayliffe *et al.* (1998) and the Tasmanian speleothem data set. In the Naracoorte region speleothem deposition has been intermittent and appears to have been strongly influenced by available moisture (Ayliffe *et al.*, 1998). In Tasmanian caves continuous growth has occurred since the Last Interglacial (LIG) with only one exception, the LGM. This indicates that speleothem growth in the Naracoorte area is more sensitive to moisture changes than in Tasmania where it is affected more strongly by low temperatures as has been shown to be the case in north-western Europe (Baker *et al.*, 1993a).

4.5.3. Age Determination of Yarrangobilly Flowstones

Three sections of Yarrangobilly flowstone, JC-F1, JC-F2, and JC-F4, were analysed using the TIMS $^{230}Th/^{234}U$ dating technique and the results of 18 samples are given in Table 4.3. From these results, and due to the limited time-frame of the project, it was decided to concentrate the research effort on JC-F1. Minor elements were measured along the growth axis of JC-F1, JC-F2, and JC-F4 using a laser ablation ICP-MS, the results are given in Chapter 5. Stable isotope analyses were performed only on JC-F1, the results are described in Chapter 6.

4.5.3.1. Yarrangobilly Flowstone Sample JC-F1

Sample weights for TIMS $^{230}Th/^{234}U$ dating varied from 4 to 5 grams, the amount of the JC-F1, approximately 3 or 4 kg, allowed the luxury of fairly capacious samples. The dimensions of individual samples varied from 2 to 3 mm for z-axis (vertical), 10 mm for y-axis, and approximately 50 to 90 mm for x-axis. The relatively large sample sizes ensured that ample U and Th was available for analysis. This was particularly helpful when measuring ^{230}Th in the upper section of JC-F1 due to the low concentration found in young samples. The large sample sizes also compensate for the relatively low uranium concentration of JC-F1, approximately 100 nmol g^{-1}, and gives increased confidence in the age and error estimates. The age estimates from Yarrangobilly have not been included in the age frequency histogram calculations (Section 4.5.1) as the Yarrangobilly Karst is outside the main study area.

Table 4.3 **Results of Uranium-series dating of Yarrangobilly flowstone samples JC-F1aa, JC-F2, and JC-F4, error estimates are reported as ± 2σ. The dashed lines indicate the position of hiatuses, the dotted lines are inferred hiatuses.**

Sample Name	Distance From Base (mm)	^{238}U (nm/g)	± ^{238}U (nm/g)	^{230}Th (nm/g)	$\frac{^{230}Th}{^{238}U}$ (Act)	± $\frac{^{230}Th}{^{238}U}$ (Act)	$\frac{^{234}Th}{^{238}U}$ (Act)	$\frac{^{230}Th}{^{232}Th}$ (Act)	Age (years)	± 2_ error	Growth Rate (mm ka^{-1})
JC-F1(1)	267	0.1903	0.00015	5.82E-07	0.1812	0.00290	1.8411	57	11.04	0.23	
JC-F1(2)	260	0.4171	0.00025	1.90E-06	0.2699	0.00205	1.7333	68	17.91	0.17	5.27
JC-F1(3)	235	0.5497	0.00050	3.05E-06	0.3289	0.00202	1.6996	99	22.65	0.16	11.07
JC-F1(4)	195	0.5989	0.00058	4.04E-06	0.3999	0.00117	1.8050	228	26.27	0.09	15.08
JC-F1(5)	180	0.5403	0.00035	3.72E-06	0.4077	0.00229	1.7800	283	27.26	0.17	9.15
JC-F1(6)	145	0.6545	0.00034	4.93E-06	0.4466	0.00282	1.7361	684	31.09	0.21	2.88
JC-F1(7)	100	1.1875	0.00162	1.44E-05	0.7200	0.00214	1.9656	111	46.74	0.14	
JC-F1(8)	93	0.4856	0.00025	7.46E-06	0.9100	0.00230	1.6225	1042	82.02	0.23	1.23
JC-F1(9)	73	0.2715	0.00019	5.10E-06	1.1130	0.00789	1.7444	459	98.28	0.73	0.53
JC-F1(10)	26	0.1071	0.00010	2.41E-06	1.3352	0.01701	1.2937	7	187.54	1.91	
JC-F1(11)	18	0.1265	0.00014	3.80E-06	1.7808	0.01751	1.9464	22	338.61	4.48	0.91
JC-F1(12)	4	0.0923	0.00015	2.04E-06	1.3128	0.01036	1.2728	44	354.54	3.29	
JC-F2(1)	99	0.0377	0.00017	1.93E-07	0.3041	0.08819	1.7703	6	20.22	6.23	0.40
JC-F2(5)	88	0.1086	0.00008	1.20E-06	0.6536	0.01646	1.7860	2	47.81	1.50	1.79
JC-F2(2)	37	0.2256	0.00017	3.66E-06	0.9624	0.01876	1.8301	3	75.96	2.04	
JC-F2(3)	34	0.0578	0.00013	1.13E-06	1.1634	0.01538	1.8671	97	96.52	2.00	0.28
JC-F2(4)	4	0.1302	0.00016	3.32E-06	1.5112	0.21267	1.6347	11	203.19	53.62	
JC-F4(1)	49	0.1267	0.00050	1.28E-06	0.5986	0.00924	1.9655	19	38.30	1.49	0.85
JC-F4(2)	1.5	0.3913	0.00050	6.61E-06	1.0007	0.00568	1.6426	52	94.56	0.98	

Detrital contamination was monitored with the $^{230}Th/^{232}Th$ activity ratio ($^{230}Th/^{232}Th_{Act}$) and a figure greater than 20 (Schwarcz, 1980) indicates that no correction of the age is necessary, although a figure greater than 100 is considered a better threshold for TIMS age estimates (Li *et al.*, 1989). Of the twelve JC-F1aa dates eleven $^{230}Th/^{232}Th_{Act}$ values were above the minimum threshold of 20, with 5 greater than 100, with only one value below 20. This value corresponds to the sample immediately above hiatus H1 and probably indicates the presence of detrital material, clay and dust, accumulated on the surface as the hiatus spanned approximately 150,000 years. Roberts (1998) has observed similar results for samples that were adjacent to hiatuses.

The results of twelve TIMS U-series age estimates for flowstone sample JC-F1aa are presented in Table 4.3. The flowstone started growing at approximately 354.6 ± 3.3 ka and ceased deposition sometime in the Holocene, however, the growth was discontinuous as indicated by three obvious hiatuses. These hiatuses occurred between 338.6 ± 4.5 and 187.5 ± 1.9 ka (H1), between 82.0 ± 0.2 and 46.7 ± 0.1 ka (H2), and between 17.9 ± 0.2 and 11.0 ± 0.2 ka (H3). The top date of the flowstone represents an averaged age as it was very difficult to extract enough material for two separate samples. This break in deposition corresponds to a period sometime after the LGM, not contemporaneous with it as might have been expected. A distance/age model is presented in Figure 4.3.

Growth phases and hiatuses occur at or very close to MIS boundaries. The first section of growth started approximately mid-way through MIS 10 and ceased at or close to the boundary between MIS 10 and MIS 9. The first hiatus, H1, extended over several isotope stages including MIS 9, MIS 8, and MIS 7 before growth restarted at the boundary of MIS 7 and MIS 6, continuing until late MIS 5. The second hiatus, H2, spanned MIS 4 before deposition recommenced early MIS 3, continuing into the middle of MIS 2, ceasing at or close to the LGM. The duration of hiatus, H3, the growth period following this, and the final cessation of calcite deposition is unknown, further analyses are required to resolve the age range of the top section.

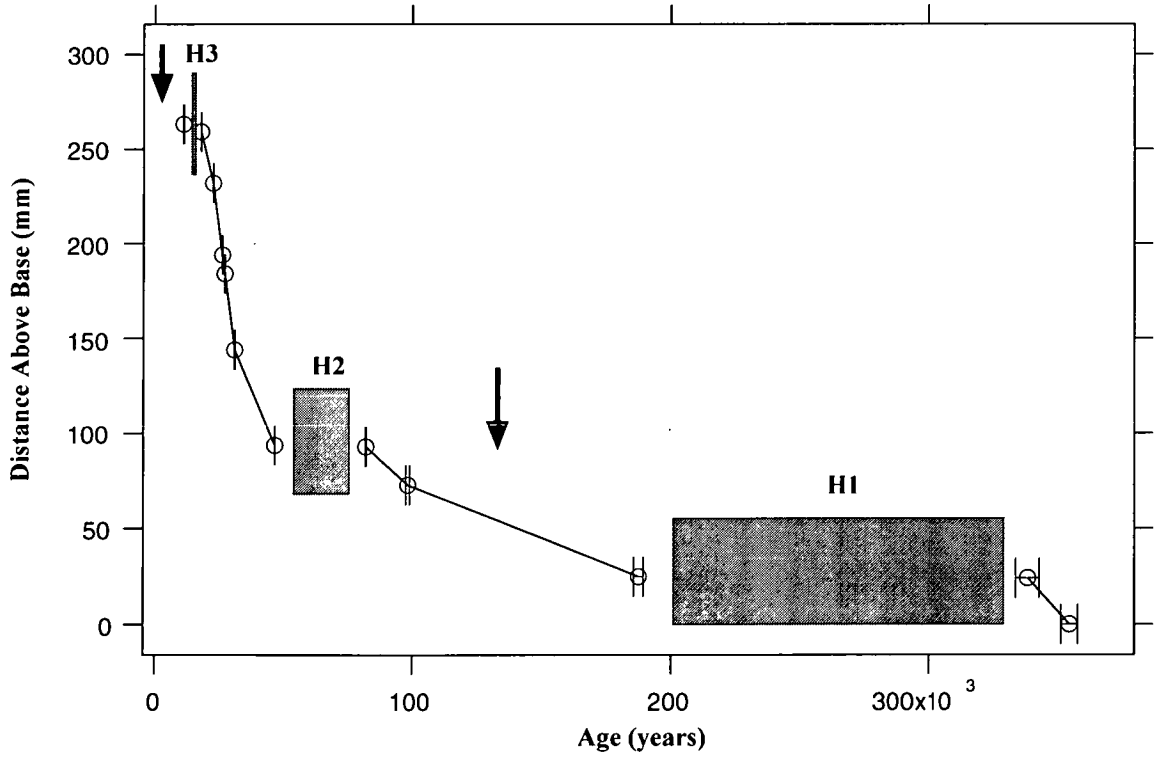

Figure 4.3. Distance-Age model for Yarrangobilly flowstone sample, JC-F1aa, based on TIMS $^{230}Th/^{234}U$ dating, error bars are 2σ. The location of hiatuses are indicated by grey areas, inferred hiatuses by black arrows.

JC-F1aa growth rates varied considerably ranging from a minimum of 0.53 mm ka^{-1} to a maximum of 15.10 mm ka^{-1}, assuming that the calcite deposition rate was constant between samples, the average extension rate is 5.77 mm ka^{-1}. The fastest growth occurred in the upper section between 31.1 ± 0.2 and 22.6 ± 0.2 ka, and the slowest rate of growth between 187.5 ± 1.9 and 98.3 ± 0.7 ka. This extended period of slow growth may be due to one or more indistinct hiatuses that may have escaped detection because of the spacing of dated samples. The calcite fabric changes with the growth rate. In the section below H2 the calcite is dense, columnar or palisade (Kendall and Broughton, 1978), macrocrystalline calcite. Above H2 the structure of the calcite consists of approximately 1 mm diameter, needle-like columns or fibrous, acicular calcite (Kendall and Broughton, 1978). Above H3 the calcite is more like that found below H2. Fluid inclusions are abundant throughout the flowstone but distinct layers of maximum density do occur.

Gonzalez *et al.* (1992) have suggested that calcite crystal fabric and habit may give some clues on the degree of supersaturation of the parent solution as well as providing constraints on the nature of the water flow and whether the transport of reactants is fast or slow. In a detailed investigation of the petrography of speleothem calcite, Ayalon *et al.* (1999) observed that large, well-developed crystals with a preferred orientation occurred between 60 and 17 ka, a period of cooler and drier conditions in the region. They suggested that the large crystals were due to slow and constant water flow over the speleothem surface. After 17 ka, warmer and wetter conditions caused the speleothem calcite crystals to become small and anhedral. The dramatic decrease in crystal size is interpreted as reflecting a significant increase in the water flow over the spleothem surface.

4.5.3.2. Yarrangobilly Flowstone Sample JC-F2

This section of flowstone is approximately 100 mm thick and started growing at approximately 203.2 ± 53.6 ka and deposition ceased at around 20.2 ± 6.2 ka (Table 4.3). A distance/age model is presented in Figure 4.4. The basal date requires a second measurement as some problems have been encountered during analysis, specifically beam instability during Th measurement, a factor that has contributed to the large error associated with the top date. Another contributing factor to the large error is the very low ^{230}Th content of the basal sample which may have been due to detrital contamination, mainly clays, affecting the ion exchange resin during the chemical extraction procedure. One date, taken at approximately 67 mm from the base, had to be rejected outright as problems were encountered with both the uranium and thorium beam stability and the age estimate obtained was also not in stratigraphic order.

Calcite deposition was not continuous as there are two obvious hiatuses at 35 mm, H1, occurring between 96.5 ± 2.0 and 76.0 ± 2.0 ka, and at 82 mm, H2, however this hiatus was not resolved temporally. The rate of growth of F2 varied from 0.28 mm ka^{-1} for the section below H1 and at 1.79 and 0.40 mm ka^{-1} for the section above H1 assuming that there was no significant break in deposition at H2. The relatively slow growth rate is also reflected in the nature of the calcite as it is fairly uniform, except for the colour, and consists of dense, columnar macrocrystalline calcite. While detrital contamination was significant in 4 samples, as

indicated by the $^{230}Th/^{232}Th$ ratios being less than 20 (Schwarcz, 1980) and 100 (Li *et al.*, 1989), no attempt has been made to correct the age estimates.

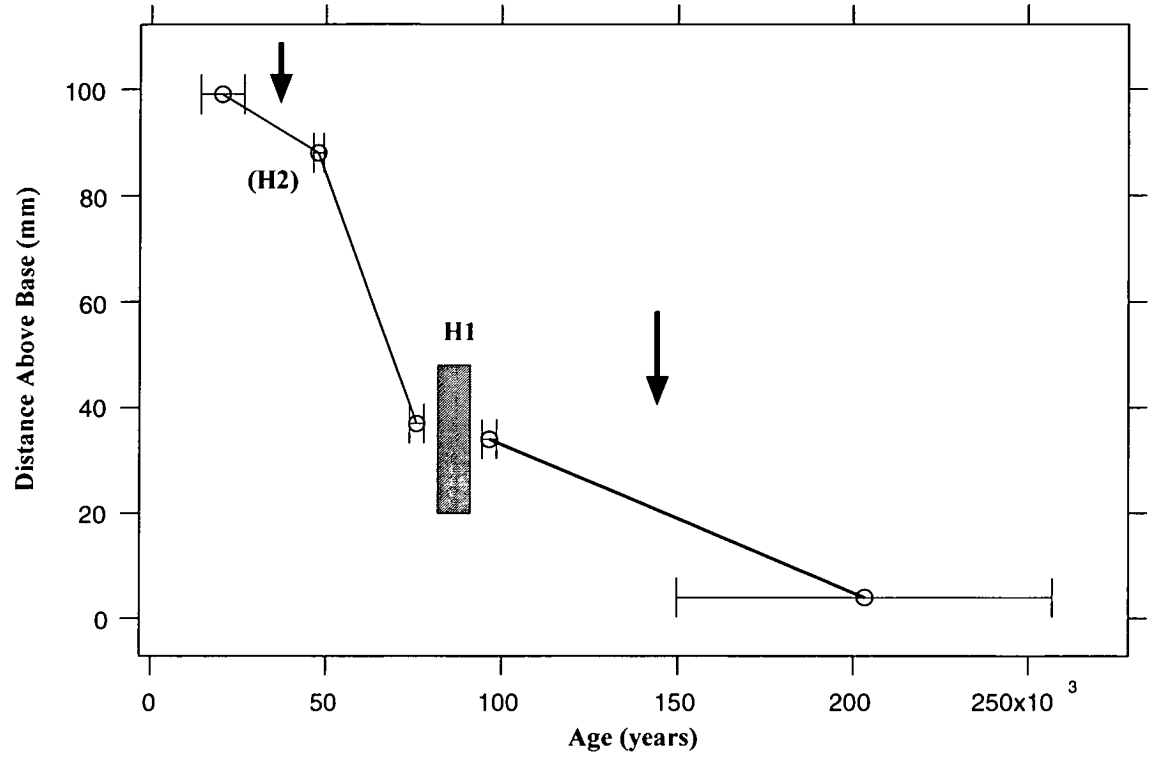

Figure 4.4. Distance/Age model for Yarrangobilly flowstone sample, JC-F2, based on TIMS $^{230}Th/^{234}U$ dating, error bars are 2σ. The location of hiatuses are indicated by grey areas, inferred hiatuses by black arrows.

4.5.3.3. Yarrangobilly Flowstone Sample JC-F4

This section of flowstone is approximately 50 mm thick and started growing at approximately 94.6 ± 1.0 ka and ceased deposition at around 38.3 ± 1.5 ka (Table 4.3). Calcite deposition was apparently continuous although there appears to be a hiatus at the very top of the sample and another analysis immediately below it is required to confirm its existence and duration. The flowstone grew at approximately 0.85 mm ka^{-1} assuming constant growth and no breaks in calcite deposition. The flowstone consisted of columnar, macrocrystalline calcite, although a characteristic of this sample was the tendency for it to come apart very easily suggesting little inter-crystalline strength, *ie* acicular (Kendall and Broughton, 1978), unlike the other two Yarrangobilly samples.

It has been assumed that no significant detrital contamination occurred with this sample and no corrections have been attempted. Although the $^{230}Th/^{232}Th$ ratio for the top sample was 19, a figure slightly below the figure of 20 recommended by Schwarz (1980) and well below 100 (Li *et al.*, 1989), this may have been due to an apparent hiatus but further analyses are required

to confirm this. The basal date had a $^{230}Th/^{232}Th$ ratio of 52 and is considered acceptable although not ideal.

4.5.4. Patterns of Deposition of Yarrangobilly Flowstone Discussion

The growth period of a speleothem and changes in the rate of calcite deposition both have the potential to provide very important palaeoenvironmental signals (Baker *et al.*, 1998b; Hellstrom, 1998). However, the growth of speleothems is controlled by a complex suite of factors including:

(1) the concentration of Ca^{2+} in the seepage water;
(2) the rate at which the CO_2 outgasses from solution;
(3) water supply and film thickness;
(4) transport of reacting species to and away from the calcite surface; and
(5) temperature and soil processes.

Various attempts have been made to model the rate of calcite precipitation on the growth surface of a speleothem. Dreybrodt (1981) has proposed a numerical model of the rate of speleothem growth based on the calcium ion concentration of the seepage water and the rate at which CO_2 outgasses from the water layer into the cave atmosphere.

Recent observations of the growth rates of speleothems in the field by Baker *et al.* (1998b) show the calcium ion concentration to be the dominant effect. There are a number of factors controlling the concentration of Ca^{2+} in solution, including the soil temperature, soil moisture, soil depth, climate seasonality, vegetation, bedrock characteristics such as purity, porosity, and permeability, and the equilibrium state of the seepage water (Baker *et al.*, 1998b). These factors complicate attempts to interpret palaeoenvironmental conditions from speleothem growth rate variations. However, some of these conditions can be elucidated from other palaeoenvironmental proxy records such as pollen abundance in sediment cores from both marine and lake settings or stable isotope measurements of various calcareous marine microfossils in ocean sediment cores.

The growth phases and hiatuses of the Yarrangobilly flowstone samples provide important additional evidence of Late Quaternary palaeoenvironmental history in southern NSW with strict temporal control. It appears that present day environmental conditions are not highly conducive to speleothem growth, although further investigations are needed to confirm this. While some speleothem deposition is occurring in sections of the tourist caves, as evidenced by calcite growth on chicken wire, a reconnaissance of "wild" caves in the Yarrangobilly Karst is required in order to gauge the full extent of modern calcite deposition, particularly of flowstones. Observations so far indicate that calcite precipitation is occurring on a limited scale in the Yarrangobilly Caves at present.

The three Yarrangobilly flowstones have some overlapping growth periods, however, JC-F2 requires more dates to confirm the full extent. None of the hiatuses correspond temporally suggesting that local factors may be affecting the flowstone's water supply thereby governing its growth. The use of age estimates as a climate signal requires a greater number of measurements, but a regional or global palaeoenvironmental signal may still be present in a

geochemical form *ie* variations in stable isotope ratios and minor element concentrations. Further sampling is required to investigate the timing of hiatuses, by stacking their ages, as this would help differentiate the degree to which local and global factors are determining flowstone growth. As Hellstrom (1998) has pointed out, flowstones are often fed by more than one source of seepage water and are therefore more likely to grow for extended periods. On the other hand stalagmites, while growing for shorter periods of time, may provide useful "windows" to check against extended palaeoenvironmental records from flowstones.

A tentative palaeoenvironmental interpretation is presented for the Yarrangobilly flowstones, based on the $^{230}Th/^{234}U$ dates and the estimated growth rates. While some of the shortcomings of using flowstones have been mentioned previously, the author fully acknowledges the limitations of basing an interpretation on such a restricted data set. However, some important general observations can be made on an area where very little palaeoenvironmental information currently exists in the hope that this will stimulate discussion and further research.

It is hypothesised that surface water availability plays a key role in the growth of speleothems at Yarrangobilly and that this has varied considerably in the past as evidenced by hiatuses and changes in the rate of growth. Periods of speleothem growth seem to occur during the cooler phases of glacial-interglacial cycles, although several more $^{230}Th/^{234}U$ dates are required on JC-F1 to investigate the relationship of growth phases to the Last Interglacial. A cessation of deposition would suggest that water supply is significantly reduced during the warmer phases of glacial-interglacial cycles due possibly to a change in atmospheric circulation.

Supporting evidence, although lacking the strict temporal control possible with speleothems, comes from several Australian palaeoenvironmental records such as sequences of aeolian, fluvial, and lacustrine sediments dated by a variety of methods. These sequences provide evidence of wetter or drier conditions over many regions such as the Lake Ayre Basin, desert dunefields, and the large river systems that drain the Australian highlands. The growth record of JC-F1 suggests that wetter conditions were experienced by the Yarrangobilly area during MIS 6 and 5, and 3 through to the LGM. For other areas the evidence suggests wetter conditions during MIS 4 and a drier conditions in MIS 3 (Wasson, 1986; Nanson *et al.*,1992).

4.5.5. YB-1 Internal Standard

The upper 150 mm of white/pale coloured, macrocrystalline calcite was cut from a section of flowstone similar to the YBJC-F1AA sample, previously collected from Yarrangobilly Caves by Dr John Stone. John Hellstrom initiated the idea to make an internal standard for U-series dating using the following method. The white horizon, thought to be around 25 ka in age, was cut into 2 kg of 30 mm cubes using a diamond-tipped rock saw and cleaned in an ultrasonic bath with alternating solutions of acetone and deionised water.

The blocks were broken into smaller fragments, randomised, and crushed in a tungsten swing mill. The resulting powder was sieved through a 30 micron mesh, producing approximately 1.5 kg of fine powder for use as an internal speleothem standard, YB-1, for TIMS $^{230}Th/^{234}U$ dating (Hellstrom, 1998). The standard was run as a check on the performance of the machine and

user and, like the sample blank, provided a useful benchmark for gauging the quality of each batch. The YB-1 standard results are shown in Table 4.4.

As has already been observed by Hellstrom (1998) the internal speleothem standard, YB-1, has proved a difficult one in which to measure the U and Th isotopes successfully. While the $^{234}U/^{238}U$ ratio of the standard is fairly well established, the age of the standard is not as well known but an average age of 30.6 ± 1.1 ka (n = 8) has been determined. Repeat measurements of the standard indicate that speleothem dates from the RSES laboratory have an external precision fully consistent with their reported errors, despite a change of $^{233}U/^{229}Th$ spike in the chemical procedure and several replacement secondary electron multipliers on the Finnigan MAT 261 mass spectrometer.

Continued measurements of the standard will improve the statistics of the sample but a better check would be to provide several samples to another laboratory to measure, this has been initiated but so far no results have become available.

Table 4.4. Results of TIMS $^{234}U/^{230}Th$ analysis of YB-1 internal standard at RSES, ANU. The average age of the sample is 30.6 ± 1.1 ka where n = 8. (* = U-1 spike, † = U-2 spike, § = values used in average calculation)

Sample Name	^{238}U (nmol g^{-1})	± error	^{230}Th (nmol g^{-1})	$^{230}Th/^{238}U$ act	± error	$^{234}U/^{238}U$ act	$^{230}Th/^{232}Th$ act	Age (years)	± error (years)
JD1*§	0.4708	0.00083	3.55E-06	0.447	0.018	1.756	286	30294	1375
JD2†§	0.4690	0.00097	3.55E-06	0.449	0.018	1.759	286	31371	1408
JD3†§	0.4711	0.00067	3.55E-06	0.447	0.018	1.758	286	31245	1418
JD4†§	0.6055	0.00184	4.48E-06	0.438	0.008	1.751	445	30665	638
JD#5†§	0.6366	0.00125	4.61E-06	0.429	0.006	1.753	237	29920	481
JD#6†	0.8010	0.00286	4.61E-06	0.341	0.005	1.760	236	23074	391
JD#7†	0.8007	0.00174	4.61E-06	0.341	0.005	1.756	237	23134	374
JD#8†§	0.6372	0.00059	4.48E-06	0.416	0.018	1.751	357	28959	1370
JD#9†	0.6189	0.00121	4.03E-06	0.385	0.071	1.756	290	26487	5290
JD#10†§	0.6164	0.00185	4.75E-06	0.449	0.010	1.757	535	31450	825
JD#11†§	0.6124	0.00053	4.49E-06	0.428	0.013	1.751	406	29870	984

4.5.6. Growth Rates of Soda Straw Stalactites

4.5.6.1. Assessment of ^{210}Pb Levels in Soda-straw Stalactites

Preliminary work involved assessing the concentrations of ^{210}Pb and ^{226}Ra in fragments of soda-straw stalactites from several caves, the results are given in Table 4.5. In all of the samples measured from Risbys Basin the concentrations of ^{226}Ra were less than 0.1 dpm g^{-1} indicating that most of ^{210}Pb in the calcite must be derived from the water feeding the speleothem and that there is a low risk of contamination of ^{210}Pb by ^{226}Ra from the cave atmosphere. The concentrations of ^{210}Pb in soda-straw stalactites vary greatly with concentrations in Frankcombe Cave up to 100 times higher than those of other sites, a section of FC-SS1 has a level of 2,028.92 dpm g^{-1} compared to an average figure of approximately 20 dpm g^{-1} for Risbys Basin. The contrasting levels of ^{210}Pb are probably related to the amount of ^{222}Rn in the water feeding the speleothems as groundwaters may contain very high concentrations of ^{222}Rn (Baskaran and Iliffe, 1993; Tanahara *et al.*, 1997).

Table 4.5. ^{210}Pb analyses of soda-straw stalactite fragments from several Tasmanian caves. Measurements by Gary Hancock (CSIRO).

Sample	^{210}Pb Activity (dpm g^{-1})	Error (dpm g^{-1})
BDTH-Hollow	51.21	1.21
BDTH-SS1 Average for all segments	221.71	26.00
BDTH-SS5 Average for all segments	194.04	34.22
FC-SS1 Average for all segments	823.05	20.41
RB-Filled	12.41	0.78
RB-Hollow	16.69	1.33
RB-SS1 Average for all segments	31.54	1.17
Average =	**192.95**	
Standard Deviation =	**290.88**	

4.5.6.2. Excess ^{210}Pb Dating Results

Four soda-straw stalactites, BDTH-SS1, BDTH-SS5, FC-SS1, and RB-SS1, were broken/cut into segments varying in length from 20 to 40 mm and measurements taken of the ^{210}Pb concentration for each segment and the results of the analyses are given in Table 4.6. In theory the tip section should have the largest ^{210}Pb activity and decrease as the distance from the tip increases. In most of the samples analysed in this study the ^{210}Pb activity did not show a simple age related decline. This suggests that contamination, both from atmospheric ^{210}Pb adsorbing onto the outer surface of the soda-straw stalacite and also from ^{210}Pb from percolation water plating out on the inner surface of the soda-straw stalacite, may have influenced the

results. For example, BDTH-SS5 does not have the simple age related decline and instead has mixed ^{210}Pb activities along its length which suggests that surface contamination may have influenced the measurements. Results of the three bottom segments from the sample RB-SS1 are diametrically opposite to the age decline model and no reason can be given for this occurrence, therefore no ages have been calculated for this particular sample.

Comparisons between ^{210}Pb activity measurements of the matrix and the inner and outer surfaces of two soda-straw stalactites by Tanahara *et al.* (1998) observed that the activity in the inner margin is low in comparison to the innner and outer surfaces suggesting that ^{210}Pb intake is confined to the growing tip. Measurements of the ^{210}Pb activity of the outer surface of the soda-straw stalactites suggests that adsorption of ^{210}Pb onto the outer surface contributes a significant amount of ^{210}Pb therefore acid cleaning of the inner and outer surfaces is required. Since the Tasmanian samples were not pretreated in this way there is an unknown amount of atmospheric ^{210}Pb contributed from both the inner and outer surfaces and this may be the reason for the indifferent results.

In spite of this problem the ages and growth rates of the samples were calculated using a technique normally applied to calculating age models for sediment cores *ie* sedimentation rate using the Constant Initial Concentration (CIC) model (Gale *et al.*, 1995). This method uses the y-intercept (m) and slope (b) data of log/linear regression lines (Table 4.7) in the following equation:

Equation 4.4.

$$y = \frac{\left[m \times \ln\left(\frac{\exp\left(-b/m\right)}{2} \right) + b \right]}{22.26}$$

The result is a sedimentation rate which can be used to calculate the age of a segment, however, the results are maximum estimates for growth rate and minimum ones for age. The average calculated growth rates for BDTH-SS1 and BDTH-SS5 are 4.17 and 0.91 mm year^{-1}, respectively.

4.5.6.3. AMS Radiocarbon Dating Results

Four soda-straw stalactites, BDTH-SS1, BDTH-SS5, RB-SS4 and RB-SS5, had samples of approximately 50 μg taken from the growing tip, base, and from various places along their lengths. The ^{14}C content of the calcite was analysed by AMS and the results are given in Table 4.8. Ages are corrected for the apparent age effect (or DCP) by subtracting the y-intercept, calculated from linear regression (Table 4.9), from the uncorrected ages, the results have not been calibrated to calendar years. The slope gives the distance from the tip of the "zero age". This methodology follows the example of Williams *et al.* (1999) using the same assumptions *ie* that the apparent age effect has been constant for the entire depositional period of the speleothem. All of the radiocarbon dates of the samples analysed are in stratigraphic order with no age inversions (Table 4.8). The calculated growth rates for the BDTH soda-straw stalactites vary between approximately 0.02 to 1.1 mm year^{-1}. No ages or growth rates were calculated for the Risby Basin Cave samples as an inadequate number of samples were analysed.

Table 4.6. **^{210}Pb analyses of vertical segments of four soda-straw stalactites from three Tasmanian caves, Burning Down The House Cave (BDTH) and Frankcombe Cave (FC), Florentine Valley, and Risbys Basin Cave (RB), Risbys Basin, Tasmania. Average growth rates for BDTH-SS1 and BDTH-SS5 are 4.2 mm year^{-1} and 0.91 mm year^{-1}, respectively. Measurements done at ANSTO (Dr Hendrik Heijnis) and CSIRO (Gary Hancock). The age (Age# column) corresponds to the middle of the segment and the following column (Segment Age Range) gives the age of the base and top of the segment, respectively.**

Sample	Mid-Segment Distance from Base (mm)	^{210}Pb Activity @ 1-1-98 (dpm g^{-1})	Error (dpm g^{-1})	Age# (years)	Segment Age Range (years)
BDTH-SS1 (0-33)	16.5 base	82.90	6.60	63.5	57.2 - 69.7
BDTH-SS1 (33-53)	43.0	79.20	14.20	54.7	52.2 - 57.2
BDTH-SS1 (53-74)	63.5	161.00	13.50	48.9	46.2 - 52.2
BDTH-SS1 (74-94)	84.0	158.10	32.20	43.7	41.3 - 46.2
BDTH-SS1 (94-116)	105.0	192.70	21.60	38.9	36.5 - 41.3
BDTH-SS1 (116-136)	126.0	187.30	35.40	34.6	32.7 - 36.5
BDTH-SS1 (136-152)	144.0	293.30	32.70	30.3	27.9 - 32.7
BDTH-SS1 (152-172)	162.0	210.90	25.50	25.2	22.6 - 27.9
BDTH-SS1 (172-192)	182.0	193.20	29.20	20.2	17.8 - 22.6
BDTH-SS1 (192-217)	204.5	302.90	23.60	15.3	12.7 - 17.8
BDTH-SS1 (217-238)	227.5	402.50	51.20	10.3	7.9 - 12.7
BDTH-SS1 (238-290)	264.0 tip	396.50	26.30	4.0	0.0 - 7.9
BDTH-SS5 (0-20)	10.0 base	153.20	22.20	108.2	96.2 -120.3
BDTH-SS5 (20-44)	32.0	237.00	42.10	84.2	72.2 - 96.2
BDTH-SS5 (44-66)	55.0	199.20	35.20	60.1	48.1 - 72.2
BDTH-SS5 (66-88)	77.0	247.10	43.00	35.0	21.9 - 48.1
BDTH-SS5 (88-110)	99.0 tip	113.70	28.60	10.9	0.0 - 21.9
FC-SS1 (C1) thin	226.1 base	322.29	7.23	–	–
FC-SS1 (C2) thick	226.1	178.92	2.71	103.12	n/c
FC-SS1 (B)	320.5	2028.92	56.02	68.74	n/c
FC-SS1 (A)	528.5 tip	762.05	15.67	5.84	n/c
RB-SS1 (41-80)	60.0 base	42.41	1.57	n/c	n/c
RB-SS1 (121-160)	140.0	48.92	1.87	n/c	n/c
RB-SS1 (201-240)	220.0	62.77	2.53	n/c	n/c
RB-SS1 (281-320)	300.0	36.71	1.26	n/c	n/c
RB-SS1 (361-400)	380.0	35.30	1.26	n/c	n/c
RB-SS1 (441-480)	460.0	29.82	1.08	n/c	n/c
RB-SS1 (521-560)	540.0	24.76	0.90	n/c	n/c
RB-SS1 (601-640)	620.0	22.53	0.66	n/c	n/c
RB-SS1 (681-720)	700.0	17.77	0.78	n/c	n/c
RB-SS1 (761-800)	780.0	24.04	0.96	n/c	n/c
RB-SS1 (841-880)	860.0	24.22	0.96	n/c	n/c
RB-SS1 (921-960)	940.0	22.65	0.66	n/c	n/c
RB-SS1 (1001-1040)	1020.0 tip	18.07	0.72	n/c	n/c

Table 4.7. **Equations for logarithmic regression lines through ^{210}Pb activity measurements of segments taken from the longitudinal axis of three Tasmanian soda-straw stalactites, BDTH-SS1, BDTH-SS5, and RB-SS1. Sub-sampled data are made up of those measurements closest to the tip section. Column "y" is calculated using equation Equation 4.4.**

Sample	Regression Equation	R^2	n	y (mm year^{-1})
BDTH-SS1	y = 133.6 * ln(x) – 570.98	0.8408	12	4.41
sub-sample	y = 101.11 * ln(x) – 375.61	0.4981	6	3.15
BDTH-SS5	y = -29.372 * ln(x) + 205.95	0.0586	5	0.91
sub-sample	y = -104.96 * ln(x) –517.49	0.4362	5	3.27
RB-SS1	y = -702.29 * ln(x) - 1832.8	0.7573	13	21.37
sub-sample	y = 237.8 * ln(x) – 40.991	0.1944	5	7.18

Table 4.8. **AMS Radiocarbon results of several soda-straw stalactites from two Tasmanian caves. Ages are corrected for the apparent age effect by subtracting the y-intercept, calculated from linear regression (Table 4.9) and the distance from the tip is the slope of the regression line. Corrected ages have not been calibrated to calendar years.**

Sample	Distance from Tip (mm)	Percent Modern Carbon	+/- 1σ	Uncorrected Age [BP] (years)	+/- 1σ	Corrected Age [BP] (years)	Growth Rate (mm year^{-1})
BDTH-SS1 (0) base	290	73.55	0.83	2470.0	90	937.5	1.09
BDTH-SS1 (74)	192	74.33	0.71	2380.0	80	847.5	0.27
BDTH-SS1 (136)	136	76.36	0.61	2170.0	70	637.5	0.12
BDTH-SS1 (192)	74	81.23	0.81	1670.0	80	137.5	0.51
"Zero age"	4	-	-	1532.5	-	0	0.02
BDTH-SS1 (290) tip	0	82.89	1.17	1510.0	120	160.0	
BDTH-SS5 (0) base	110	69.05	0.61	2980.0	80	1033.7	0.15
BDTH-SS5 (66)	66	71.51	0.94	2690.0	110	743.7	0.08
"Zero age"	10	-	-	1946.3	-	0	0.27
BDTH-SS5 (110) tip	0	78.85	0.41	1910.0	50	36.3	
RB-SS4 (Base)	270	67.56	0.43	3150.0	60	2820.0	nc
RB-SS4 (Tip)	0	96.03	1.05	330.0	90	0	
RB-SS5 (Base)	290	64.36	0.76	3540.0	100	3050.0	nc
RB-SS5 (Tip)	0	94.04	0.72	490.0	65	0	

Table 4.9. Regression equations of AMS Radiocarbon results (Table 4.8) of several soda-straw stalactites from two Tasmanian caves.

Sample	Equation	R^2	n
BDTH-SS1	y = 3.667x + 1532.5	0.8992	5
BDTH-SS3	y = 9.982x + 1946.3	0.9795	3
RB-SS4	y = 10.444x + 330	-	2
RB-SS5	y = 10.517x + 490	-	2

4.5.7. Excess ^{210}Pb Dating of Soda-straw Stalactites Discussion

As noted previously none of the segments of soda-straw stalactites analysed in this study were pretreated in any way. In hindsight, and following the example of Tanahara *et al.* (1998), a pre-treatment step is necessary in order to reduce contamination from atmospheric plating out of radon on the exterior surface and plating out of radon from the seepage water onto the inside surface. Tanahara (pers. comm.) states that the pretreatment step is important as the concentrations of ^{210}Pb on the exterior and interior surfaces are much higher than the ^{210}Pb levels in the soda-straw stalactites inner margin, only this latter ^{210}Pb will reflect the age of the bulk of the sample.

The error that may have been introduced by the lack of pretreatment of samples in this study will be treated as a systematic one by assuming it to be constant for all samples. This assumption may not be valid since the distribution of radon in the cave may vary in space and time. There is some support for the assumption from measurements made by Tanahara *et al.* (1998) of the ^{210}Pb activities of rinsing solutions of the inner and outer surfaces of two soda-straw stalactites.

This study has highlighted the need for careful sample selection, a point also acknowledged by Tanahara (pers. comm.), who has recognised the problem of sampling bias. Much more work needs to be done on the factors controlling the sources and supply of the parent and daughter isotopes to speleothem calcite. Akiro Tanahara is currently investigating some of the environmental influences in caves on ^{210}Pb and ^{226}Ra and their eventual incorporation into calcite (Tanahara *et al.*, 1997).

4.5.8. AMS Radiocarbon Dating of Soda-straw Stalactites Discussion

The application of radiocarbon dating to soda-straw stalactites relies on the assumption that the apparent age effect (dcp) has remained constant for the entire the depositional period. There is also the implicit assumption of continuous growth. A further complicating factor is that

the ^{14}C activity in the atmosphere and other reservoirs, and thus in the initial activity of the samples dated, has varied over time (Stuiver *et al.*, 1998). A calibration dataset is necessary to convert conventional radiocarbon ages into calibrated years (cal yr).

Genty and Massault (1997) observed that the dcp in seepage water appears to be homogeneous between sites within a cave but will vary by up to 15 % between sites. There also appears to be a dependence on the type of surface vegetation. This is of particular concern given the potential rapidity of vegetation change and the effect it may have on the dcp, but further investigation is required.

Genty *et al.* (1998) have demonstrated that ^{14}C activity in speleothem calcite is affected by the rate of turnover of soil organic matter (SOM). At two different sites they observed that speleothem ^{14}C activity rose dramatically after the bomb tests and peaked at approximately 1970 but following this peak ^{14}C activity remained constant at one site while at the other it has gradually fallen. The karst areas surrounding the caves from which the soda-straw stalactite samples used in this study were collected, have been subject to forestry plantation management practices. Although these activities occurred predominantly after the nuclear bomb tests their influence may be just a dramatic.

Prior to these disturbances the wet sclerophyll forest in the Florentine Valley was inherently stable in its community structure and composition over the last several hundred years (Colhoun, 1988). Since the samples analysed in this study are unlikely to be more than several hundred years old, any major changes in the vegetation community can be attributed to anthropogenic activities or fire activity (Wells and Hickey, 1999). In Frankcombe Cave there are approximately fifty soda-straw stalactites growing along a fissure in the cave roof with almost all of them having several discrete dark brown rings. The feature has also been observed in several other soda-straw stalactites in another cave in the Florentine Valley. It is hypothesised that they are due to forestry activity causing a major short term increase in the mobility of SOM.

The assumption of a linear growth rate may not be appropriate in accounting for the dcp in speleothem calcite. Major disturbances, such as fire or forestry activities, may have significant impacts on the SOM turnover and therefore the ^{14}C activity of speleothem calcite.

The application of excess ^{210}Pb dating was supposed to aid in determining the apparent age effect but the major disparity between the calculated ages from the methods is not encouraging. However, there are still some problems with the excess ^{210}Pb dating technique that require further investigation

4.6. Conclusions

The application of high resolution TIMS $^{230}Th/^{234}U$ age determination to a number of stalagmites and flowstones has yielded important information regarding terrestrial palaeoenvironments in southeast Australia in the Late Pleistocene. An age frequency histogram compiled from 37 new TIMS $^{230}Th/^{234}U$ dates together with a number of existing uranium series age estimates

provided clues on periods of greater moisture availability in southeastern Australia, especially during the last 50 ka. The timing of glacial maxima can also be inferred by the lack of speleothem growth. The age frequency results bear this out as there are two major periods in the last 200 ka where no speleothem growth occurs, from 150 to 125 ka and from 22 to 19 ka, suggesting that severe climatic conditions during the Penultimate Glacial may have been of much longer duration than during the Last Glacial.

The growth phases and hiatuses of the Yarrangobilly flowstone samples, determined by high precision TIMS $^{230}Th/^{234}U$ age determinations, provide important information about palaeoenvironmental history in NSW. Periods of greater moisture availability are suggested by the dramatic increase in growth rates in the upper section of JC-F1, from approximately 30 to 22 ka. Further sampling is required to investigate the timing of hiatuses as this will help to discriminate between local and global factors influencing flowstone growth. Although the number of samples is small the results are very enouraging and hopefully will stimulate further work in this karst area.

In order to provide temporal frameworks for several soda-straw stalactites two radiometric methods were tried, excess ^{210}Pb and AMS ^{14}C dating. Although the application of this techniques did not lead to a totally successful outcome, some important directions for future research have been identified.

Chapter 5

Minor Elements in Speleothems

5.1. Introduction

In nature, pure calcium carbonate is exceptional and unlikely given the thermodynamic hurdles that need to be overcome during precipitation (Morse and Mackenzie, 1990). Usually calcium carbonate is contaminated during precipitation by numerous elements present in percolation water, derived from the weathering of rock and decomposition of vegetation and soil. The concentration of minor elements in calcite is controlled by both the composition of the parent solution and the conditions under which precipitation occurs. If an understanding of the factors controlling minor element concentrations in contemporary speleothem calcite under present day conditions is achieved then determining past environmental changes above the cave should be possible with more ancient samples.

Note that in order to avoid confusion in this study, particularly when referring to minor (>1 % by weight) and trace (from 0.1 to 1 % by weight) elements, the term "minor element" refers to both minor and trace elements as some of the elements investigated are, by definition (Gill, 1997), minor and trace elements.

Most early studies of the minor element composition of speleothems have concentrated on the controls of speleothem colour by minor elements (Gascoyne, 1977; Hill and Forti, 1997; White, 1981; White and Brennan, 1989). Until quite recently very few studies have looked at the minor element composition of speleothems specifically to investigate their palaeoenvironmental significance, an area as yet poorly investigated, but with considerable potential (Gascoyne, 1992). Exceptions are Gascoyne (1983), Goede and Vogel (1991), and Goede (1994). Technological advances in analytical techniques have further stimulated studies of the minor element composition of speleothems for the following reasons:

(1) the precision and accuracy of analyses has increased;

(2) the size of sample required for analysis has decreased considerably;

(3) the time taken to process a large number of samples is greatly reduced; and

(4) the achievable sampling resolution has significantly increased.

For example, Roberts *et al.* (1998) used an ion microprobe to investigate annual magnesium and strontium variations at intervals of approximately 2-4 μm, along a 2.4 mm section of stalagmite.

This chapter provides some background information on possible factors influencing the minor element composition of speleothems and the partitioning of minor elements into calcite. A

review of the current literature on the theoretical background and environmental controls on the partitioning of minor elements, especially magnesium, strontium, barium, and uranium, into calcite is given. This is followed by a discussion on the sources of minor elements and their incorporation into speleothem calcite. The methodology of the study is discussed in detail starting with some background information on the techniques used, their application to speleothems, and finally the results of the study are presented and discussed.

5.2. Theoretical Background

A significant body of work exists on the environmental controls on the minor element composition of low temperature calcite cements and inorganic marine carbonates but, as has been pointed out previously, very little effort has been directed towards low temperature, inorganic secondary calcite deposits. The following sections discuss previous studies of speleothems that have investigated their minor element content followed by several sections discussing the main factors influencing the minor element composition of low temperature, freshwater carbonates, especially speleothems.

5.2.1. Previous Studies of Minor Elements in Speleothems

Many early studies of minor elements in speleothems were attempts to explain their colour variations. However, Gascoyne (1983) was the first to try to interpret minor element variations in terms of palaeoenvironmental change. Gascoyne (1983) observed that the partition coefficient of magnesium of contemporary cave water and calcite is temperature dependent, but this is not the case with the partition coefficient of strontium. It was suggested that variations in speleothem magnesium-calcium ratios could be used as a palaeothermometer, however, it was soon recognised that changes to the concentration of magnesium in waters feeding the speleothem would be the principal factor limiting its use as a palaeothermometer.

Goede and Vogel (1991) demonstrated that many minor elements showed significant variations in concentration along the length of a stalagmite that they attributed to environmental change. Goede (1994) compared variations of magnesium and strontium concentrations in a stalagmite against stable isotope changes and found significant correlations. The results were encouraging and stimulated further research into minor elements, especially investigation of strontium isotope ratios as a proxy for aeolian dust (Goede *et al.*, 1998).

Recent work has shown that there are many factors influencing the variations in concentration of certain minor element species in speleothems, and that complex interactions, that are not yet fully understood, make interpretations in relation to past environmental change less than straight forward (Roberts, 1997). It should be possible, however, to calibrate the minor element records against other proxies or historic records in order to get a qualitative record for any given site. It has also been observed that fine scale variations in certain minor elements are useful in resolving annual cycles, therefore they can be applied as a dating tool in a similar fashion to UV luminescence records (Roberts *et al.*, 1998).

In order to study palaeoenvironmental changes Hellstrom (1998) has used solution introduction and laser ablation ICP-MS to investigate variations in the concentrations of minor elements present in New Zealand speleothem calcite. Initial screening of 37 elements has found that magnesium, strontium, barium, thorium, and uranium are present in measurable quantities and that it is possible to obtain repeatable measurements with these particular elements. Attempts have also been made to analyse several other minor elements, including sodium, aluminium, zinc, yttrium, lanthanum, and lead, but these were unsuccessful as the ability to duplicate the results for these elements was questionable and there is little or no information pertaining to the factors controlling their incorporation into calcite.

The study has been useful in constraining some of the main factors influencing variations in the concentration of five elements in New Zealand speleothems by comparing the minor element analyses with measurements of growth rate, $\delta^{18}O$, $\delta^{13}C$, and luminescence variations. Magnesium content has been interpreted as being influenced by water residence time, strontium and barium respond primarily to changes in the concentration of CO_2 in the soil atmosphere, thorium as an indicator of detrital contamination, and uranium may relate to changes in the water and soil chemistry. However, the author highlights the need for further investigations into the factors influencing minor element content, suggesting that a comprehensive water and environmental sampling program is the only way that significant progress will be made in this field of research.

5.2.2. Minor Element Partition Coefficients

The study and application of partition coefficients has been an important tool in trying to understand various earth processes and particularly the environments under which they formed, for example the deposition and diagenesis of carbonate minerals. An understanding of the factors controlling the co-precipitation of "foreign" ions into natural carbonates has considerable potential in the study of palaeoenvironments (Morse and Bender, 1990). The simplest form of describing the co-precipitation of minor elements from solutions into solids is the non-thermodynamic homogenous partition coefficient (D), first derived by Henderson and Kracek (1927 quoted in Morse and Mackenzie, 1990), and usually applied to compositionally homogeneous solids:

Equation 5.1

$$D = \frac{[Tr/Cr]_{solid}}{[Tr/Cr]_{solution}}$$

where [Tr/Cr] is the molar ratio of a "trace", *ie* a particular minor element, to a "carrier", *ie* calcium, in the solid and liquid phases (Morse and Bender, 1990). The equation assumes that the solution composition remains constant during calcite precipitation, however, in many experiments aimed at establishing various minor element activity ratios, this has not been the case and significant difficulties can be encountered when applying the derived partition coefficients to natural waters.

Morse and Bender (1990) note that, despite the large body of experimental work on the partition coefficients of calcite, researchers are still no closer to being able to precisely model

the composition of calcite even if many of the parameters are well established. Therefore, applying these derived partition coefficients to older carbonates, where only the composition is accurately known, in order to infer the conditions of formation via the partition coefficients is "nebulous" at the very least.

It should also be obvious that the application of Equation 5.1 to natural carbonates is not without its problems as they are anything but homogeneous in composition. While some work has been done on the behaviour of minor element partition coefficients at different temperatures, little data exists on the effect of pressure on partition coefficients, therefore, it is generally regarded as having little if any impact (Morse and Mackenzie 1990). Factors affecting partition coefficients also include the reaction rate, precipitation rate, and the presence of other impurities. Several recent experimental studies (Lorens, 1981; Pingitoire and Eastman, 1986) strongly suggest that some partition coefficients are precipitation rate dependent therefore implying non-equilibrium conditions, and adding yet another compositional controlling variable (Morse and Bender, 1990).

It was suggested by Morse and Bender (1990) that the application of partition coefficients to low temperature natural systems is valid only under the conditions with which they were determined. They also note that as further experimental investigations reveal an increasing number of parameters influencing partition coefficients, their application to natural systems becomes more questionable. As Roberts (1997) points out, the application of partition coefficients to speleothem calcite has severe limitations. At best it may provide a loose framework within which likely environmental influences can be implied.

5.2.3. Factors Affecting Minor Element Partitioning into Calcite

As noted by Roberts (1997) there are two main methods of determining empirical values for partition coefficients, laboratory experiments, where calcite is precipitated under controlled conditions, and field studies, where coexisting water and calcite are analysed. In the case of experimentally derived minor element partition coefficients, the limitations of applying the results to natural systems are many, given the multitude of possible controlling variables. The factors which have received the most attention are temperature, partial pressure of CO_2, precipitation rate, and the effect of other minor elements present in the parent solution.

This section discusses these factors and their influence on the partitioning (D) of the most commonly investigated minor elements, namely the alkaline earth elements magnesium, strontium, and barium, into calcite. Some observations and discussion on uranium will also be given. Hellstrom (1998) and Roberts (1997) have also given reviews of the factors influencing minor element partitioning into calcite.

5.2.3.1. Effect of Temperature on Minor Element Partition Coefficients

Temperature has been widely investigated as a possible controlling factor on some minor element partition coefficients, particularly magnesium (Gascoyne, 1983; Oomori *et al.*, 1987; Burton and Walter, 1991). The results of temperature dependency experiments using inorganic marine settings (Mucci, 1987; Oomori *et al.*, 1987; Burton and Walter, 1991) sharply contrast with the one study using field based observations of karst systems (Gascoyne, 1983).

In the latter study a significantly steeper regression line of temperature and D_{Mg} is the distinguishing feature. Gascoyne (1983) has found that the temperature dependency of D_{Mg} was 0.0017 $°C^{-1}$ but he did not consider the possibility of other factors influencing the results.

Theoretically a temperature change of several degrees will significantly affect the magnesium content of calcite precipitated from a given solution (Hellstrom, 1998), while the strontium content has been shown to have no such temperature dependence (Katz *et al.*, 1972; Gascoyne, 1983). If temperature is a controlling factor on the magnesium concentration of speleothems then the most dramatic changes should occur in response to large temperature variations such as those that occur in glacial to interglacial transitions or from stadials to interstadials. Several recent studies of speleothem minor element composition, including Goede (1994), Hellstrom (1998) and Roberts *et al.* (1998), support the notion that magnesium content is not directly influenced by temperature and that residence time of seepage waters in the overlying carbonate rocks may be a more important factor.

5.2.3.2. Influence of Partial Pressure of CO_2 on Minor Element Partition Coefficients

Several studies have investigated the relationship between PCO_2 and minor element partition coefficients, however, the results of experimental data are not conclusive. Studies on the relationship between PCO_2 and D_{Mg} have so far not produced a clear answer (Gonzalez and Lohmann, 1988; Burton and Walter, 1991; Hartley and Mucci, 1996). For example, Burton and Walter (1991) have claimed that partial pressure of CO_2 has an important effect on the incorporation of magnesium in calcite. They found that the D_{Mg} has an inverse linear relationship with PCO_2.

Hellstrom (1998) argues that there is a strong relationship between the $\delta^{13}C$ and PCO_2 as variations in speleothem $\delta^{13}C$ have been shown to be caused by changes in vegetation activity through changes in the PCO_2 of the soil. He has observed that the close correlation between the Sr/Ca and Ba/Ca traces and the $\delta^{13}C$ results suggests that variations in soil PCO_2 may be a dominant influence on strontium and barium concentrations in speleothem calcite.

5.2.3.3. Effect of Calcite Precipitation Rates on Minor Element Partioning

Several studies have shown that the precipitation rate of calcite is a significant factor influencing minor element partition coefficients (Lorens, 1981; Morse and Bender, 1990; Tesoriero and Pankow, 1996). It has been observed that precipitation rate has a strong positive correlation with strontium (Lorens, 1981; Pingitore and Eastman, 1986) and barium partition coefficients (Tesoriero and Pankow, 1996), but its effect on magnesium partition coefficients is still unclear and controversial (Mucci and Morse, 1985; Given and Wilkinson, 1986; Gonzalez and Lohmann, 1988).

5.2.3.4. Changes to Ion-Calcium Ratios in the Precipitating Solution

Experimental studies suggest that the partition coefficient of an element bears some relationship to the minor element to calcium ratio (Mucci and Morse, 1983; Pingitore and Eastman, 1986; Howson *et al.*, 1987; Banner, 1995). The D_{Mg} is inversely related to the Mg/Ca ratio of the precipitating solution at values between 1 and 5.13 (Mackenzie *et al.*, 1983), but at Mg/Ca values less that one there is no observable effect on D_{Mg} (Howson *et al.*, 1987). The

latter situation, where Mg/Ca is less than one and there is no change to D_{Mg}, is the most likely situation in cave settings (Roberts, 1997). An inverse relationship exists between the Sr/Ca ratio of the precipitating solution and D_{Sr} (Pingitore and Eastman, 1986; Banner, 1995).

5.2.4. Factors Affecting Minor Element Sources and Supply

It is apparent that the minor element composition of speleothems is influenced by two principal factors:

(1) temporal changes in the minor element composition of seepage waters; and

(2) variations in the depositional process which effects the partitioning of minor elements between the percolation water and the speleothem calcite.

Concerning the first factor there are many influences on the evolution of percolation waters, that ultimately supply speleothems. Therefore, consideration must be given to the whole hydrogeochemical system, as the source of minor elements is highly variable in both time and space. In considering the above factors one must also take note of the temporal scale at which the minor element variations are being investigated as different factors may become dominant at different temporal scales, this may also be applicable to stable isotope records (Chapter 6). Goede (in prep) suggests that the factors influencing the composition of minor elements in speleothem calcite can be conveniently examined at three different temporal scales, glacial/interglacial (10^4–10^5 years), millenial (10^3–10^4 years), and secular ($<10^2$–10^3 years).

At the glacial/interglacial scale large excursions in environmental conditions are to be expected and may possibly contain glacial to interglacial transitions (for example Hellstrom, 1998). It would be expected that at these scales the effects of temporal changes in such factors as cave temperature, supply of terrestrial dust (for example Goede *et al.*, 1998), vegetation cover (Hellstrom *et al.*, 1998), *etc*, would be maximised thus the response of the minor elements should be fairly dramatic. At the millenial scale minor element records are less likely to show the full range of environmental excursions, depending of course on where the record fits in time, however it is still possible that significant trends in the minor elements may be present although relating them to environmental changes can be more problematical. Secular scale changes may allow annual and other short term quasi-periodical environmental fluctuations to be investigated. In circumstances where the speleothem is collected with a known date the variations in minor element composition may be compared with historical climate records or with measurements of environmental variables *in situ*, for example drip water rates or seepage water composition.

Influences on percolation water include the aerosol/dust content of precipitation, soil formation and weathering processes, and limestone bedrock dissolution (Gascoyne, 1983). The major causes of variation in the minor element composition of percolation water consist of changes in the partial pressure of soil CO_2, water residence time, seepage pathways, and fluctuations in dissolved ions, from the carbonate bedrock, soil, and other rock types that may be present, and soil organic matter (Hellstrom, 1998). The influence of elements derived intermittently from incidental sources such as atmospheric dust, sea salt, pollen and spores, and fire products, should not be overlooked.

Sector zoning of calcite (described earlier in Section 2.5.4) may present major difficulties when studying minor element variations of speleothem calcite on a microscale, particularly as there is potential for significant lateral variation of minor element concentrations along temporal horizons (Reeder and Grams, 1987; Hellstrom, 1998).

It is likely that considerable noise and possible site specific factors will be associated with any palaeoenvironmental signal in speleothem calcite, due to the complexity of the system. As many of the factors will interact with each other to a degree, working out the principal environmental factors or at least narrowing them down may be feasible in the current research climate. Relatively little research has been done on the variations in minor element composition of cave seepage waters, although Dr Ian Fairchild (University of Keele) and several of his students are currently investigating the minor element geochemistry of both seepage water and speleothems in several European karst areas (Fairchild *et al.*, 1996). The following sections discuss those factors which are most likely to be the dominant factors controlling the minor element composition of speleothems.

5.2.4.1. Changes in the Partial Pressure of Soil CO_2

Soil processes have a significant and direct impact on both the partial pressure of CO_2 and the pH of percolation water. The high partial pressure of dissolved CO_2 in the soil atmosphere has been shown to be directly related to temperature, and will therefore vary seasonally. Dörr and Münnich (1989) have found that the dissolved CO_2 partial pressure of soil moisture can be an order of magnitude higher in summer than in winter. This suggests that in areas where surface temperature fluctuates markedly between seasons, seasonal variations in the PCO_2 and pH of soil water will also occur. It follows then that significant changes in groundwater acidity will have major impacts not only on the absolute and relative concentrations of dissolved mineral species in the water but also on the dissolution of the carbonate bedrock.

5.2.4.2. Fluctuations of Dissolved Ions and Soil Organic Matter

Since soil CO_2 directly affects the pH of seepage water it follows that the dissolution of organic and inorganic material will show seasonal fluctuations. Organic acids are also able to form complexes with many cations and in some cases this is the only way that those ions can be transported in natural waters. Binding of some metal ions by organic acids may also reduce certain ion species' activity (Benedetti *et al.*, 1996). Accurately predicting these effects on the ion concentrations of natural waters temporally and spatially is very difficult. Since pH and possibly drip water temperature vary seasonally it is argued that the reactions between organic acids and some ionic species may be significantly altered by these changes. Roberts *et al.* (1998) observed an inverse relationship between annual variations in the Sr/Ca ratio and luminescence intensity, high luminescence is interpreted as indicating high organic acid concentrations.

Baker *et al.* (1998a) have shown that organic material in speleothems and the waters that feed them consist mainly of humic and fulvic acids, derived from the decomposition of organic material and the activity of surface vegetation. It has also been demonstrated that annual variations exist in the organic acid content of speleothems (see Section 2.6.8). Shortwave UV

light stimulates the organic acids and the resultant luminescence differences are recorded and measured (Baker *et al.*, 1993b; Shopov *et al.*, 1994; Baker *et al.*, 1996a). These studies support the notion that seasonal fluctuations of the organic acids in cave seepage water do occur but the mechanisms controlling them are still not well understood. Toth (1998) investigated seasonal differences in the dissolved organic carbon concentrations and luminescence characteristics of cave seepage waters. However, the author points out that the results are likely to be site-specific and will remain so until more is known about the factors controlling organic acids in seepage waters and more studies have been done of individual sites.

5.2.4.3. Changes in Water Residence Time

The path water takes from when it enters the surface until it infiltrates a cave may involve considerable distance and time. Longer residence times in soils and underlying bedrock will potentially increase the relative contribution of dissolved metals from resistant mineral phases to the seepage water. Therefore, if this contribution is significantly different from that of the more easily leached minerals, the geochemistry of the seepage waters is affected by the residence time (Hellstrom, 1998). For example, longer water residence times in carbonate rocks favour the dissolution of dolomite over calcite therefore increasing the magnesium concentration and possibly lowering the strontium concentration, as strontium is present in much lower concentrations in dolomite than in calcite (Roberts *et al.*, 1998). The effect of longer water residence times on reactions between organic acids and cations should not be overlooked.

Genty and Deflandre (1998) investigated the variation of a stalactite's drip rate and seepage water conductivity in relation to precipitation. They observed a strong positive correlation (R^2 value of 0.98) between the interannual drip rate variation and the effective precipitation, calculated using the Thornthwaite formula, therefore the greater the water excess the greater is the drip rate and thus the volume of water flowing through the stalactite. The drip- and flow-rate of the stalactite exhibit a distinct seasonal pattern consisting of three stages starting with an abrupt flow-rate increase in the autumn/early winter, then a high flow-rate regime in winter/early spring, followed by a gradual decrease through late spring/summer. Conductivity also shows a strong seasonality and a positive correlation with flow rate.

5.2.4.4. Variations in the Dominant Pathway of Seepage Water

The flowpath of water through the soil is relatively simple but on entering the pore and fracture space (subcutaneous zone, Williams, 1983) the flowpath can become much more complex. Aquifer volume and flow rate have the potential to influence the minor element geochemistry of groundwaters, for example high flow regimes may utilise rock pore space and fractures, whereas low flow regimes may favour transport primarily via rock pore space (Benedetti *et al.*, 1996; Genty and Deflandre, 1998). Therefore, the influence of temporally and, possibly, spatially variable flow regimes is very important on those factors affected by residence times.

It is hypothesised that the residence time and mixing of waters of different ages may influence the degree of annual layering in speleothems as a longer residence time or longer flowpath may have the effect of "averaging" the seasonal signal.

5.3. Methodology

Microbeam analytical techniques are greatly increasing our understanding of earth processes through the study of major- and minor-elements in a wide range of natural materials. In this study, two different microbeam instruments, an inductively coupled plasma-mass spectrometer (ICP-MS) and an electron microprobe, were used to collect high-resolution minor element data from speleothems. ICP-MS, although a relatively new analytical technique, is gaining wide acceptance in many earth science investigations. The technique allows for high resolution, multi-element analysis of natural materials with good sensitivity, very low detection limits, and good accuracy and precision (Rollinson, 1993). Electron microprobe analysis is a standard technique used in mineralogy and petrology, although it has limited application to other geochemical investigations. Sample descriptions are given in Tables 3.1 and 4.1.

5.3.1. Inductively Coupled Plasma Mass Spectrometry (ICP-MS)

5.3.1.1. Previous ICP-MS Studies of Speleothems

The applications of ICP-MS are wide ranging and much of it is beyond the scope of this thesis. It is pertinent, however, to mention some of the applications related to this research. Hellstrom (1998) has been one of the first speleothem workers to utilise both solution-introduction and laser-ablation ICP-MS in minor element studies of speleothems.

Published work, using ICP-MS specifically on speleothems, includes research by Halicz *et al.* (1997) who used solution introduction ICP-MS to measure low U and Th concentrations in cave deposits. Bar-Matthews *et al.* (1991) used ICP-Atomic Emission Spectrometry (AES) to investigate the major and minor element composition of a range of carbonate deposits from Soreq Cave, Israel. Railsback *et al.* (1994) used solution introduction ICP-MS to analyse concentrations of various ions in two water samples taken from Drotskys Cave, northwestern Botswana. Studies of other carbonates have used corals (Sinclair *et al.*, 1998) and shells of various species to investigate pollution (Fuge *et al.*, 1993), and sea water temperature and productivity (Girard and Albarede, 1996; Lea and Martin, 1999) Numerous papers have been published on the use of ICP-MS on geological materials (Eggins *et al.*, 1998b; Butler and Nesbitt, 1999).

Vadillo *et al.* (1998) used laser-induced breakdown spectrometry (LIBS) to investigate spatial distributions of Mg and Sr along the axial and radial growth axis of a stalactite from Nerjas Cave in Malaga, Spain. LIBS uses a precisely focused laser beam, a pulsed Nd:YAG laser, to irradiate the sample which at the interface between sample and laser beam produces a high-temperature plasma where vaporisation and ionisation of the sample occurs (Vadillo *et al.*,1998). Spectral analysis of the plasma in the spot area gives a precise elemental analysis of the sample.

An advantage of this technique is the relative rapidity of data acquisition at a fraction of the cost of other microbeam techniques. However, Vadillo *et al.* (1998) have used a relatively coarse sampling resolution, a 1 mm sampling interval, which in comparison to other microbeam

techniques makes interpretation of minor element data problematical, especially if one is trying to identify seasonal variations. The authors highlight the need for more work on the analytical technique particularly on ablation efficiency, and the effects the quality of the sample surface has on results, standardisation of procedures and quantification of minor element concentrations (Vadillo *et al.*, 1998).

5.3.1.2. Laser Ablation and Solution Introduction ICP-MS Methodology

ICP-MS is an analytical technique that uses a high temperature plasma, commonly argon, to dissociate molecules and ionise atoms. Ions are extracted through a pinhole-sized aperture into a pumped intermediate area, from which it is further sampled through a second aperature into a high-vacuum ion lens region of a mass spectrometer (Rollinson, 1993). The plasma (see Figure 5.1) is generated and sustained by an intense radio frequency (RF) field. The RF field is produced by a copper tube, coiled up to 4 times around the end of the quartz torch glass, acting as an antenna and through which cooling water flows. At the end of the torch glass, an induction region is created by the intense electromagnetic field within the bounds of the coil. The plasma torch is ignited by passing a high voltage spark through the argon gas, which ionises some of the argon atoms.

The mixture of argon gas and ions passes into the induction area where it becomes coupled to the oscillating induction field. Continuous collisions occur within the field between electrons and argon atoms thereby producing more argon ions, and in effect creating a self-supporting plasma as long as the RF field maintains the induction and there is a continuous supply of argon gas. Sample ionisation occurs through heating by the central core of the plasma, which reaches a temperature of around 10,000 K. Sample ionisation is extremely efficient and occurs at temperatures between 5,000 and 7,000 K (Perkins and Pearce, 1995). Ions of all masses from the sample are extracted into a mass spectrometer which sorts the ions by mass using a quadrapole mass filter.

All ICP-MS work was performed at the Research School of Earth Sciences (RSES), Australian National University (ANU) under the supervision of, and with assistance from, Mr Les Kinsley and John Hellstrom. The machine at RSES is a Fisions VG Plasmaquad PQ-2. This instrument can be set up to analyse samples using either solutions, by injection as an aerosol into the plasma, or by laser ablation where the sample is ablated directly by the laser, producing microparticulate material, and introduced into the plasma via a helium/argon carrier gas.

RSES Laser Ablation Stage Setup

The ablation setup utilises a Lambda Physik LPX 120I argon-fluoride excimer laser with a wavelength of 193 nm. The maximum power output of the laser is approximately 60 W, but for most analyses of speleothems the laser is operated between 5 and 15 W with a pulse rate of between 5 and 30 Hz. Stalagmites and flowstones are polished to a flat planar surface prior to analysis, in order to clean the sample surface before an analysis scan. The power settings are varied depending on whether the laser was ablating the sample surface as a cleaning step, ie pre-ablation, or ablating the sample for data acquisition. Generally, the power settings for pre-ablation runs are twice that of a sample scan.

The laser beam is masked through an aperture and, although a fairly wide range of sizes and shapes is possible, most work with speleothems uses a rectangular spot approximately 20 (x) by 200 (y) μm. It is found that with smaller spot sizes an increase in the number of pulses per second, with a maximum of approximately 30 Hz, is necessary to ensure that enough sample is ablated. Much also depends on the sensitivity and background noise of the machine. Sample ablation occurs in a chamber containing an argon-helium gas mixture, at atmospheric pressure, and this gas flow carries the ablated sample through the pulse-smoothing cell and from there to the ICP-MS. The RSES laser ablation ICP-MS system has been described in detail by Eggins *et al.* (1997) and in Sinclair *et al.* (1998).

RSES Solution Introduction Setup

Solution ICP-MS has been used to measure the uranium concentrations of samples used for age determination prior to analysis by the TIMS method (Chapter 4). The procedure involves dissolving 2-5 mg of speleothem sample in 9.0 ml of clean 2% HNO_3 in an acid cleaned test tube, and then adding 1,000 μl of previously prepared $^{233}U/^{115}In$ spike solution. A blank and standard are also prepared, the blank made up of 9.0 m*l* of clean 2% HNO_3 and 1,000 μ*l* of $^{233}U/^{115}In$ spike solution, the standard containing 9.0 m*l* of clean 2% HNO_3 and 1,000 μ*l* of a $^{238}U/^{232}Th$ standard solution. The solutions are allowed to equilibrate overnight, then loaded into a Gilson auto-sampler attached to the ICP-MS. Sample, standard, and blank details, dilution factor, ^{233}U and ^{115}In concentrations, are entered into the ICP-MS control software and after the analysis run is finished, uranium concentration results are output as blank subtracted, solid concentrations. The uranium concentrations from the ICP-MS analysis has an average analytical error of several percent. The results shown in Table 4.1 are used to calculate spike weights in the TIMS U-series dating of the speleothem samples.

5.3.1.3. Application of ICP-MS to Speleothems in this Study

Sample preparation for laser work has involved mounting the samples on a 50 mm by 60 mm glass "stage", prior to mounting on the sample cell stage. The sample cell restricts travel of the stage to approximately 50 mm, thus the maximum sample size is 50 mm (X-axis) x 50 mm (Y-axis). The X- and Y-axial directions of the stage are controlled by two hand operated micrometers (± 5-10 μm), but an added capability on the Y-axis is a small DC electric motor which allows the micrometer to be turned at a constant rate from 1.5 μms^{-1} up to 85 μms^{-1}. The motor driven axis allows the user to scan continuously along the surface of the sample at a constant rate.

For soda-straw stalactite mounts, the unbroken soda-straw stalactites were first sectioned into pieces up to 50 mm in length by carefully sawing with a razor blade until they broke or could be separated without causing shattering. The soda-straw stalactite sections are held in place on a glass microscope slide using "blue-tack", the slide is then put into the sample cell stage using "blue-tack" to hold it in place. The only cleaning process that the specimens are exposed to was a pre-ablation run. In hindsight, an ultrasonic cleaning step to get rid of any dust on the surface should have been added prior to mounting the soda-straw stalactite on the glass microscope slide.

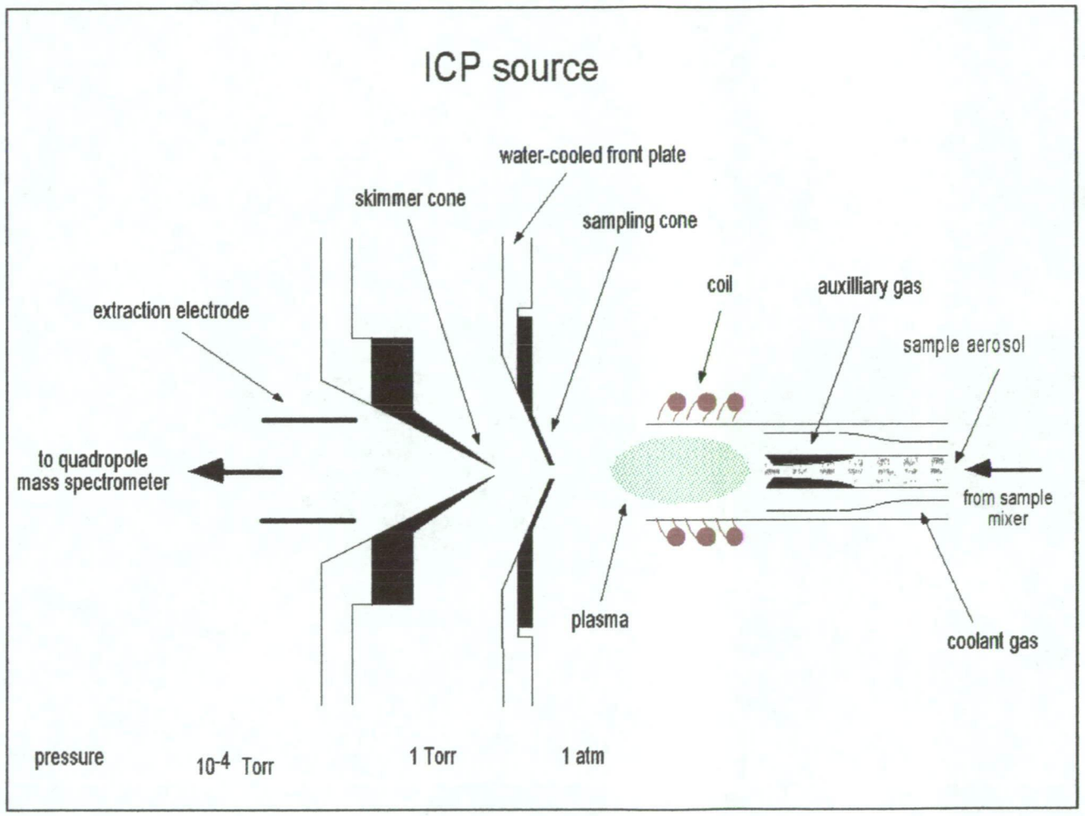

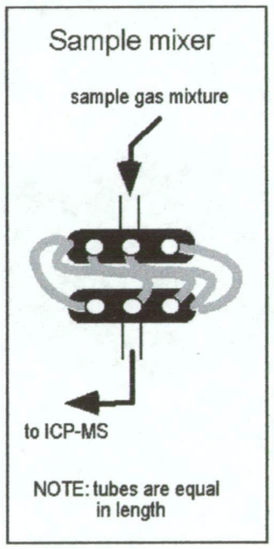

Ar + He + sample
gas flow to ICP-MS
via sample mixer

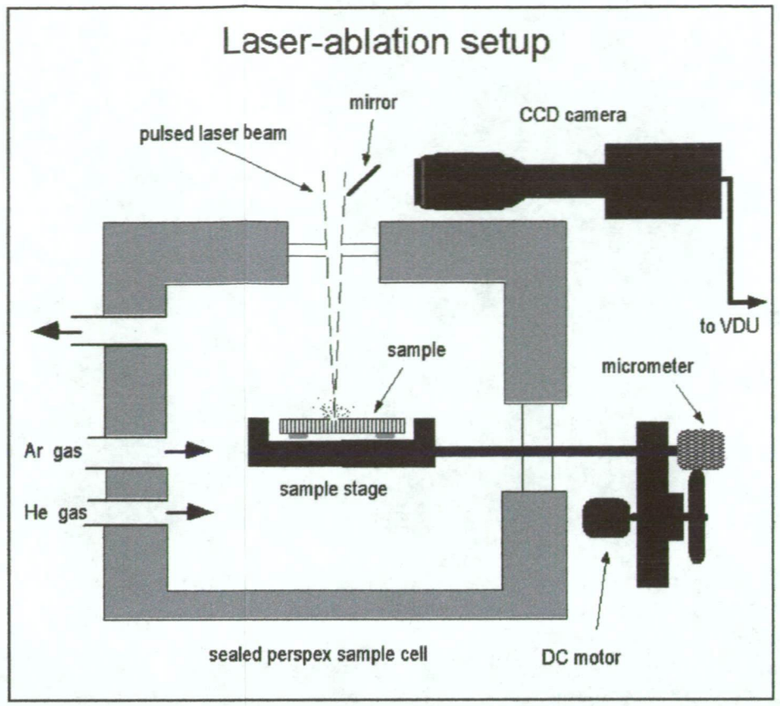

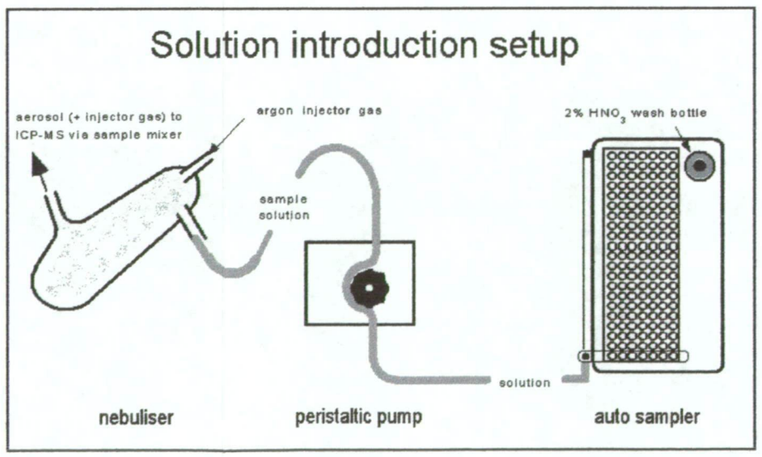

Figure 5.1. **Schematic diagram of ICP-MS apparatus at Research School of Earth Sciences, ANU, Canberra. Diagram shows both solution introduction tool as well as the laser ablation stage setup. The ICP-MS at RSES is a Fisions VG Plasmaquad PQ-2 and the laser ablation setup utilises a Lambda Physik LPX 120I argon-fluoride excimer laser with a wavelength of 193 nm. The sample mixer randomises the sample before it enters the plasma.**

One potential problem with the analysis of the soda-straw stalactites is the uneven surface presented to the laser. The surface sometimes appears to have horizontal bands that may be physically manifested as ribs, several tens of microns in height. Hellstrom (1998) tried mounting a piece of soda-straw stalactite in epoxy resin and then polishing the sample to get a planar surface. The main problem with this approach is the potential loss of data. Since the outer surface of the soda-straw stalactite is deposited first, we can assume that its outside surface is a temporal sequence with the oldest calcite at the base and the youngest at the tip. Thus, any polishing may disturb the record by exposing calcite of a different age and thereby introducing uncertainty into the stratigraphic sequence of the surface to be sampled. Samples analysed with the electron microprobe have to be mounted in epoxy resin as there is no other way of preparing them for analysis due to the nature of the instrument. Studies using other microbeam techniques may have significant errors associated with temporal disturbance if the samples require similar preparation and polishing.

Flowstone and stalagmite mounts were analysed in a similar manner to the soda-straw stalactite mounts but were cut into sections 50 mm by 5-10 mm using a diamond saw. The sections were glued to glass slides, using dyed epoxy resin, and the sample surface polished. The epoxy resin was dyed red in order to identify any areas of the surface contaminated by resin. It can also provide a useful marker in the ICP-MS data set if present on the sample surface as calcium ion intensity drops significantly when epoxy resin is sampled by the ICP-MS.

It must be noted that all data collected in this study are qualitative and not semi-quantitative or quantitative. The data is reported as "normalised counts per second" *ie* all element measurements are normalised to calcium (^{48}Ca) and no calibration of absolute concentration data is attempted. Normalising to calcium assumes that the mass ratios of the elements remain constant with fluctuations in total signal strength and that calcium content is always 4×10^8 ppb. A disadvantage of this approach is the addition of any calcium signal noise to the noise associated with each element (Hellstrom, 1998). It has been considered unnecessary to convert the minor element data to a quantitative form given the nature of the study and, as Hellstrom (1998) points out, the relative internal variations of a speleothem are of more interest that the absolute concentrations.

The lack of a suitable carbonate standard hinders a fully quantitative approach. Attempts with a silica glass standard, NBS-612, provided crude concentration estimates but in switching from a silicate- to a carbonate-matrix the machine sensitivity and some isotope background levels are adversely affected and take considerable time to return to normal levels (Hellstrom, 1998). Calibration of concentration data has not been attempted for these reasons especially considering the difficulty that Sinclair *et al.* (1998) have encountered in creating a standard for coral analysis.

It must be pointed out that the magnesium ICP-MS data for some of the samples is of relatively poor quality because of contamination of the sample chamber by carbonate powder by another user prior to, and unknown by this researcher at the time and obviously beyond his control. Although the sample chamber had been cleaned, the results indicate that a much

more thorough cleaning procedure was required. The contamination significantly reduced the magnesium signal to noise ratio. It is estimated from previous measurements that the magnesium background signal was increased by a factor of approximately five or more.

Unfortunately the analyses have not been repeated due to time and cost constraints but attempts will be made to repeat some at a future time. The contamination was treated as a systematic error on the assumption that the error remained constant throughout the analyses. The ICP-MS results were treated by bacground subtracting an additional twenty percent from the signal, assuming that this was the contamination contribution to the overall signal. This is valid given the qualitative nature of the results and the interest is predominantly in the pattern of variations over time. In order to get fully quantitative results a much more rigorous procedure for calibration will have to be followed.

5.3.1.4. ICP-MS Data Processing

Data from the laser ablation ICP-MS of speleothems have been processed using spreadsheets (MS Excel™) and signal processing software (Igor Pro™). It is necessary to remove the headers put in by the ICP-MS control software but this is easily done in a text editor, for example, BBEdit™. A later version of the ICP-MS control software allows the user to eliminate the headers prior to export. MS Excel™ has been used to pre-process the data prior to importing into Igor Pro™. Pre-processing includes deleting unnecessary headers in the raw ICP-MS output, background subtraction, calcium normalisation, drift correction, and removal of "spikes" in the data.

Background subtraction is necessary to eliminate machine noise. This is done by selecting a few hundred data points from the start and end of each element acquisition, calculating the average for each element, and subtracting this value from the data. Each element was normalised to ^{48}Ca, or ^{46}Ca if ^{48}Ca was not analysed, on the presumption that the mass ratios are constant despite fluctuations in signal strength, caused mainly by sample surface defects in the speleothem such as holes, cracks and, on some occasions, epoxy resin.

As acquisitions usually run for a considerable length of time, up to 50 minutes, it is necessary to correct for drift in the machine's sensitivity, as variation in the order of a few percent is likely to occur over a run of a few hours. A standard, AM-1 (Hellstrom, 1998), is usually analysed at the start and finish of each run, usually when the sample cell is opened to change samples or after the ICP-MS has been re-tuned, and an easily identifiable block of several hundred data points is used to correct the elemental data by interpolating over the time between measurements of the standard. See Sinclair *et al.* (1998) for a more detailed discussion of sensitivity drift.

Temporal sequences of trace element data collected by the ICP-MS occasionally suffer from large spikes, described here as single extreme outliers and easily identified as being spurious. They are presumably caused by dislodgement and entrainment into the plasma of relatively large discrete particles resulting from the ablation of the sample. The data are spike filtered using a running standard deviation filter which works by rejecting any point that is more than three standard deviations from the mean of the twenty points immediately adjacent to it. The

rejected point is replaced with the mean value of the six closest points (Hellstrom, 1998; Sinclair *et al.*, 1998). The data can be smoothed using a 15 point running triangular mean or it can be imported, unsmoothed, into the signal processing software.

Wavemetrics Igor Pro™ was used to analyse and graph the laser ablation ICP-MS data as this package was able to deal with the very large files generated, the largest consists of approximately 60,000 measurements *ie* slice numbers. The large files are generated when scanning at very high resolution, that is, ablating the surface at speeds of a few microns per second. For example, a section of soda-straw stalactite around 50 mm long and scanned at 5 μms^{-1} will take approximately 160 minutes to complete, generating a file of up to 25,000 measurements. As indicated by Hellstrom (1998), these large data sets require considerable desktop computing power in order to be analysed and graphed.

Prior to analysis in Igor Pro™, the majority of data files require trimming in order to get rid of the background component of the scan. In all acquisitions, the first few hundred analyses are measurements of machine background before commencing acquisition of sample data. Background measurements were also made close to the end of the acquisition. The cropped data were then smoothed in order to reduce high frequency noise in the signal. The majority of smoothing in the initial stages of analysis utilises a smoothing spline, a least squares variant of a cubic spline, Hellstrom (1998) has also tried band-pass and low-pass filtering using Fast Fourier transforms. Wavelet analysis has been applied with some success by Hellstrom (1998) and the technique has also been employed in this study.

Following the example of Roberts *et al.* (1998) correlations between minor element pairs have been done on the low frequency data, *ie* untreated, and the high frequency data, *ie* detrended. The data were detrended by subtracting a 50-point running mean. This has the effect of enhancing the high frequency structure and removes any long term temporal trends. The sheer magnitude of some of the data sets has required specialist software and considerable desktop computing power for analysis. It has also required developing analytical procedures and applying specialist data analysis tools to the results.

5.3.2. Electron Microprobe Microanalysis

5.3.2.1. Electron Microprobe Methodology

Electron microprobe analysis uses the X-ray spectrum emitted from the surface of a solid sample bombarded by a focused beam of electrons to acquire discrete chemical analyses (Reed, 1995). The technique is capable of measuring all elements heavier than boron in a wide range of natural earth and synthetic materials. All analyses used in this study were performed at the Central Science Laboratory (CSL), University of Tasmania (UTAS) using a Cameca SX-50 Electron Probe Microanalyser under the supervision of, and with assistance from, Mr Wis Jablonski and Dr Andrew McNeil.

The Cameca SX-50 electron microprobe uses wavelength dispersive (WDS) detectors to perform analyses, employing crystals that diffract characteristic x-rays emitted from the sample according to their wavelength. X-rays are diffracted by a suitable analysing crystal (LiF: lithium fluoride; PET: penta-erythritol; TAP: thallium acid phthallate) and measured in counts per

second by gas flow proportional detectors. These detectors allow very high precision, quantitative chemical analysis to be performed by comparing the intensities of the characteristic X-rays generated by the elements in the sample by reference to X-ray intensities measured in standard materials.

Instrumental calibration is carried out using standard reference materials, both internal and external, and employing either the ZAF (atomic number effects, absorption, and fluorescence) matrix correction procedure or a comparison standard technique. The diameter of the electron beam can be controlled to analyse sample volumes smaller than a few cubic micrometres (Reed, 1995; Rollinson, 1993)

Relative to laser ablation ICP-MS analysis, sample preparation for electron microprobe analysis is more complicated. Samples must be conductive, provided with a planar, well polished surface, and must be physically compatible with the specimen stage. Maximum sample dimensions for the CSL SX-50 are either, a diameter of 24.5 mm or, a rectangular slide of 40 mm (X) by 18 mm (Y) by 4 mm (Z). The sample is first cut to size using a diamond saw, mounted in epoxy resin, polished, and coated with gold or carbon.

5.3.2.2. Previous Electron Microprobe Studies of Speleothems

Since its commercial development in the 1960s, the electron microprobe has become a standard analytical tool for mineralogists, petrologists, and other earth and materials scientists. Several authors have used electron microprobes to study, at very high resolutions, the trace element content of speleothems. Fairchild *et al.* (1996) used an electron microprobe, and also an ion microprobe, to study chemical variations in soda-straw stalactites from Belgium and Eire (Ireland), the soda-straw stalactites were analysed because they showed repetitive bands, between 2 to 5 per millimetre in width, along their entire length. The geochemistry of a stalagmite from Drotskys Cave in northern Botswana has been studied using an electron microprobe by Railsback *et al.* (1994). The study examined differences in Mg and Sr concentrations in annual aragonite and calcite layers.

5.3.2.3. Application to Speleothems in This Study

A 110 mm long soda-straw stalactite from Risbys Basin Cave, RB-SS2, has been cut up into six lengths of approximately 20 mm and individual sections mounted in 24.5 mm diameter epoxy resin mounts, followed by polishing and gold coating. Seven elements (F, Mg, Cl, Mn, Fe, Br, and Sr) were analysed using the CSL SX-50 electron probe micro-analyser, with Ca added to the element menu in another series of analyses. All samples were analysed using a 15 kV accelerating voltage, a 10 nano-amp beam current, a 10 to 15 µm beam diameter, and 30 second counting times. Analyses were performed at 500 µm intervals. Two rectangular slides were also prepared using Yarrangobilly flowstone material, YBJC-F2 and YBJC-F3, and a 50 mm stalagmite, FC-S4, from Frankcombe Cave in the Florentine Valley.

5.3.3. Establishing Chronologies Using Non-Destructive Techniques

This section describes attempts to date several soda-straw stalactites using two methods, counting the seasonal variations of minor elements, or autocorrelation, and the use of

dendrochronological equipment. Assistance was given by John Hellstrom who helped undertake the onerous task of processing some of the data by counting the peaks and troughs along the several metres of FC-SS5 ICP-MS printouts and demonstrating that a useful chronology could be created. The results have since been replicated by the author using the method developed by John Hellstrom.

5.3.3.1. Incremental Counting

The method assumes that the speleothem is active at the time of collection and that deposition has been continuous over the life of the speleothem, thereby giving a "zero" age *ie* the year of collection, or that an independent means of dating the sample has been used, for example AMS radiocarbon dating. The sample is analysed at high resolution using laser ablation ICP-MS, an essentially non-destructive analytical technique. A rectangular laser ablation "spot" gives the best results and the X-dimension, perpendicular to the speleothem growth axis, should be at least five times greater than the Y-dimension.

The results are processed according to the method described in Section 5.3.1.4. Establishing the chronology is done by counting the years from peak to peak, or trough to trough, back from the "zero" age. In some cases, the "years" are not particularly clear. However, with careful analysis the chronology can be established with several assumptions and "best guesses".

5.3.3.2. Tree Ring Measuring Equipment

Equipment normally used for dendrological analysis, a Velmex "TA" system, has been utilised in this study to investigate the ring features seen in soda-straw stalactites (Figure 5.2a) and stalagmite growth layers (Figure 5.2b and c). The Velmex "TA" system consists of a Unislide® aluminium measuring stage with Acurite® Mini-scale digital linear encoder, with a resolution of 1 μm or 0.001 mm ± 5.0 μm m^{-1}, attached to a Quick-Chek® QC-1000 digital display unit. A microscope with a cross-hair reticule is used to view the sample at up to 40x magnification, the cross-hair aids in accurately identifying measurement points. Controlling software, PJK5.v5, was installed on a Macintosh computer. Data from the system have been processed in terms of distance in microns between consecutive rings, viewed through the microscope, in years from a starting date. COFECHA, a data quality control program, has been used to check the dating of samples. It identifies dating conflicts or mistakes by comparing segments of one sample against those of another, or a number of samples (Allen, 1998).

One of the main problems involved in measuring soda-straw stalactites has been identification of a consistent marker to start/end a year. In tree ring studies, the identification of rings is much simpler as summer and winter growth, equal to one year, are conspicuous through abrupt phloem density differences. In order to overcome this problem, multiple measuring runs of up to 20 were performed on individual segments and the results checked in COFECHA. Where major conflicts occur, for example if series lengths do not correspond, the series has been rejected outright. The remaining series are averaged and the results used as the final chronology.

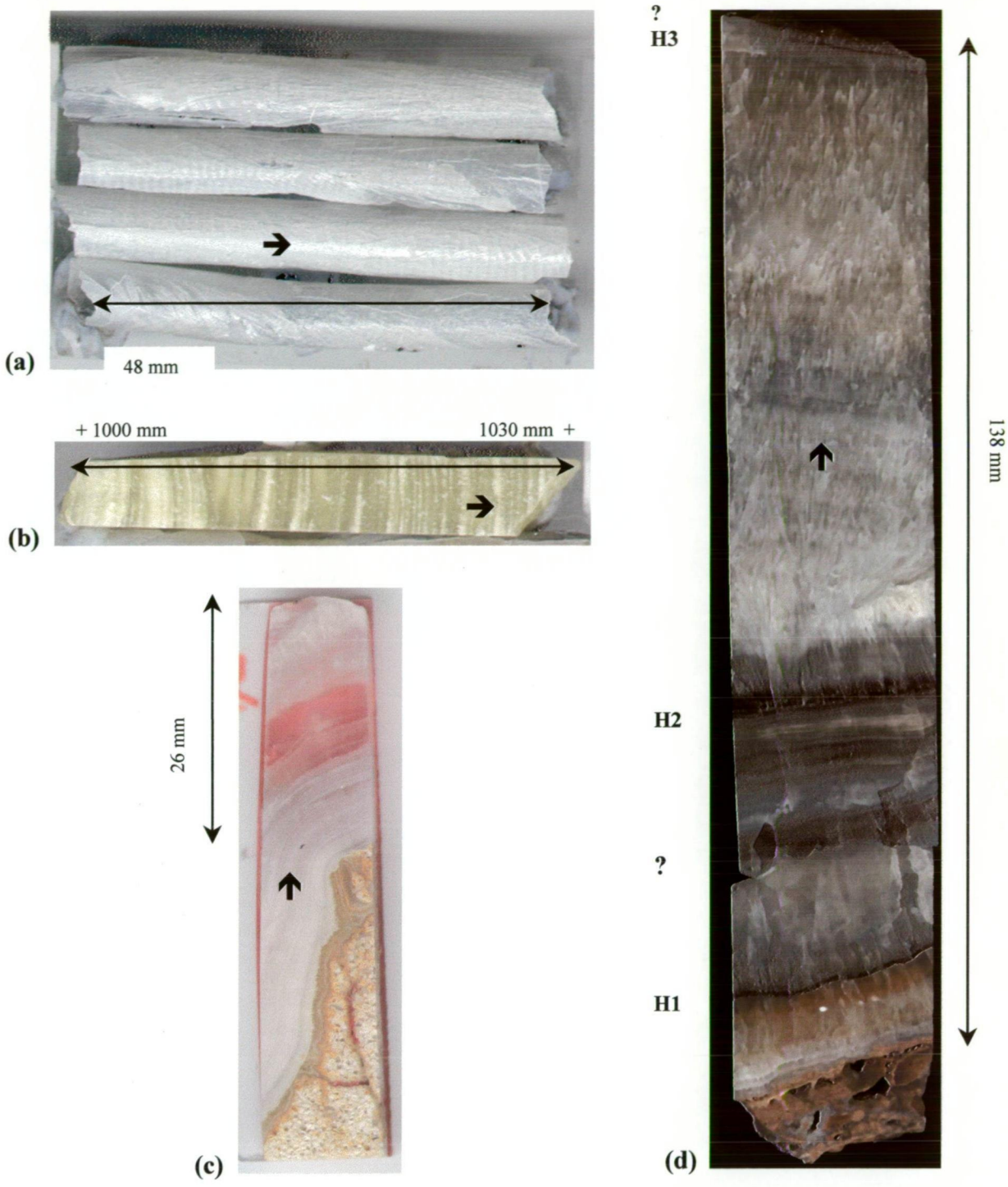

Figure 5.2. **(a) Photograph of FC-SS5, a soda-straw stalactite from Frankcombe Cave, Florentine Valley, Tasmania. Note surface banding feature, arrow indicates growth direction.**
(b) Photograph of CTH-S1, a stalagmite from Top Hole, Croesus Cave, Mole Creek, Tasmania. Note fine scale laminations, arrow indicates growth direction.
(c) Photograph of BFM-J96, a stalagmite from Browns Folly Mine, Bath, England. Note fine scale laminations.
(d) Photograph of JC-F1, a flowstone section from Jersey Cave, Yarrangobilly, New South Wales. Note grey colouring, hiatuses are marked with a letter, "H", and a number from 1 to 3, question marks are approximate positions of inferred hiatuses.

5.4. Laser Ablation ICP-MS Results

This section presents the results for several soda-straw stalactites, stalagmites, and flowstones analysed, in almost all cases for their entire length, at low- and high-resolution using laser ablation ICP-MS. All samples used in this chapter are described in Chapter 3. Several soda-straw stalactite samples have distinct and easily identifiable quasi-periodical minor element oscillations, these variations are inferred to be annual. Analysis of several stalagmite and flowstone sections by laser ablation ICP-MS enables investigation of long term minor element fluctuations and their relationship to past environmental conditions. Some of the stalagmite samples have high frequency minor element oscillations that are hypothesised to be annual. In several soda-straw stalactite and stalagmite samples, the extent of lateral variation in the minor element composition of the longitudinal growth axis has been investigated by parallel laser ablation ICP-MS analysis.

5.4.1. ICP-MS Analysis of Browns Folly Mine Stalagmites

Three stalagmite samples, BFM-92-5, BFM-93-2, and BFM-J96 (Figure 5.2c), from the Browns Folly Mine, Bathford, Wiltshire, England were analysed with laser ablation ICP-MS. These were investigated because some luminescence work on a number of samples and a detailed examination of the water chemistry at the site has already been done by Dr Andy Baker, results of which are published in Baker *et al.* (1998b). An additional advantage of these samples is that the minimum and maximum ages of the samples are well constrained as they were active at the time of collection, thereby giving a zero minimum age, and their maximum age is approximately 160 years since mining had been abandoned by 1836 in the section from where the samples were collected. Therefore the minimum theoretical growth rate for a speleothem can be calculated using the vertical height over the known maximum deposition period (Baker *et al.*, 1998b).

5.4.1.1. BFM-92-5 and BFM-93-2 Minor Element Screening Results

Initially a suite of minor elements: magnesium, aluminium, calcium, iron, copper, strontium, yttrium, cadmium, iodine, caesium, barium, lanthanum, lead, thorium and uranium, are measured in order to establish which elements are present in high enough concentrations to analyse. Two stalagmites, 92-5 (16 mm high) and 93-2 (22 mm high), have been analysed with laser ablation ICP-MS at low resolution, *ie* the sample has been scanned at a fast speed with a relatively large spot size (75 μm), using the expanded set of elements. The results for these preliminary scans are presented in Figure 5.3 (a) and (b), and Figure 5.4 (a) and (b), together with luminescence profiles of the stalagmites provided by Dr Andy Baker. Note that all elements are normalised to calcium (^{48}Ca).

Almost all of the minor element analyses, specifically iron, copper, yttrium, caesium, and lanthanum, seem to be records of machine/background noise with occasional peaks thus they have not been investigated any further. The peaks may be related to ablation of clay or dust particles present in the calcite matrix or appear through molecular interference *ie* counting of compounds with the same molecular weight as the target species, an idiosyncrasy of the ICP-MS system.

Lead is interesting as it may indicate increasing contamination of the environment by the burning of fuels with an additive (Figure 5.3b and Figure 5.4b) but further investigation is required to test this hypothesis. Some elements, aluminium, cadmium, iodine, and thorium, are present in concentrations high enough to be above background levels but, as in the study of Hellstrom (1998), the repeatability of the measurements is questionable. Hellstrom (1998) does not attempt to analyse these particular elements any further because of the instability of the counts per second, leading to poor counting statistics, and due to the low signal to background ratios.

Drift of the machine's analytical sensitivity is apparent, as evidenced by an increase, for example aluminium, or decrease, for example caesium, in the overall minor element signal. Hellstrom (1998) discusses methods of treating ICP-MS results in order to account for drift. Subsequent analyses have all been treated to eliminate machine drift. In this case the results have not been treated in order to illustrate one of the potential problems associated with ICP-MS analysis. Drift correction is achieved by measurement of a standard, AM-1 (Hellstrom, 1998), at the beginning and end of a sampling run, usually when the sample chamber is opened in order to change samples.

5.4.1.2. BFM-J96 Minor Element Results

Subsequent laser ablation ICP-MS analyses has used a more restricted set of minor elements with only magnesium, strontium, barium, and uranium analysed. All are normalised to calcium (^{48}Ca). This allows an increase in the "dwell" time for each element, *ie* the time spent counting on a given mass number by the instrument during each circa 1 second sweep of the mass range, such that elements of low abundance, *eg* uranium, were given higher dwell times than elements with high abundance, *eg* calcium or magnesium. The results of two separate scans, approximately 200 μm apart, of BFM-J96 (Figure 5.2c)using laser ablation ICP-MS at low-resolution, approximately 50 μm s^{-1}, and high-resolution, approximately 15 μm s^{-1}, are presented in Figure 5.5 and Figure 5.6, respectively.

There are some significant differences between the low- and high-resolution scans but this is most likely due to spatial variation because of the slight lateral offset of the scans. Since the fine scale structures of the results are relatively difficult to see in Figure 5.6, several "windows" of approximately 30 years along BFM-J96 are presented in Figure Figure 5.7 (a) to (e). The windows, from the high-resolution scan, show various features such as high- and low-frequency quasi-periodical minor element variations, positive and negative correlations between elements and pairs of elements, and possible growth rate variations.

A correlation matrix of the low (untreated) and high (detrended) frequency records for the high resolution analysis of BFM-J96 is presented in Table 5.1. In the low frequency results there is a weak positive correlation ($r = 0.61$) between the Sr and Ba but no other elements correlate very strongly, there is no correlation ($r = -0.0001$) at low frequency between Mg and Sr. In the high frequency results there is a strong positive correlation between the Sr and Ba ($r = 0.57$) and a weak positive correlation between the Mg and Sr ($r = 0.10$). The strong positive correlations between the Sr and Ba suggests that the processes controlling Sr and Ba geochemistry are very similar and are not significantly influenced by different temporal scales.

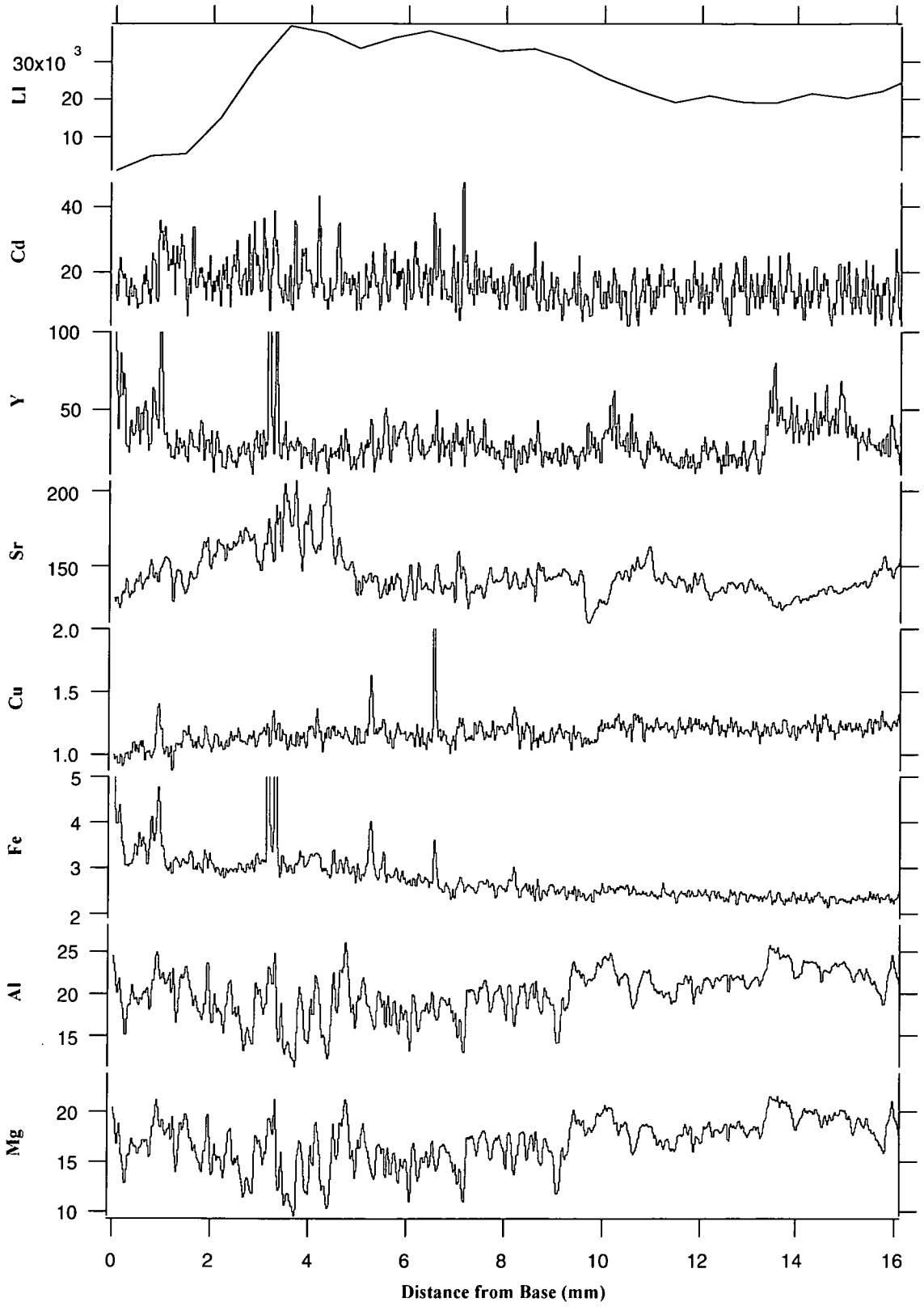

Figure 5.3 (a). Results of laser ablation ICP-MS analysis of BFM-92-5 together with luminescence intensity (LI) results. These scans were done in order to select minor elements in speleothem calcite present in sufficient concentrations to enable further analysis. Axes are from the bottom magnesium, aluminium, iron, copper, strontium, yttrium, and cadmium, and units are in normalised counts second^{-1}.

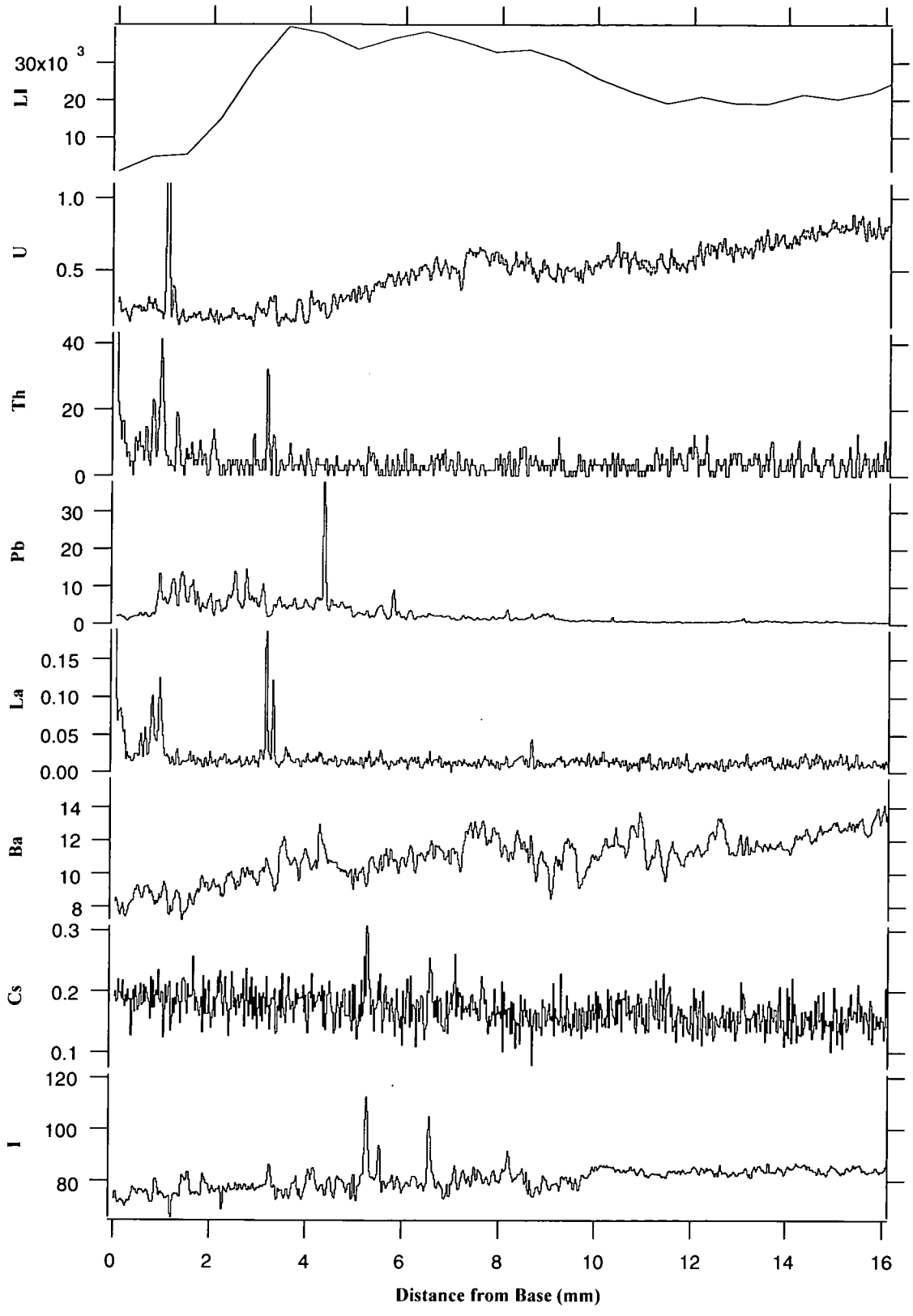

Figure 5.3 (b). **Results of laser ablation ICP-MS analysis of BFM-92-5 together with luminescence intensity (LI) results. These scans were done in order to select minor elements in speleothem calcite present in sufficient concentrations to enable further analysis. Axes are from the bottom iodine, cesium, barium, lanthanum, lead, thorium, and uranium, and units are in normalised counts second^{-1}.**

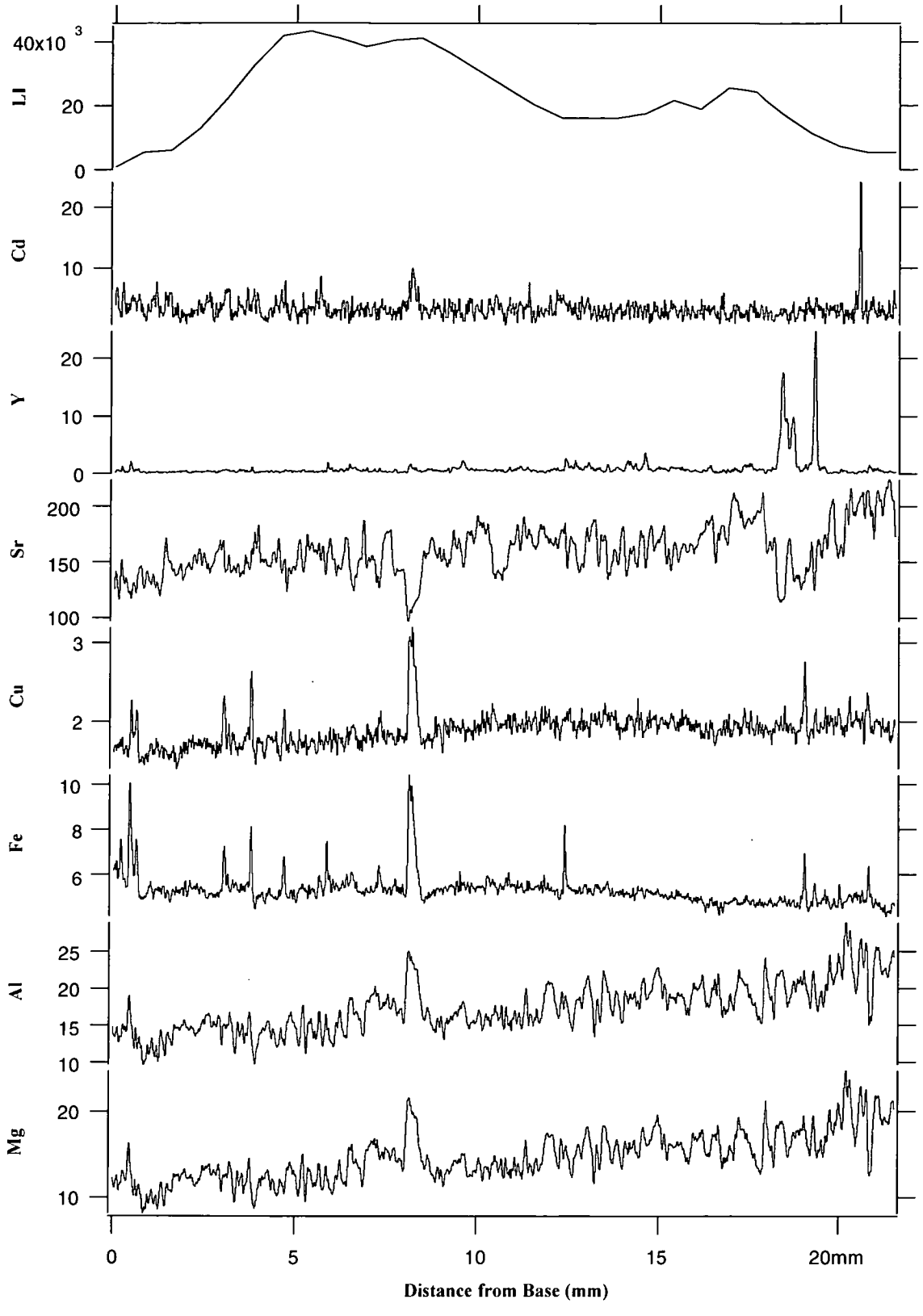

Figure 5.4 (a). **Results of laser ablation ICP-MS analysis of BFM-93-2 together with luminescence intensity (LI) results. These scans were done in order to select minor elements in speleothem calcite present in sufficient concentrations to enable further analysis. Axes are from the bottom magnesium, aluminium, iron, copper, strontium, yttrium, and cadmium, and units are in normalised counts second^{-1}.**

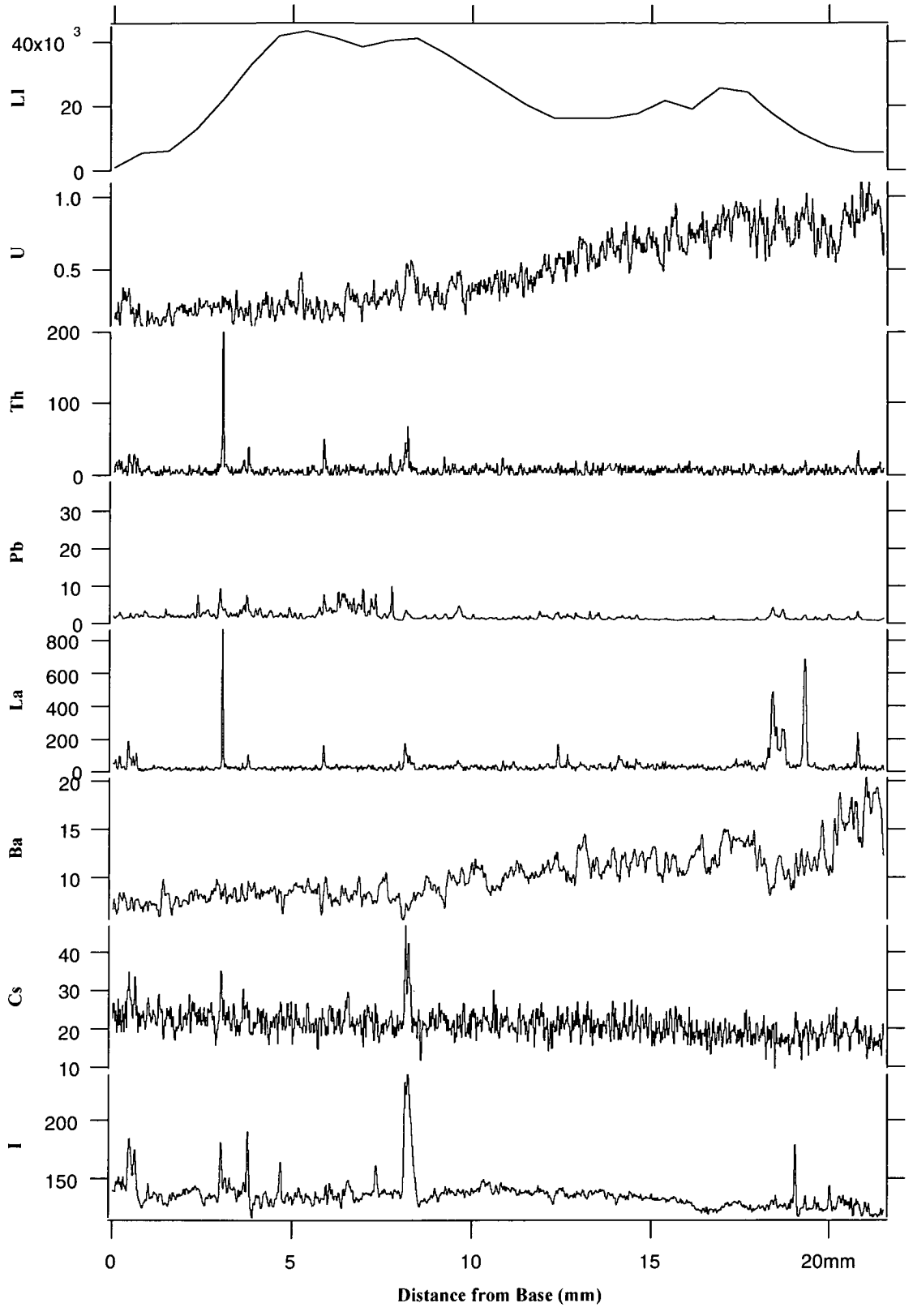

Figure 5.4 (b). **Results of laser ablation ICP-MS analysis of BFM-93-2 together with luminescence intensity (LI) results. These scans were done in order to select minor elements in speleothem calcite present in sufficient concentrations to enable further analysis. Axes are from the bottom iodine, cesium, barium, lanthanum, lead, thorium, and uranium, and units are in normalised counts second^{-1}.**

Visual inspection of the BFM-J96 results reveals that the relationships between the elements are complex, for example very strong positive correlations exist between Sr and Ba between 1975 and 1980 in Figure 5.7 (a), 1930 and 1945 in Figure 5.7 (b), 1905 and 1920 in Figure 5.7 (c), 1865 and 1872 in Figure 5.7 (d), 1851 and 1861 in Figure 5.7 (e), at both the high- and low-frequencies in some cases. But also note that Mg and U appear to be negatively correlated in some sections and positively correlated in others. This clearly illustrates the problems of analysing discrete sections of a sample as the degree of correlation may change significantly between sections.

Table 5.1. Correlation coefficients (r) for the low frequency (untreated, UT) and high frequency (detrended, DT) records from high-resolution laser ablation ICP-MS analysis of BFM-J96. DT correlation coefficients are shaded.

Element	Mg	Sr	Ba	U
Mg	$_{DT}\backslash^{UT}$	-0.001	0.02	0.29
Sr	0.10	$_{DT}\backslash^{UT}$	0.61	0.06
Ba	0.095	0.57	$_{DT}\backslash^{UT}$	0.18
U	0.081	-0.007	0.005	$_{DT}\backslash^{UT}$

5.3.1.3. BFM-J96 Chronology

The minimum average growth rate of BFM-J96 is 0.163 mm year^{-1} (162.5 μm year^{-1}), calculated using the height of 26 mm and the maximum period of deposition of 160 years. Since the width of the laser ablation window (20 μm) is small enough to sample at sub-annual resolution, dating by autocorrelation was attempted by counting the seasonal cycles of the minor elements. The minimum growth rate suggests that the number of years per millimetre should be approximately 6, assuming that deposition of BFM-J96 has been constant and continuous. It is anticipated that identifying individual years would be straightforward given the large seasonal temperature differences between winter and summer, and that although precipitation is relatively constant throughout the year effective precipitation would be much reduced in summer.

In order to construct a chronology, the seasonal patterns of minor elements are used to identify individual years. The slice number and corresponding year are recorded in order to create a time/distance function by linear interpolation. In comparison with other samples the identification of a seasonal pattern was extremely difficult, and the accuracy of the chronology is questionable. Instrumental temperature records, monthly from 1921 to 1991, and precipitation records, monthly from 1866 to 1991, for Bath, located approximately 50 km from Browns Folly Mine, are plotted against the minor element results of BFM-J96 in Figure 5.8 (a) and (b). Given the difficulty in establishing a chronology it is very difficult to see any clear relationship between the instrumental climatic data and the minor element variations.

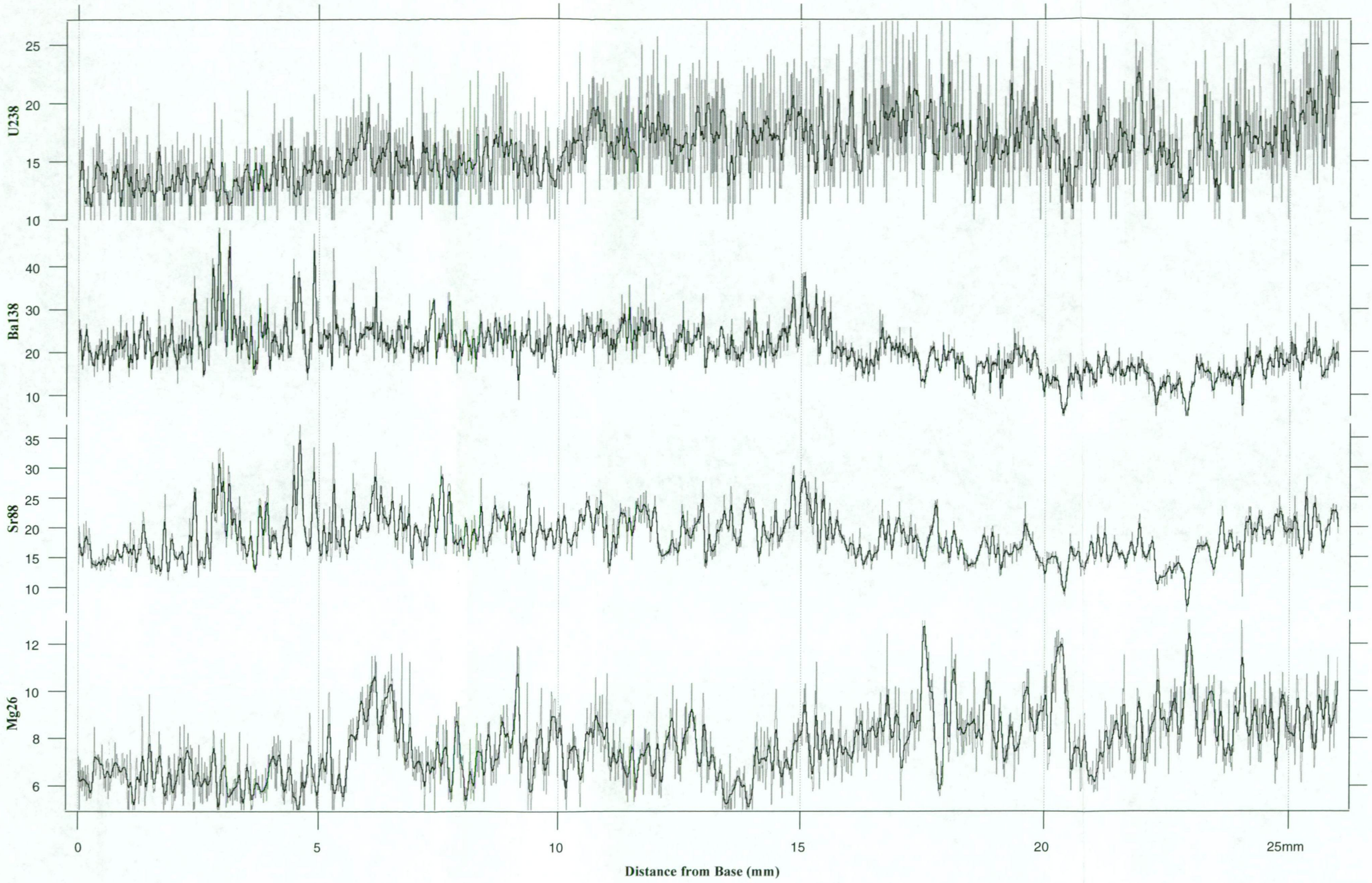

Figure 5.5. **Results of low resolution laser ablation ICP-MS analysis of BFM-J96 (5.2c) plotted versus distance from base. Since mining was abandoned in 1886 the maximum period of deposition is approximately 160 years, the sample was collected in 1996. Axes are from the bottom: magnesium, strontium, thorium, and uranium, and units are in normalised counts second^{-1}.**

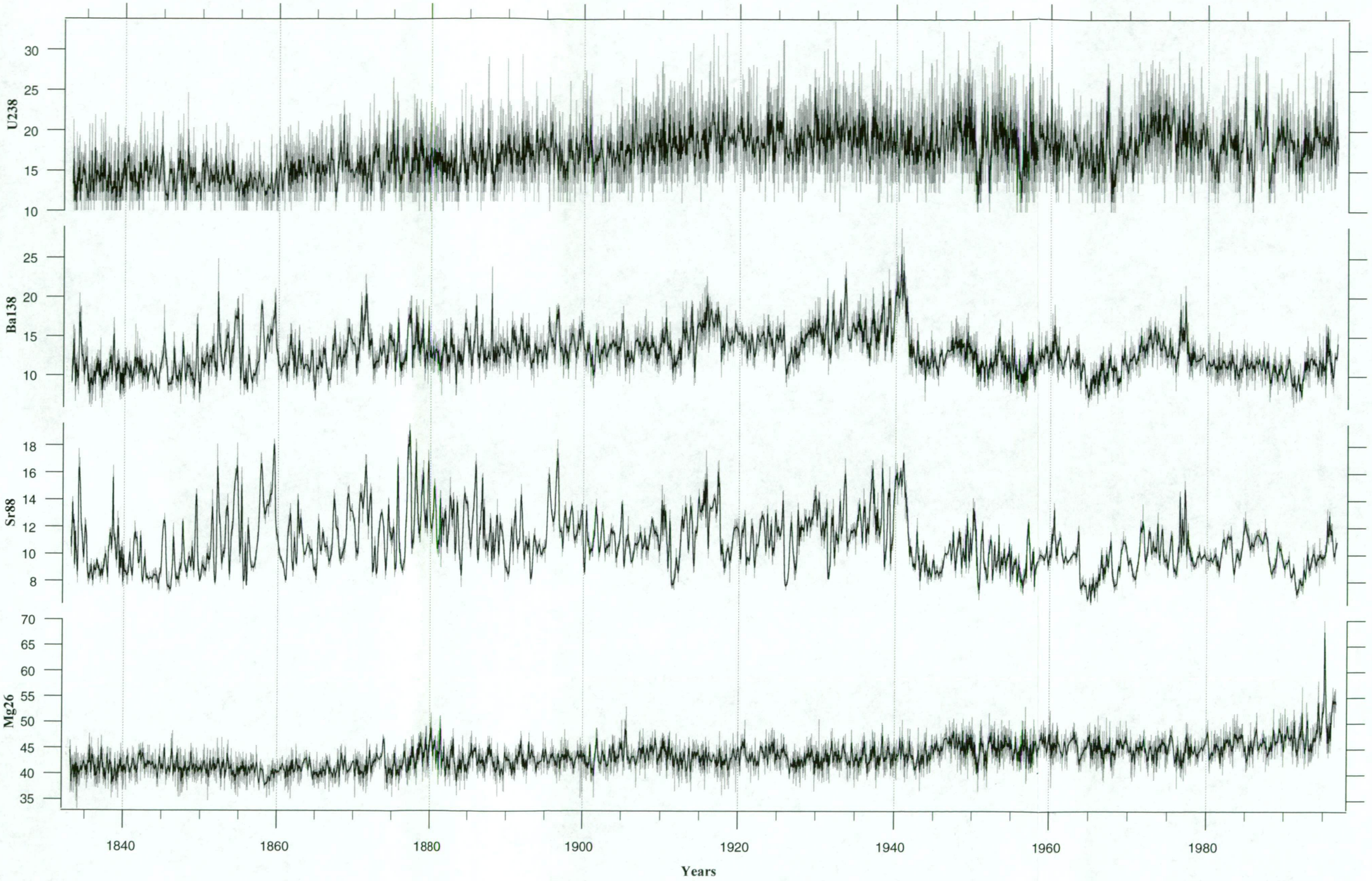

Figure 5.6. **Results of high resolution laser ablation ICP-MS analysis of BFM-J96 (5.2c) plotted versus distance from base. Since mining was abandoned in 1886 the maximum period of deposition is approximately 160 years, the sample was collected in 1996. Axes are from the bottom: magnesium, strontium, thorium, and uranium, and units are in normalised counts second^{-1}.**

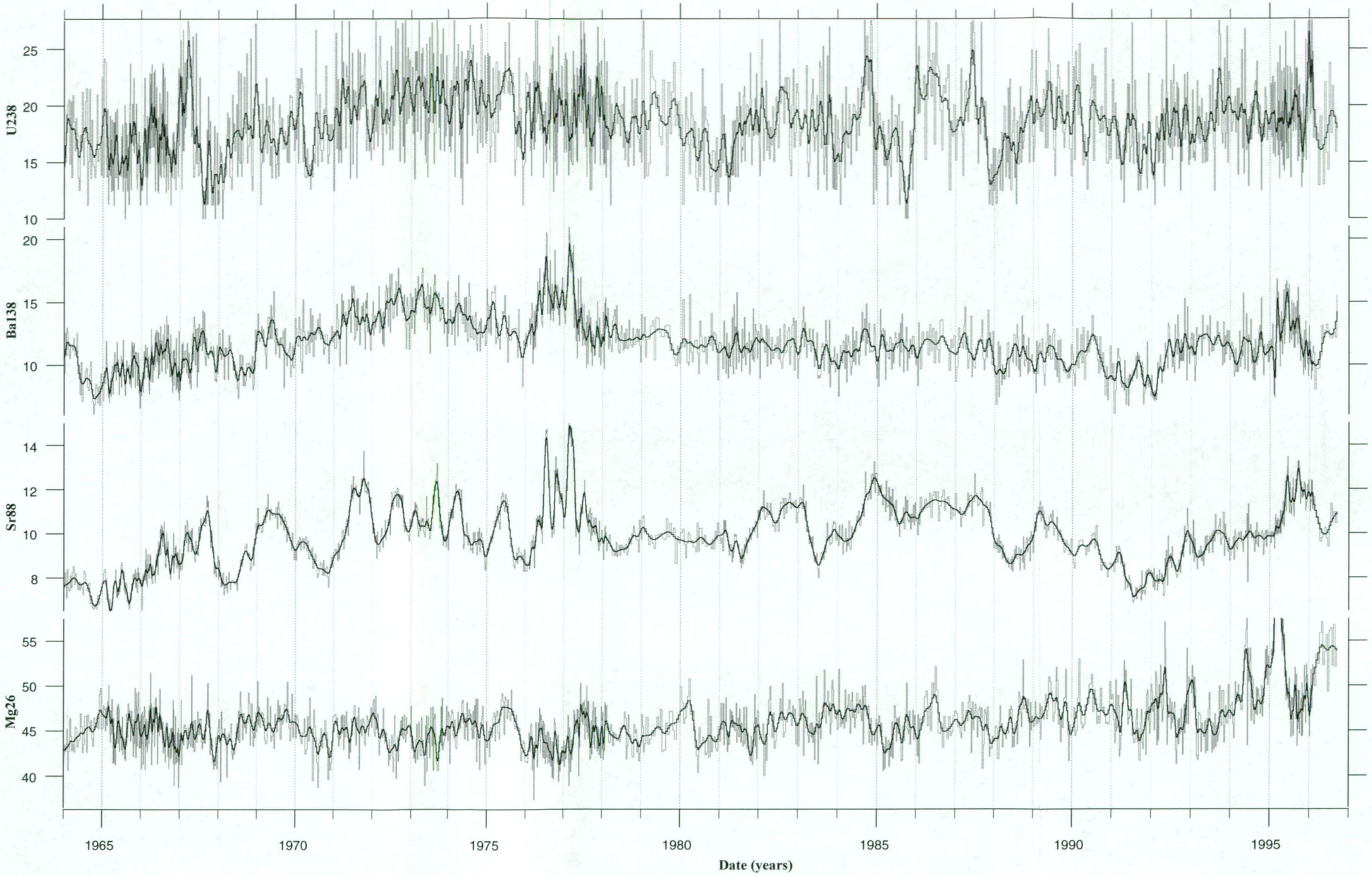

Figure 5.7 (a). **Results of high resolution laser ablation ICP-MS analysis of BFM-J96 (5.2c) plotted versus age in years, in this graph from 1965 to 1996. Since mining was abandoned in 1886 the maximum period of deposition is approximately 160 years, the sample was collected in 1996. The chronology was established by autocorrelation by counting the seasonal pattern of the minor elements and assuming that growth was continuous. Axes are from the bottom: magnesium, strontium, thorium, and uranium, and units are in normalised counts second^{-1}.**

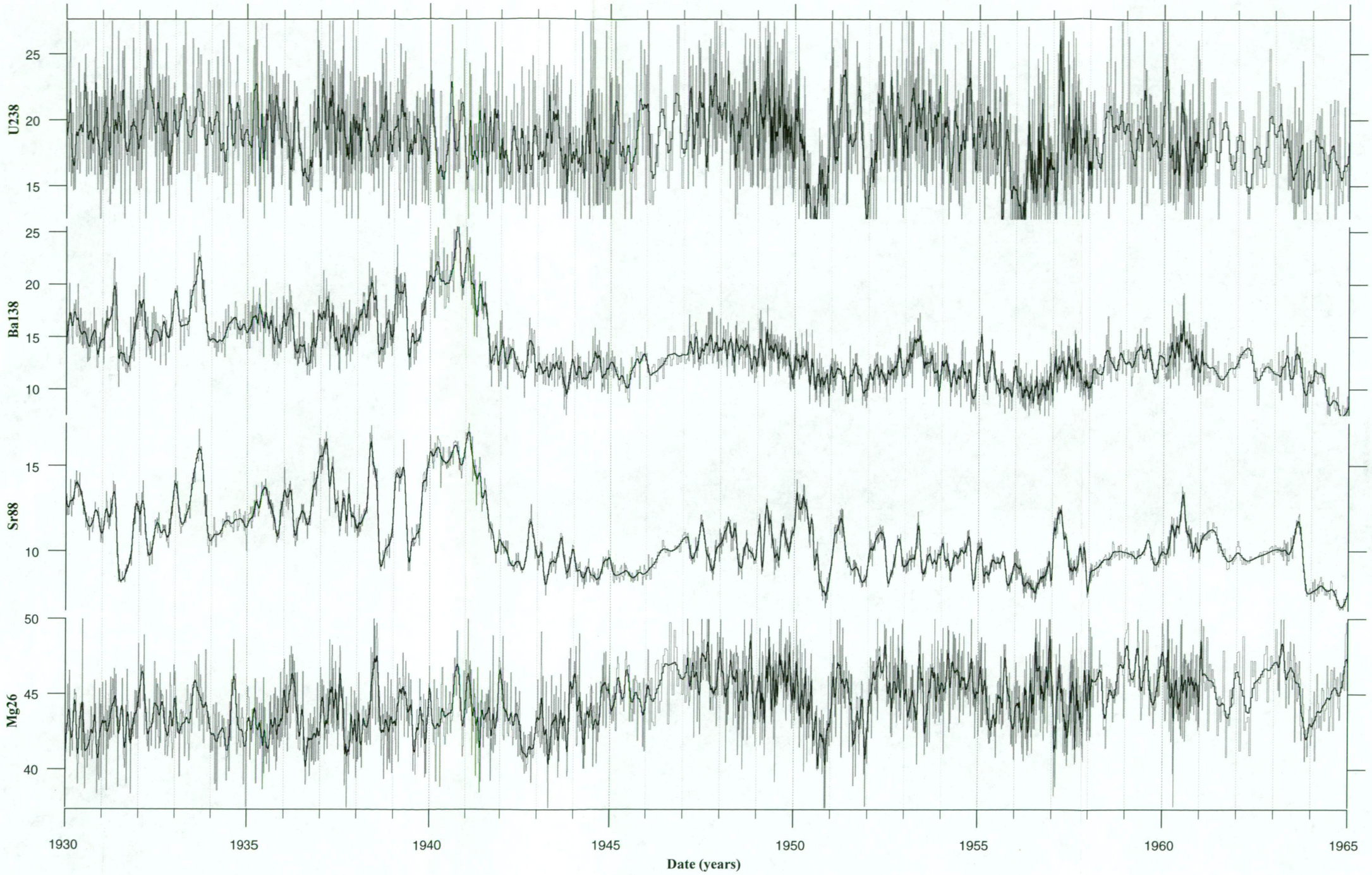

Figure 5.7 (b). **Results of high resolution laser ablation ICP-MS analysis of BFM-J96 (5.2c) plotted versus age in years, in this graph from 1930 to 1965. Since mining was abandoned in 1886 the maximum period of deposition is approximately 160 years, the sample was collected in 1996. The chronology was established by autocorrelation by counting the seasonal pattern of the minor elements and assuming that growth was continuous. Axes are from the bottom: magnesium, strontium, thorium, and uranium, and units are in normalised counts second^{-1}.**

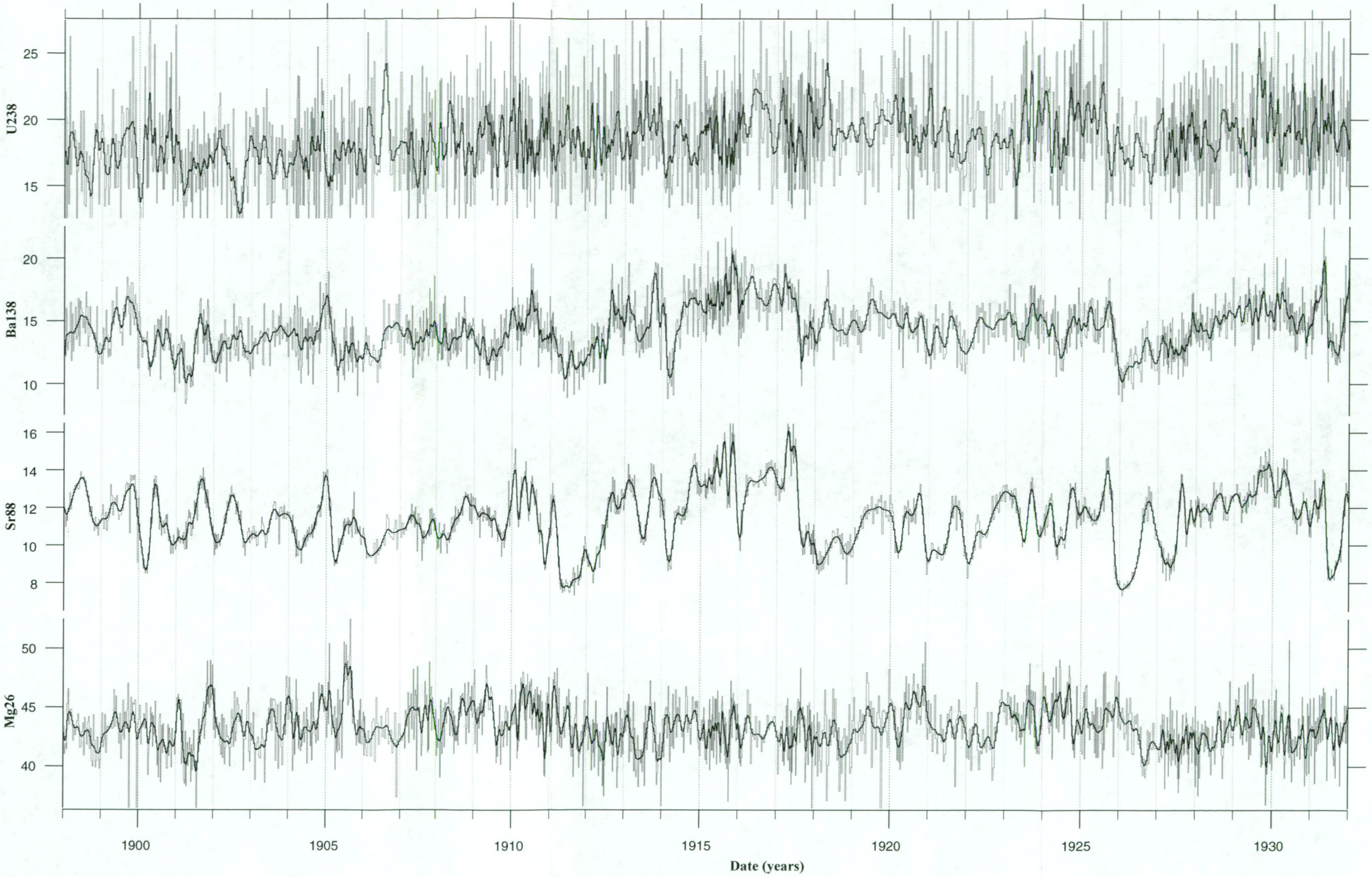

Figure 5.7 (c). **Results of high resolution laser ablation ICP-MS analysis of BFM-J96 (5.2c) plotted versus age in years, in this graph from 1900 to 1930. Since mining was abandoned in 1886 the maximum period of deposition is approximately 160 years, the sample was collected in 1996. The chronology was established by autocorrelation by counting the seasonal pattern of the minor elements and assuming that growth was continuous. Axes are from the bottom: magnesium, strontium, thorium, and uranium, and units are in normalised counts second^{-1}.**

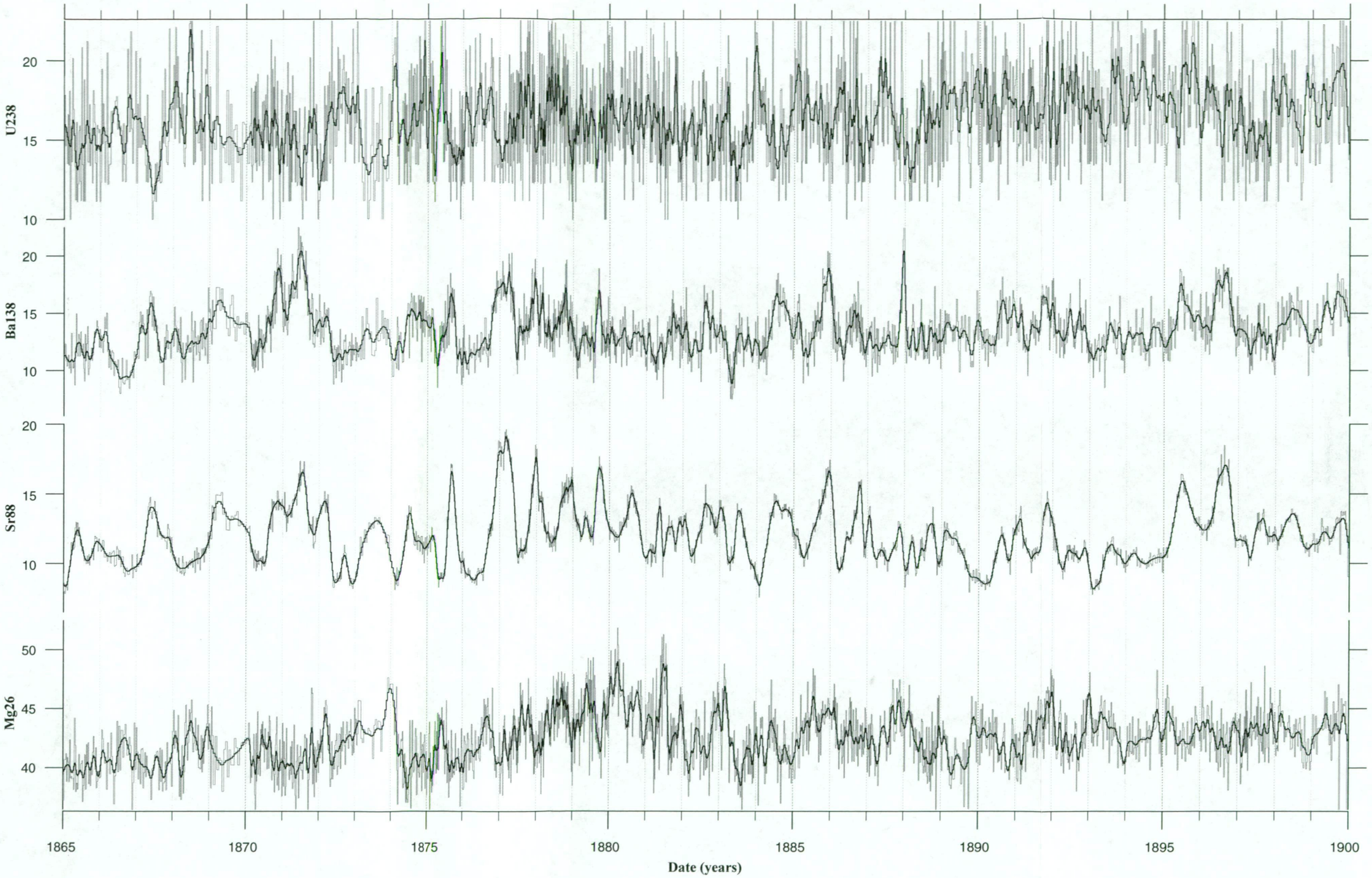

Figure 5.7 (d). **Results of high resolution laser ablation ICP-MS analysis of BFM-J96 (5.2c) plotted versus age in years, in this graph from 1865 to 1900. Since mining was abandoned in 1886 the maximum period of deposition is approximately 160 years, the sample was collected in 1996. The chronology was established by autocorrelation by counting the seasonal pattern of the minor elements and assuming that growth was continuous. Axes are from the bottom: magnesium, strontium, thorium, and uranium, and units are in normalised counts second^{-1}.**

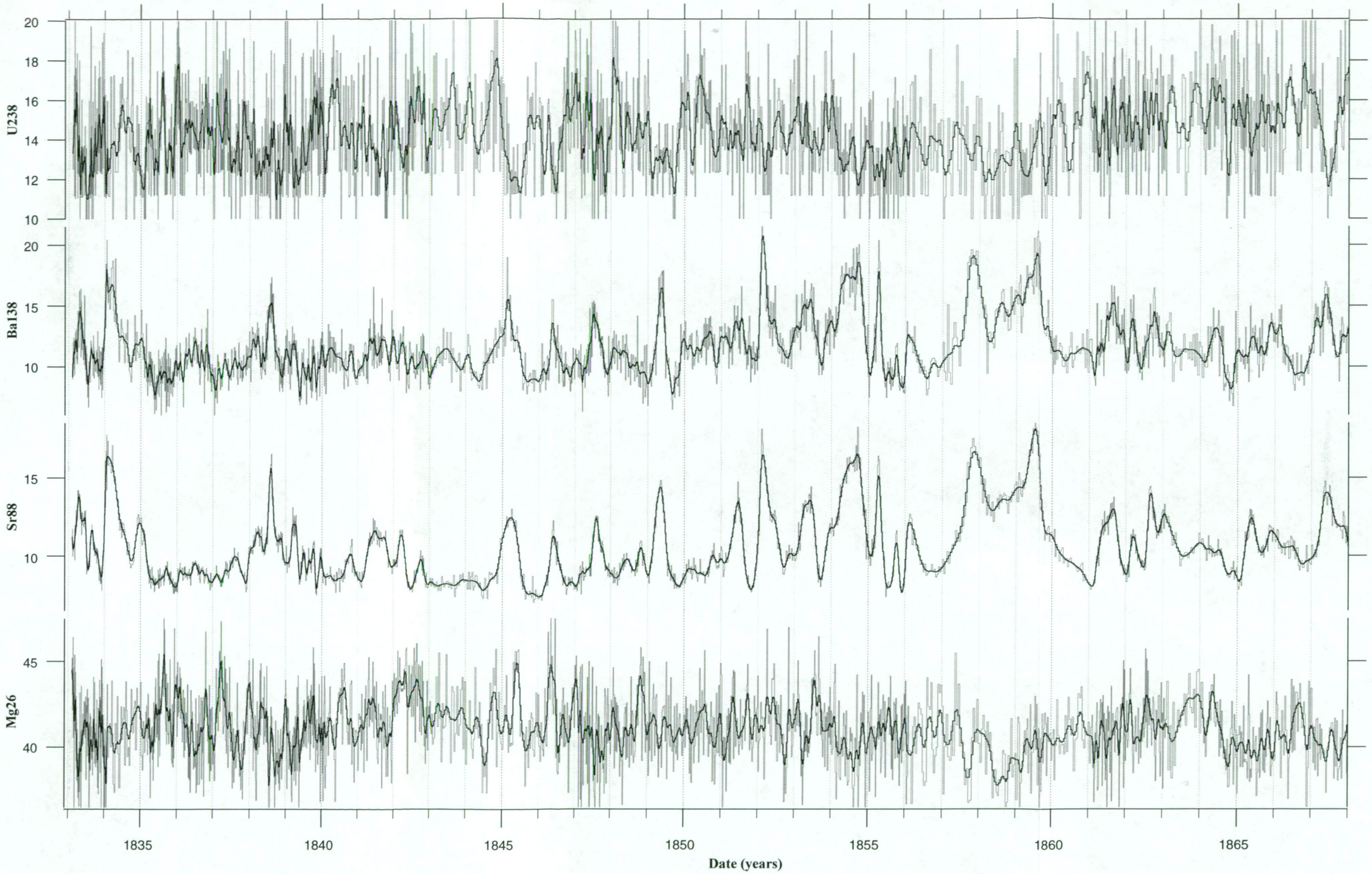

Figure 5.7 (e). **Results of high resolution laser ablation ICP-MS analysis of BFM-J96 (5.2c) plotted versus age in years, in this graph from 1835 to 1865. Since mining was abandoned in 1886 the maximum period of deposition is approximately 160 years, the sample was collected in 1996. The chronology was established by autocorrelation by counting the seasonal pattern of the minor elements and assuming that growth was continuous. Axes are from the bottom: magnesium, strontium, thorium, and uranium, and units are in normalised counts second^{-1}.**

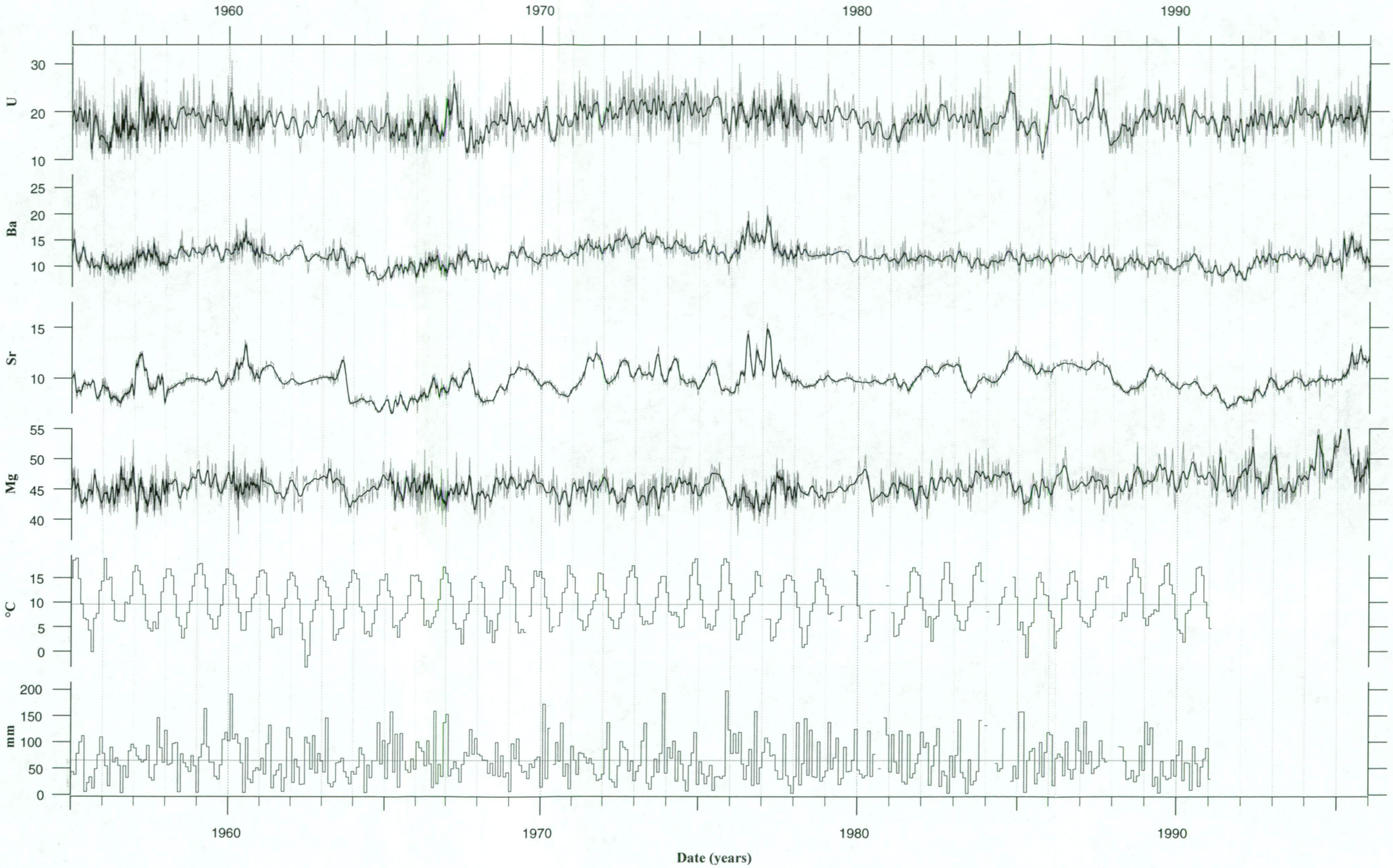

Figure 5.8 (a). **Results of high resolution laser ablation ICP-MS analysis of BFM-J96 (5.2c) plotted versus age in years, in this graph from 1960 to 1996, together with instrumental climate data from Bath, located approximately 50 km from Browns Folly Mine. The chronology was established by autocorrelation by counting the seasonal pattern of the minor elements and assuming that growth was continuous. Axes are from the bottom: monthly precipitation in mm, monthly temperature in °C, magnesium, strontium, thorium, and uranium, and units are in normalised counts second^{-1}.**

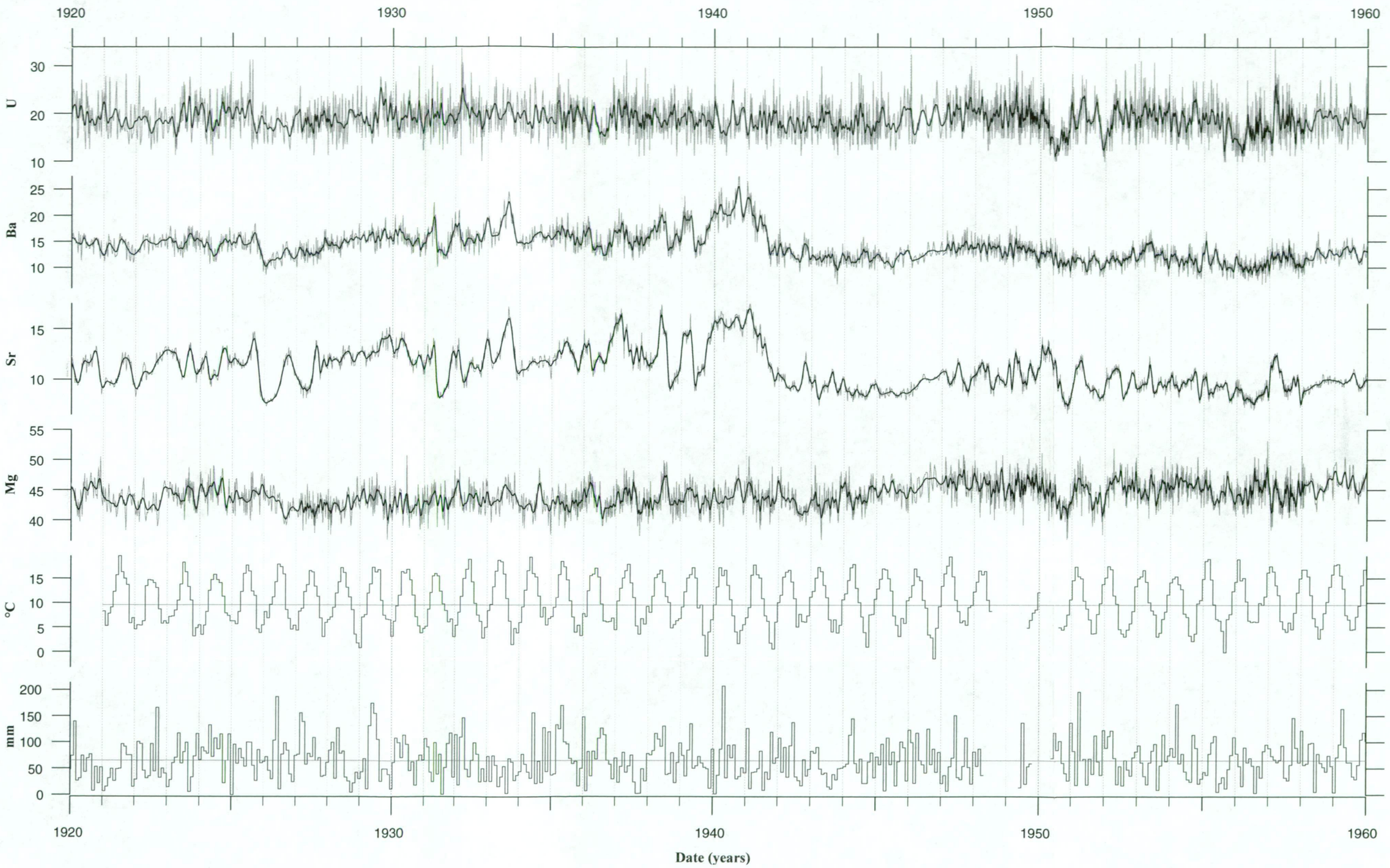

Figure 5.8 (b). **Results of high resolution laser ablation ICP-MS analysis of BFM-J96 (5.2c) plotted versus age in years, in this graph from 1920 to 1960, together with instrumental climate data from Bath, located approximately 50 km from Browns Folly Mine. The chronology was established by autocorrelation by counting the seasonal pattern of the minor elements and assuming that growth was continuous. Axes are from the bottom: monthly precipitation in mm, monthly temperature in °C, magnesium, strontium, thorium, and uranium, and units are in normalised counts second^{-1}.**

5.4.2. FC-SS5 Minor Element Results

This 151 mm long soda-straw stalactite has been collected from Frankcombe Cave, Florentine Valley, Tasmania, Australia, and is shown in Figure 5.2a. The results of a single high-resolution laser ablation ICP-MS analysis of magnesium, strontium, barium, and uranium along the growth axis of FC-SS5 are plotted against distance along the 151 mm analysis track in Figure 5.9. Two other analyses of the tip section were done only to investigate the lateral variation of minor elements in soda-straw stalactites, these results are presented in Figure 5.14.

In Figure 5.9 it is relatively difficult to see the fine scale structure of the FC-SS5 results therefore several "windows" of up to approximately 15 years long are presented in Figure 5.10 (a) to (i). These higher resolution windows show various features of the results such as high and low frequency oscillations, positive and negative correlations between elements and pairs of elements, and possible growth rate variations. Overall the most striking feature is the consistency of peaks and troughs in the Sr and Ba results, it is also evident in the Mg and U traces but not to the same extent.

5.4.2.1. FC-SS5 Minor Element Relationships

A correlation matrix of the low-frequency (untreated) and high-frequency (detrended) records for the whole length of FC-SS5 together with results for the upper, middle, and lower segments are presented in Table 5.2. Both the low and high frequency results have strong positive correlations between Sr and Ba and very similar r-values, 0.90 and 0.88 respectively. The strength of the association suggest that the processes controlling Sr and Ba geochemistry are very similar and do not vary significantly at different temporal scales.

A positive correlation is also found between Mg and U, ($r = 0.61$) in the untreated results but in the detrended results the correlation is weaker ($r = 0.32$). In the untreated results the correlations between the other elements do not exceed r-values of 0.10 suggesting that there is no relationship at low frequencies. At the higher frequencies weak positive relationships occur between the Mg-Sr ($r = 0.36$) and Mg-U ($r = 0.32$) and a weak negative relationship between Mg-Ba ($r = -0.35$). It is interesting to compare the r-values with some of the high resolution windows in Figure 5.10 (c and d) and note that the majority of Mg peaks are synchronised with troughs in Sr content and have a positive correlation, yet the Sr and Ba are strongly correlated and Mg has a negative relationship with Ba. This highlights the need for several more higher quality analyses to investigate the elemental relationships as it is difficult to say whether these relationships are real or whether they are an artefact of the Mg data processing.

5.4.2.2. Discrete Features in the FC-SS5 Minor Element Results

Two very large peaks in the Sr and Ba results, at approximately 1959 (22 mm) and 1965 (27 mm) and similar peaks in the Mg and U results at around 1959, in Figure 5.10(h), are related to a ridge feature on the surface of FC-SS5, that is visible under a microscope. It suggests that physical features on the surface may influence minor element composition but further investigation is required.

Table 5.2. Correlation coefficients (R) for the low frequency (untreated, UT) and high frequency (detrended, DT) records from high-resolution laser ablation ICP-MS analysis of FC-SS5. The numbers in brackets in the first column relate to the number of slices used and DT correlation coefficients are shaded.

Segment	Element	Mg	Sr	Ba	U
All	Mg	$_{DT}\backslash^{UT}$	0.04	-0.08	0.60
(n = 56954)	Sr	0.36	$_{DT}\backslash^{UT}$	0.90	0.03
	Ba	-0.35	0.88	$_{DT}\backslash^{UT}$	-0.03
	U	0.32	-0.10	-0.08	$_{DT}\backslash^{UT}$

Several low frequency oscillations are evident in the FC-SS5 results, for example in Figure 5.10(b) there is a broad high with a period of approximately 6 mm starting at about 1793 (132 mm) and ending at around 1805 (138 mm). The length of the wave suggests that it may be related to a sunspot or Schwabe cycle but further investigation is required to confirm this. Interestingly the Sr and Ba scans and the Mg and U results at both low- and high-frequency correlate positively and the correlation between the pairs of scans, *ie* Sr and Ba versus Mg and U, correlate negatively.

At approximately 1908 (66 mm) a significant reduction in all of the minor element concentrations is observed and shown in Figure 5.10(g). This type of feature is not observed anywhere else along the analysis track. It could be related to a surface defect, such as a hole or crack in the calcite surface or might have been caused by a surface event inducing a sudden change in the water chemistry.

5.3.2.3. Spectral Analysis of FC-SS5

The marked cyclicity of the Sr and Ba results, and to a certain extent the Mg results, strongly suggest the presence of an annual signal evidenced by the considerable structure at the higher frequencies. The quasi-periodic variations have been investigated by spectral analysis, using the multi-taper method (MTM) from Ghil and Yiou (1996) and the results presented in Figure 5.11 (a) to (d). In order to test spectral analysis results, a subsample of the FC-SS5 data was taken between approximately 1840 and 1880 and analysed separately. The results are shown in Figure 5.12 (a) to (d). There are no significant differences between the analyses, even more encouraging is that the dominant wavelengths remain very close. The frequency of 0.0304, present as the dominant frequencies in the Sr and Ba spectral analysis results, corresponds to a figure of 240 sample slices in excellent agreement with the average number of slice numbers per year, 246 (± 72, 1σ).

The dominant frequencies in the Mg and U spectral analysis results are 0.0266 or 274 sample slices and 0.0305 or 239 sample slices. All of these results strongly support the conclusion that the high-frequency oscillations observed in the Sr and Ba results are annual. The uranium trace of FC-SS5 does exhibit some cyclicity but not to the same degree as the other elements, the reason for this requires further investigation. This could be done by only measuring uranium and calcium with the instrument dwell time maximised for uranium, ensuring a good signal to background ratio.

5.4.2.4. Shape and Phase Relationships Between Minor Elements in FC-SS5

In order to investigate the shape and phase relationships of minor elements in a normal year, an average annual cycle for FC-SS5 has been derived. The method involves identifying each year and corresponding sample slice number. A linear interpolation is done with the same number of points as the minor element data and allows them to be plotted against time. A smoothing spline interpolation, a least squares variant of a cubic spline, is used to adjust each year to the same number of data points, in this case each year consists of a 30 point sequence. The smoothing spline data have been divided into two-yearly segments (60 points) in order to get a complete annual cycle and the data averaged, the result is an "average" year.

The results for the full data set together with a data subsample that excludes the large peaks are presented in Figure 5.13. Strontium and barium variations represent summer peaks and the trough between them autumn/winter/spring, whereas the magnesium and uranium results are, at the very least, severely lagged or very close to being diametrically opposite. The patterns of strontium and barium concentrations look very similar except that the second barium peak is much smaller than the first whereas the strontium peaks are nearly equal. The patterns of magnesium and uranium concentrations are interesting because they appear to be inversely related to those of strontium and barium. Troughs in magnesium and uranium concentrations appear to lag behind the peaks in strontium and barium concentrations.

5.4.2.5. Lateral Variation of Minor Elements in FC-SS5

Investigation of lateral variation in the minor element composition of FC-SS5 was done by several parallel laser ablation ICP-MS analyses. The tip section was scanned along three different tracks using laser ablation ICP-MS and the results are presented in Figure 5.14. No correlation analysis has been attempted between the scans due to the differences in resolution of the scans which produce traces of different lengths. However, It is evident that some spatial variability exists in the minor element composition of FC-SS5, but the cyclicity of the minor elements is common to the three scans giving confidence in its reproducibility along different analysis tracks and their use for autocorrelation. Future attempts at analysing the lateral variations of minor elements in speleothems should try to ensure that the resolution of the analysis track is the same, that the tracks are parallel, and that the analyses are done consecutively in order to minimise experimental error.

Chronologies were established by autocorrelation of minor element results, determined by laser ablation ICP-MS, and measurements of surface growth rings with dendrochronological equipment (Section 5.3.3). Both techniques rely on the assumption that the sample was

active at the time of collection and has been growing continuously. The minor element chronology is dependent on the assumption that the Sr and Ba peaks at the tip of the sample *ie* the minimum age, represent a summer maximum as the sample was collected in late February. Using the autocorrelation method chronologies were determined independently by the author and by Mr John Hellstrom. They obtained activity periods of 1765 to 1996 and 1769 to 1996. The author also used the dendrochronology method to obtain an activity period from 1774 to 1996.

The closeness of the three results gives a great deal of confidence in the chronology particularly as one was established by a different method. Ideally a radiometric dating method such as AMS radiocarbon or ^{210}Pb excess dating (Chapter 4) should have been applied in order to provide precise independent temporal control (for example, Genty *et al.*, 1998 or Tanahara *et al.*, 1998). Unfortunately this was not attempted with FC-SS5 as the AINSE dating work (Chapter 4), that could have provided such control, was done prior to the ICP-MS analysis being initiated.

5.4.2.6. Comparison of FC-SS5 Minor Element Results with Instrumental Records

Attempts were made to compare the growth record of FC-SS5 and instrumental climate records from several stations located in the vicinity of the Junee-Florentine Valley, including Maydena and Strathgordon. The growth record of FC-SS5 was calculated using the measured ring width results from the incremental counting and dendrochronological methods (see Section 5.3.3). Annual recharge/effective precipitation was calculated using the Thornthwaite model. No significant correlations ($R < \pm 0.4$) were observed between the ring width data and climate records, including interannual variation and lagged data. Lag calculations of up to 12 months were done to simulate the delay that precipitation has in reaching the sample. Further investigation is required to see if the lack of correlation between the climate data and the growth rate is due to the climate stations being so far from the site, placing a station above the cave would be ideal, or due to other factors.

5.4.2.7. Analysis of UV Luminescence Microbanding of FC-SS5

Luminescence microbanding of FC-SS5 was investigated by photographing the sample under a UV fluorescent tube and data processing followed the method of Hellstrom (1998). Luminescence banding was present but sporadic thus no detailed analysis of a pattern or comparison with the minor element data was possible. The sections where luminescence banding was present appeared to have a similarly cyclic pattern in light intensity, measured by converting the image to grey scale, to the minor elements. Further work will be required to investigate the relationship between the minor elements and the luminescence banding.

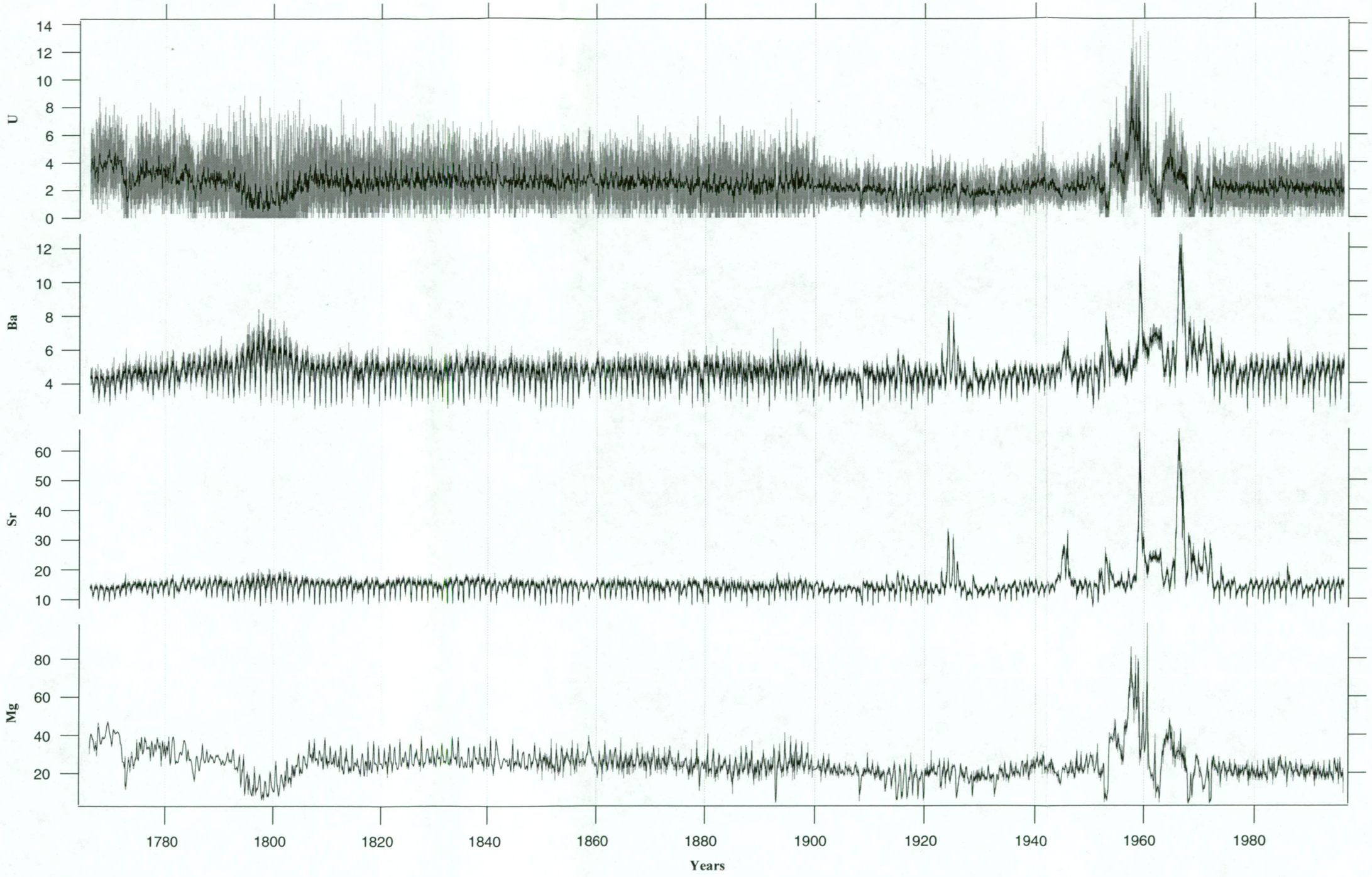

Figure 5.9. Results of minor element analysis of FC-SS5 (Figure 5.2a), a 151 mm long soda-straw stalactite from Frankcombe Cave, Tasmania, using high resolution laser ablation ICP-MS. Axes are from the bottom magnesium, strontium, thorium, and uranium, and units are in normalised counts second^{-1}. The most striking feature is the regularity of the quasi-periodical minor element variations along the entire length of the sample. The two major peaks in the minor element scans at approximately 1959 and 1965 are associated with a ridge feature on the surface of the soda-straw stalactite.

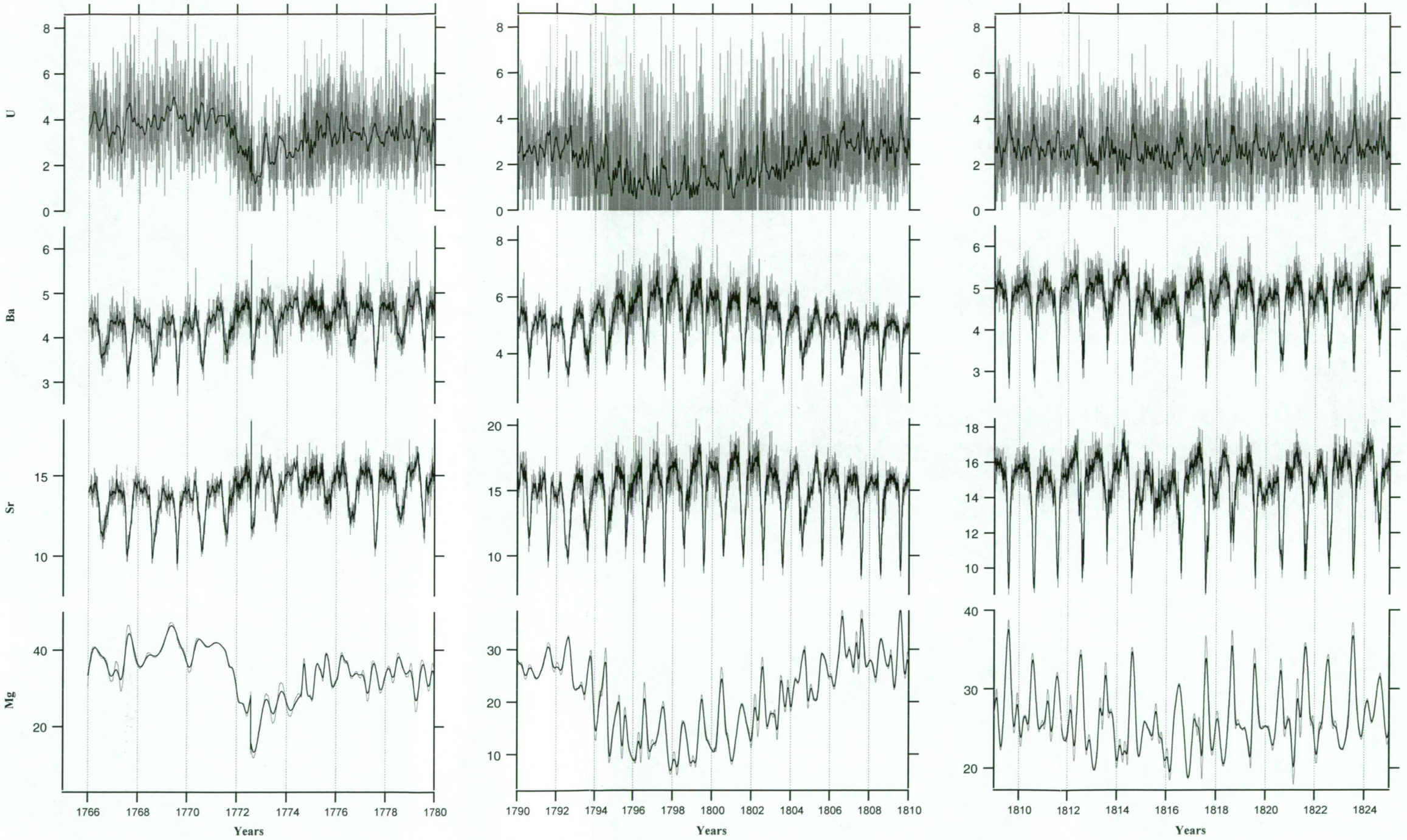

Figure 5.10 (a) to (c). **Results of minor element analysis of FC-SS5 (Figure 5.2a), a 151 mm long soda-straw stalactite from Frankcombe Cave, Tasmania, using high resolution laser ablation ICP-MS. The three diagrams, (a), (b), and (c), correspond to the time periods, respectively 1766 to 1780, 1790 to 1810, and 1809 to 1825. The chronology is based on autocorrelation of minor element patterning on the assumption that the sample was active at the time of collection and that growth was continuous. Y-axis units are in normalised counts second^{-1}.**

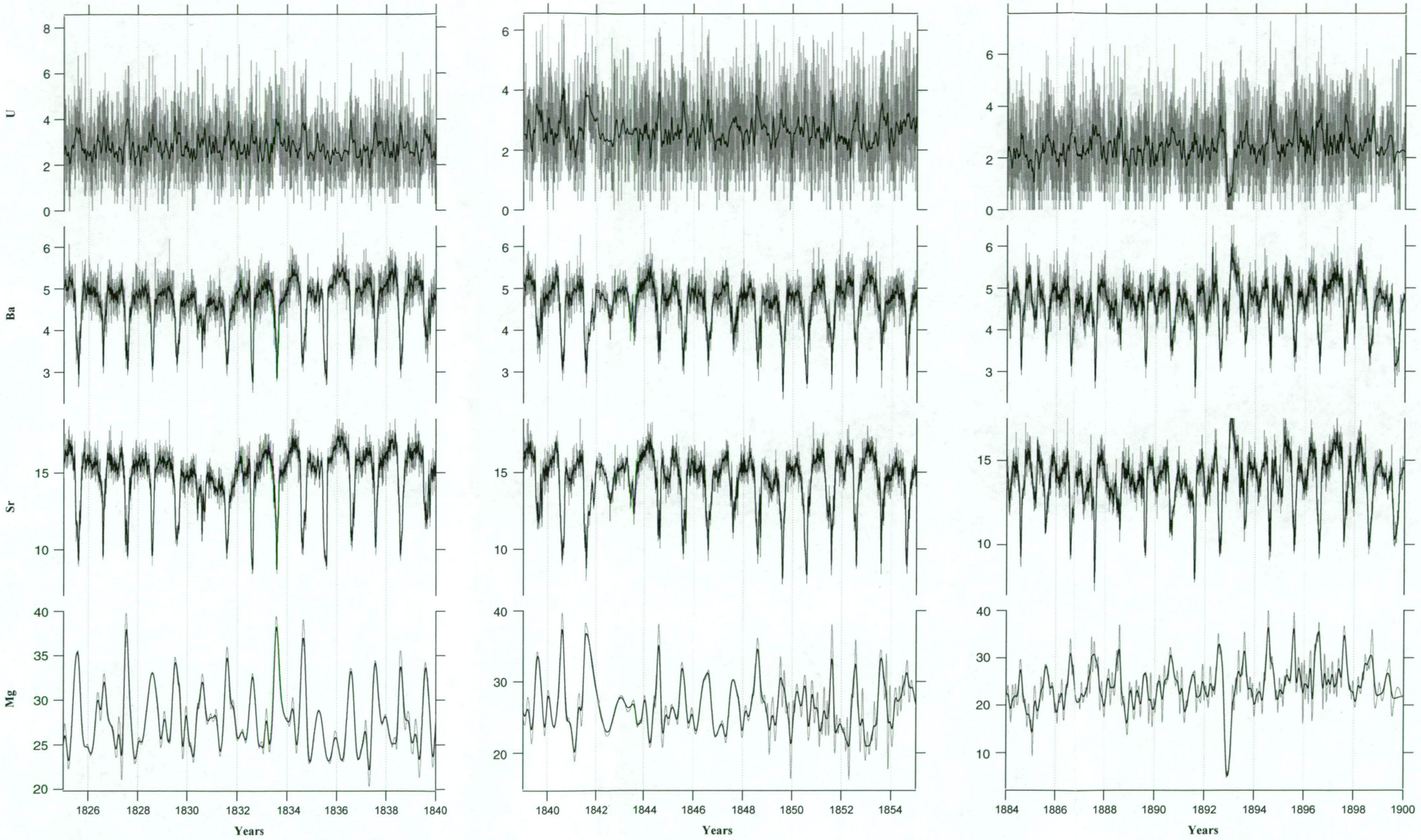

Figure 5.10 (d) to (f). Results of minor element analysis of FC-SS5 (Figure 5.2a), a 151 mm long soda-straw stalactite from Frankcombe Cave, Tasmania, using high resolution laser ablation ICP-MS. The three diagrams, (d), (e), and (f), correspond to the time periods, respectively 1825 to 1840, 1839 to 1855, and 1884 to 1900. The chronology is based on autocorrelation of minor element patterning on the assumption that the sample was active at the time of collection and that growth was continuous. Y-axis units are in normalised counts second^{-1}.

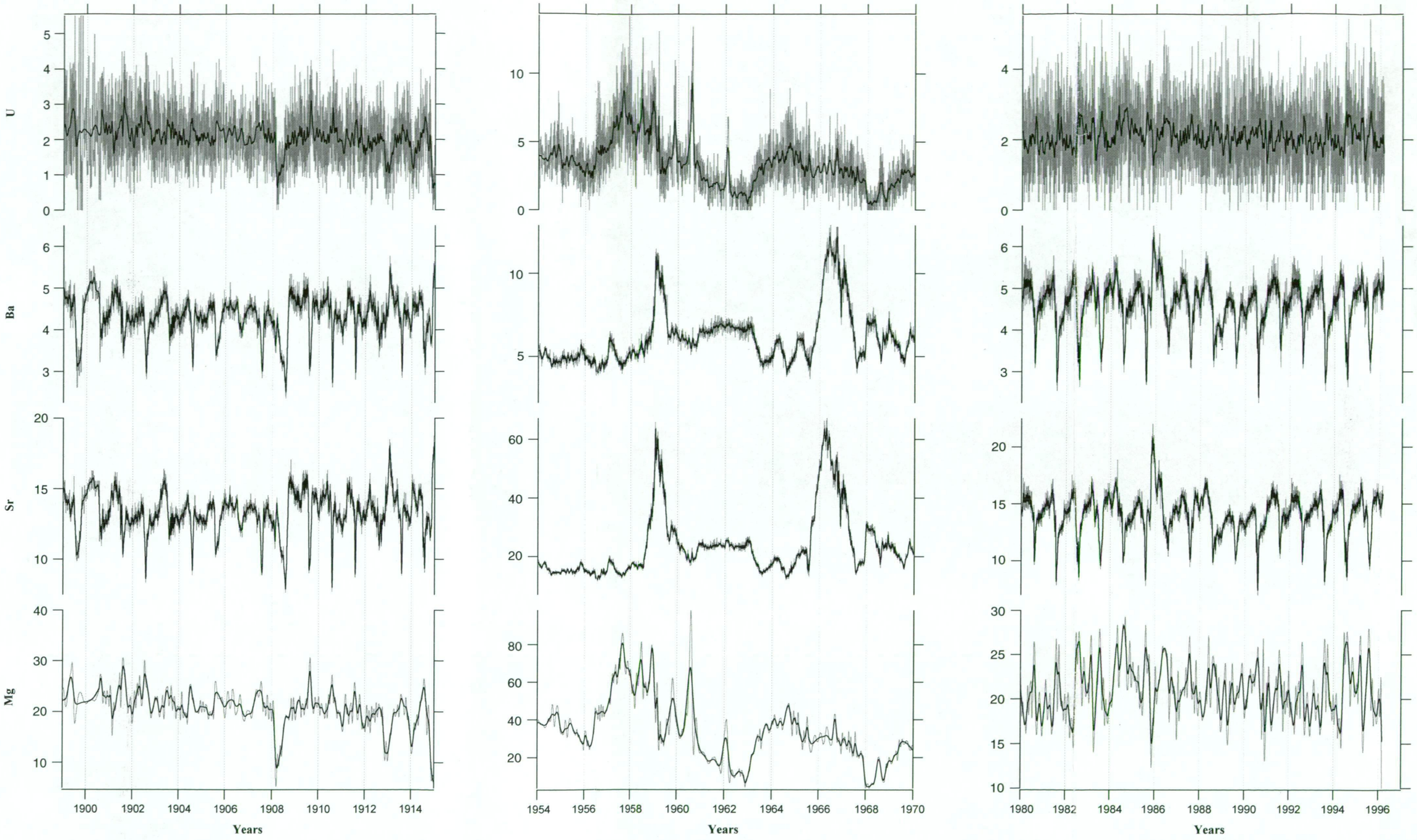

Figure 5.10 (g) to (i). **Results of minor element analysis of FC-SS5 (Figure 5.2a), a 151 mm long soda-straw stalactite from Frankcombe Cave, Tasmania, using high resolution laser ablation ICP-MS. The three diagrams, (g), (h), and (i), correspond to the time periods, respectively 1899 to 1915, 1955 to 1969, and 1980 to 1996. The chronology is based on autocorrelation of minor element patterning on the assumption that the sample was active at the time of collection and that growth was continuous. Y-axis units are in normalised counts second^{-1}.**

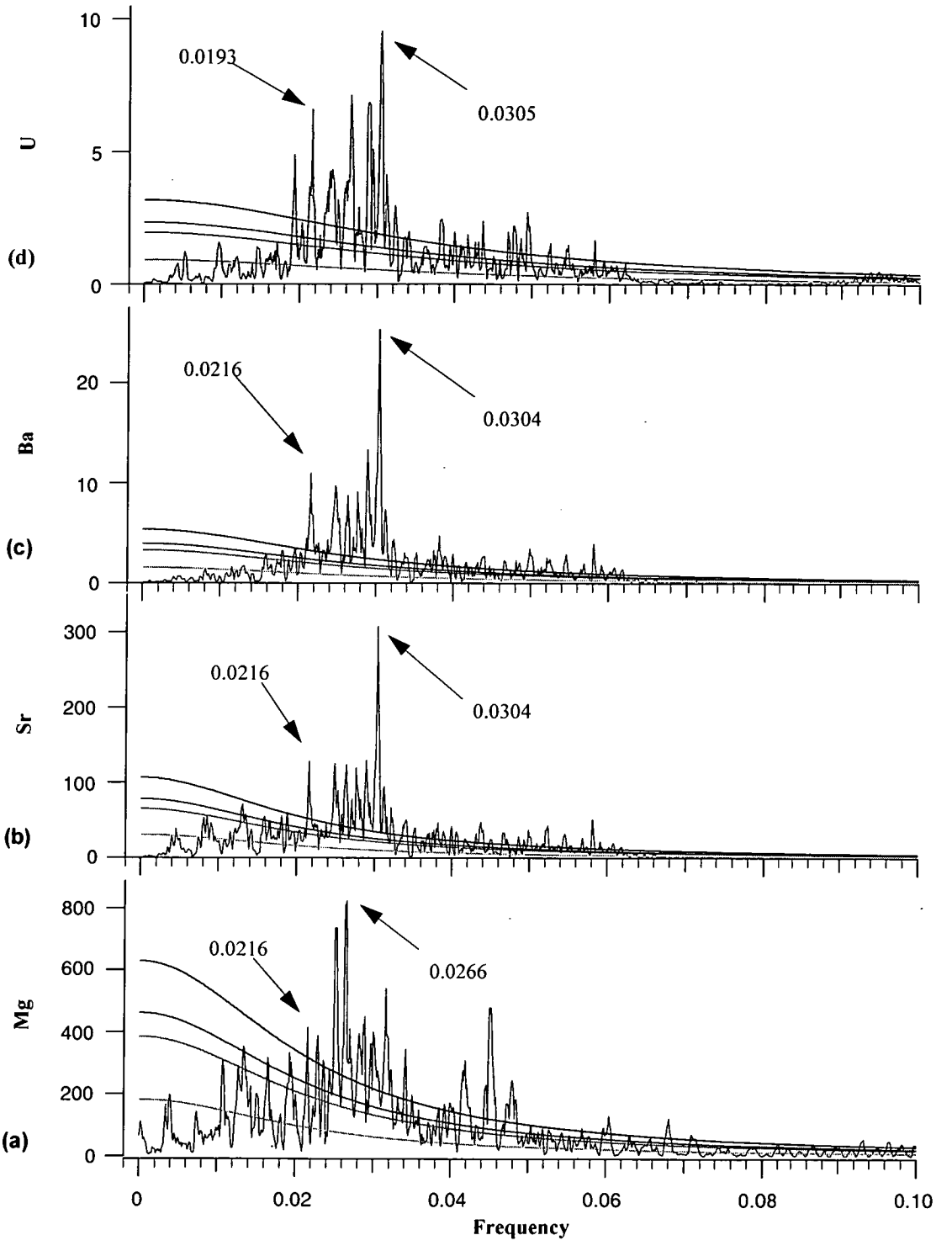

Figure 5.11. **Power spectra (n = 56954) of high-resolution laser ablation ICP-MS analysis of FC-SS5 (see Figure 5.2a), a 151 mm long soda-straw stalactite from Frankcombe Cave, Tasmania. Curved lines are levels of significance starting at 50 % (light grey, bottom line), 90 %, 95 %, and 99 %, respectively. Data have been pretreated by subtracting the median and filtering the two ridge features, represented as two large spikes in the raw data (Figure 5.9) and likely to skew the spectral analysis. Graphs (a), (b), (c), and (d) correspond respectively to, magnesium, strontium, barium, and uranium scans, and units are in normalised counts second^{-1}. Numbers on graphs are frequencies and are discussed in Section 5.3.2.3.**

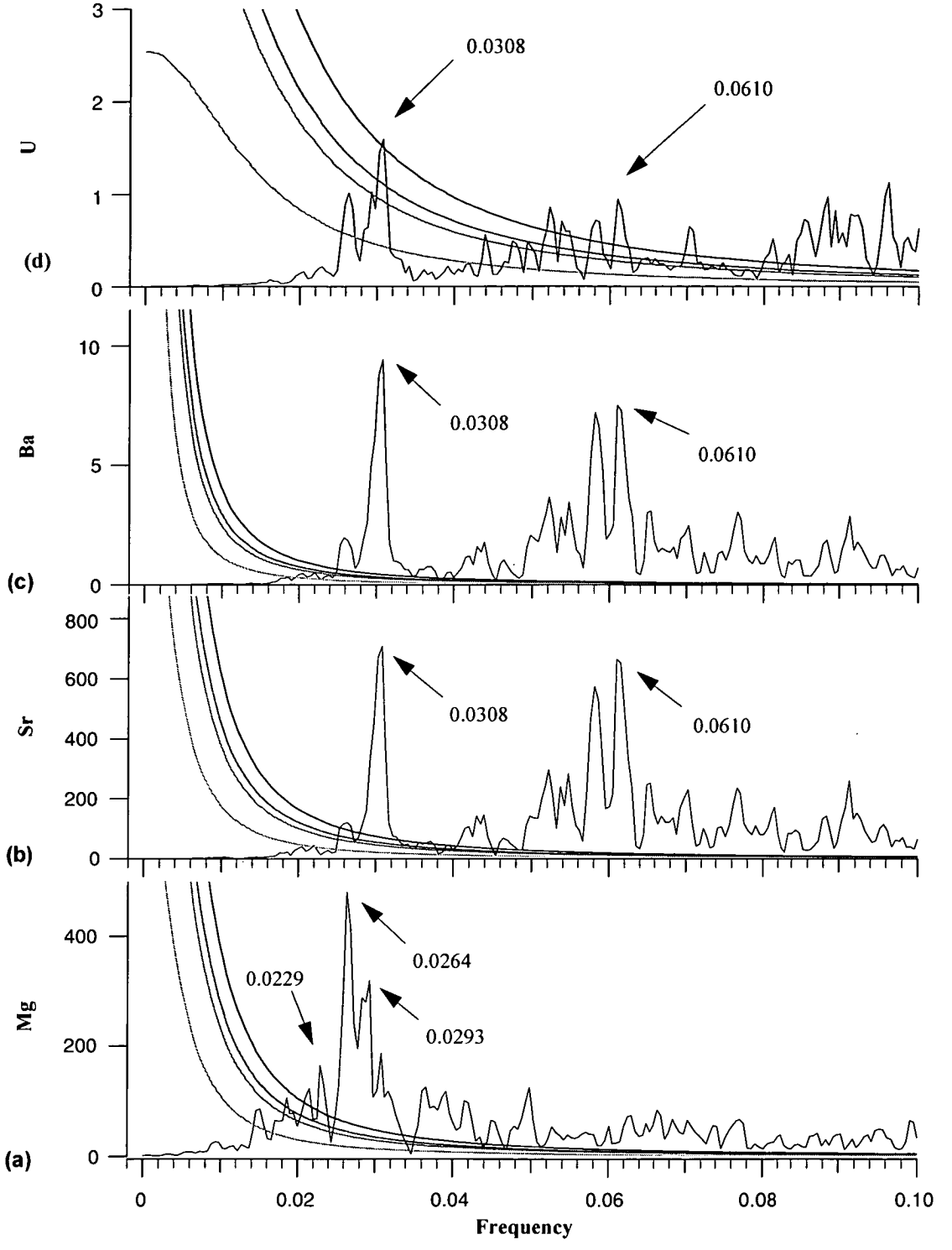

Figure 5.12. **Power spectra of a subsampled data set (n = 8000) from the high-resolution laser ablation ICP-MS analysis of FC-SS5 (Figure 5.2a), a 151 mm long soda-straw stalactite from Frankcombe Cave, Tasmania. Curved lines are levels of significance starting at 50 % (light grey, bottom line), 90 %, 95 %, and 99 %, respectively. Data have been pretreated by subtracting the median and filtering the two ridge features, represented as two large spikes in the raw data (shown in Figure 5.9) and likely to skew the spectral analysis. Graphs (a), (b), (c), and (d) correspond respectively to, magnesium, strontium, barium, and uranium scans, and units are in normalised counts second^{-1}. Numbers on graphs are frequencies and are discussed in Section 5.3.2.3.**

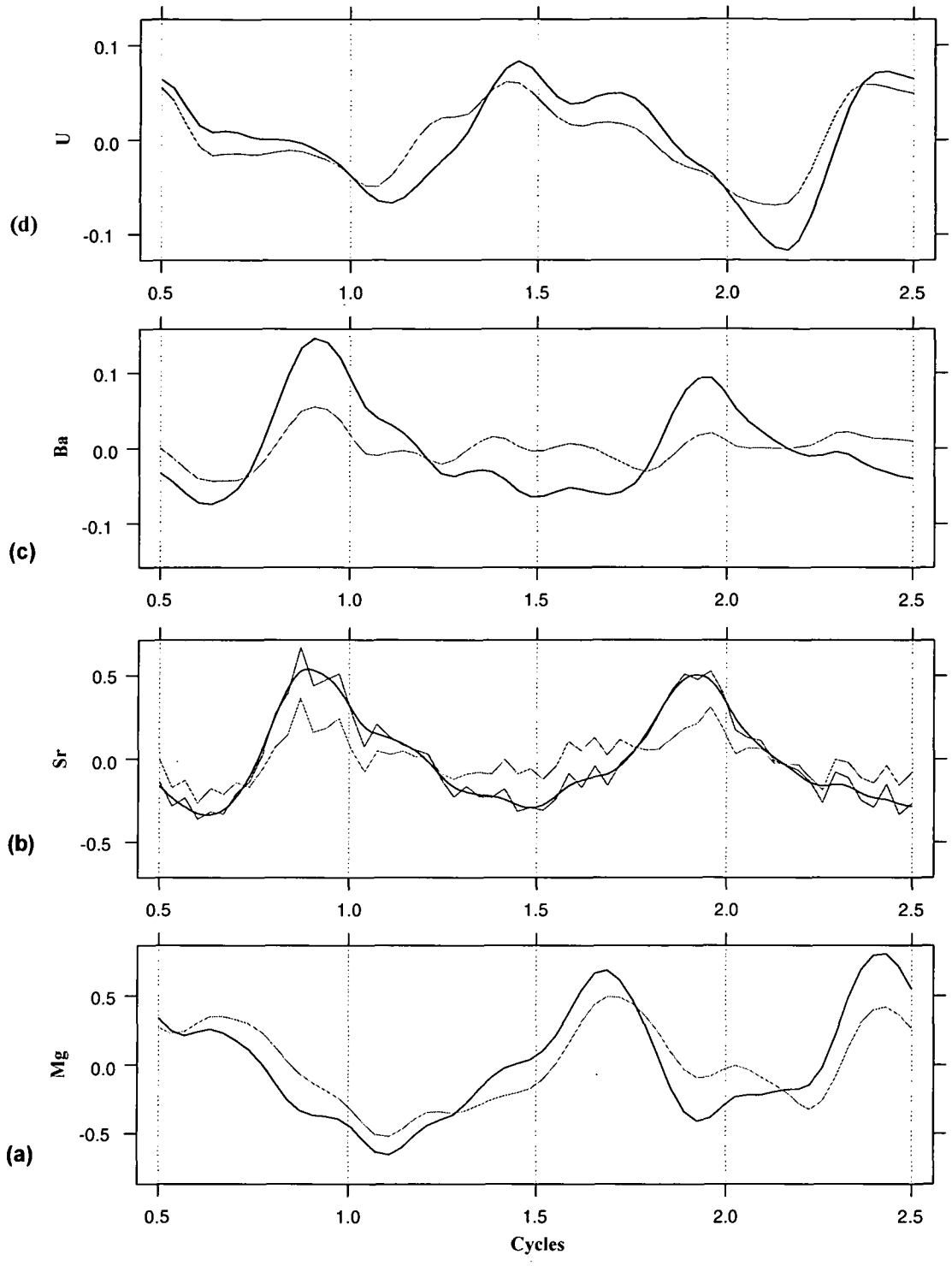

Figure 5.13. Graph of an "average" year from the high-resolution laser ablation ICP-MS analysis of FC-SS5 (Figure 5.2a), a 151 mm long soda-straw stalactite from Frankcombe Cave, Tasmania. Graphs (a), (b), (c), and (d) correspond respectively to, magnesium, strontium, barium, and uranium scans, and units are in normalised counts second^{-1}. Light grey lines represent complete data sets and black traces are the data minus several years adjacent to and containing the two large spikes (shown in Figure 5.9). Strontium data (b) have a smoothing spline (black line) through the subsampled data (dark grey line) together with the complete data set (light grey line).

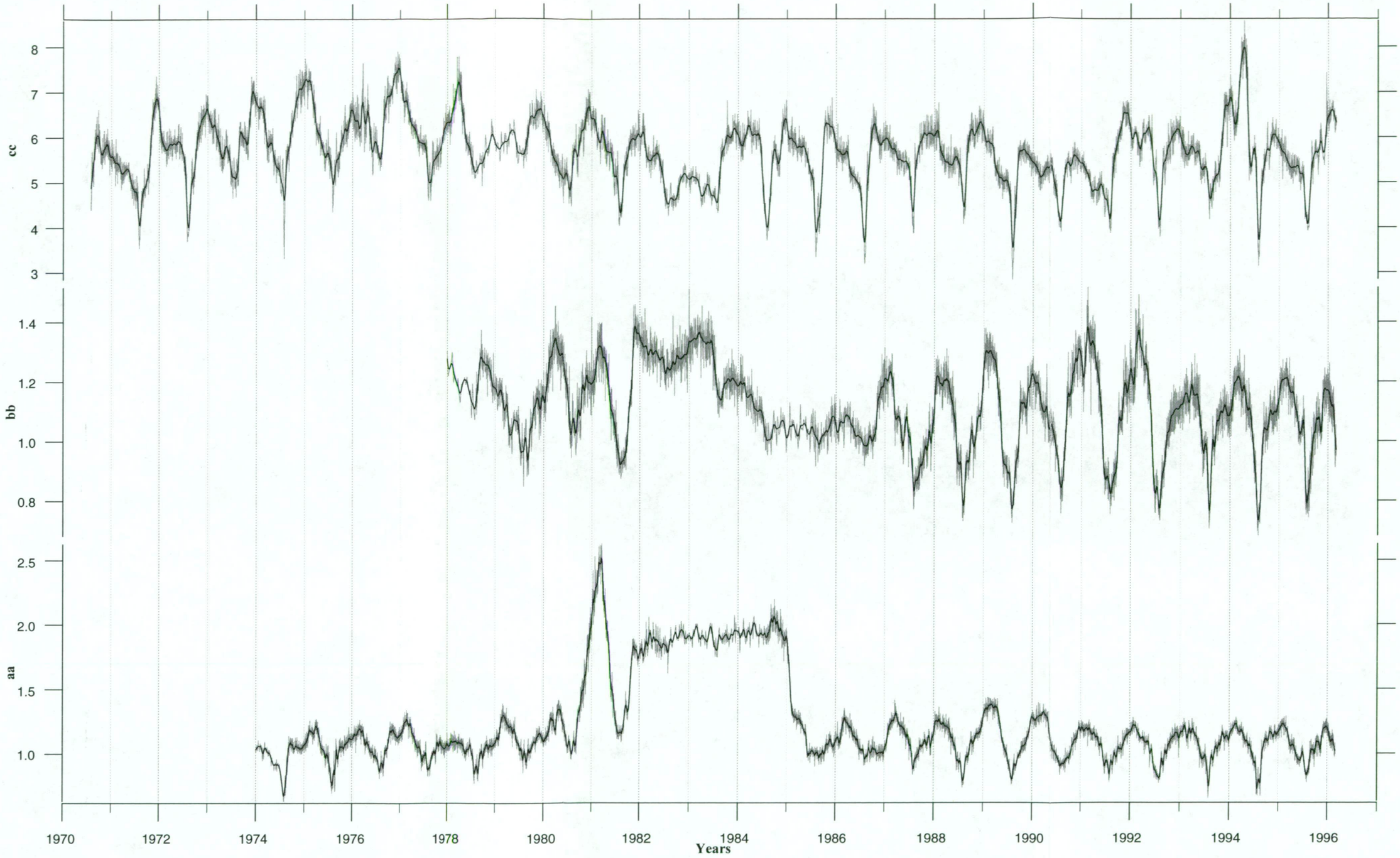

Figure 5.14. **Strontium results of three separate high-resolution laser ablation ICP-MS analyses of FC-SS5 (Figure 5.2a), a 151 mm long soda-straw stalactite from Frankcombe Cave, Tasmania. The two lower scans, aa and bb axes, were done at 90° to the top, cc axis, scan, and parallel to each other, approximately 100 µm apart. Y-axis units are in normalised counts second^{-1}.**

5.4.3. Results of ICP-MS Analysis of BDTH Soda-Straw Stalactites

Samples were collected from Burning Down The House Cave, Florentine Valley, Tasmania, Australia. Since these samples came from the same chamber it was anticipated that they would be showing close similarity in their patterns of minor element variation due to their close proximity to one another and the possibility that they shared a common source of seepage water. It would in fact be a good test of the ability to duplicate minor element results in different samples.

Analysis of the magnesium, strontium, barium, and uranium composition along the growth axis of BDTH-SS1 (35 mm long) and BDTH-SS3 (28 mm long) by laser ablation ICP-MS indicates that there are quasi-periodical variations in their minor element contents. Since the laser ablation ICP-MS results of BDTH-SS6 do not have similar minor element cyclicity this sample has not been analysed further. The minor element results of laser ablation ICP-MS analysis are plotted against distance for BDTH-SS6 in Figure 5.15, and for BDTH-SS1 (bottom) and BDTH-SS3 (top) in Figure 5.16.

No chronologies could be constructed for these samples using either of the techniques used with FC-SS5 or BFM-J96 due to the relatively low growth rate, estimated to be approximately 100 $\mu m\ year^{-1}$.

5.4.3.1. Minor Element Relationships in BDTH Soda-straw Stalactites

A correlation matrix of the low-frequency, *ie* untreated, and high-frequency, *ie* detrended, minor element records for both the whole and a subsample of BDTH-SS1 and BDTH-SS3 are presented in Table 5.3. Correlations between the minor elements have been obtained on subsamples of the data due to the presence of several large peaks/spikes in the data and also because the lower section of the data does not appear to have quasi-periodical minor element variations. In some cases there are major differences in the correlation coefficients between the complete and sub-sampled data therefore only the sub-sampled relationships will be considered.

The Sr and Ba concentrations have a strong positive relationship in both the sub-sampled low and high frequency records of BDTH-SS1, r values of 0.83 and 0.90 respectively, and BDTH-SS3, r values of 0.85 and 0.93 respectively. These results suggest that the processes controlling Sr and Ba geochemistry do not change very much over different temporal scales. Significant differences in the minor element relationships occur between the BDTH-SS1 and BDTH-SS3 data. In some cases the relationships are not consistent between samples, for example the Mg-Sr, Mg-Ba, Sr-U, and Ba-U have a negative relationship in BDTH-SS1 and a positive relationship in BDTH-SS3. It is difficult to account for these, particularly as the samples came from the same location, but it is possible that evaporation or other site specific factors may explain some of the variability. Although no clear explanation can be given for the observed differences between the minor element relationships, these results highlight the need for further investigations.

Table 5.3. **Correlation coefficients (r) for the low frequency (untreated, UT) and high frequency (detrended, DT) records from high-resolution laser ablation ICP-MS analysis of BDTH-SS1 and BDTH-SS3. Correlations were done on subsamples of the data as there are several large spikes and the first section of data does not appear to have quasi-periodical minor element variations. DT correlation coefficients are shaded.**

Sample	Element	Mg	Sr	Ba	U
BDTH-SS1	Mg	$_{DT}$|^{UT}	-0.15	-0.06	-0.02
(n = 10860)	Sr	-0.24	$_{DT}$|^{UT}	0.91	-0.05
	Ba	-0.17	0.90	$_{DT}$|^{UT}	-0.06
	U	0.04	-0.04	-0.9	$_{DT}$|^{UT}
Sub-sample	Mg	$_{DT}$|^{UT}	-0.36	-0.17	0.09
(2500-6500)	Sr	-0.69	$_{DT}$|^{UT}	0.84	-0.06
(n= 4000)	Ba	-0.33	0.83	$_{DT}$|^{UT}	-0.11
	U	0.21	-0.21	-0.26	$_{DT}$|^{UT}
BDTH-SS3	Mg	$_{DT}$|^{UT}	0.91	0.91	0.63
(n = 10686)	Sr	0.91	$_{DT}$|^{UT}	0.92	0.57
	Ba	0.92	0.93	$_{DT}$|^{UT}	0.70
	U	0.60	0.54	0.64	$_{DT}$|^{UT}
Sub-sample	Mg	$_{DT}$|^{UT}	0.7570	0.72	0.34
(7000-10500)	Sr	0.69	$_{DT}$|^{UT}	0.87	0.39
(n = 3500)	Ba	0.64	0.82	$_{DT}$|^{UT}	0.40
	U	0.35	0.41	0.40	$_{DT}$|^{UT}

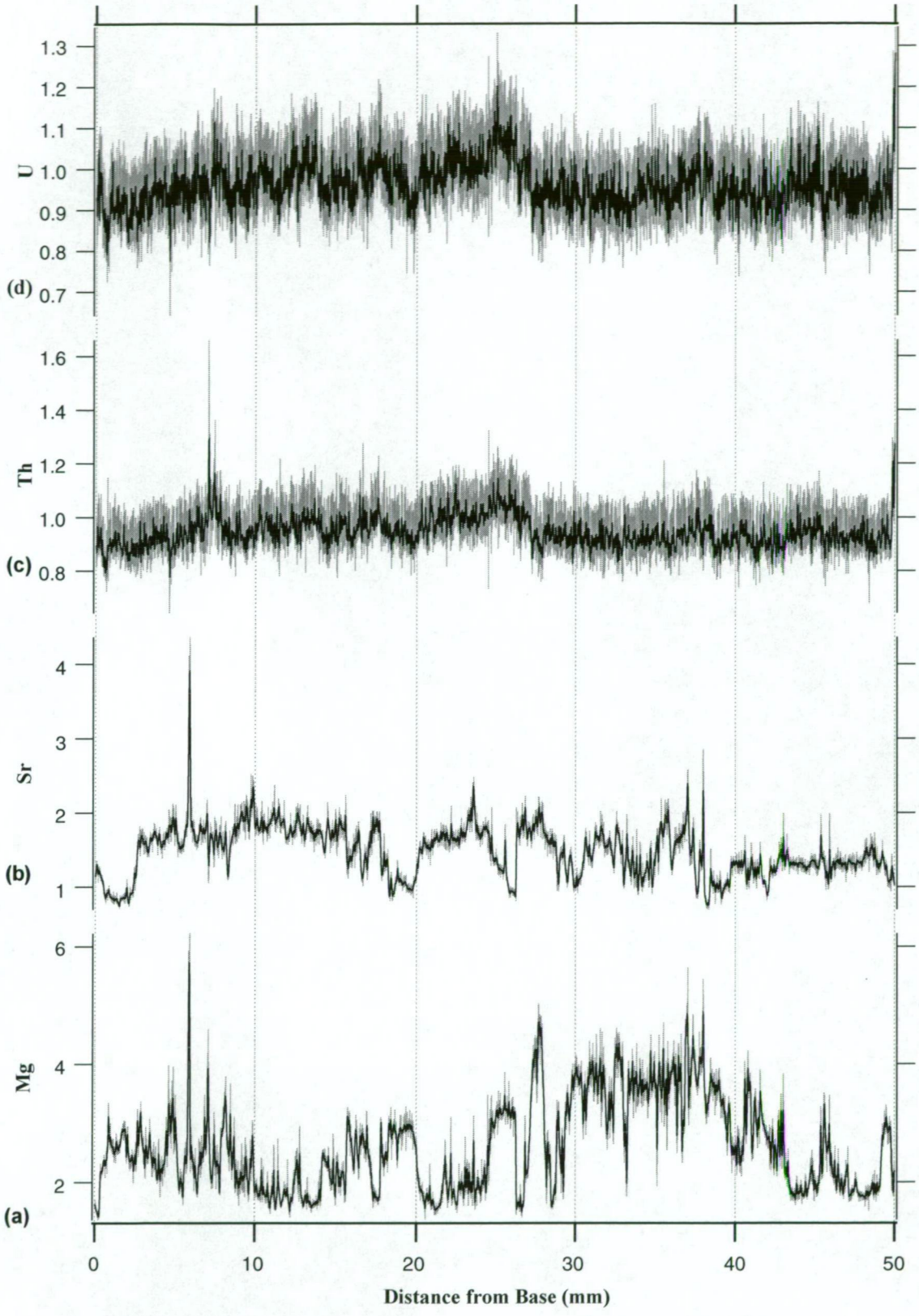

Figure 5.15. Results of laser ablation ICP-MS analysis of tip section of BDTH-SS6, a soda-straw stalactite from Burning Down The House Cave, Florentine Valley, Tasmania. Axes are from the bottom: magnesium, strontium, thorium, and uranium, and units are in normalised counts second^{-1}. Light grey line is raw data and black line is a smoothing spline.

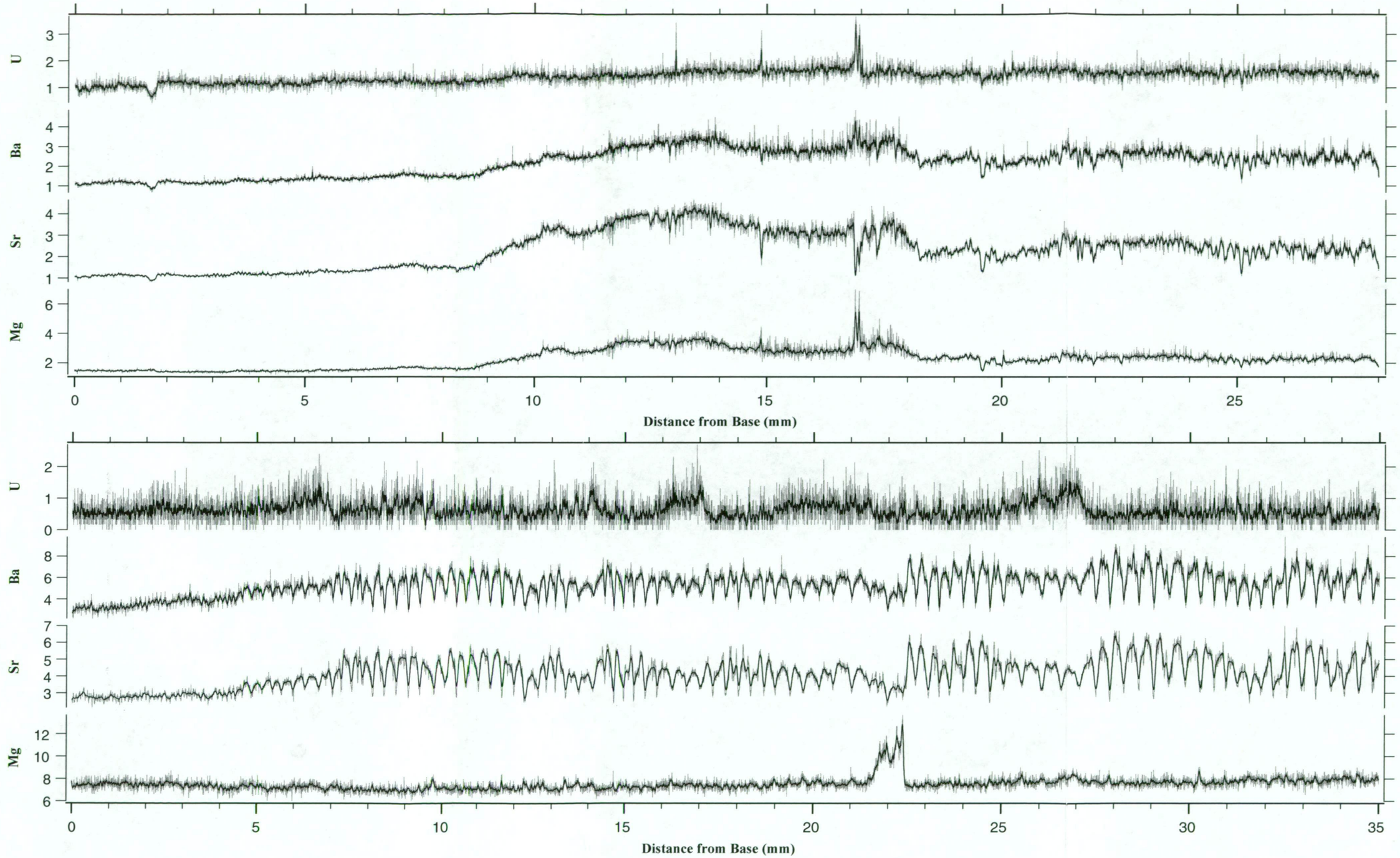

Figure 5.16. Results of laser ablation ICP-MS analysis of tip sections of BDTH-SS1 (bottom) and BDTH-SS3 (top), two soda-straw stalactites from Burning Down The House Cave, Florentine Valley, Tasmania. Axes are from the bottom magnesium, strontium, barium, and uranium, and units are in normalised counts second^{-1}. Light grey line is raw data and black line is a smoothing spline.

5.4.4. Results of ICP-MS Analysis of a Section of Stalagmite from CTH-S1

This stalagmite, from Top Hole, Croesus Cave, Mole Creek, Tasmania, has discernible laminations for almost its entire length and it is hypothesised that they may be annual, although counting of the laminations between two TIMS $^{230}Th/^{234}U$ dates was inconclusive. The spectacular results of the soda-straw stalactite FC-SS5 analyses indicate that annual cyclicity in the minor element composition of speleothems is present but further investigation is required to see whether it was present in other speleothem samples. CTH-S1 has been selected because it has very clearly defined laminations and also has been dated by several TIMS $^{230}Th/^{234}U$ analyses, 8,647 ± 499 years for the basal age and 4,302 ± 131 years at 1,020 mm above the base, giving a calculated growth rate of 0.2347 mm $year^{-1}$ between these samples. It is pertinent to investigate the relationships between the minor elements to see if they are similar to those of recent samples. The variation of the minor element composition of CTH-S1 was investigated by two parallel laser ablation ICP-MS analyses along the growth axis of the pre-ablated surface of a sample taken from between 1,000 and 1,030 mm from the base (Figure 5.2b). The results of the laser ablation ICP-MS are plotted against distance along the 30 mm analysis track in Figure 5.17.

A correlation matrix of the low-frequency, *ie* untreated, and high-frequency, *ie* detrended, minor element records for the two parallel scans, A and B, of CTH-S1 is presented in Table 5.4 In both the low-frequency and detrended results of the CTH-S1A amd CTH-S1B results strong positive relationships occur between Sr and Ba concentrations. These results suggest that Sr and Ba are sensitive to similar controls but that the controls are not temporally dependent. All other element pairs are weakly positively correlated with no r values exceeding 0.30. It is interesting to note that the relationships do not change significantly between the untreated and detrended results. This suggests that the relationships are not significantly affected at different timescales.

Table 5.4. Correlation coefficients (r) for the low frequency (untreated, UT) and high frequency (detrended, DT) records from two parallel high-resolution laser ablation ICP-MS analyses of CTH-S1. DT correlation coefficients are shaded.

Sample	Element	Mg	Sr	Ba	U
CTH-S1A	Mg	$_{DT}\backslash^{UT}$	-0.04	-0.001	0.04
(n = 11884)	Sr	0.12	$_{DT}\backslash^{UT}$	0.92	0.25
	Ba	0.20	0.87	$_{DT}\backslash^{UT}$	0.31
	U	0.09	0.12	0.20	$_{DT}\backslash^{UT}$
CTH-S1B	Mg	$_{DT}\backslash^{UT}$	-0.11	-0.06	-0.05
(n = 11347)	Sr	0.08	$_{DT}\backslash^{UT}$	0.90	0.19
	Ba	0.14	0.86	$_{DT}\backslash^{UT}$	0.23
	U	0.05	0.11	0.17	$_{DT}\backslash^{UT}$

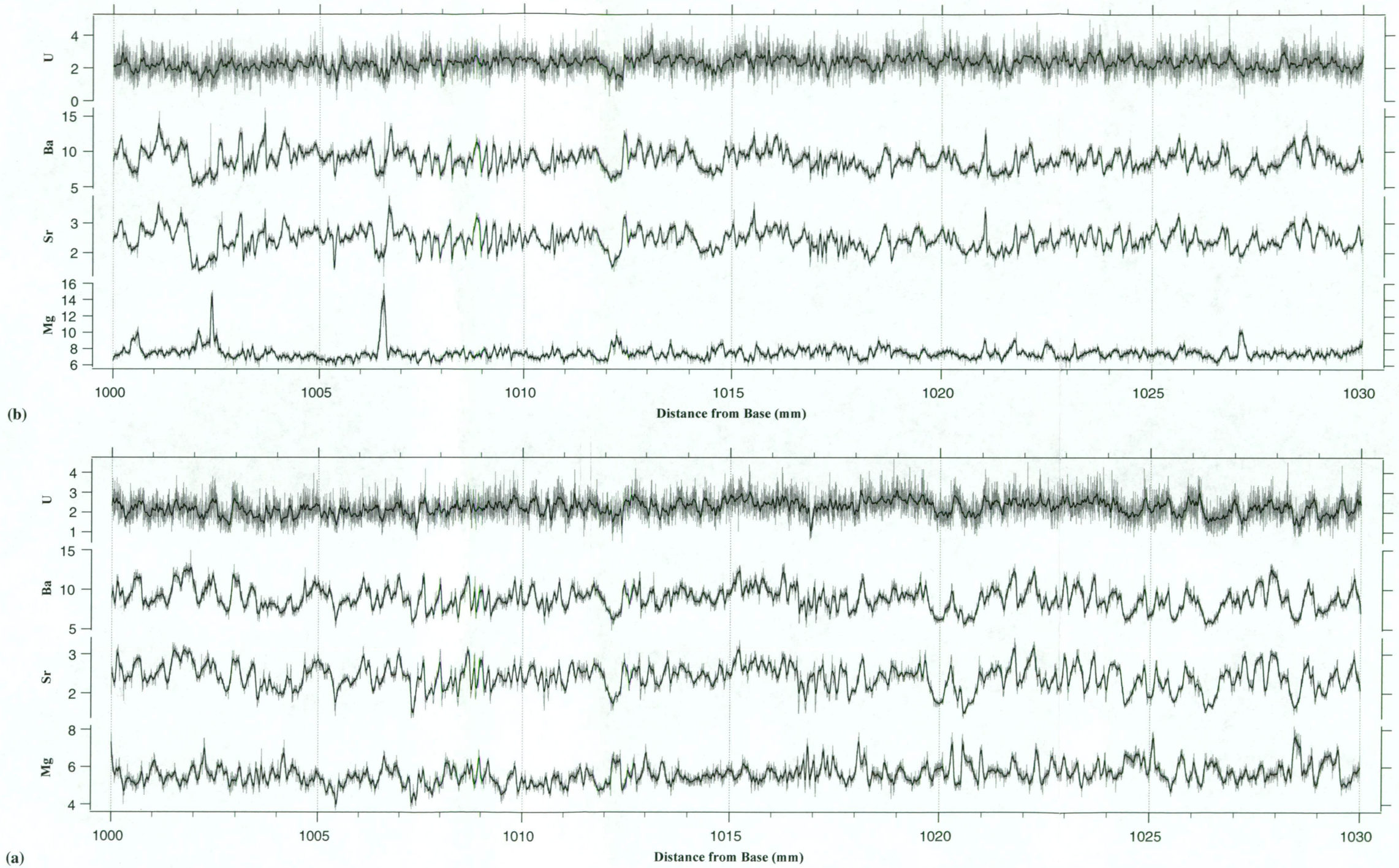

Figure 5.17. Results of two parallel laser ablation ICP-MS analyses of a sub-sample taken at between 1000 and 1030 mm from the base of CTH-S1 (Figure 5.2b), stalagmite from Top Hole, Croesus Cave, Mole Creek, Tasmania. Axes are from the bottom: magnesium, strontium, barium, and uranium, and units are in normalised counts second^{-1}. Light grey line is raw data and black line is a smoothing spline. Distance from the base is marked on the x- axis.

5.4.5. Results of ICP-MS Analysis of Stalagmite FC-S4

This stalagmite was collected from Frankcombe Cave, Florentine Valley, Tasmania, from the same chamber as the sample FC-SS5. The magnesium, strontium, barium, and uranium composition of FC-S4 was investigated by laser ablation ICP-MS analysis along the longitudinal axis of a pre-ablated surface. The results of the laser ablation ICP-MS are plotted against distance along the 28 mm analysis track in Figure 5.18.

This stalagmite was found very close to FC-SS5 and, since this sample has been shown to exhibit very strong minor element cyclical variations, it had been expected that FC-S4 would show similar trends. FC-S4 has not been dated using any radiometric methods and it was hoped that dating by autocorrelation would be possible. However, this proved not to be the case. It is also relevant to investigate the relationships between the minor elements to see if they are similar to FC-SS5. A correlation matrix of the low-frequency, *ie* untreated, and high-frequency, *ie* detrended, minor element data for two parallel scans, FC-S4aa and FC-S4bb, are presented in Table 5.5. In FC-S4aa and FC-S4bb a strong positive relationship occurs between Sr and Ba in both the untreated and detrended results, with r-values of 0.92 and 0.81, and 0.83 and 0.75, respectively. The similarity between the untreated and detrended results suggests that there is little, if any, temporal control on the factors controlling Sr and Ba.

In the untreated results the Mg-Sr and Mg-Ba relationships are not consistent between the two scans but in the detrended results the relationsips are very similar. In the case of the FC-S4aa scan the Mg-Ba relationship has an r-value of –0.30 in the low frequency and a r-value of 0.31 in the high frequency results, a similar situation occurs with the Mg-Sr with r-values of –0.18 and 0.20 respectively. The causes of these differences are not apparent and further analyses are required to investigate this, a two-dimensional scan of the surface may provide more information than several parallel one-dimensional tracks.

Table 5.5. Correlation coefficients (r) for the low frequency (untreated, UT) and high frequency (detrended, DT) records from high-resolution laser ablation ICP-MS analysis of FC-S4 (n = 6172). DT correlation coefficients are shaded.

Element	Mg	Sr	Ba	U
Mg-aa	$_{DT}$|^{UT}	-0.18	-0.30	-0.33
Sr-aa	0.31	$_{DT}$|^{UT}	0.92	0.28
Ba-aa	0.20	0.81	$_{DT}$|^{UT}	0.31
U-aa	-0.04	0.12	0.13	$_{DT}$|^{UT}
Mg-bb	$_{DT}$|^{UT}	0.19	0.01	-0.24
Sr-bb	0.37	$_{DT}$|^{UT}	0.83	0.12
Ba-bb	0.26	0.75	$_{DT}$|^{UT}	0.09
U-bb	-0.06	0.08	0.09	$_{DT}$|^{UT}

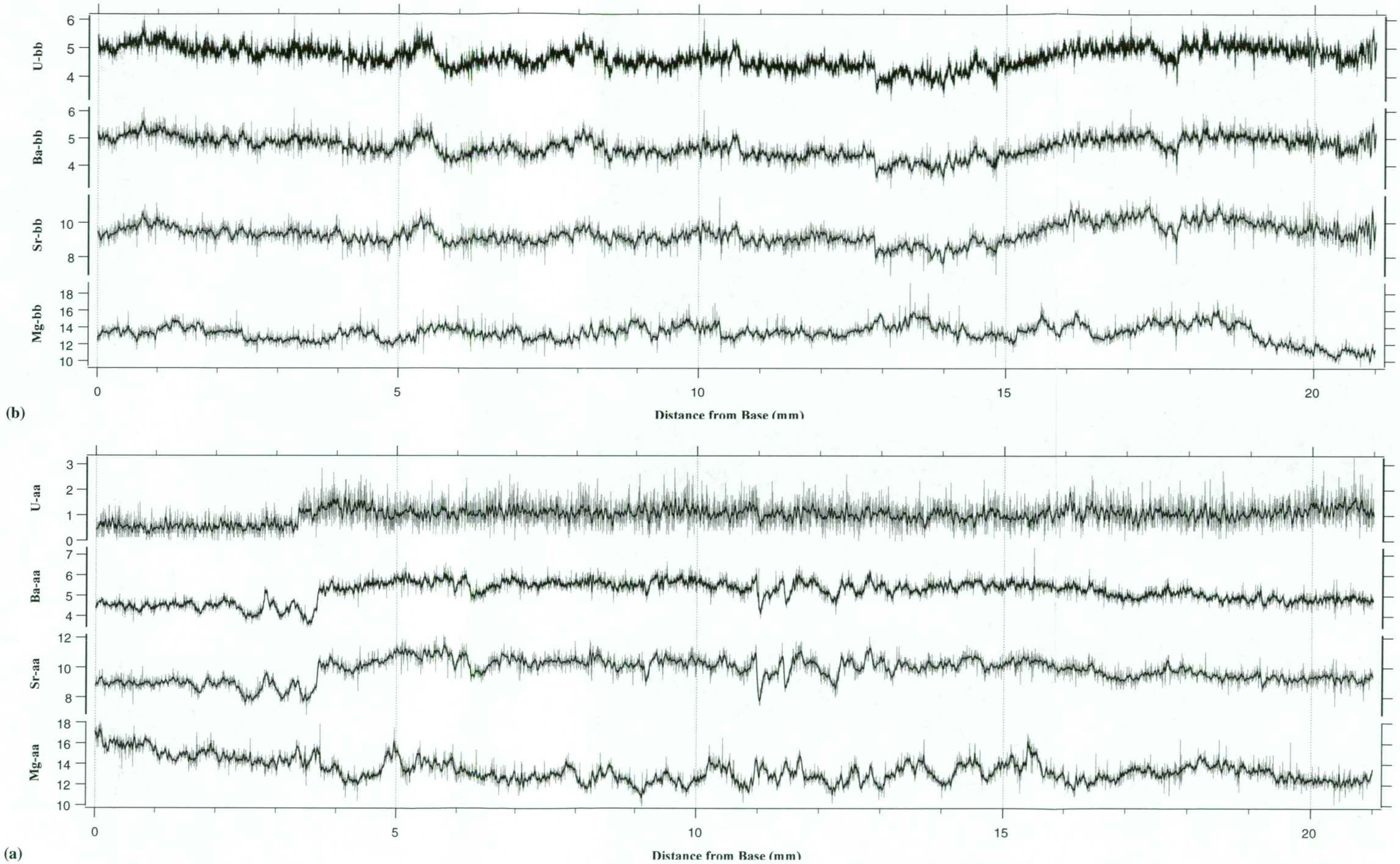

Figure 5.18. Results of two parallel laser ablation ICP-MS analyses of FC-S4, a stalagmite from Frankcombe Cave, Florentine Valley, Tasmania. Axes are from the bottom: magnesium, strontium, barium, and uranium, and units are in normalised counts second^{-1}. Light grey line represents raw data and black line is a smoothing spline. Distance from the base is marked on the x- axis.

5.4.6. Results of ICP-MS Analysis of Flowstone Samples JC-F1aa and JC-F1bb

The magnesium, strontium, barium, and uranium compositions of JC-F1aa (Figure 5.2d) and JC-F1bb were investigated by laser ablation ICP-MS analysis along the growth axis of a pre-ablated surface. The results of laser ablation ICP-MS are plotted against distance along the analysis tracks of JC-F1aa in Figure 5.19 (a), and JC-F1bb in Figure 5.19 (b). The sample JC-F1aa has been dated using TIMS $^{230}Th/^{234}U$ analyses. Investigation of the long-term variations of minor elements in speleothems was deemed a worthwhile exercise particularly as a stable isotope (Chapter 6) profile was also analysed for this sample. Hellstrom (1998) has observed a significant positive relationship between Ba concentration and $\delta^{13}C$ values in a New Zealand speleothem and has suggested that barium concentrations may also be indicative of vegetation productivity.

A correlation matrix of the low-frequency, *ie* untreated, and high-frequency, *ie* detrended, minor element records for JC-F1aa and JC-F1bb is presented in Table 5.6. Again the most striking feature is the strong positive relationship between Sr and Ba in both the low- and high-frequency results. The consistancy of the relationship supports the general observation that there is a distinct lack of temporal dependence by these elements and that similar geochemical factors govern their behaviour. In the untreated results weak negative relationships between Sr-U and Ba-U are observed and are consistent betweem the two JC-F1 samples. These relationships are significant as they may relate to changes in soil chemistry (Hellstrom, 1998). The weak positive relationship between the Mg-Sr and Mg-Ba pairs is consistent between the low- and high-frequency results in both samples. Roberts *et al.* (1998) attributed changes in the relationships to possible variations in the residence time of seepage waters.

Table 5.6. Correlation coefficients (r) for the low frequency (untreated, UT) and high frequency (detrended, DT) records from high-resolution laser ablation ICP-MS analysis of JC-F1aa (Figure 5.2d) and JC-F1bb. DT correlation coefficients are shaded.

Sample	Element	Mg	Sr	Ba	U
JC-F1aa	Mg	$_{DT}\backslash^{UT}$	0.24	0.20	0.08
(n = 11884)	Sr	0.22	$_{DT}\backslash^{UT}$	0.78	-0.38
	Ba	0.16	0.81	$_{DT}\backslash^{UT}$	-0.25
	U	-0.02	-0.21	0.60	$_{DT}\backslash^{UT}$
JC-F1bb	Mg	$_{DT}\backslash^{UT}$	0.28	0.22	0.08
(n = 11347)	Sr	0.30	$_{DT}\backslash^{UT}$	0.78	-0.42
	Ba	0.23	0.79	$_{DT}\backslash^{UT}$	-0.26
	U	0.08	-0.31	-0.12	$_{DT}\backslash^{UT}$

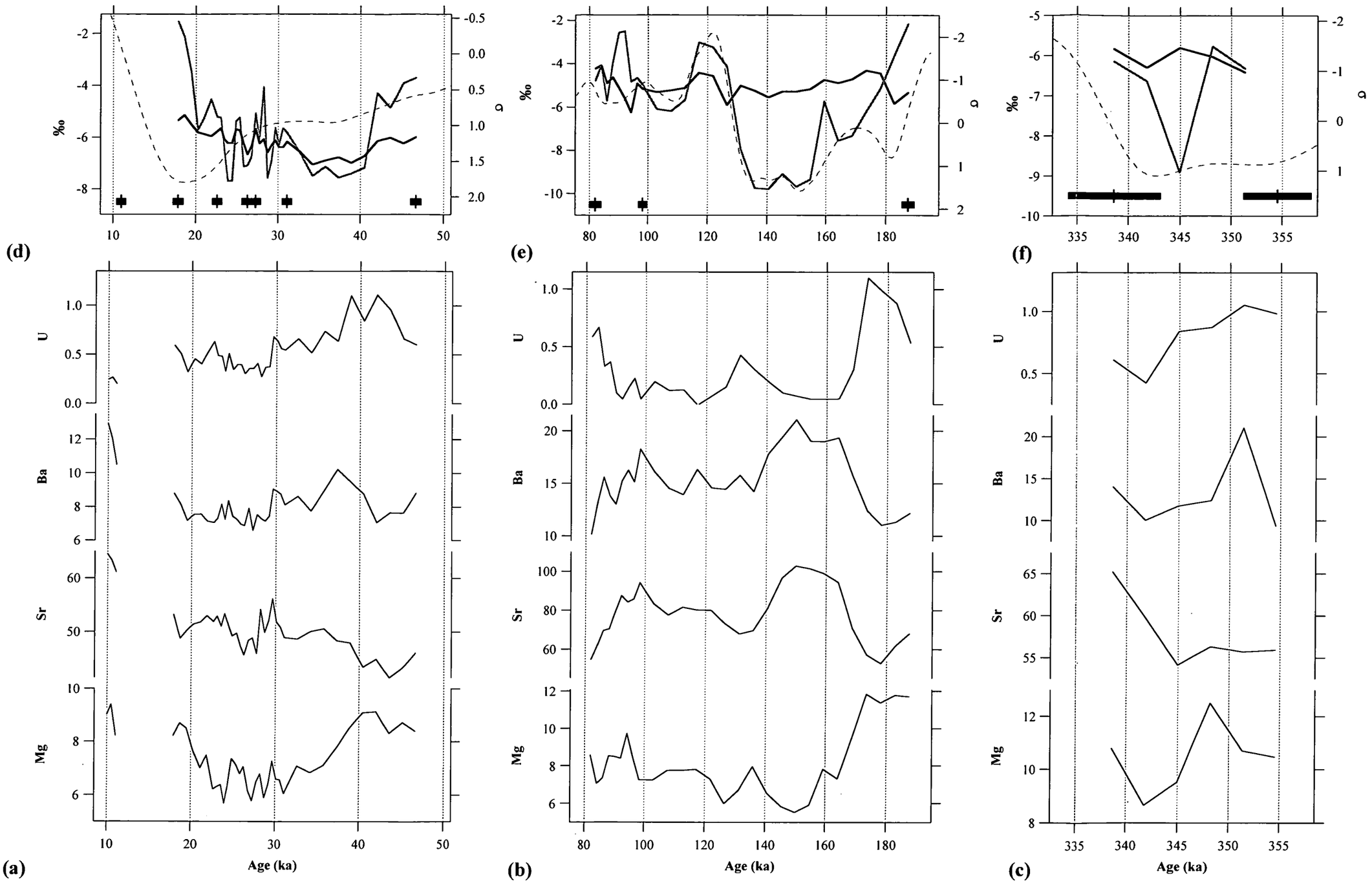

Figure 5.19 (a). Comparison of the results of laser ablation ICP-MS and stable isotope analysis of JC-F1aa (Figure 5.2d), a section of flowstone from Jersey Cave, Yarrangobilly, New South Wales, Australia. Graphs (a) to (c) are the minor element analyses. Axes are from the bottom: magnesium, strontium, barium, and uranium, and units are in normalised counts second^{-1}. Graphs (d) to (f) are oxygen (dark line) and carbon (grey line) isotope results of samples taken from the longitudinal profile, dashed grey line is the SPECMAP record. Black bars are age estimates with 2 sigma errors. Ages are in thousands of years and the gaps between the graphs are depositional hiatuses. The thickness of JC-F1aa (Figure 5.2d) is 138 mm and that of JC-F1bb is 110 mm.

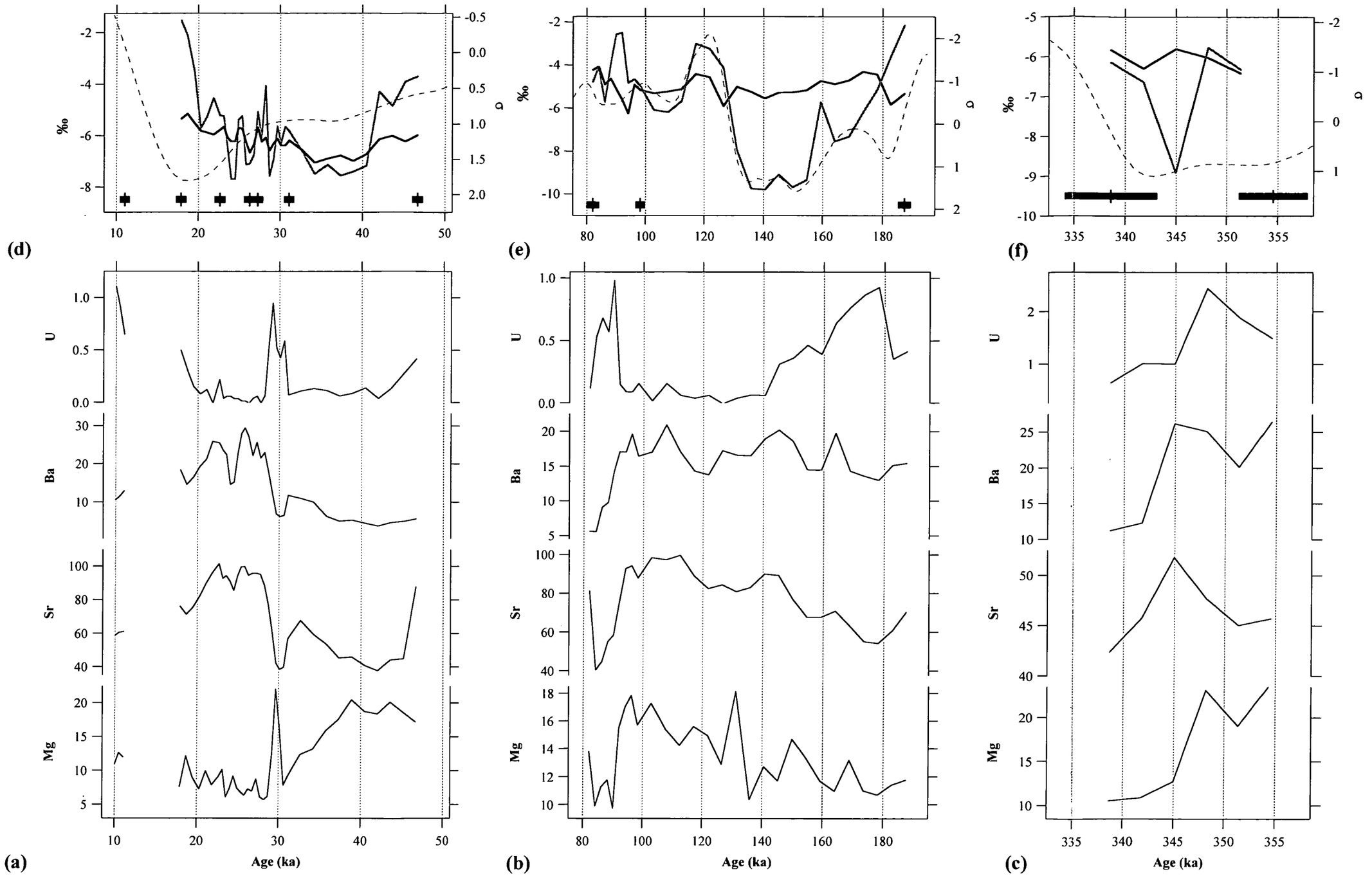

Figure 5.19 (b). Comparison of the results of laser ablation ICP-MS and stable isotope analysis of JC-F1aa (Figure 5.2d), a section of flowstone from Jersey Cave, Yarrangobilly, New South Wales, Australia. Graphs (a) to (c) are the minor element analyses. Axes are from the bottom: magnesium, strontium, barium, and uranium, and units are in normalised counts second^{-1}. Graphs (d) to (f) are oxygen (dark line) and carbon (grey line) isotope results of samples taken from the longitudinal profile, dashed grey line is the SPECMAP record. Black bars are age estimates with 2 sigma errors. Ages are in thousands of years and the gaps between the graphs are depositional hiatuses. The thickness of JC-F1aa (Figure 5.2d) is 138 mm and that of JC-F1bb is 110 mm.

5.4.7. Results of ICP-MS Analysis of Yarrangobilly Flowstone Sample JC-F2

The magnesium, strontium, barium, and uranium composition of JC-F2 was investigated by laser ablation ICP-MS analysis along the growth axis of a pre-ablated surface. The results of laser ablation ICP-MS are plotted against distance along the 100 mm analysis track in Figure 5.20. A correlation matrix of the low-frequency, *ie* untreated, and high-frequency, *ie* detrended, minor element records for JC-F2 is presented in Table 5.7. In this sample of Yarrangobilly material there are correlations between several minor element pairs not seen in other samples from this site.

In both the low- and high-frequency results strong positive correlations between the pairs Mg-Sr, Mg-Ba, and Sr-Ba are observed with r values greater than approximately 0.70, weak positive relationships occur with the pairs Mg-U, Sr-U, and Ba-U with r-values less than approximately 0.40 and greater than 0.20. The strong relationship between Sr and Ba is also observed here but it also has several relationships between elements that are not observed in other samples. Further ICP-MS scans together with stable isotope analyses are required to investigate the significance of these relationships and how they are affected by environmental change.

Table 5.7. Correlation coefficients (r) for the low frequency (untreated, UT) and high frequency (detrended, DT) records from high-resolution laser ablation ICP-MS analysis of JC-F2 (n = 1177). DT correlation coefficients are shaded.

Element	Mg	Sr	Ba	U
Mg	$_{DT}\backslash^{UT}$	0.81	0.77	0.31
Sr	0.75	$_{DT}\backslash^{UT}$	0.85	0.03
Ba	0.68	0.72	$_{DT}\backslash^{UT}$	0.24
U	0.36	0.21	0.44	$_{DT}\backslash^{UT}$

5.4.8. Results of ICP-MS Analysis of Yarrangobilly Flowstone Sample JC-F4

The magnesium, strontium, barium, and uranium composition of JC-F2 was investigated by laser ablation ICP-MS analysis along the growth axis of the pre-ablated surface. The results of laser ablation ICP-MS are plotted against distance along the 49 mm analysis track in Figure 5.21. A correlation matrix of the low-frequency, *ie* untreated, and high-frequency, *ie* detrended, records for JC-F4 is presented in Table 5.8. The consistent strong positive relationship between Sr and Ba in the low- and high-frequency correlations seen in the other samples is again present with r-values of 0.63 and 0.57, respectively. Relationships between the other minor elements vary considerably between the untreated and detrended results suggesting that there is a high degree of structure at the higher frequencies (Mg-Sr, Mg-Ba, and Ba-U) but in some cases the opposite is true (Sr-U).

Table 5.8. Correlation coefficients (r) for the low frequency (untreated, UT) and high frequency (detrended, DT) records from high-resolution laser ablation ICP-MS analysis of JC-F4 (n = 595). DT correlation coefficients are shaded.

Element	Mg	Sr	Ba	U
Mg	$_{DT}\backslash^{UT}$	0.37	0.07	-0.05
Sr	0.57	$_{DT}\backslash^{UT}$	0.63	-0.46
Ba	0.24	0.57	$_{DT}\backslash^{UT}$	0.03
U	-0.16	-0.19	0.37	$_{DT}\backslash^{UT}$

5.5. Electron Microprobe and Ion Chromatography

This section presents the results of electron microprobe and ion chromatography analysis of several Australian speleothems, one from Risbys Basin Cave,Tasmania, RB-SS2, and two from Jersey Cave, Yarrangobilly, New South Wales, JC-F1 and JC-F2. Ion chromatography has been used to test the hypothesis that the dark grey to black layering present in the Yarrangobilly samples (Figure 5.2d) was caused by fire and that this effect could be identified by variations in bromine and chlorine (Mano and Andreae, 1994). Initial attempts to test this hypothesis have been made with electron microprobe analysis. However, despite the encouraging results obtained from the electron microprobe at the CSL at the University of Tasmania, Hobart, several problems were encountered with the electron microprobe used at RSES at ANU in Canberra, mainly to do with interferences from other elements during the analysis of bromine and chlorine. The RSES electron microprobe, although from the same manufacturer as the CSL instrument, is a much earlier model than the one located at the CSL and this may have contributed to the inability of the RSES machine to accurately resolve variations in bromine and chlorine.

5.5.1. Results of Electron Microprobe Analysis of RB-SS2

Electron microprobe analyses have been taken from the middle of the soda-straw stalactite wall at intervals of approximately 500 microns or 0.5 millimetres, a major disadvantage of this technique in comparison to laser ablation ICP-MS is the low level of temporal resolution due to the large sample interval. Seven elements: bromine, chlorine, fluorine, iron, manganese, magnesium and strontium, were present in sufficient concentrations to be sampled and multiple analyses were carried out to see if cyclic variations could be detected. The results are presented in Figure 5.22. Very few analyses of fluorine and strontium fall below the machine detection limits whereas a significant number of the bromine, chlorine, iron, manganese, and magnesium measurements do so.

5.5.2. Ion Chromatograph Results for JC-F1 and JC-F2

Results of ion chromatography indicate that neither bromine or chlorine are related to the observed grey and black layers. However, the method used to extract the elements may have been flawed and further investigation is required.

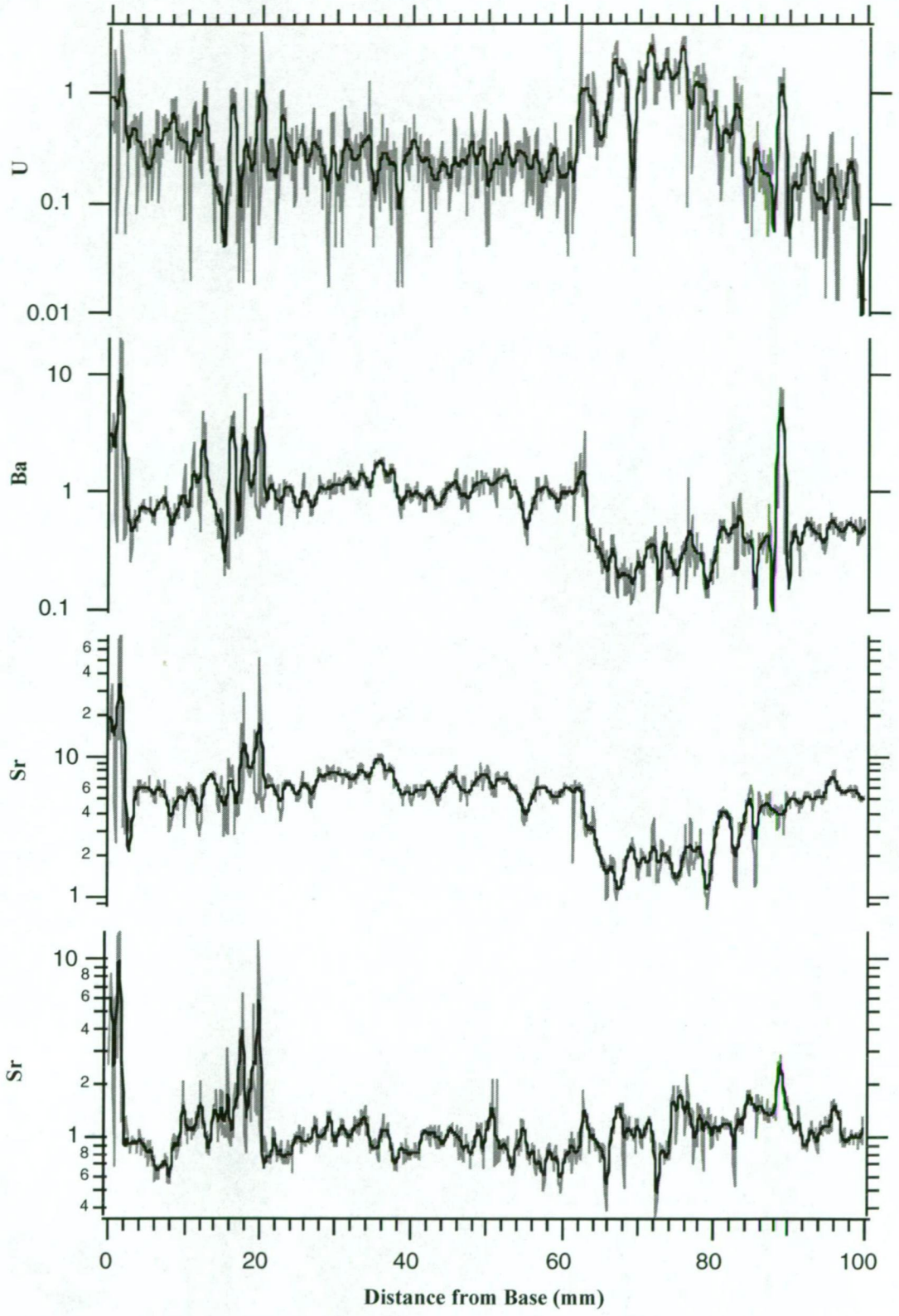

Figure 5.20. Results of a low-resolution laser ablation ICP-MS analysis of the flowstone JC-F2 from Jersey Cave, Yarangobilly, New South Wales, Australia. The thickness of sample is 100 mm. Axes are from the bottom magnesium, strontium, barium, and uranium, and units are in normalised counts second^{-1}.

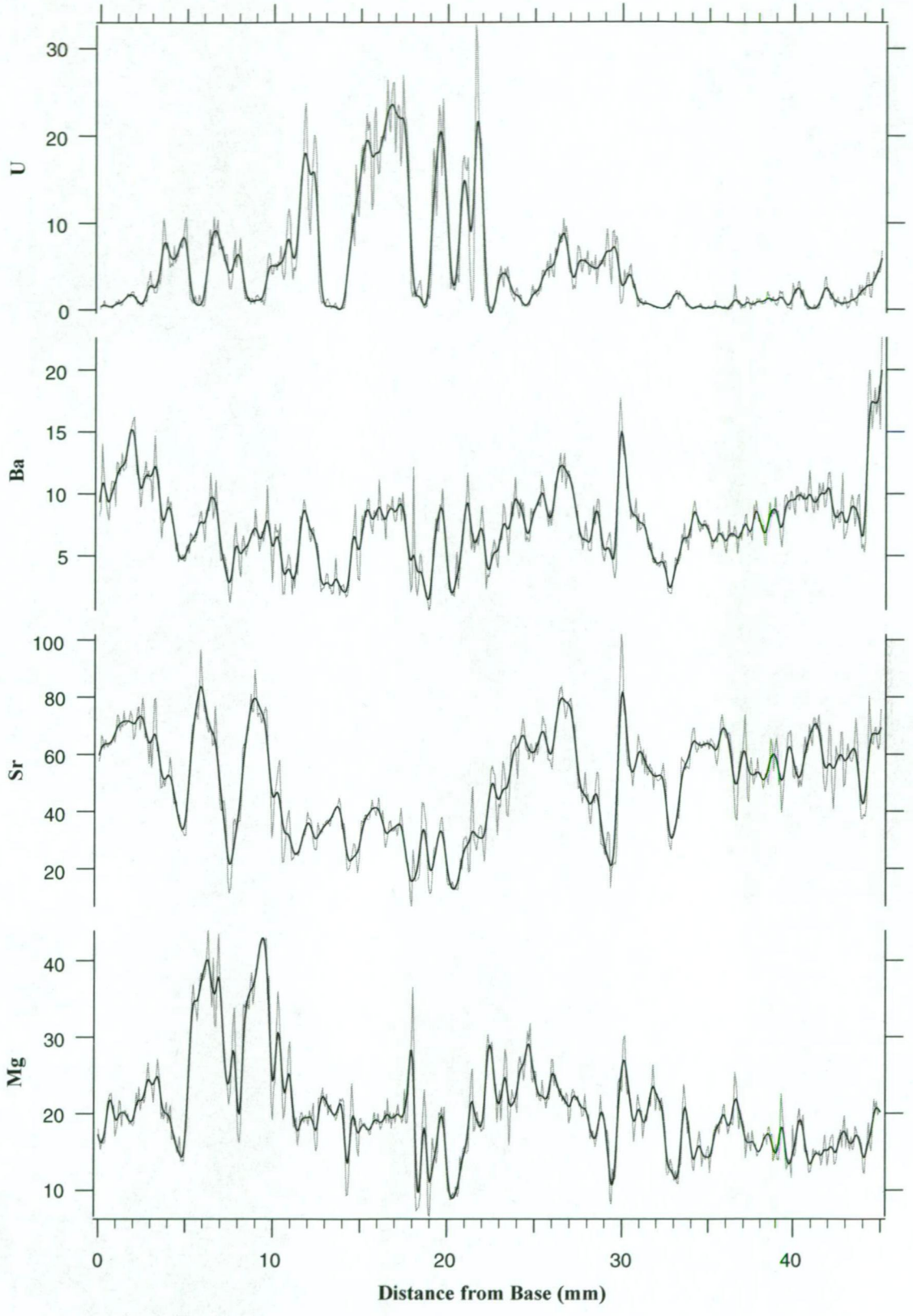

Figure 5.21. **Results of a low-resolution laser ablation ICP-MS analysis of the flowstone JC-F4 from Jersey Cave, Yarangobilly, New South Wales, Australia. The thickness of sample is 50 mm. Axes are from the bottom: magnesium, strontium, barium, and uranium, and units are in normalised counts second^{-1}.**

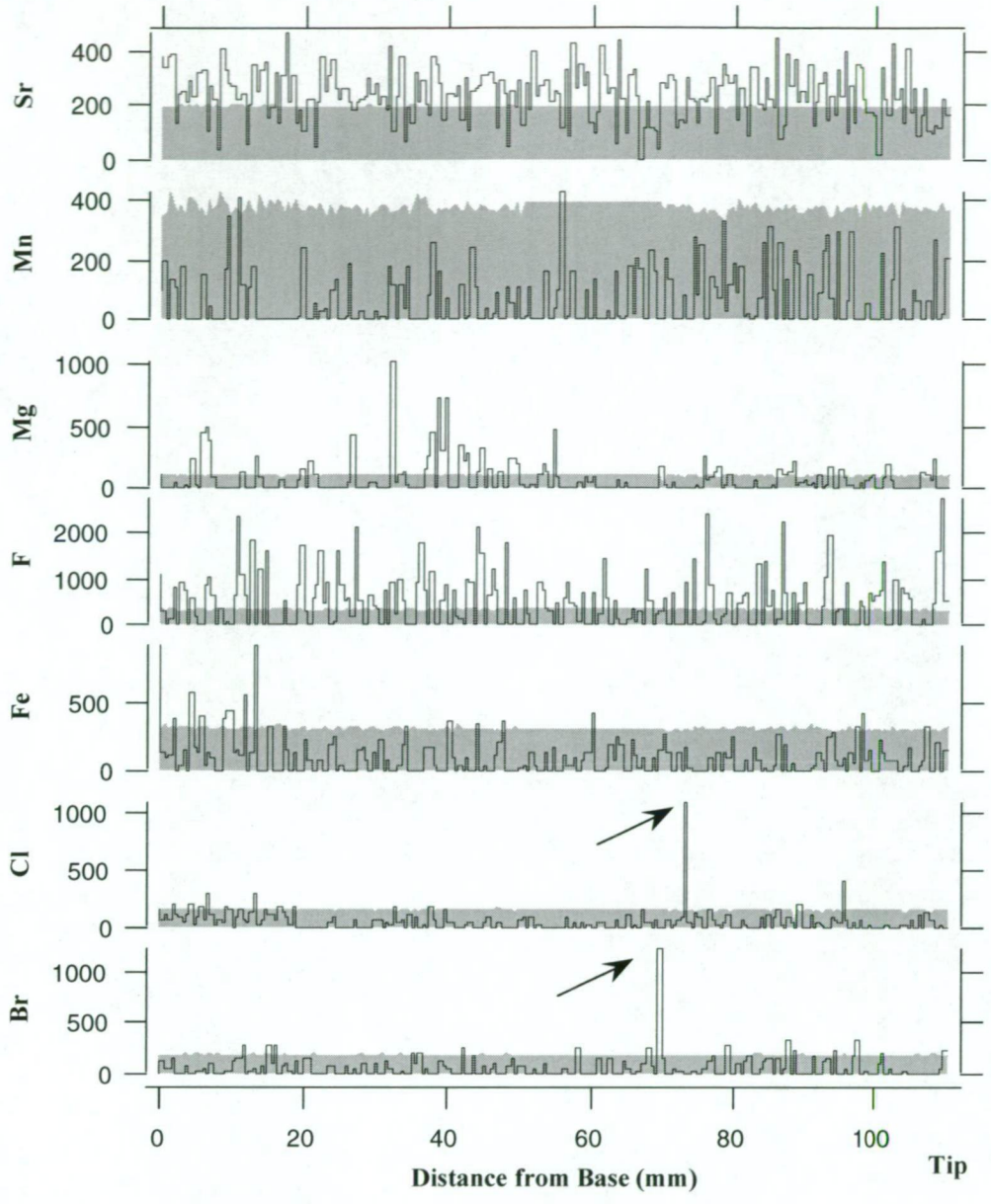

Figure 5.22. **Results of minor element analysis of RB-SS2, a straw stalactite from Risbys Basin Cave, Tasmania, using an electron microprobe and sampled at 0.5 mm intervals. Seven elements: bromine (Br), chlorine (Cl), iron (Fe), fluorine (F), magnesium (Mg), manganese (Mn), and strontium (Sr), were analysed. The strongest peak in bromine and chlorine traces (marked by arrows) are tentatively interpreted as being due to 1967 bushfires in Tasmania. Grey shading indicates the machine detection limits for each element.**

5.6. Discussion

The following discussion will not attempt to cover all of the ICP-MS results, but the more important findings will be examined in detail. The discussion will focus mainly on the soda-straw results paying particular attention to FC-SS5, as this is the most outstanding of the laser ablation ICP-MS analyses, and to a lesser extent the BDTH soda straws, which are characterised by having similar cyclical variations in the minor elements. The ICP-MS results of the stalagmite, BFM-J96, will be discussed in relation to the water chemistry data provided by Dr Andy Baker. The impact of lateral variation will also be discussed using results from the FC-SS5 tip comparison, from analyses of the stalagmites FC-S4 and CTH-S1, and from the analysis of the Yarrangobilly flowstone material JC-F1. Some attention will first be given to the advantages and disadvantages of using the laser ablation ICP-MS method.

5.6.1. Comments on the Laser Ablation ICP-MS Methodology

Both this study and that of Hellstrom (1998) clearly illustrate some of the advantages of the laser ablation ICP-MS technique over other microbeam analytical methods particularly in relation to sample preparation (*ie* very little is required in comparison to SIMS or electron microprobe analysis), to the speed of data acquisition and sample throughput. The laser ablation ICP-MS system lags behind other microbeam techniques in regard to the spatial resolution of the analysis, although this is being addressed by newer generations of laser ablation ICP-MS instrumentation.

Of great concern, and requiring further investigation, are possible intra-crystalline minor element variations due to crystal zoning, an effect that may have detrimental impacts on the interpretation of very high resolution minor element analyses of speleothems (Reeder and Grams, 1997). Hellstrom (1998) has noted that it is very easy to disturb the temporal sequence of soda-straw stalactites when preparing samples for analysis particularly by those analyses that require a flat planar surface such as the SIMS or electron microprobe techniques. Therefore, results from the study of soda-straw stalactites that have been prepared for analysis by cutting and polishing should be treated with some caution.

The lack of a calcite standard selected specifically for speleothems is a major drawback for this type of study, particularly if comparisons are going to be made with other geochemical analyses. Hellstrom (1998) demonstrated that there is good agreement between fully quantitative solution introduction ICP-MS results and qualitative laser ablation ICP-MS analyses, although the former technique will give more accurate results. As the results of this study are qualitative only with the principal intention to investigate the nature of minor element variations in speleothems, it was deemed unnecessary to develop a calcite standard, the difficulties of which are discussed by Sinclair *et al.* (1998). Further extension of this type of study using laser ablation ICP-MS will require development of a suitable speleothem calcite standard so that analyses can be treated as fully quantitative and comparable with results obtained from other geochemical analyses.

5.6.2. Correlations Between Minor Elements

The positive correlations between several of the minor element pairs shown in Table 5.9 are of real significance in nearly all of the samples analysed with laser ablation ICP-MS, particularly as they agree very closely with the results of Roberts *et al.* (1998). In almost every sample the Sr and Ba minor element pairs have strong positive correlations and most r values are greater than 0.50 for both the low- and high-frequency results, notable exceptions are BFM-J96 and YBJC-F4 with relatively weak positive correlations.

Roberts *et al.* (1998) argue that there is an indirect temperature effect on the partitioning of Sr and Ba into speleothem calcite, suggesting that it may be related to the calcite precipitation rate which is itself a complex function of temperature, water supply, and the concentration of PCO_2 and Ca^{2+}. Since temperature directly affects PCO_2 and Ca^{2+} concentrations, the rate of precipitation of speleothem calcite increases with positive temperature fluctuations *ie* it will increase during spring with the maximum occurring in late summer, and decrease during autumn with the minimum occurring in late winter.

The influence of lag effects between cause and effect have not been considered here, or in the FC-SS5 chronology as seepage water at these sites have not been sampled over time. Using monthly sampling intervals Goede (1981) found a lag time of up to two months in the hardness of seepage water relative to surface temperature changes at two drip sites in Frankcombe Cave, Florentine Valley, Tasmania.

It has been shown that seasonal changes in temperature that induce oscillations in soil PCO_2 also influence the pH of groundwaters (Dörr and Münnich, 1989). It is argued that the variations observed in uranium are influenced by seasonal changes in pH as the uranyl ion is sensitive both to pH changes and to fluctuations in other dissolved species. Close scrutiny of variations in uranium content and its relationship to the other minor elements analysed (for example Figure 5.10d to Figure 5.10f) reveals that the majority of the U and Mg peaks coincide but have a negative relationship with Sr and Ba. These relationships are supported in the correlation matrix, although the middle and lower sections of FC-SS5 (Table 5.2) have stronger relationships between the elements.

Although the Mg results in this study have an unknown systematic error, because of the sample chamber contamination problem reported earlier, this is assumed not to have affected the pattern of variation. Most samples have positive correlations between the Sr and Ba results, however FC-SS5 has weak negative correlations between the Mg and the Sr-Ba results, a pattern similar to that observed by Roberts *et al.* (1998). According to these authors the nature of the correlations is indicative of a size dependent relationship, reflected by variations in ionic radii, since Ba^{2+} and Sr^{2+} ions are larger than Ca^{2+} ions they positively correlate but negatively correlate with Mg^{2+}, which has a smaller ionic radius than Ca^{2+}. However, not all of the results fit this model indicating that there are other geochemical factors influencing the minor element relationships, both on a temporal and spatial scale.

There are major differences in the correlations between the annual records, for example FC-SS5, and the long term records, for example the Yarrangobilly samples, clearly illustrating that

the temporal scale does have a significant influence. Factors that may have the greatest influence over long time scales include changes in flow path resulting in longer residence times or exposure of geochemically different carbonate. Further investigation is required to establish whether the seepage water feeding the speleothems is a mixture of waters, *ie* the catchment area contains several lithologically different bedrock types, or if it is from a single source, *ie* the catchment contains a single bedrock type (Roberts, 1997).

Table 5.9. **Summary of the relationships between the four minor elements (Mg, Sr, Ba, and U) in all of the samples analysed by laser ablation ICP-MS. The table shows both the untreated (UT) and detrended (DT) results with positive relationship indicated by a "+" symbol and a negative relationship indicated by a "=" symbol. The number of symbols relates to the size of the r-value, one symbol equivalent to an r-value between 0 and ± 0.30, two symbols equivalent to an r-value between ± 0.31 and ± 0.70, and three symbols equivalent to an r-value greater than ± 0.71. Roberts *et al.* (1998) correlation coefficients are also shown for comparison.**

Sample	Type	T	Mg-Sr	Mg-Ba	Mg-U	Sr-Ba	SrU	Ba-U
BFM-J96	st	UT	=	+	+	+ +	+	+
(n = 9663)		DT	+	+	+	+ +	=	+
FC-SS5	ss	UT	+	=	+ + +	+ + +	+	=
(n = 56954)		DT	+ +	= =	+ +	+ + +	=	=
BDTH-SS1 (sub)	ss	UT	= =	=	+	+ + +	=	=
(n = 4000)		DT	= =	= =	+	+ + +	=	=
BDTH-SS3 (sub)	ss	UT	+ + +	+ + +	+ +	+ + +	+ +	+ +
(n = 3500)		DT	+ +	+ +	+ +	+ + +	+ +	+ +
CTH-S1a	st	UT	=	=	+	+ + +	+	+ +
(n = 11884)		DT	+	+	+	+ + +	+	+
CTH-S1b	st	UT	=	=	=	+ + +	+	+
(n = 11347)		DT	+	+	+	+ + +	+	+
FC-S4aa	st	UT	=	= =	= =	+ + +	+	+
(n = 6172)		DT	+ +	+	=	+ + +	+	+
FC-S4bb	st	UT	+	+	=	+ + +	+	+
(n = 6172)		DT	+ +	+	=	+ + +	+	+
JC-F1aa	fl	UT	+	+	+	+ + +	= =	=
(n = 11884)		DT	+	+	=	+ + +	=	=
JC-F1bb	fl	UT	+	+	+	+ + +	= =	=
(n = 11347)		DT	+	+	+	+ + +	= =	=
JC-F2	fl	UT	+ + +	+ + +	+ +	+ + +	+	+
(n = 1177)		DT	+ +	+ +	+ +	+ + +	+	+ +
JC-F4	fl	UT	+ +	+	=	+ +	= =	+
(n = 595)		DT	+ +	+	=	+ +	=	+ +
Roberts *et al.* (1998)	st	UT	=	+ +		+ +		
(n = 1150)		DT	= =	=		+ + +		

5.6.3. ICP-MS Analysis of FC-SS5

The minor element variations observed in FC-SS5 (Figure 5.9) are almost certainly annual and are remarkably similar to the results of a 2.4 mm section of stalagmite analysed by Roberts *et al.* (1998) using SIMS. One of the most significant results is that annual cyclicity of the minor elements can be traced for the whole length of the sample and a chronology established using autocorrelation. Another significant finding is that the surface ridging is also annual and that this morphological feature can be measured with dendrochronological equipment. The results can be used not only to determine sample ages, but also to investigate growth rate variations.

The closeness of the FC-SS5 chronologies, established by two independent methods, indicates that soda-straw stalactites have great potential as a palaeoenvironmental proxy recorder over the last few hundred up to several thousand years. However, it does assume that deposition was continuous and continued right up to the time the specimen was collected. Considerable work is required to investigate further the parameters controlling surface ridges and the cyclicity of the minor element composition of soda-straw stalactites.

The distinct cyclicity of the FC-SS5 minor element data indicates that there is a very strong seasonal influence controlling the partitioning of Sr and Ba into calcite, more or less in antiphase with the U and Mg. Table 5.10 outlines some of the factors that may influence the minor element composition of speleothem calcite and indicates their seasonal response. Previous studies have demonstrated very strong relationships between several of the variables listed in Table 5.10 such as water conductivity and calcium concentration (Langmuir, 1971), or the concentration of organic acids and discharge (Baker *et al.*, 1997a).

A study of seepage water hardness at Frankcombe Cave by Goede (1981) has concluded that it has a strong positive correlation with mean monthly temperature but moisture availability has some influence. Moore (1962) has demonstrated that annual pH variations are related to the seasonal fluctuation of CO_2, driven by the activity of soil microrganisms and vegetation, with seepage water slightly alkaline in winter with pH values of approximately 8, and slightly acidic in summer with pH values around 6.5. Fluctuations of CO_2 concentrations in the cave atmosphere change by almost two orders of magnitude between the seasons with higher CO_2 concentrations occurring in summer (Moore, 1962). Moore (1962) suggested that stalactite growth is subdued or retarded in winter with most of growth occurring in the warmer months. The FC-SS5 minor element results support this idea.

The two climate stations nearest to Frankcombe Cave, Butlers Gorge (Lat: 42.28°S; Long: 146.27°E: Elevation: 666 m) and Maydena (Lat: 42.76°S; Long: 146.60°E; Elevation: 270 m), have mean summer (DJF) temperatures of 12.0°C and 14.5°C respectively, and mean winter (JJA) temperatures of 3.7°C and 5.8°C respectively, mean daily potential evaporation at Maydena is 3.5 mm in summer and 0.7 mm in winter. Given the large temperature range between the summer and winter mean temperatures at Butlers Gorge and Maydena of 8.3°C and 8.7°C, respectively, it is likely that temperature fluctuations directly influence soil biological activity and PCO_2 concentrations in seepage water, and consequently the pH of the seepage

water to such a degree as to produce the cyclic fluctuations not only of PCO_2 in solution but also of the minor elements observed in FC-SS5. A program of water collection and analysis of the minor element composition of the seepage water in Frankcombe Cave will be needed to investigate the seasonal concentrations and relationships of the major ion species, specifically Mg, Sr, Ba, and U together with concentrations of the organic acids and other relevant environmental data.

Table 5.10 **Some of the factors that may influence the minor element composition of speleothem calcite. Pitty (1966) lists a number of factors that could cause differences in the quantities of dissolved carbonate in karst groundwater together with their effects on the "solute concentration" and the possibility of temporal lags.**

		Summer	Winter
Minor Element Ratios	Mg and U	↓	↑
	Sr and Ba	↑	↓
Factors	Surface Mean Annual Temperature	↑	↓
	Soil PCO_2	↑	↓
	Vegetation activity	↑	↓
	Seepage Water pH	↑ (acid)	↓ (alkaline)
	Calcite Precipitation	↑	↓
	Residence Time	↑	↓
	Surface Water Excess	↓	↑
	Seepage Water Drip Rate	↓	↑
	Seepage Water Conductivity	↓	↑
	Organics	↑	↓
	Ca^{2+} Concentration	↑	↓
	Water Hardness	↑	↓
	Bedrock Weathering Rates	↑	↓
	Cave Mean Annual Temperature	↑	↓
	Seepage Water Temperature*	↑	↓

The complete ICP-MS scan of FC-SS5 has two significant peaks at 1959 and 1965 (Figure 5.9) that may be related to some kind of surface crystal defect but its exact nature needs further study. Hellstrom (1998) and Roberts (1997) discuss the potential problems that crystal zoning may have both on the reliability of records obtained by micro-sampling and also to their lateral reproducibility within samples. They rightly point out that extreme caution should be exercised in interpreting results when relying on a single minor element trace along the longitudinal axis of a speleothem, and suggest that the lateral variation should first be assessed by two dimensional rastering, an application of laser ablation ICP-MS that has already been shown to be extremely useful (Hellstrom, 1998).

The results of three separate scans of varying lengths from the tip of the lowest section of FC-SS5 (Figure 5.14) suggest that there is significant lateral variation in minor element composition. It is encouraging to note that the cyclicity of the minor elements is laterally continuous around the diameter of the soda-straw stalactite and congruous with surface banding. However, further investigation of other samples is required to confirm this, preferably using laser ablation ICP-MS analysis to produce two dimensional maps up to two mm wide. (Hellstrom, 1998).

5.6.4. ICP-MS Analysis of Browns Folly Mine Stalagmite, BFM-J96

It was anticipated that an annual scale chronology could be produced from the BFM-J96 minor element results using the peaks and troughs as yearly markers, however this has proved very difficult. Unlike FC-SS5, which has very clear and distinct annual cycles, an annular minor element pattern in BFM-J96 is difficult if not impossible to distinguish. An attempt was made to construct a chronology using the Ba and Sr traces in order to identify individual years. This attempt yielded a chronology that is very close to the 160 year maximum age but not much confidence is placed on its reliability. The main problem is in distinguishing one year from another by the annual minor element pattern given that the growth rate probably varies considerably. Measured growth rates, determined both from annual laminations and total sample thickness assuming 160 years growth, vary from approximately 0.05 to 0.25 mm $year^{-1}$, implying that the analysis may not have resolved some years, further complicated by the assumption that there have been no breaks in deposition. The difficulty in identifying yearly cycles not only in stalagmites but soda-straw stalactites as well raises several important issues regarding annual layering:

(1) Are the factors controlling the minor element composition of stalagmites the same as those controlling soda-straw stalactites?

(2) What key geochemical factors, for example pH, PCO_2, Ca^{2+} concentration, *etc*, govern the laying down of annual patterns of variation in minor element composition?

(3) Does sample depth below the surface influence the degree of minor element cyclicity?

(4) Is there a relationship between water temperature and small variations in cave temperature and does this influence minor element composition?

One of the major differences between the soda-straw stalactites on the one hand and stalagmites and flowstones on the other is that the former are created by a hanging drop and the latter are formed by flowing water. The presence of flowing water considerably complicates interpretation of minor element deposition and may explain the lateral variation observed in stalagmites due to progressive minor element depletion of the solution as it moves across the growth surface. Further study is required to investigate the variation of minor elements along both stalagmite and flowstone growth surfaces.

5.6.5. ICP-MS Analysis of Yarrangobilly Flowstones

Comparisons between minor element scans and a number of stable isotope analyses will be presented in Chapter 6 together with a more detailed discussion of the results since the factors controlling the composition of stable isotopes in speleothem calcite are better understood and may provide additional clues as to the possible influences on the minor element composition of speleothems. However some preliminary discussion of the Yarrangobilly flowstones will be presented.

The positive correlation between Sr and Ba is consistent in all of the samples at both low- and high-frequency suggesting that strontium and barium respond to similar geochemical factors, a situation also observed in New Zealand flowstones by Hellstrom (1998). It has been suggested previously that variations in the strontium and barium composition of speleothem calcite may be caused by an indirect temperature effect (Roberts, 1997). The weak negative correlation between the minor element pairs Sr–U and Ba–U in the low frequency results of JC-F1 may be related to changes in groundwater chemistry caused by variations in vegetation productivity, a similar situation was found in New Zealand flowstones by Hellstrom (1998). The stable isotope and growth rate data, calculated from the $^{230}Th/^{234}U$ age estimates, may provide additional evidence to support these hypotheses and will be discussed further in Chapter 6.

5.6.6. Lateral Variation in the Minor Element Composition of Speleothems

In this study laser ablation ICP-MS analysis has been used exclusively to investigate minor element variations in the three types of speleothems used for palaeoenvironmental interpretations allowing both short and long term variations to be studied and, to a limited degree, lateral spatial variation. Most samples have been analysed with a single analysis scan but in several cases a repeat scan was done parallel to the first, approximately 200 µm from the first, allowing some assessment of lateral spatial variation. A raster map of the speleothem surface, following the procedure of Hellstrom (1998), would be a better method for studying the lateral variation of minor element composition in speleothems. This was not attempted with any of the samples due to the relative difficulty and time consuming nature of rastering with the current laser ablation stage set up. The current stage apparatus at the RSES, ANU, Canberra is in the process of being fully computerised thus making it significantly easier to collect and process data. At the same institution, installation of a new and more sensitive ICP-MS is imminent.

The most significant result of all the lateral variation analyses was the similarity apparent between all three FC-SS5 scans, at least in the ability to be able to discriminate individual years but more work is needed to investigate the quantitative relationships between separate scans. The relative lack of similarity between the scans of the stalagmite samples is not surprising given the potential depletion of minor elements as the precipitating solution travels down the growth surface. The lack of similarity between the two JC-F1 scans is not surprising as these samples are essentially randomly picked samples from a flowstone and their exact orientation and location relative to each other is unknown.

5.7. Conclusions

This study has shown that laser ablation ICP-MS is an extremely useful tool for the investigation of minor element fluctuations in the three main types of speleothems used for palaeoenvironmental investigations, namely soda-straw stalactites, stalagmites, and flowstones. Five elements: magnesium (^{26}Mg), strontium (^{88}Sr), barium (^{138}Ba) and uranium (^{238}U) were selected for analysis as they were found in suitable concentrations for analysis and gave reproducible results from duplicate measurements. All results were normalised to calcium (^{48}Ca). The technique has permitted extremely high resolution analyses to be done on samples which encompass three different temporal scales, interglacial/glacial (10^4–10^5 years), millenial (10^3–10^4 years), and secular ($<10^2$–10^3 years).

Lateral variations in speleothem minor element composition have also been investigated by laser ablation ICP-MS and the results indicate that significant lateral variations can occur in stalagmites and flowstones due to the nature of their formation while soda-straw stalactites show only very minor lateral differences. Further investigation is required on the lateral fluctuation of absolute concentrations.

Nearly all samples showed high positive correlations between the Sr and Ba results suggesting that strontium and barium concentrations are controlled by the same environmental parameters at all temporal scales, this appears not to hold true for Mg and U. At the secular scale the elements seem to be responding to seasonal changes in the acidity of the seepage water, responding to changes in the PCO_2 and biological activity of the soil and vegetation above the cave. At the higher temporal scales several factors may be operating to produce discernible changes in the minor element composition of speleothems but the traces must be compared with other palaeoenvironmental records in order to narrow down the dominant factors (see Hellstrom, 1998 for an example). Ayalon *et al.* (1999) have shown that a close relationship between Sr and Ba occurs even when a significant amount of strontium has been derived from an exogenic source suggesting that barium may also be supplied from such a source.

The most significant results have come from the study of the soda-straw stalactite, FC-SS5, which shows distinct cyclicity in its minor element content. The regularity of the quasi-periodical signal strongly supports an annual origin and on this basis a chronology for the sample has been constructed by autocorrelation using two independent methods, namely the minor element signal and the surface ridging of the sample, the results agreed with each other very closely (± 5 %). The method assumes that the sample has grown continuously and was either active at the time of collection or that at least the minimum age of the youngest material is accurately known. Comparison of minor element results with instrumental climate data did not yield any significant correlation but this may be due to the climate stations for which data were available being at some considerable distance from the cave in an area with a local relief of approximately 1,000 metres.

Chapter 6

Stable Isotopes in Speleothems

6.1. Introduction

There are approximately 300 stable isotope species in nature and 62 elements possess at least two or more isotopes with one usually predominant and the others present in trace quantities. The study of light stable iostopes such as oxygen, carbon, sulpur, hydrogen, *etc* has allowed a greater understanding of a whole suite of earth processes. Such studies were made possible with the development of the mass spectrometer by H.C. Urey and his collegues. The fractionation of light stable isotopes during physical and chemical processes records the environmental conditions under which they occurred by altering their relative abundances.

Therefore analyses of stable isotope ratios can potentially be used to reconstruct changes in environmental conditions (Ehleringer and Rundel, 1988). However, the environmental signal may be masked by fractionation caused by other natural processes thereby making the reconstruction process more difficult. It is therefore vital to consider all of the possible influences on the final delta (δ) value (Hellstrom, 1998). This chapter briefly examines the background of stable isotope studies and then discusses the main factors influencing oxygen and carbon isotope ratios with specific reference to speleothems.

6.1.1. Stable Isotope Variations in Nature

Variations in the stable isotope ratios of many minerals have been shown to reflect the environmental conditions prevalent during deposition (Gray, 1981). The isotopic composition of a sample is expressed using differential notation:

Equation 6.1

$$\delta X_{standard} = \left[\left(R_{sample} - R_{standard} \right) \Big/ R_{standard} \right] \times 1000$$

where $\delta X_{standard}$ is the isotope ratio in delta units relative to a standard. R_{sample} and $R_{standard}$ are the absolute isotope ratios of the sample and the standard, respectively. Multiplying by 1000 enables the results to be expressed in parts per thousand (‰) or "per mil" (Ehleringer and Rundel, 1988). Samples of gas are prepared and the isotopic ratios of the elements measured by mass spectrometry.

6.1.1.1. Oxygen

Oxygen, the most abundant element in the terrestrial crust, has three stable isotopes with relative abundances of 99.7630 % for ^{16}O, 0.0375 % for ^{17}O, and 0.1905 % for ^{18}O (Bowen, 1991). Most

research has focussed on the oxygen isotope ratio $^{18}O/^{16}O$, particularly in relation to climate studies, because of their abundance, a large reservoir of oxygen exists in the oceans, and reactivity, as oxygen forms compounds with most other elements. The relative ease with which natural abundance variations can be measured also makes oxygen an ideal isotope for environmental studies (Gray, 1981).

6.1.1.2. Carbon

There are two stable isotopes of carbon with relative abundances of 98.89 % for ^{12}C and 1.11 % for ^{13}C (Bowen, 1991). For geological and biological materials, naturally occurring variations in the isotopic ratios of carbon are generally in the range between -40 and 20 ‰. Its participation in many biological and geological processes, along with oxygen, means that the study of $^{13}C/^{12}C$ ratios has made important contributions to our understanding of earth systems (Ehleringer and Rundel, 1988).

6.1.1.3. Hydrogen

Hydrogen has two stable isotopes with relative abundances of 99.9852 % for ^{1}H and 0.0148 % for ^{2}H, or deuterium (Bowden, 1988). The large relative mass differences mean that the isotope ratios of hydrogen in geological and biological materials can vary by up to 70 %, the maximum possible in stable nuclides, in meteoric water the range is in the order 400 ‰. Its abundance and participation in the hydrological cycle, particularly with isotopes of oxygen, make it ideal for investigating environmental change and various biological and geological processes (Faure, 1985).

6.2. Isotopic Composition of Meteoric and Percolation Water

In natural waters δD and $\delta^{18}O$ values are normally expressed relative to the Standard Mean Oceanic Water (SMOW) standard (Craig, 1961). All figures in the following discussion are given relative to SMOW unless otherwise indicated. To convert $\delta^{18}O$ results from SMOW to PDB a figure of 29.94 ‰ is subtracted.

6.2.1. Meteoric Water

Spatial and temporal variation of stable isotope ratios in precipitation occurs because of the preferential evaporation of lighter isotopes, due to vapour pressure differences between the isotope pairs ^{18}O and ^{16}O for oxygen and ^{2}H and ^{1}H for hydrogen, in the moisture source areas resulting in water vapour enriched in the lighter isotopes relative to the moisture source (Dansgaard, 1964). When water vapour reaches the target area, with condensation processes forming raindrops or ice crystals, the heavier isotopes tend to condense preferentially and the fractionation process is reversed. The earth's atmospheric circulation, temperature and other geographical factors combine to produce the global pattern observed in the oxygen isotope ratios of precipitation (Schotterer *et al.*, 1996).

Dansgaard (1964) identified global patterns in the isotopic variations of oxygen ($\delta^{18}O$) and hydrogen (δD) of precipitation and concluded that they were influenced by several key factors.

The factors include a temperature dependence, termed the "temperature effect", a relationship with the amount of precipitation, the "amount effect", and a negative relationship between elevation and the isotopic ratio, the "altitude effect". The temperature at which vapour condensation takes place is the key factor governing the $\delta^{18}O$ of precipitation, and as the distance from the moisture source increases so to does the depletion of the heavier isotopes (^{2}H and ^{18}O). Therefore, the greater the fall in temperature, the more condensation will occur resulting in lower heavy isotope concentrations relative to the original water source (Bradley, 1986).

Investigations of the relationship between the mean annual $\delta^{18}O$ of precipitation and temperature allows calculation of the temperature effect, a value of approximately 0.7 ‰ $°C^{-1}$, assuming that the $\delta^{18}O$ variation is controlled by local temperature. The amount effect is considered to be predominant in tropical precipitation (Dansgaard, 1964) but can significantly influence the isotopic composition of summer precipitation in temperate regions including Tasmania (Goede, 1982).

6.2.2. Percolation Water

Vadose seepage waters are isotopically homogenised to varying degrees depending on the extent of mixing within the soil and epikarst zone. Short mixing times combined with rapid recharge of water give rise to marked seasonal variation in the isotopic composition of water while the converse produces values that are relatively constant (Thompson *et al.*, 1976, Yonge *et al.*, 1985). Yonge *et al.* (1985) found that seepage water sampled throughout the year from a number of caves in North America approximated to the isotopic composition of the winter weighted mean annual precipitation for the region with values on or close to the Meteoric Water Line (Craig, 1961):

Equation 6.2 $$\delta D = 8 \times \delta^{18}O + d$$

where *d*, deuterium excess, is equal to 10. In contrast, Goede (1998) has found that for Tasmanian cave sites the isotopic composition of seepage water approximates that of the weighted mean winter precipitation ($\delta D = 7.0 \times \delta^{18}O + 6.9$). This has been attributed to high evapotranspiration rates during the summer months leaving little surplus water for downward percolation.

6.3. Stable Isotope Variations in Speleothems

6.3.1. Calcite Deposition

Karst landscapes and caves develop in limestone bedrock usually due to the dissolution of calcium carbonate by carbonic acid. High concentrations of CO_2 are frequently found in the soil atmosphere due to biological processes and partially dissolve in percolation water to yield carbonic acid thus greatly increasing the rate of dissolution of underlying limestone. When seepage waters subsequently come in contact with a cave atmosphere, where CO_2 concentrations are usually much lower than in soils, they quickly become highly supersaturated

due to outgassing of CO_2 and calcium carbonate will be precipitated (Buhmann and Dreybrodt, 1985; Dreybrodt, 1988).

The temperature of the soil and the partial pressure of CO_2 in the soil, which are controlled by the surface temperature, govern the supersaturation of the seepage water (Dreybrodt, 1999). The depositional process can be characterised by the following equation:

Equation 6.3

$$Ca^{2+} + 2HCO_3^- \rightarrow CO_2 + H_2O + CaCO_3$$

Precipitation of calcium carbonate from thin water films is controlled by four main mechanisms that act independently but any one can determine the overall rate:

(1) Kinetics of precipitation at the phase boundary between the $CaCO_3$-H_2O-CO_2 system and the limestone.

(2) Kinetics of conversion of carbonic acid (H_2CO_3) to CO_2.

(3) Mass transport of dissolved ions by diffusion to phase boundaries.

(4) Rate of outgassing of CO_2 from solution into the cave atmosphere.

Palaeoenvironmental studies of speleothems have been concentrated on uniform diameter stalagmites because they grow relatively rapidly and often continuously over time periods in excess of 10^4 years. The rate of water supply is the main factor determining speleothem shape. The nature of their growth is well understood and a detailed discussion can be found in Dreybrodt (1988). It is notable that the supersaturation of the parent water and uniform diameter stalagmite shape are dependent on climatic variables therefore permitting palaeoenvironmental signals to be recorded by speleothems (Dreybrodt, 1999)

6.3.2. Stable Isotope Fractionation During Speleothem Formation

Hendy (1971) has suggested three modes of calcium carbonate deposition that might affect the isotopic composition of speleothems:

(1) the equilibrium loss of carbon dioxide;

(2) the kinetic loss of carbon dioxide; and

(3) the evaporation of water.

The use of isotopic ratios in speleothems as sources of palaeoenvironmental data depends on the maintenance of isotopic equilibrium conditions between bicarbonate ions (HCO_3^-) and aqueous carbon dioxide ($CO_{2(aq)}$). Isotopic equilibrium is maintained only if carbon dioxide outgasses slowly from the host dripwater (Hendy, 1971). Under isotopic equilibrium conditions, the fractionation of oxygen isotopes between parent dripwater and speleothem calcite is temperature dependent at a rate of -0.24 ‰°C^{-1} (Hendy and Wilson, 1968) and can yield important information about regional palaeoenvironments.

The controlling mechanisms that affect the isotopic composition of speleothems will be discussed below. Hendy's modes (2) and (3) result in the formation of calcite with stable isotope ratios that cannot be used for palaeoenvironmental studies. Deposition under conditions of isotopic equilibrium is most likely when humidity of the cave atmosphere is at or close to 100 percent and

where air movement is restricted. Here thermal equilibrium is reached with the surrounding bedrock and cave temperatures will usually be equivalent to the surface mean annual temperature within approximately 1°C (Gascoyne, 1992).

For most speleothems in temperate climate caves, oxygen isotope ratios can be used as a proxy of mean annual temperature only when seepage waters are homogenised isotopically and do not show significant seasonal variation in the rate of supply. In some temperate west coast environments the dominant influence affecting oxygen isotope ratios appears to be strong glacial-interglacial latitudinal shift in the moisture source area, *e.g.* Vancouver Island, Tasmania and Norway (Gascoyne *et al.*, 1980; Gascoyne *et al.*, 1981; Goede *et al.*, 1998; Lauritzen, 1995). In contrast, oxygen isotope values of speleothems from tropical environments are influenced predominantly by the amount of precipitation (Fisher *et al.*, 1996). Many tropical regions are also subject to a strong seasonality in moisture receipts *ie* the wet and dry seasons.

Goede (1998) has found that the bulk of seepage water in several Tasmanian caves has been derived from winter precipitation and argues that, since the oxygen isotope ratio of Tasmanian precipitation shows a strong seasonal dependence on temperature, Tasmanian $\delta^{18}O$ values in speleothem calcite should be interpreted in terms of mean winter temperature rather then mean annual temperature. Due to a dominance of winter precipitation and high evapotranspiration rates in summer, a similar situation is likely to exist at Naracoorte.

6.3.3. Fluid Inclusions

In certain circumstances small amounts of water are trapped in cavities and crystal boundary defects during calcite precipitation (Kendall and Broughton, 1978). These small reservoirs of ancient water, approximately 10 to 50 μm in size, are thought to be the remnants of the parent drip water responsible for the growth of the speleothem. Due to the possibility of oxygen isotopic exchange with the host calcite, the deuterium/hydrogen ratio (δD) is measured, a simple conversion via the empirical relationship of Craig (1961) allows the $\delta^{18}O$ to be estimated (Equation 6.2). It has been demonstrated that the δD values of contemporary fluid inclusions from actively growing speleothems are similar to the modern percolation waters at a particular cave (Harmon *et al.*, 1979; Yonge *et al.*, 1985).

As mentioned in Section 6.2.2, the δD of percolation water is closely related to the isotopic composition of the meteoric water on the surface above the cave (*eg* Yonge *et al.*, 1985; Goede, 1998). Estimates of cave palaeotemperatures are possible by converting the fluid inclusion δD measurements to $\delta^{18}O$ (Equation 6.2) and substituting the result into the following equation derived by O'Neil *et al.* (1975):

Equation 6.4

$$10^3 \ln \alpha_{c-w} = 2.78 \times 10^6 \times T^{-2} - 2.89$$

where α_{c-w} is the water-calcite fractionation constant and T is temperature in °K.

The main problem with this approach has been the successful extraction of water from the fluid inclusions, firstly without fractionation occurring and secondly in such a way that a large enough sample is obtained for analysis. Early attempts used crushing techniques or a combination of

heating and crushing (Yonge, 1981; Goede *et al.*, 1986) which significantly improved sample yield but made the extraction procedure very complicated because at high temperatures the limestone is decomposed yielding a large volume of CO_2 that has to be separated from the water vapor.

Recent attempts at extracting water from fluid inclusions without significant fractionation occurring have been much more encouraging (Dennis *et al.*, 1996; Rowe *et al.*, 1998). It is suggested that the method may be improved by direct extraction by laser ablation, *eg* UV laser, and analysis by a mass spectrometer able to analyse very small quantities of sample. Dr Michael Palin (RSES, ANU) is currently using this technique to analyse fluid inclusions in carbonate rocks in order to investigate their diagenetic history. It may be possible to apply the method with minor modifications to analyse fluid inclusions in speleothem calcite.

6.3.4. Testing for Equilibrium Deposition

To confirm that calcium carbonate has been deposited in isotopic equilibrium with the seepage water, that is that the loss of CO_2 from solution during calcite precipitation is sufficiently slow so that isotopic equilibrium is maintained between the aqueous carbon dioxide, bicarbonate ions, and the water (Hellstrom, 1998), the following tests can be made (Hendy and Wilson, 1968; Schwarcz, 1986; Lauritzen, 1995):

(1) Degree of positive correlation of paired values of $\delta^{18}O$ and $\delta^{13}C$ taken from the centre of the core along the vertical axis of the speleothem. If strong positive correlation is absent it provides good evidence of deposition under equilibrium conditions. However, the presence of a strong positive correlation does not necessarily indicate absence of equilibrium conditions since such a relationship may also be due to common environmental factors causing covariation (Goede, 1998).

(2) Paired values of $\delta^{18}O$ and $\delta^{13}C$ of at least seven calcite samples taken in sequence along an individual growth layer should not show a significant trend towards progressively heavier isotopic values from the centre of the core outwards. The test should be repeated for a number of growth layers (Hendy and Wilson, 1968, Hendy, 1971).

(3) There should be no significant correlation between $\delta^{18}O$ and $\delta^{13}C$ values along a growth layer as it may indicate a kinetic isotopic effect such as rapid loss of CO_2 (Gascoyne, 1992).

If any of these criteria are violated then it must be suspected that kinetic fractionation has occurred and that the spurious $\delta^{18}O$ and $\delta^{13}C$ values have produced which may mask any variation specifically due to climatic effects. For example, evaporation causing a rapid loss of CO_2 will negate any relationship between temperature and final $\delta^{18}O$.

Hellstrom (1998) investigated the validity of correlating $\delta^{18}O$ and $\delta^{13}C$ to infer isotopic equilibrium by using synthetic oxygen and carbon isotope records to simulate the effects of kinetic fractionation by the addition of a noise signal to these records. He suggested testing for covariation versus time using the first derivatives of $\delta^{18}O$ and $\delta^{13}C$ which should, theoretically, allow isolation of the variation due entirely to kinetic fractionation and, therefore, allow testing for it empirically. Repeated runs of

the simulation indicate that records with a first derivative correlation coefficient less than approximately 0.3 do not suffer from any significant bias due to kinetic fractionation (Hellstrom, 1998), therefore the method may provide a powerful method of testing for equilibrium conditions.

6.3.5. Controls on the Isotopic Composition of Speleothem Calcite

6.1.1.1 Oxygen Isotope Ratios

In temperate environments, variations in oxygen isotope values of speleothems that are deposited under conditions of isotopic equilibrium are controlled by three main factors (Harmon *et al.*, 1978):

(1) Changes in the temperature of the cave environment during deposition (temperature effect). Such changes are usually related directly to changes in mean annual temperature at the surface.

(2) Shifts in the isotopic composition of seawater due to the accumulation and ablation of glacial ice on land estimated by Shackleton (1987) at approximately 1.5 ‰ SMOW for a full glacial-interglacial cycle (ice volume effect) but it may be as small as 1.0 ‰ (Schrag *et al.*, 1996).

(3) Fluctuations in the isotopic composition of precipitation caused by temperature and humidity fluctuations at sites of evaporation and precipitation, sometimes accentuated by changes in the geographical location of moisture source areas (surface changes effect).

Factors 1 and 2 will cause speleothem calcite to become enriched in ^{18}O during cold periods while factor 3 generally has the opposite effect. The majority of stalagmites studied around the world show a negative relationship between $\delta^{18}O$ values of speleothem calcite and temperature indicating the dominance of factors 1 and 2.

In some caves, particularly those in cooler temperate West Coast climates (*e.g.* Norway, Tasmania, and Vancouver Island), factor 3 is dominant causing a positive relationship between the $\delta^{18}O$ values of speleothem calcite and palaeotemperature (Gascoyne *et al.*, 1980; Gascoyne *et al.*, 1981; Goede *et al.*, 1986; Lauritzen, 1995).

6.3.5.1. Carbon Isotope Ratios

Causes of variation of carbon isotope ratios within a single speleothem deposited under conditions of isotopic equilibrium has long been a contentious issue. However, the issue has been clarified by recent research results (*e.g.* Hellstrom *et al.*, 1998). The carbon isotope composition of speleothems will be influenced by whether the water passes through the limestone as a closed or an open system (Baker *et al.*, 1997). However, it is presumed unlikely that open and closed conditions would alternate during the growth of a single speleothem and this factor is therefore disregarded as being a major cause of internal variation.

It has also been suggested that $\delta^{13}C$ variations could in part reflect variable amounts of calcite precipitation in the flow-path above the cave. If this were to be so, a positive correlation would be expected between $\delta^{13}C$ values and magnesium content (Baker *et al.*, 1997, Roberts *et al.*, 1998).

No such relationship has been found. Explanation of temporal changes can be considered in terms of three major hypotheses:

(1) Changes in the relative abundance of two groups of plants that follow different photosynthetic pathways: C3 and C4 (Brook *et al.*, 1990; Dorale *et al.*, 1992; Talma and Vogel, 1992). C4 plants are predominantly tropical grasses and require high summer temperatures (Teeri and Stowe, 1976; Tieszen *et al.*, 1979).

(2) Changes in vegetation productivity, that control the amount of isotopically light organic matter supplied to the soil, which is broken down to provide CO_2 derived directly from the atmosphere. Carbon isotope variations in soil carbonates (Quade *et al.*, 1989) and subaqueous wallcrust in a karst spring (Coplen *et al.*, 1994) have also been attributed to this cause. Provided that soil thickness and texture does not change significantly during the life of the stalagmite, CO_2 concentrations in the soil can be expected to be function of the level of vegetation activity.

(3) Changes in the isotopic composition of carbon in atmospheric CO_2, with glacial periods being characterised by less negative values. One of the most reliable estimates so far of glacial-interglacial change suggests a change of 0.7 ‰ (Marino *et al.*, 1992).

Since the third hypothesis can only account for relatively minor variations, major changes will be interpreted in terms of the first two hypotheses.

6.4. Methodology

6.4.1. Sampling

Stalagmites are bisected longitudinally using a diamond-saw blade, one half is set aside for reference while the other half is used for isotope and/or minor element sampling and to provide samples for uranium series dating. Flowstones are cut perpendicular to the direction of growth in order to get a planar surface from which to acquire samples. In this study the flowstone samples used in this study were already broken into pieces and loosely followed the methodology of Hellstrom (1998) for cutting and preparing the samples for analysis. Hellstrom (1998) describes an excellent method for extracting cores from flowstones *in situ* and the techniques for mounting and extracting samples for age estimates, minor element, and stable isotope analyses. It is suggested that this methodology be followed by other speleothem workers in the future.

Stable isotope samples are extracted using a 1.6 mm diameter tungsten-carbide dental drill. Growth layers are sampled in order to test for conditions of isotopic equilibrium. Using a dental drill, a set of seven closely spaced 1.6 mm diameter holes are drilled within each growth layer from the centre outwards and analysed for $\delta^{18}O$ and $\delta^{13}C$.

6.4.2. Stable Isotope Analysis

For all oxygen and carbon isotopic analyses of calcite, carbon dioxide gas was prepared by reacting samples with 100% H_3PO_4 in a vacuum. Measurements of isotopic ratios are expressed

as per mil (‰) using the delta (δ) notation relative to the PDB (PeeDee Belemnite) standard. The isotopic ratios were determined using a VG-SIRA Series II mass spectrometer with a minimum measurement precision of approximately 0.02 ‰.

Dripwaters were prepared for oxygen isotope analysis by equilibration with CO_2 gas at 25°C for five hours in a VG-Isoprep 18. After drying, the gas samples were analysed on a VG-SIRA Series II mass spectrometer with a minimum analytical precision of around 0.02 ‰ relative to the SMOW standard.

To determine the nature of the relationship between $\delta^{18}O$ values of speleothem calcite and past temperatures, the isotopic composition of contemporary calcite deposited at isotopic equilibrium has to be determined. This has been done by sampling actively growing soda-straw stalactites at various underground sites within the study areas. Analyses can show a wide range of $\delta^{18}O$ values since some may not have been deposited under conditions of oxygen isotope equilibrium. However, it is assumed that a large enough sample was taken from individual caves for one or more individuals to have been deposited at or close to isotopic equilibrium and they can be identified by having the most negative values for both $\delta^{18}O$ and $\delta^{13}C$ (Goede and Hitchman, 1984; Goede *et al.*, 1986). In order to independently test the value of contemporary calcite an estimate of present day cave temperature (T) can be made using the expression of Craig (1965):

Equation 6.5

$$T\,(°C) = T_{MAT} - 4.2\left(\delta^{18}O_c - \delta^{18}O_w\right) + 0.13\left(\delta^{18}O_c - \delta^{18}O_w\right)^2$$

where T_{MAT} equals the surface mean annual temperature. Using the mean value of drip water ($\delta^{18}O_w$) and the value for modern calcite ($\delta^{18}O_c$) and substituting these in Equation 6.5, a temperature estimate is obtained. This value can be checked by measuring the cave temperature with a thermometer.

6.5. Results and Discussion

Theoretically Australia is not the most ideal place in which to recover Quaternary palaeoenvironmental records due to its relatively stable geological context, resulting in much thinner sequences with which to study, especially when compared to a geologically active environment such as New Zealand. As such the Australian palaeoenvironmental record is best described as patchy and incomplete with most records having poor temporal frameworks. The majority of the continent is arid with a humid margin that does not extend much more than 100 kilometres from the coast, thus in Australia most Quaternary palaeoenvironmental records predominantly reflect changes in available moisture (Kershaw and Nanson, 1993). Most of these records are severely limited by the material available with which to date them and rely mainly on a combination of radiocarbon dating and correlation to oxygen isotope stages (Chappell, 1991). Speleothems can be precisely dated with TIMS $^{230}Th/^{234}U$ dating (Chapter 4) and have been shown to reflect periods of greater moisture availability (for example, Ayliffe *et al.*, 1998; Desmarchelier *et al.*, 2000).

This section discusses the results of the analysis of contemporary calcite, dripwater, growth layer analyses, and stable isotope profiles of two stalagmites, LT and SC-S11 from Little Trimmer Cave, Tasmania and Victoria Fossil Cave, South Australia respectively, and a section of flowstone, JC-F1 from Jersey Cave, New South Wales. The discussion sections will demonstrate the potential that speleothems have in providing precisely dated, high-resolution, terrestrial palaeoenvironmental records with which to compare other proxy records against.

6.5.1. Modern Calcite and Growth Layer Analysis

6.5.1.1. Tasmanian Modern Calcite and Growth Layer Analysis

The present day isotopic composition of speleothem material from Little Trimmer Cave, Mole Creek, Tasmania, was determined by multiple analyses of calcite removed from two plastic funnels used to collect dripwater during 1979 (Goede *et al.*, 1982). The values obtained were -3.75 ‰ (PDB) for the $\delta^{18}O$ and -12.21 ‰ (PDB) for the $\delta^{13}C$. However, a $\delta^{18}O$ value of –4.0 ‰ (PDB) has been estimated from nearby Lynds Cave (Goede and Hitchman, 1983) by sampling sod-straw stalactite tips. This is regarded as a better estimate of the present day $\delta^{18}O$ of speleothem calcite as the Little Trimmer Cave drip site has a very fast mean drip rate and has been observed to respond quickly to isotopically heavy summer rainfall which may have biased the oxygen isotope composition of the lowstone towards a higher value (Goede, 1998: p. 185).

The first test for isotopic equilibrium suggested by Hendy and Wilson (1968) involves the degree of positive correlation between $\delta^{18}O$ and $\delta^{13}C$ values of samples taken along the longitudinal axis. A weak but statistically significant negative correlation was found (Table 6.1) confirming deposition under conditions of isotopic equilibrium (Figure 6.1). The second test involves examination of sets of seven samples from each of twelve growth layers. These sets show no significant correlation beween paired $\delta^{18}O$ and $\delta^{13}C$ values with one exception where the changes are relatively small. Overall the evidence is strongly in favour of deposition under isotopic equilibrium conditions.

Table 6.1 Descriptive statistics for two stalagmites, LT from Little Trimmer Cave, Mole Creek, Tasmania, and SC-S11 from Victoria Fossil Cave, Naracoorte, South Australia, and a flowstone, JC-F1 from Jersey Cave, Yarrangobilly, New South Wales.

	LT		SC-S11		JC-F1	
	$\delta^{18}O$	$\delta^{13}C$	$\delta^{8}O$	$\delta^{13}C$	$\delta^{18}O$	$\delta^{13}C$
n	283		90		74	
Minimum	-5.58	-11.25	-4.95	-9.17	-7.06	-9.78
Maximum	-3.12	-5.45	-2.58	-3.70	-4.05	-1.53
Mean	-4.84	-8.44	-3.94	-6.58	-5.66	-5.64
Correlation Coefficient	-0.3843		0.7732		0.3093	
1st Derivative	0.0335		0.6586		0.3072	
Regression Equation	y = -0.1563x – 6.1518 R^2= 0.1477		y = 1.929x + 1.0191 R^2= 0.5978		y = 0.1145x – 5.0119 R^2= 0.0957	

An additional test of equilibrium conditions suggested by Hellstrom (1998) is the analysis of the first derivatives from the longitudinal isotope profile. Longitudinal $\delta^{18}O$ and $\delta^{13}C$ profiles whose first derivatives have a correlation coefficient of less than approximately 0.3 suggests that the sample suffers from insignificant bias due to kinetic fractionation. The R-value of the first derivatives analysis of the LT stalagmite isotope profile is 0.0335 confirming that the LT stalagmite did grow in conditions of isotopic equilibrium.

6.5.1.2. Naracoorte Modern Calcite and Growth Layer Analysis

The isotopic composition of contemporary calcite was determined by sampling twelve actively growing soda-straw stalactites at two sites within Victoria Fossil Cave. Results of these analyses together with four dripwater samples from Spring Chamber are listed in Table 6.2. As expected, analyses show a wide isotopic range presumably because many were not deposited under conditions of oxygen isotope equilibrium. However, it is assumed that this is a large enough sample for one or more individuals to have been deposited at or close to isotopic equilibrium and they can be identified by having the most negative values of both $\delta^{18}O$ and $\delta^{13}C$, as shown in Figure 6.2, (Goede and Hitchman, 1984; Goede *et al.*, 1986). The technique provides an estimate of -4.76 ‰ PDB for the $\delta^{18}O$ of contemporary calcite. The modern calcite value was tested with Equation 6.5 using the mean value of drip water, -4.98 ‰ SMOW (-4.76 ‰ PDB), -4.76 ‰ PDB for modern calcite. A temperature estimate of 16.9°C is obtained and since this value is very close to the one actually measured (16.8°C) it confirms the estimate of the isotopic value of contemporary calcite.

There is a significant degree of positive correlation between the $\delta^{18}O$ and $\delta^{13}C$ values of 90 samples taken from the longitudinal profile of SC-S11 (Table 6.1 and Figure 6.3) so the first test is inconclusive. If correlation were due to fractionation effects, a linear relationship would have been expected but this is not the case. Paired values of $\delta^{18}O$ and $\delta^{13}C$ along four selected growth layers do not show a single trend towards heavier isotopic values from the centre of the core outwards and provide strong support for deposition under conditions of isotopic equilibrium.

Statistically significant correlations between $\delta^{18}O$ and $\delta^{13}C$ within a growth layer is absent in three of the four layers occurring only in growth layer GL-D which is located in the tapering tip of the speleothem. On examination of the data this appears to be due to a significant trend towards isotopically lighter values in $\delta^{13}C$ ($R^2 = 0.783$, df = 5, t = 4.2481, $P < 0.01$) but not in the case of $\delta^{18}O$ values. This is indicative of rapid loss of CO_2 from the depositional surface as the drip rate declines, suggesting that the amount of dripwater is less, resulting in a thinner water film (Dreybrodt, 1999), as indicated by the tapering tip. The hypothesis that the material has been deposited predominantly under conditions of isotopic equilibrium is supported and allows interpretation of oxygen and carbon isotope changes along the growth axis in terms of environmental change over the growth period of the speleothem, except perhaps for a minor fractionation effect on carbon isotope values near the tip which will not affect the interpretation that follows.

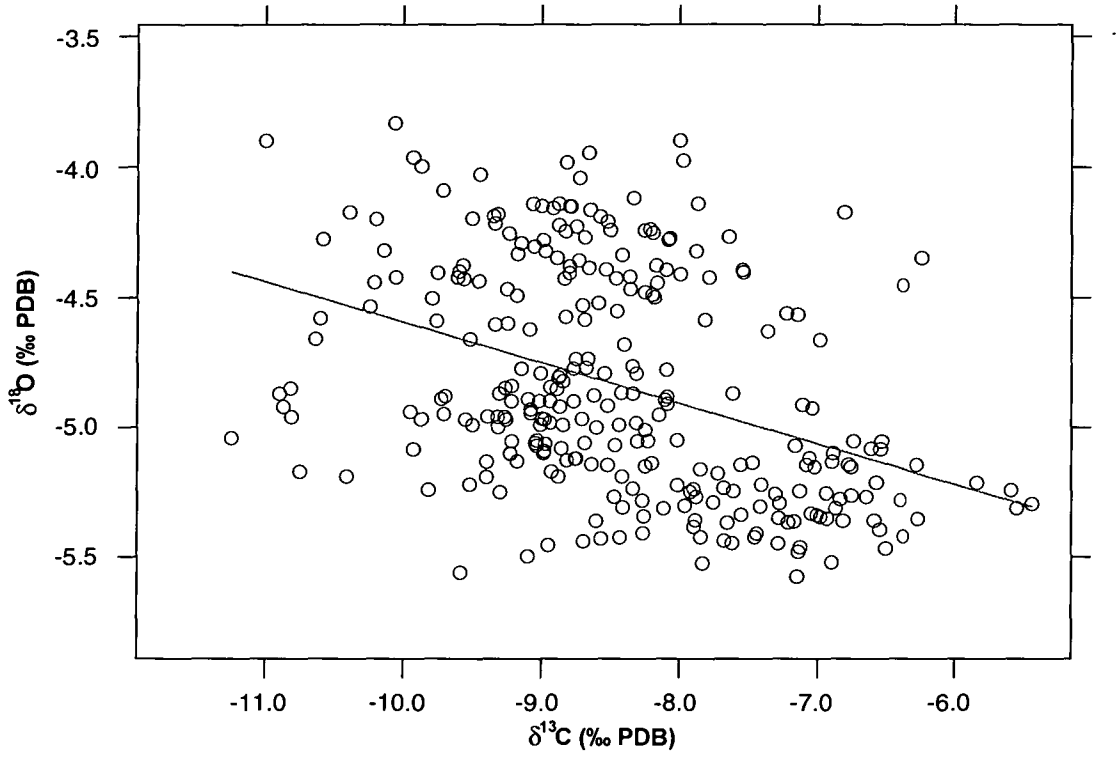

Figure 6.1. **Scatter plot of 283 $\delta^{18}O$ and $\delta^{13}C$ values of samples taken from the longitudinal profile of the LT stalagmite. A weak but statistically significant negative correlation was found (r = -0.39), regression line is also plotted (y = -0.1563x – 6.1518).**

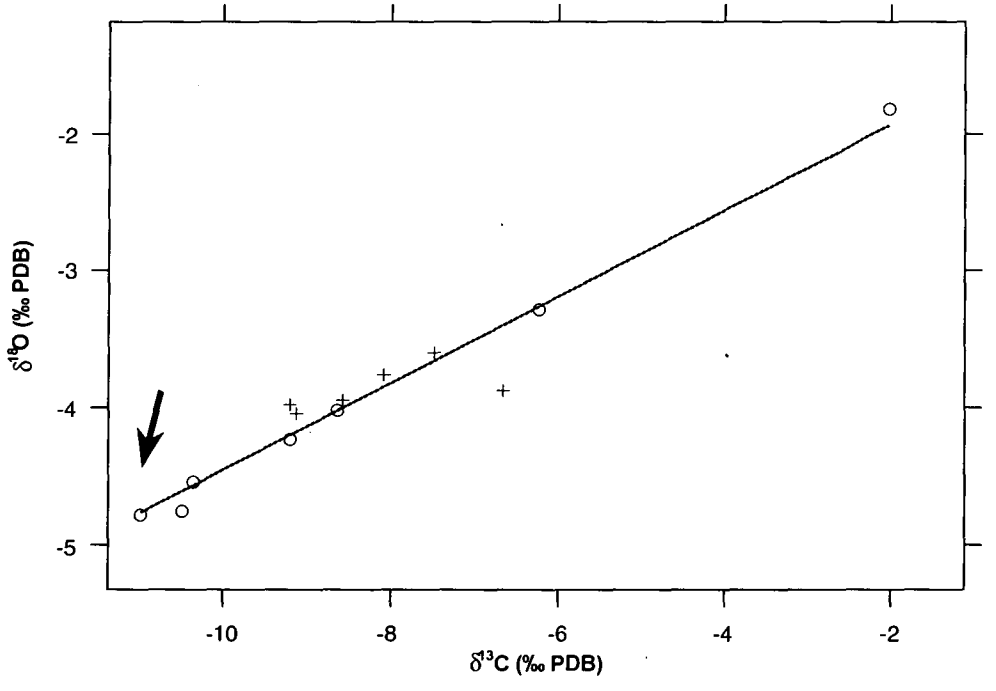

Figure 6.2 **Scatter plot of $\delta^{18}O$ and $\delta^{13}C$ results of twelve actively growing straw stalactites at two sites within Victoria Fossil Cave, Naracoorte. The most negative values (isotopically lightest) of the $\delta^{18}O$ and $\delta^{13}C$ results are assumed to have been deposited at or close to isotopic equilibrium, thus the $\delta^{18}O$ value for modern calcite is –4.76 ‰ PDB (marked by arrow). A regression line is plotted, y = 0.305x – 1.372, with an r-value of 0.99.**

Table 6.2. **Results of $\delta^{18}O$ and $\delta^{13}C$ analyses of twelve actively growing soda-straw stalactites from Spring and New Formation Chamber, Victoria Fossil Cave, Naracoorte, South Australia together with four dripwater samples from Spring Chamber. Isotopic ratios are given in per mil (‰) and versus the PDB standard unless otherwise indicated.**

Location	Sample #	Description	$\delta^{18}O$	$\delta^{13}C$
Spring Chamber	S1B	dripwater	-4.878 ± 0.013 (SMOW)	
	S1A	dripwater	-4.921 ± 0.013 (SMOW)	
	S2A	dripwater	-5.123 ± 0.016 (SMOW)	
	S2B	dripwater	-4.997 ± 0.004 (SMOW)	
Spring Chamber	NAS-1	straw stalactite	-3.949 ± 0.011	-8.571 ± 0.012
	NAS-2	straw stalactite	-3.981 ± 0.015	-9.199 ± 0.015
	NAS-3	straw stalactite	-4.047 ± 0.005	-9.120 ± 0.006
	NAS-4	straw stalactite	-3.602 ± 0.010	-7.484 ± 0.009
	NAS-5	straw stalactite	-3.759 ± 0.008	-8.084 ± 0.005
	NAS-6	straw stalactite	-3.878 ± 0.008	-6.659 ± 0.008
New Formation Chamber	NAN-7	straw stalactite	-4.756 ± 0.017	-10.487 ± 0.004
	NAN-8	straw stalactite	-4.022 ± 0.005	-8.635 ± 0.012
	NAN-9	straw stalactite	-4 .234 ± 0.004	-9.200 ± 0.005
	NAN-10	straw stalactite	-4.545 ± 0.008	-10.358 ± 0.009
	NAN-11	straw stalactite	-3.288 ± 0.018	-6.227 ± 0.011
	NAN-12	straw stalactite	-4.783 ± 0.023	-10.985 ± 0.017
	NAN-13	straw stalactite	-1.818 ± 0.012	-2.026 ± 0.009

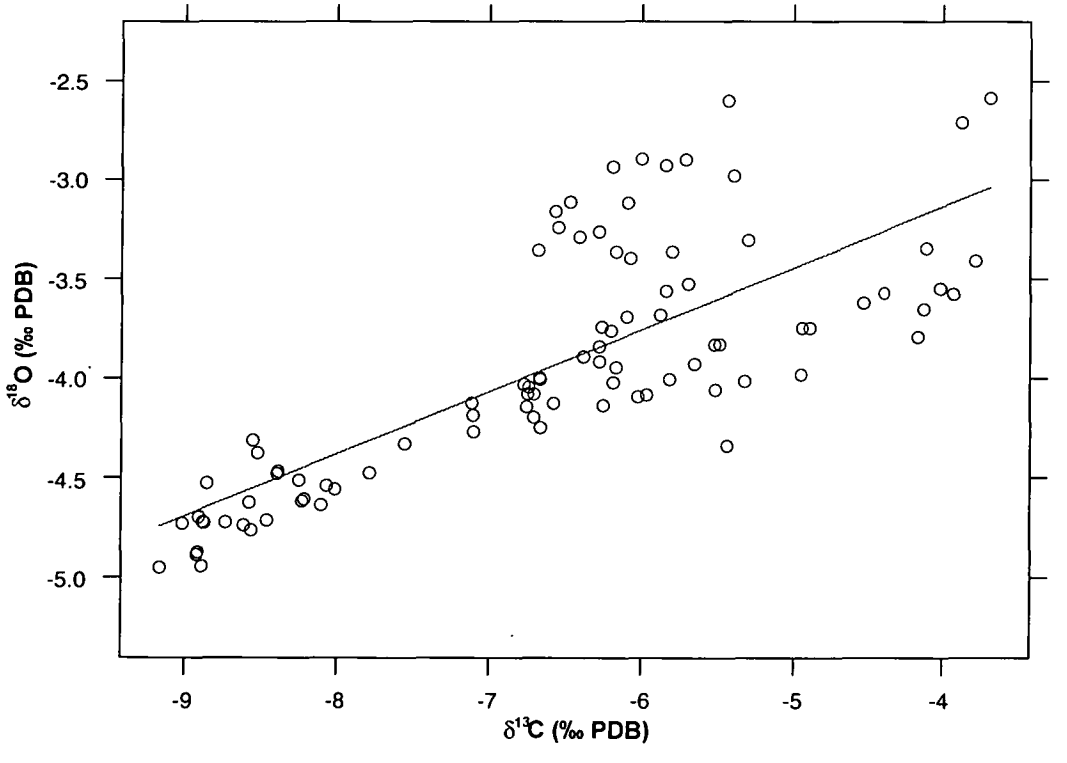

Figure 6.3 **Scatter plot of 90 $\delta^{18}O$ and $\delta^{13}C$ values of samples taken from the longitudinal profile of the SC-S11 stalagmite. A significant positive correlation between the $\delta^{18}O$ and $\delta^{13}C$ values is observed (r = 0.77), with the linear regression line shown (y = 1.929x + 1.0191).**

6.5.1.3. Yarrangobilly Modern Calcite and Growth Layer Analysis

To determine the nature of the relationship between $\delta^{18}O$ values of speleothem calcite and past temperatures in Jersey Cave, Yarrangobilly, five actively growing soda-straw stalactites were collected from several sites within Jersey Cave the results of these analyses are listed in Table 6.3. The results show a wide isotopic range since many were not deposited under conditions of oxygen isotope equilibrium. However, it is assumed that this is a large enough sample for one or more individuals to have been deposited at or close to isotopic equilibrium and they can be identified by having the most negative values of both $\delta^{18}O$ and $\delta^{13}C$, as shown in Figure 6.4, (Goede and Hitchman, 1984; Goede *et al.*, 1986). The technique provides a value of -7.49 ‰ (PDB) for the $\delta^{18}O$ and -10.3 ‰ (PDB) for the $\delta^{13}C$ of contemporary calcite.

No growth layers were analysed in JC-F1 in order to test for deposition under equilibrium conditions due to financial constraints. The $\delta^{18}O$ and $\delta^{13}C$ isotope results from the longitudinal profile are positively correlated but it is not statistically significant (Table 6.1). An additional test suggested by Hellstrom (1998) using the correlation of the first derivatives of the isotopic profile also supports the hypothesis that sample has been deposited under conditions of isotopic equilibrium (Table 6.1), where records whose first derivatives have a correlation coefficient of approximately 0.3 suffer from insignificant bias due to kinetic fractionation. Attempts will be made to analyse several growth layers along the x- and y-axis *ie* perpendicular to one another. This will allow investigation of spatial variation as well as test for deposition under conditions of isotopic equilibrium.

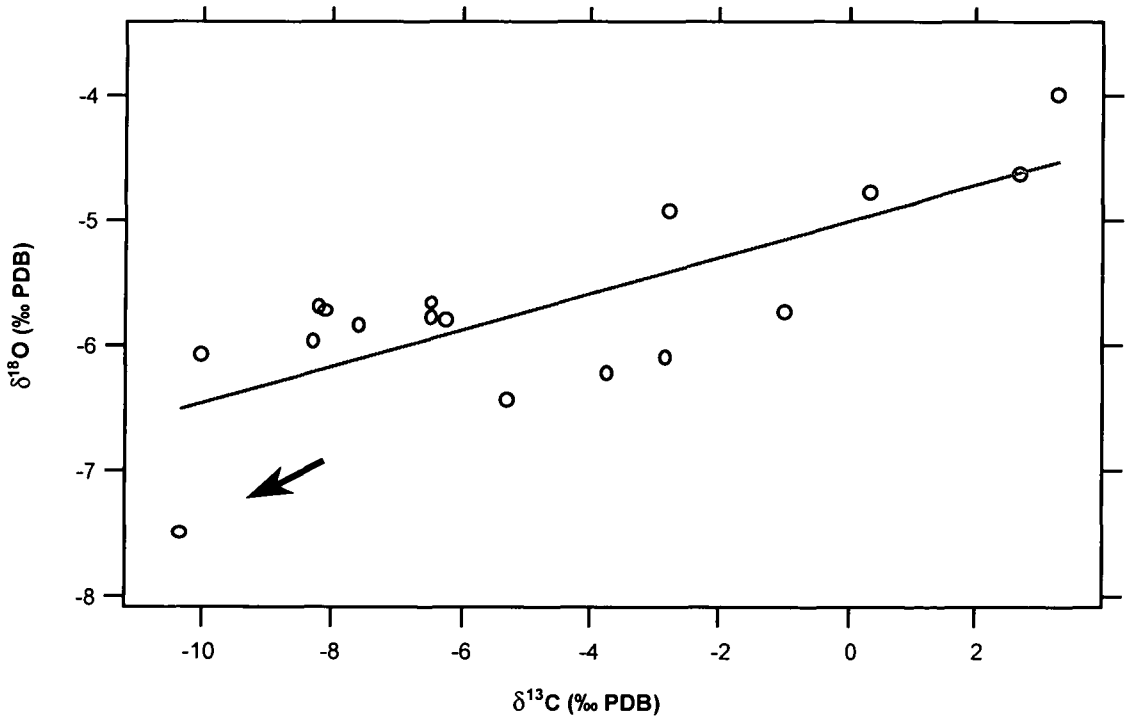

Figure 6.4 **Scatter plot of $\delta^{18}O$ and $\delta^{13}C$ results of five actively growing straw stalactites from Jersey Cave, Yarrangobilly. The most negative values (isotopically lightest) of the $\delta^{18}O$ and $\delta^{13}C$ results are assumed to have been deposited at or close to isotopic equilibrium, thus the $\delta^{18}O$ value for modern calcite is estimated at –7.49 ‰ PDB (marked by arrow).**

Table 6.3. Results of stable isotope analyses of actively growing soda-straw stalactites from Jersey Cave, Yarangobilly. All figures have an precision of 0.030 ‰ or better.

Sample	$\delta^{13}C_{PDB}$ (‰)	$\delta^{18}O_{PDB}$ (‰)
Y-JC-0a	-8.214	-5.695
Y-JC-0b	-8.109	-5.729
Y-JC-1a	-2.836	-6.094
Y-JC-1b	-3.751	-6.232
Y-JC-1c	0.310	-4.783
Y-JC-1d	-0.995	-5.744
Y-JC-2a	2.676	-4.632
Y-JC-2b	3.235	-4.001
Y-JC-2c	-6.476	-5.786
Y-JC-3a	-2.781	-4.938
Y-JC-3b	-7.586	-5.852
Y-JC-3c	-8.293	-5.975
Y-JC-4a	-5.298	-6.438
Y-JC-4b	-6.475	-5.663
Y-JC-4c	-6.248	-5.808
Y-JC-4d	-10.331	-7.492
Y-JC-4e	-10.017	-6.083

6.5.2. LT Stalagmite Isotope Profile Results

The isotope profile is based on 283 samples taken at 5 mm intervals along the vertical axis and were analysed for both $\delta^{18}O$ and $\delta^{13}C$ and plotted as a time series against their estimated ages (Figure 6.5 and Figure 6.6) together with isotopic results from Goede *et al.* (1986). Also plotted for comparative purposes are the Vostok temperature record (Jouzel *et al.*, 1993), the RC 11-120 sea surface temperature record (Martinson *et al.*, 1997), and December insolation values for 30°S (Berger and Loutre, 1991). Both the $\delta^{18}O$ and $\delta^{13}C$ results are smoothed using a smoothing spline, a least squares variant of a cubic spline.

6.1.1.1 LT Oxygen Isotope Profile Results

The $\delta^{18}O$ results are plotted against a timescale derived from the TIMS $^{230}Th/^{234}U$ age estimates in Figure 6.5. $\delta^{18}O$ values range from -5.6 to -3.8 ‰ PDB with a mean of -4.8 ‰ PDB (Table 6.1). The most significant change occurs between approximately 89 ka and 85 ka, where $\delta^{18}O$ values rise from around -5.5 to -4.3 ‰ PDB. The estimated value for contemporary calcite determined by Goede and Hitchman (1983) is –4.0 ‰ PDB. Earlier studies (Goede *et al.*, 1986; Desmarchelier

and Goede, 1996) of the LT stalagmite have established that a positive relationship exists between temperature and the isotopic composition of speleothem calcite.

Deposition of the LT stalagmite began approximately 98 ka years ago and corresponds to OIS 5.3 (5c), a warm phase in OIS 5. An overall trend of slight cooling of approximately 0.5 to 1.0°C is suggested (Jouzel *et al.*, 1993) until about 88 ka when temperatures began to rapidly rise until the termination of the record at 84 ka, the middle of OIS 5.2 (5b). The warming period represents the largest change in the $\delta^{18}O$ and interestingly seems to have has a stepped character with approximately three easily identifiable steps of around 1 ka duration.

6.5.2.1. LT Carbon Isotope Profile Results

The $\delta^{13}C$ results are plotted against the TIMS $^{230}Th/^{234}U$ age estimates in Figure 6.6. $\delta^{13}C$ values range from -11.25 to -5.45 ‰ PDB with a mean of -8.44 ‰ PDB (Table 6.1). The wide range indicates fairly considerable surface environmental change during the depositional period. Three hypotheses were put forward in Section 6.3.5 to explain carbon isotope variations in speleothem calcite through time. The third hypothesis is considered to be only a minor factor because its maximum influence is approximately 0.7 ‰ PDB and will have limited impact on the overall $\delta^{13}C$ isotopic signal of LT which has a range of around 6 ‰. Earlier studies (Desmarchelier and Goede, 1996; Goede, 1998) have established that the $\delta^{13}C$ variation of speleothem calcite in Tasmania is highly unlikely to have been influenced by changes in the abundance of C3 and C4 plants. Therefore, the $\delta^{13}C$ variation in the LT stalagmite is best explained by changes in activity of vegetation and soil processes.

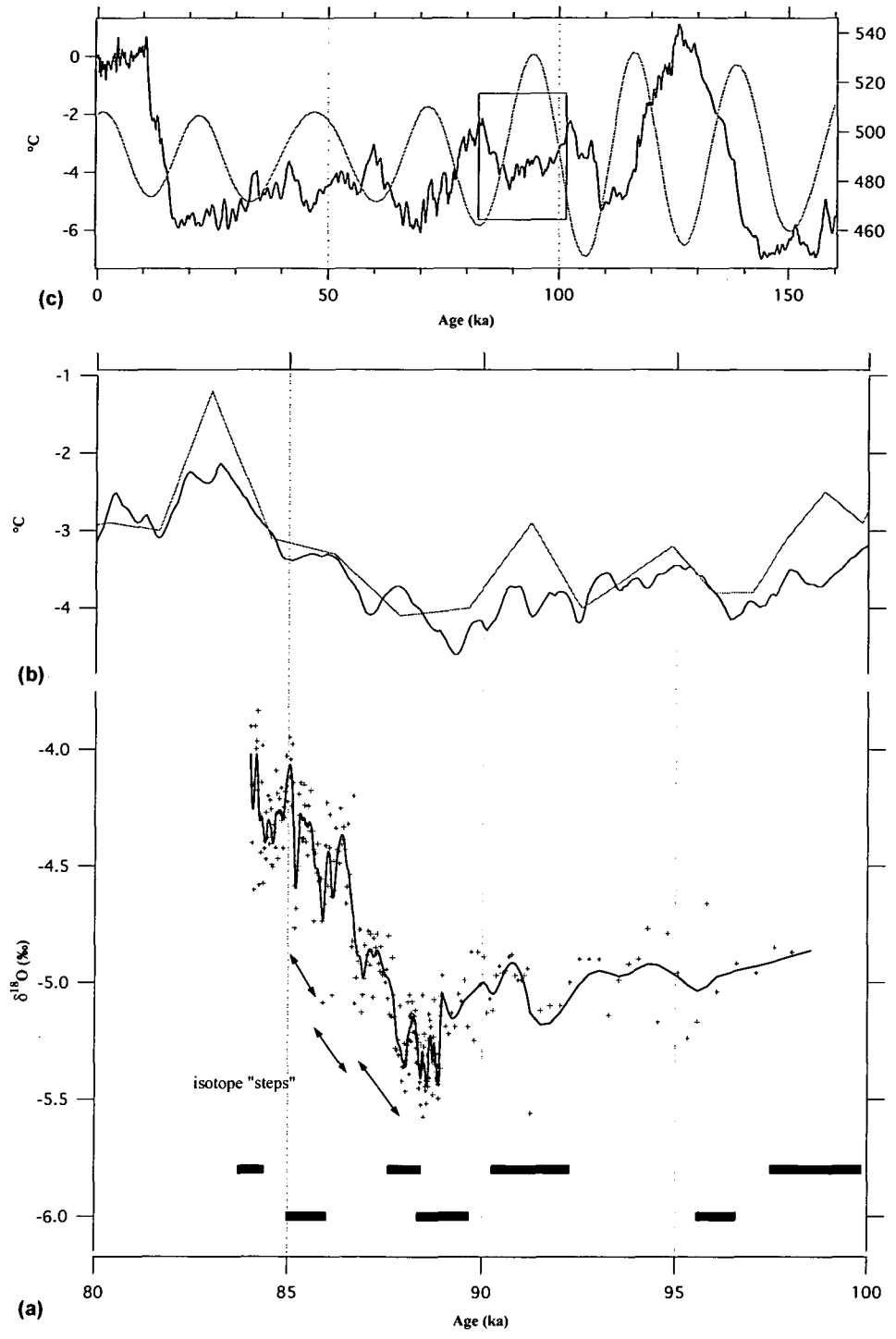

Figure 6.5. **Oxygen isotope results of samples taken from the longitudinal axis of the LT stalagmite, a 1,800 mm high sample from Little Trimmer Cave, Mole Creek, Tasmania, plotted versus age.**

(a) Dark line is smoothed LT oxygen isotope record via a smoothing spline, light dots are the raw data. Black bars on the bottom of the graph are age estimates with 2 σ errors.

(b) Dark line is the temperature difference from present mean annual temperature (°C) calculated from the Vostok ice core record (Jouzel *et al.*, 1993), light line is the temperature difference from present mean annual sea-surface temperature calculated from the ocean core RC11-120 (Martinson *et al.*, 1987).

(c) Dark line is the complete temperature difference record from Vostok with the square indicating the temporal relationship of LT to the Vostok ice core, light line is the December insolation record for 30°S (Berger and Loutre, 1991).

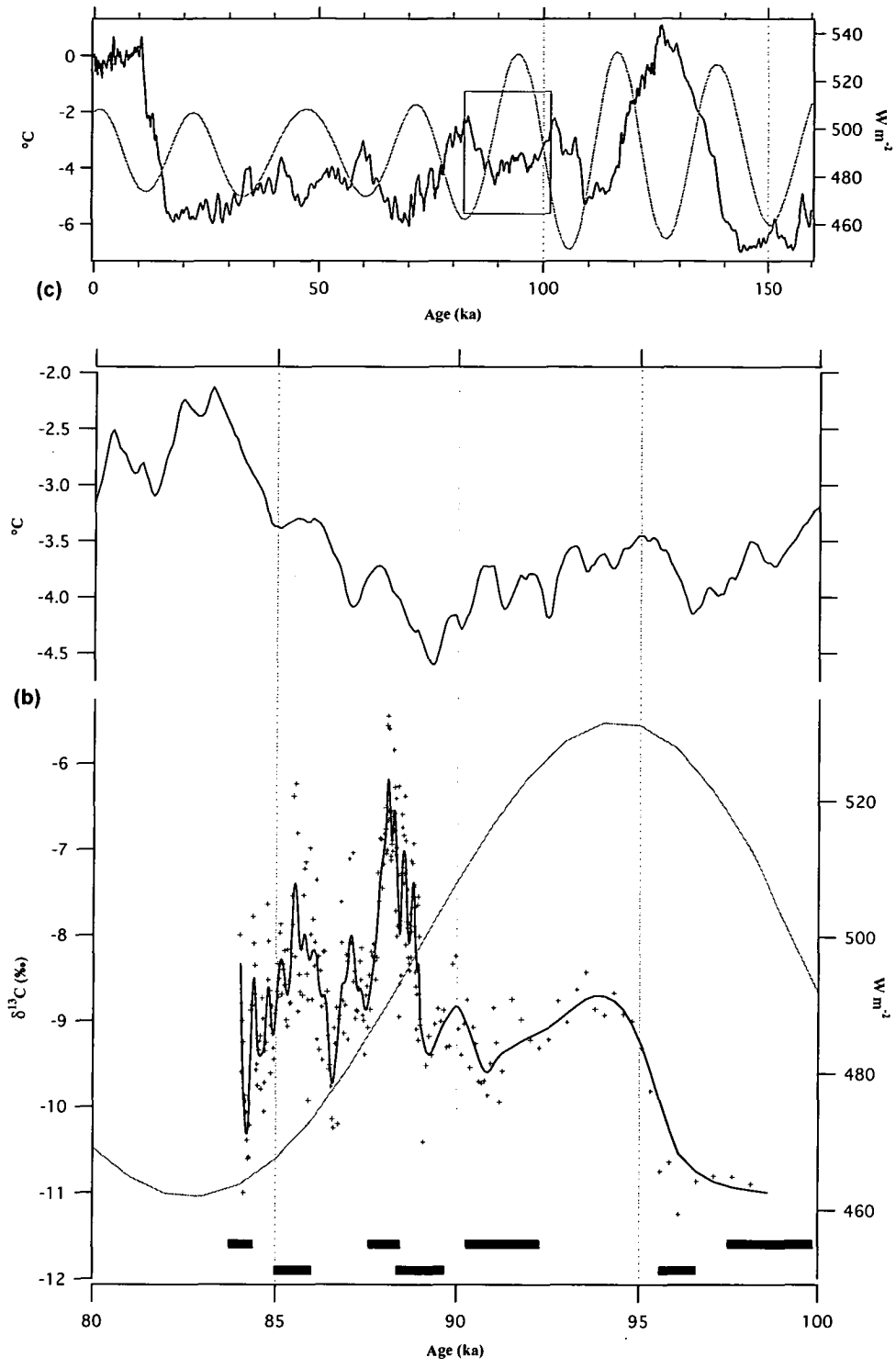

Figure 6.6. **Carbon isotope results of samples taken from the longitudinal axis of the LT stalagmite, a 1,800 mm high sample from Little Trimmer Cave, Mole Creek, Tasmania, plotted versus age.**

(a) Dark line is smoothed LT carbon isotope record via a smoothing spline, light dots are the raw data. Black bars on the bottom of the graph are age estimates with 2 σ errors.

(b) Dark line is the temperature difference from present mean annual temperature (°C) calculated from the Vostok ice core record (Jouzel *et al.*, 1993).

(c) Dark line is the complete temperature difference record from Vostok with the square indicating the temporal relationship of LT to the Vostok ice core, light line is the December insolation record for 30°S (Berger and Loutre, 1991).

6.5.3. LT Stalagmite Isotope Profile Discussion

The stalagmite was originally dated by alpha spectrometry (Goede *et al.*, 1986) but the stricter temporal constraints provided by seven TIMS $^{230}Th/^{234}U$ age determinations confirms that the stalagmite began growing early in OIS 5.3 (5c) and continued well into OIS 5.2 (5b). The TIMS $^{230}Th/^{234}U$ age estimates are a significant improvement on previous attempts at dating this sample using conventional alpha spectrometry, highlighting the considerable benefits that the TIMS technique has brought to speleothem age control. The date at which calcite deposition ceased is not known as there is a missing tip (Goede *et al.*, 1986) above the uppermost (1400 mm) U-series date. It is hypothesised that growth continued well into OIS 5.1 (5a) but it is unlikely that this will ever be confirmed unless the missing tip is located.

In Figure 6.5 the smoothed temperature record form the Vostok ice core record plotted against age, using the EGT model (ref), is compared to the LT $\delta^{18}O$ data. From approximately 89 ka to 84 ka a stepped warming pattern, with a range of around 2°C, is evident and supported by similar events of almost 1 ka duration in the LT stalagmite $\delta^{18}O$ results. A slight difference in timing between the records is attributed to possible lag effects and to the limitations of the Vostok age model. The Vostok record is dominated by a 100 ka glacial-interglacial cycle with a temperature amplitude of approximately 6°C (Lorius *et al.*, 1987).

The isotope stages in the Vostok record are identified by capital letters, commencing with A for the Holocene epoch. Vostok stage E is an interstadial characterised by two well defined temperature maxima at approximately 100 ka and 81 ka as well as several minor oscillations. The LT record corresponds to Vostok stage E (mid- to late-OIS 5) post-dating the earlier maximum and pre-dating the latter, although it could be extended further if the missing tip section were located.

In previous studies (Goede *et al.*, 1986; Desmarchelier and Goede, 1996) it has been argued that in cool, temperate climates carbon isotope variations may be interpreted largely in terms of fluctuations in vegetation activity, with more negative values indicating higher levels of activity. In Tasmania vegetation activity is seasonal and strongly influenced by moisture availability, which can be expected to be at least partly modulated by fluctuations in summer insolation. Mid-month insolation data for December at 30°S (Berger and Loutre, 1991) show increasing radiation values from a minima at 105 ka (455 W m^{-2}) to a maximum at 94 (535 W m^{-2}) followed by decreasing values to a minima at 84 ka (462 W m^{-2}). The early part of the LT stalagmite record, from 98 ka to 94 ka, indicates that with higher summer insolation values and temperature vegetation productivity decreases due to increased evaporation and consequently reduced effective precipitation. From 94 ka to 90 ka vegetation activity increases slightly as insolation decreases following the peak at 94 ka, also mirroring a decreasing temperature trend. From approximately 90 ka onwards temperature seems to be the dominant control in governing the carbon isotope composition as the insolation values decrease to a minima at 84 ka (460 W m^{-2}).

6.5.4. SC-S11 Stalagmite Isotope Profile Results

A profile of ninety samples, taken at close intervals along the vertical axis, were analysed for $\delta^{18}O$ and $\delta^{13}C$ and plotted as a time series against their estimated ages (Figure 6.7 and Figure 6.8).

Also plotted for comparitive purposes are the Vostok temperature record (Jouzel *et al.*, 1993), the RC 11-120 sea surface temperature record (Martinson *et al.*, 1987), and December insolation values for 30°S (Berger and Loutre, 1991). No smoothing was applied to the $\delta^{18}O$ and $\delta^{13}C$ results as they are effectively averaged by the nature of the sampling method.

6.5.4.1. SC-S11 Oxygen Isotope Results

The $\delta^{18}O$ results are plotted against estimated age in Figure 6.7, values range from –5.0 to -2.6 ‰ PDB with a mean value of -3.9 ‰ (Table 6.1). This should be compared with an estimated value of -4.8 ‰ for contemporary calcite. Before any interpretation is attempted it is important to determine the sign of the relationship with temperature. It can be seen that with a small number of exceptions the vast majority of values are well above the present day value.

The contemporary value represents temperature conditions which approach the maximum value of the range of temperatures experienced during the glacial-interglacial cycle of the Late Pleistocene. It appears therefore that the isotopically heaviest values of $\delta^{18}O$ represent colder climate conditions indicating a negative relationship with temperature. This is expected because examination of the time period of deposition in other palaeotemperature records such as the Vostok ice core indicates that temperatures were well below those of the Holocene and Last Interglacial (Jouzel *et al.*, 1993).

The stalagmite started growing under cold conditions (-2.5 ‰) at about 185 ka but with temperature rising rapidly to values close to those prevailing today between 178 and 162 ka. This is followed by a drop to much lower temperatures by the time the record terminates at about 157 ka. The record appears to include a mild interstadial of about 16 ka duration with temperatures similar to today that is both preceded and followed by cold climate conditions. The record shows marked similarities with the SPECMAP stack generated from deep sea core oxygen isotope data (Imbrie *et al.*, 1992) and with the pattern of $\delta^{18}O$ variations of benthic foraminifera in marine core DSDP-594 (Heusser and Van de Geer, 1994) with which it is also compared in Figure 6.7. This core site is located on the southern margin of the Chatham Rise at a depth of 1204 m, circa 250 km east of the South Island, New Zealand (45.52°S, 174.95°E).

6.5.4.2. SC-S11 Carbon Isotope Results

The $\delta^{13}C$ results are plotted against estimated age in Figure 6.8, values range from -9.2 to -3.7 ‰ PDB with a mean value of -6.6 ‰ (Table 6.1). The range is wide indicating considerable environmental change during the depositional period. In Section 6.3.5three hypotheses were put forward to explain temporal variations in carbon isotope ratios in speleothems. Hypothesis 3 is at best a minor factor since the amount of variation it could explain, approximately 0.7 ‰ PDB, is quite small. This leaves the bulk of the variance to be explained by either a change in the abundance of C3 and C4 plants and/or a change in the productivity of the vegetation provided that soil thickness has remained unchanged during the period of growth of the stalagmite.

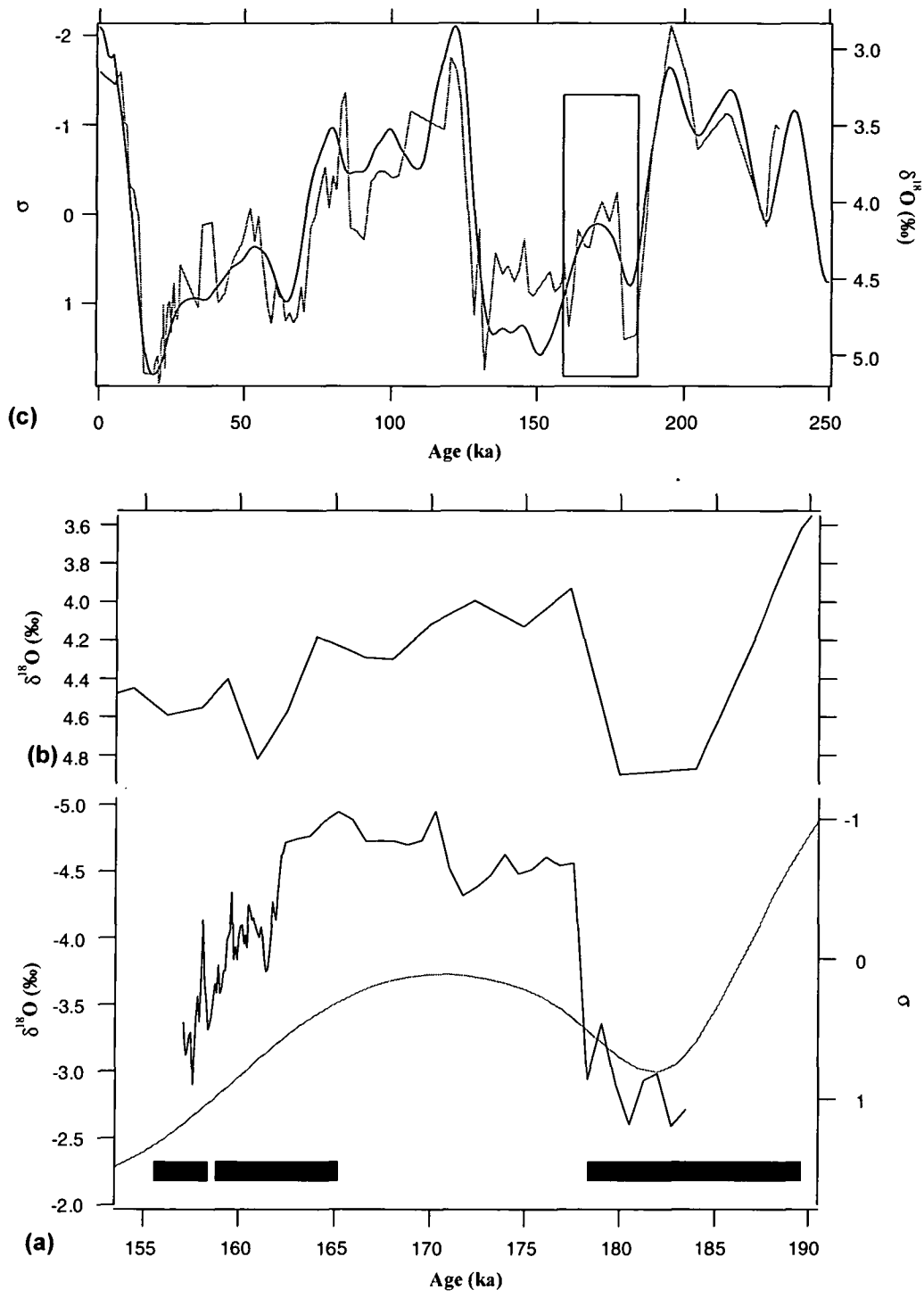

Figure 6.7. Oxygen isotope results of samples taken from the longitudinal axis of the SC-S11 stalagmite, a sample from Victoria Fossil Cave, Naracoorte, South Australia, plotted versus age.

(a) Dark line is the SC-S11 oxygen isotope record. Light line is the SPECMAP stack generated from deep-sea oxygen isotope data (Imbrie *et al.*, 1992). Black bars on the bottom of the graph are age estimates with 2 sigma errors.

(b) Dark line is the pattern of $\delta^{18}O$ variations of benthic foraminifera in marine core DSDP-594 (Heusser and Van de Geer, 1994).

(c) Dark line is the complete SPECMAP record and light line is the complete record of $\delta^{18}O$ variations of benthic foraminifera in marine core DSDP-594 (Heusser and Van de Geer, 1994). The square indicates the temporal relationship of the SC-S11 record to SPECMAP.

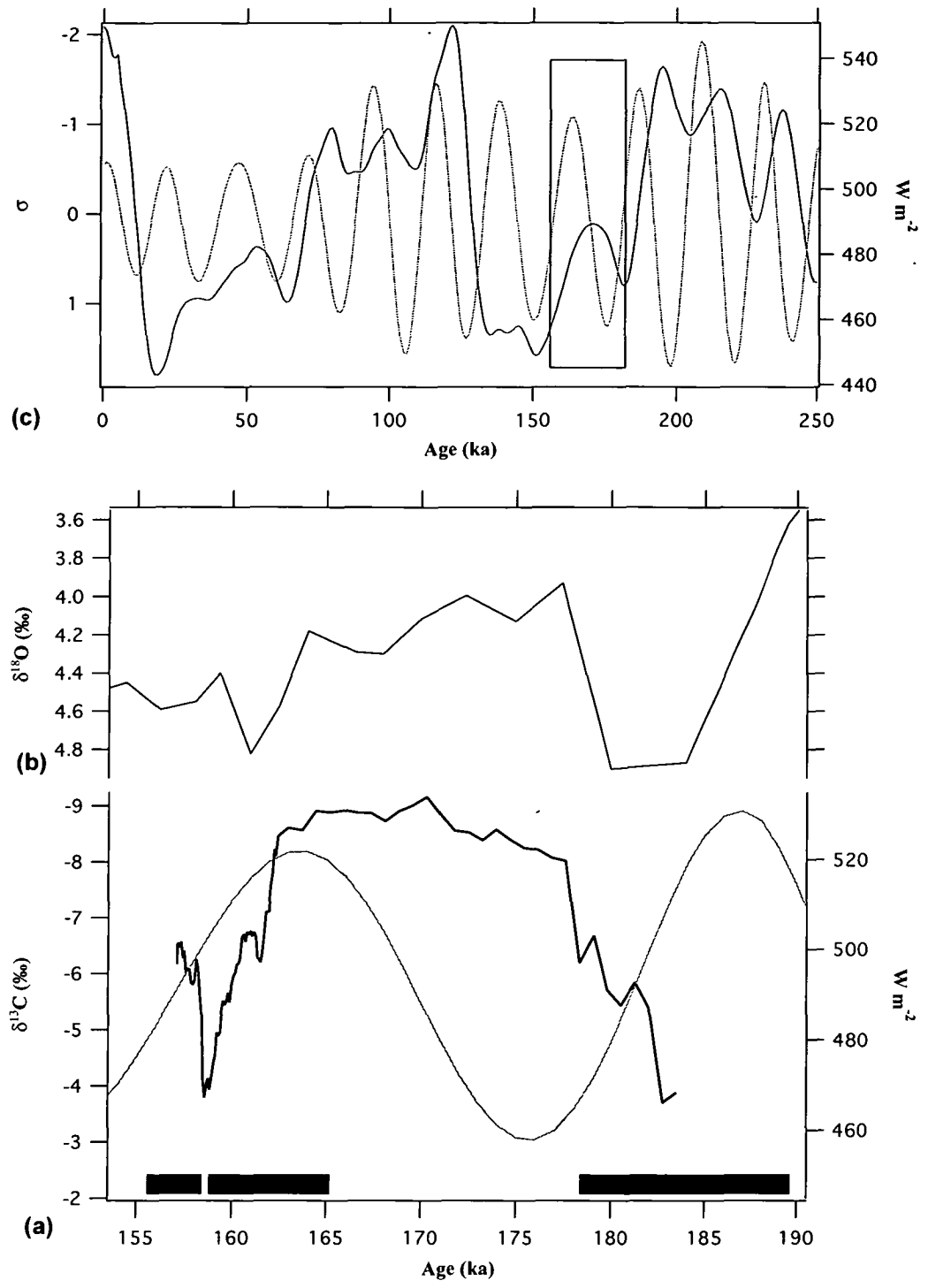

Figure 6.8. **Carbon isotope results of samples taken from the longitudinal axis of the SC-S11 stalagmite, a sample from Victoria Fossil Cave, Naracoorte, South Australia, plotted versus age.**

(a) Dark line is the SC-S11 carbon isotope record. Light line is the December insolation record for 30°S (Berger and Loutre, 1991). Black bars on the bottom of the graph are age estimates with 2 sigma errors.

(b) Dark line is the pattern of $\delta^{18}O$ variations of benthic foraminifera in marine core DSDP-594 (Heusser and Van de Geer, 1994).

(c) Dark line is the complete SPECMAP record and light line is the complete December insolation record for 30°S (Berger and Loutre, 1991). The square indicates the temporal relationship of the SC-S11 record to SPECMAP.

6.5.5. SC-S11 Stalagmite Isotope Profile Discussion

Very few late Middle Pleistocene palaeoclimatic data sets from either hemisphere are sufficiently well dated to confirm the mild interstadial conditions inferred from this profile to have occurred between 178 and 162 ka. However, an interesting and well dated record has been obtained from an excavation site in the Western Chamber of Robin Hood's Cave in Derbyshire, Britain. The site consists of a pure 30 mm thick flowstone layer with two alpha-spectrometry uranium series dates indicating an age of 165.4 + 6.0/-5.6 ka (Rowe and Atkinson, 1985). Pollen in associated clastic sediments immediately above and below the flowstone indicate the presence of grasses, thermophile trees and shrubs. They are both preceded and followed by steppe and tundra-like floras (Coles *et al.*, 1985).

A minimum estimate of temperature lowering relative to today at the beginning of the record can be obtained using Equation 6.5, if the assumption is made that isotopic composition of precipitation has not changed during the glacial-interglacial cycle. This is plausible as during cooler periods it is likely that precipitation will continue to be derived from the westerlies with the subtropical front (STF) remaining south of the site. It provides a minimum estimate of mean annual temperature lowering of 8°C, a value that would indicate full glacial conditions. Such an estimate is in good agreement with another made by Miller *et al.* (1997) using amino-acid racemization of emu eggshell to estimate a temperature change of approximately 9°C for the Last Glacial-Holocene transition.

During the interstadial, strongly negative carbon isotope ratios ranging predominantly between -8.0 and -9.0 ‰ occur. Such values are characteristic of a quite productive C3 vegetation dominating the growing season. They cannot be compared directly with the estimate of equilibrium deposition of -11 ‰ obtained from modern straw stalactites (Table 6.2, Figure 6.2), firstly because burning of fossil fuels is believed to have caused changes estimated at -2.2 ‰ in the isotopic composition of atmospheric carbon (Baskaran and Krishnamurthy, 1993) and secondly because the atmospheric carbon isotope composition during an interstadial may have differed significantly from today (Marino *et al.*, 1992). Geochemical models predict carbonate $\delta^{13}C$ values of between -14 and -6 ‰ PDB for C3 pathway plants and -6 and +2 ‰ PDB for C4 plants (Dreybrodt, 1980, quoted in Baker *et al.*, 1997) and the generally positive correlation between oxygen and carbon isotope values (Table 6.1) suggests that mild interstadial conditions are associated with maximum available moisture during the growing season.

If the less negative $\delta^{13}C$ values of between -6.0 and -3.5 ‰ PDB are indeed associated with the presence of C4 vegetation at the site, it would be expected that the time periods involved would coincide with times of high summer insolation as such a condition would favour the dominance of tropical grasses. To test this hypothesis, insolation values for 30°S in December (Berger and Loutre, 1991) have been plotted on the same diagram as the $\delta^{13}C$ variations (Figure 6.8). It can be seen that the two $\delta^{13}C$ peaks appear to trail summer insolation peaks by 3 ka and 6 ka respectively but these differences may not be real as they are comparable in magnitude to the 2σ errors quoted for the TIMS dates.

6.5.6. JC-F1 Isotope Profile Results

A longitudinal profile of seventy-one samples, taken at 5 mm intervals along the growth axis of JC-F1, were analysed for both $\delta^{18}O$ and the $\delta^{13}C$ content and plotted as a time series against their estimated ages (Figure 6.9 and Figure 6.10). Also plotted for comparitive purposes are the Vostok temperature record (Jouzel *et al.*, 1993), the RC 11-120 sea surface temperature record (Martinson *et al.*, 1987), and December insolation values for 30°S (Berger and Loutre, 1991).

6.5.6.1. JC-F1 Oxygen Isotope Results

The $\delta^{18}O$ results from the longitudinal profile of the flowstone JC-F1 are plotted against estimated age in Figure 6.9, values range from –7.06 to –4.05 ‰ PDB with a mean value of –5.66 ‰ PDB (Table 6.1). The estimated $\delta^{18}O$ value for modern speleothem calcite at Jersey Cave is –7.49 ‰ PDB. It can be seen that none of the $\delta^{18}O$ results in the JC-F1 profile fall below the present day $\delta^{18}O$ value indicating that temperatures did not exceed those of today. The isotopically heaviest values of $\delta^{18}O$ represent cool climate conditions indicating a negative relationship with cave temperature. No smoothing was applied to the $\delta^{18}O$ and $\delta^{13}C$ results due to the limited sampling resolution, approximately 5 mm.

6.5.6.2. JC-F1 Carbon Isotope Results

The $\delta^{13}C$ results from the longitudinal profile of the flowstone JC-F1 are plotted against estimated age in Figure 6.10,values range from –9.78 to –1.53 ‰ PDB with a mean value of –5.64 ‰ PDB (Table 6.1). The estimated $\delta^{13}C$ value for modern calcite is –10.33 ‰ PDB. In Section 6.3.5 three hypotheses were put forward to explain temporal variations in carbon isotope ratios in the longitudinal profiles of speleothems. Hypothesis 3 is at best a minor factor since the amount of variation it could explain, approximately 0.7 ‰ PDB, is quite small in comparison to the overall range of around 8 ‰ for JC-F1. This leaves the bulk of the variance to be explained by either a change in the abundance of C3 and C4 plants and/or a change in the productivity of the vegetation provided that soil thickness has remained essentially unchanged during the depositional period of the stalagmite.

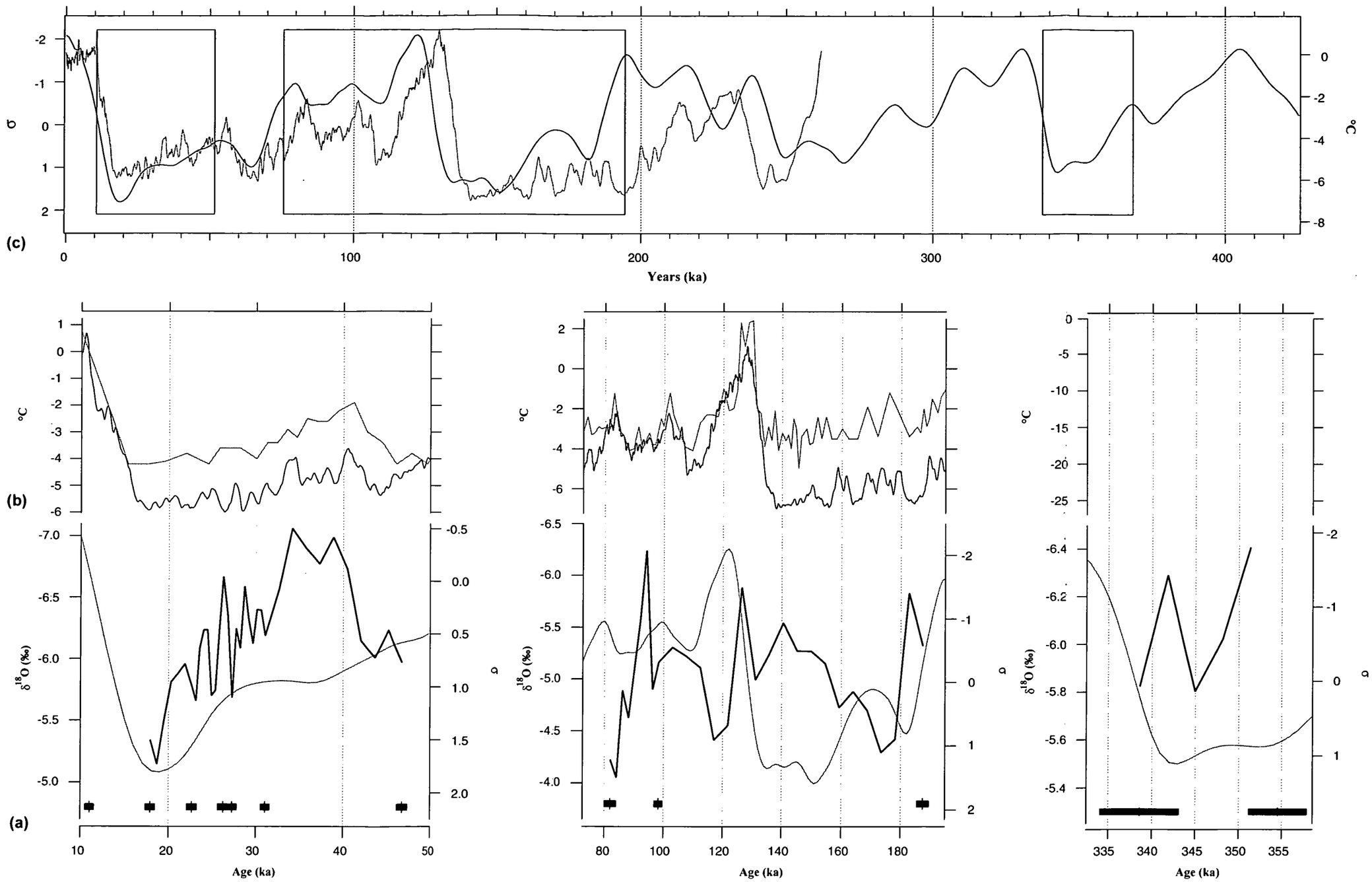

Figure 6.9. Oxygen isotope results of samples taken from the longitudinal profile of JC-F1aa, a section of flowstone from Jersey Cave, Yarrangobilly, plotted versus age.

(a) Dark line is the JC-F1aa oxygen isotope record. Light line is the SPECMAP record. Black bars are age estimates with 2 sigma errors.

(b) Dark line is the temperature difference from present mean annual temperature (°C) calculated from the Vostok ice core record (Jouzel *et al.*, 1993), light line is the temperature difference from present mean annual sea-surface temperature calculated from the ocean core RC11-120 (Martinson *et al.*, 1987).

(c) Dark line is the complete SPECMAP record and light line is the complete temperature difference record from Vostok (Jouzel *et al.*, 1993). The square indicates the temporal relationship of the JC-F1aa record.

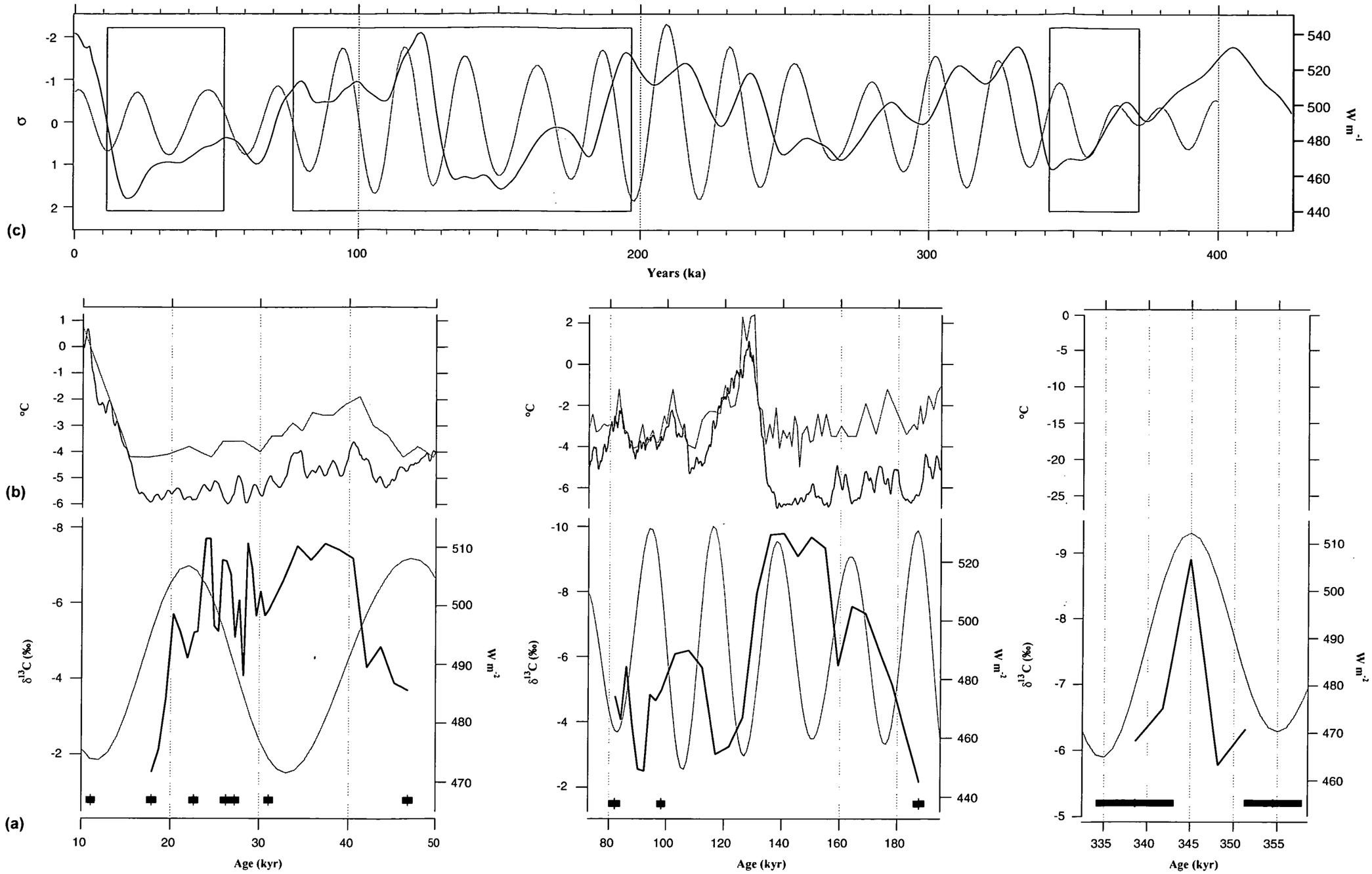

Figure 6.10. Carbon isotope results of samples taken from the longitudinal profile of JC-F1aa, a section of flowstone from Jersey Cave, Yarrangobilly, plotted versus age.

(a) Dark line is the JC-F1aa carbon isotope record. Light line is the December insolation record for 30°S (Berger and Loutre, 1991). Black bars are age estimates with 2 sigma errors.

(b) Dark line is the temperature difference from present mean annual temperature (°C) calculated from the Vostok ice core record (Jouzel *et al.*, 1993), light line is the temperature difference from present mean annual sea-surface temperature calculated from the ocean core RC11-120 (Martinson *et al.*, 1987).

(c) Dark line is the complete SPECMAP record and light line is the complete December insolation record for 30°S (Berger and Loutre, 1991). The square indicates the temporal relationship of the JC-F1aa record.

6.5.7. JC-F1 Flowstone Isotope Profile Discussion

The youngest or top section of the three JC-F1 growth phases has the best temporal control out of the sections analysed with TIMS $^{230}Th/^{234}U$ age determinations. Therefore discussion will focus mainly on this period although there will be some brief discussion on the other sections. The middle section needs at least four more TIMS $^{230}Th/^{234}U$ measurements as there appears to be a hiatus somewhere in the section between approximately 100 ka and 160 ka which may correspond to a period between the Penultimate Glacial and the Last Interglacial. The basal section of JC-F1 has insufficient stable isotope analyses to gain any clear understanding of the palaeoenvironmental conditions at that time.

The section between the two upper hiatuses of JC-F1 began growing at approximately 45 ka and ceased deposition at 18 ka. It therefore covers the latter part of the Late Pleistocene *ie* early OIS 3 to mid OIS 2. The isotopically lightest values are found between approximately 42 ka and 30 ka indicating that this was the warmest period covered by the JC-F1 record but at no stage do the $\delta^{18}O$ values exceed the contemporary value of –7.49 ‰. This period corresponds to a major interstadial recorded by lake sediments in eastern Australia from about 44 ka to 30 ka. Most of the lakes have much higher lake levels than was the case during the Holocene, for example Willandra Lakes and Lake George (Singh *et al.*, 1981), indicating a prolonged period of relatively high effective precipitation at this time (Kershaw *et al.*, 1991). However, in some lake level records from southeastern Australia, for example Lake Terang, Victoria (D'Costa, 1989), the interstadial is not as distinct.

Two possible explanations were put forward by Kershaw *et al.* (1991) to account for these differences, the first proposes that significant changes in atmospheric circulation patterns produce regional variations in effective precipitation during interglacial-glacial cycles and the second suggests that the timescale for one of the sequences is wrong. The JC-F1 isotope and growth rate record clearly shows that an interstadial influenced the Yarrangobilly region and that effective precipitation was probably higher than during OIS 5.

Since the JC-F1 record has been independently dated by TIMS $^{230}Th/^{234}U$ age estimates and does not rely on correlating key events to oxygen isotope stages, as lake and marine cores do, its chronology is difficult to question. Harle (1997) analysed the palynology of a marine core, E55-6, taken offshore from Cape Bridgewater, western Victoria to investigate regional community and climatic change in southeastern Australia. The chronology of the record was established by oxygen isotope analysis of planktic foraminifera and nannofossil smears and directly correlating the results to the marine oxygen isotope stages. Interpretation of the pollen record suggests that the wettest phase of the Last Glacial-Interglacial cycle occurred at the height of the Last Interglacial period *ie* 5.5 (e) and not during the OIS 3 interstadial as suggested by Kershaw *et al.* (1991). The JC-F1 record suggests that the Harle (1997) chronology is either wrong or that Kershaw *et al.* (1991) are right in attributing some of the differences between cores taken from eastern and southeastern Australia to regional variations in effective precipitation.

The above discussion illustrates that great care must be taken when expressing views about changes in effective precipitation particularly when the dating of a record is open to question.

One factor not mentioned by Harle (1997) was insolation which may significantly influence effective precipitation. The highest December insolation values at 30 S occur at approximately 118 ka (~530 W m^{-2}) and 95 ka (~525 W m^{-2}) and the next three insolation peaks, at around 72 ka, 48 ka, and 22 ka, have insolation values of slightly less than 510 W m^{-2} (Berger and Loutre, 1991). The lowest oxygen isotope values and the highest deposition rate in the JC-F1 record occur during the OIS 3 interstadial implying that effective precipitation was greater at this time than during OIS 5. It is suggested that the differences observed in effective precipitation are caused by both the slight variation in insolation receipts and also by the slightly lower temperatures in OIS 3 compared to OIS 5 as indicated by the Vostok temperature record. From 30 ka until deposition ceased at 18 ka the JC-F1 oxygen isotope record indicates a progressive cooling and this is supported by the majority of lake (*eg* Lake Leake and Wyrie Swamp, southeastern South Australia, Dodson, 1975; Dodson, 1977) and marine cores (*eg* SPECMAP; Harle, 1997). Throughout the period from 30 ka to 10 ka herbaceous vegetation dominates in southeastern Australia indicating cooler and drier conditions and this is supported by the JC-F1 $\delta^{18}O$ values becoming isotopically heavier.

As previously discussed in Section 6.3.5 carbon isotope variations in cool, temperate climates may be interpreted predominantly in terms of changes in vegetation activity, with more negative values indicating higher levels of activity (Goede *et al.*, 1986; Desmarchelier and Goede, 1996). High values in the JC-F1 carbon isotope record indicate higher vegetation activity.

Although the two JC-F1 minor element scans (Figure 5.19) roadly correlate there are several major differences between them which make it difficult to fully reconcile the isotopic record with the minor element results. In the JC-F1bb record the Sr/Ca and Ba/Ca ratios are low from approximately 45 ka until they suddenly increase rapidly at 30 ka. The Mg/Ca ratio is the only minor element in this period that shows similar trends between the two samples. In the JC-F1bb scan the Mg/Ca ratio gradually decreases from 45 ka to approximately 30 ka where it rises and falls sharply whereupon it stays relatively stable until deposition ceases, the JC-F1aa results have a similar pattern except they lack the spike feature present in JC-F1bb scan. Hellstrom (1998) has argued that variations in magnesium content may reflect changes in the relative residence time of cave seepage water. Given that the growth rate from 45 ka to 31 ka is low (2.9 mm ka^{-1}) compared to a rate of around 11 mm from 31 ka to 22 ka supports his suggestion that the Mg/Ca ratio in JC-F1 may be an indicator of variations in residence time but further investigation is required to test this.

As has been mentioned previously, the middle period of JC-F1 deposition occurred between approximately 180 ka and 80 ka (OIS 6 and 5) but several more TIMS $^{230}Th/^{234}U$ age determinations are needed before a definitive interpretation can be presented. However, some preliminary observations can be made about the isotope profile. It is suggested that a hiatus may occur in the period from approximately 150 ka to 130 ka and that the early period of JC-F1 growth corresponds to an interstadial in OIS 6, an event recorded in the SC-S11 stalagmite (Section 6.5.5), and that deposition of JC-F1 restarted sometime after 130 ka. The remaining isotope results seem to follow the same trends as the Vostok temperature profile.

6.6. Conclusions

6.6.1. LT Stalagmite Isotope Profile Conclusions

The LT stalagmite isotope profile covers an interval of approximately 15 ka, a period equivalent to mid- to late- OIS 5. The LT stalagmite oxygen isotope profile broadly correlates with the variations in surface mean annual temperature at Vostok (Jouzel *et al.*, 1993) and a deep sea sediment core, RC11-120 (Martinson *et al.*, 1987). As indicated by the Vostok ice core record, temperature conditions were up to 4°C cooler than present mean annual temperature. Overall the pattern is for a cooling trend for the first two-thirds of the record followed by rapid warming for the remainder, these trends are mirrored in the Vostok temperature record and also the sea-surface temperature record from RC11-120 (Martinson *et al.*, 1987). In the latter half of the LT $\delta^{18}O$ isotope record there are several isotopic "steps" of approximately 1 ka duration, it is difficult to tell whether they are related to local climatic events or to regional and/or global influences such as Dansgaard-Oeschger oscillations (Dansgaard *et al.*, 1993).

Carbon isotope variations indicate changes in vegetation activity with less negative isotopic values believed to be related to decreased vegetation activity. Previous studies (Desmarchelier and Goede, 1986, Hellstrom, 1998) have shown that summer insolation strongly influences effective precipitation, high moisture availability favours vegetation growth and speleothem deposition, and therefore insolation changes will have had significant effects on vegetation activity and speleothem deposition. In the LT stalagmite $\delta^{13}C$ results indicate that biological activity was greatly influenced by available moisture and temperature. The early part of the carbon isotope record corresponds to an insolation peak at approximately 94 ka and falling $\delta^{13}C$ values indicate that vegetation activity was decreasing as summer insolation was increasing indicating that available moisture was declining. As summer insolation continued to fall temperature became a more significant effect in controlling available moisture.

6.6.2. SC-S11 Stalagmite Isotope Profile Conclusions

The depositional record appears to be continuous and extends from approximately 185 to 157 ka, representing a period of approximately 28,000 years. In the deep sea oxygen isotope chronology it is the period equivalent of the earlier part of MIS 6, the Penultimate Glacial stage, extending from approximately 128 ka to 195 ka (Bradley, 1985). The oxygen isotope record indicates that growth commenced under full glacial conditions but that rapid warming took place leading to a major interstadial between 178 and 162 ka with mean annual temperatures in the region similar to today. It is followed by rapid cooling until the record terminates at around 157 ka. A mean annual temperature change of approximately 8°C is indicated on the assumption that there has been no change in the isotopic composition of precipitation. The indication of present day temperatures at a time when global climates are known to have been significantly cooler may be due to increased continentality associated with low sealevels.

Vegetation changes have also been dramatic. Interstadial conditions are associated with an active vegetation cover dominated by C3 plants as is the case today but probably with conditions

of greater moisture availability as speleothem deposition was more abundant than as it has been during the Holocene (Ayliffe *et al.*, 1998). Full glacial conditions in contrast appear to be associated with a sparse vegetation cover dominated by C3 grasses.

When the record is compared to the precessional cycle (Berger and Loutre, 1991), it is found likely that C3 vegetation flourished at a time when seasonality was increasing. C4 vegetation became dominant either at, or soon after, summer insolation values reached their maximum, a condition that would favour their dominance (Teeri and Stowe, 1976; Tieszen *et al.*, 1979). High moisture availability during the growing season favours both vegetation growth and speleothem deposition and appears to be strongly influenced by precessional cycles (Baker *et al.*, 1993a; Baker *et al.*, 1995; Goede, 1998).

6.6.3. JC-F1 Flowstone Isotope Profile Conclusions

The flowstone sample, JC-F1, from Jersey Cave, Yarrangobilly, New South Wales, has had three major periods of deposition and covers several key periods in the Late Pleistocence including OIS 2, 3, 5, and 6. Several more TIMS $^{230}Th/^{234}U$ age determinations are required to improve the correlation with the OIS 5 and 6 chronology but the OIS 2 and 3 period are very well constrained. The oxygen isotope results suggest that a major interstadial occurred during OIS 3 and that it was significantly wetter in the area than during the interstadials of OIS 5. Several studies of lake and marine cores from eastern and southeastern Australia have suggested that the opposite may have been true. Since these records are poorly dated in comparison to the JC-F1 record their evidence remains equivocal. Differences between the sites may also reflect regional differences in moisture receipts but more investigation on other samples and sites is required to confirm this hypothesis.

Carbon isotope variation in JC-F1 is related to vegetation activity, and, since biological response is closely related to moisture availability, summer insolation and temperature are key factors in determining this. The carbon isotope results of JC-F1 reflect sensitivity to insolation and temperature changes as higher $\delta^{13}C$ values, indicating increased biological activity and moisture availability, are associated with declining summer insolation values and *vice versa*.

Chapter 7
Summary

7.1. Summary

The overall aim of this thesis has been to investigate palaeoenvironmental change using speleothems as an information source with a range of analytical procedures at the highest resolution that is technically possible. The first aim was to investigate the age distribution of speleothems in Tasmania and how it relates to past global climate changes. The study has contributed a significant number of new TIMS age estimates to the current set of Australian speleothem dates, however many more samples are required to assess how the frequency of speleothem deposition has varied over time (for example Baker *et al.*, 1993a). The second aim was to compare several stable isotope profiles of speleothems with overlapping ages from different karst areas in order to investigate regional differences in past climate. It was anticipated that several speleothems with significant temporal overlaps would be found given the number of samples analysed by TIMS, but this was not the case and this particular aim was not fully achieved. However, the stable isotope results of three speleothems from Southeastern Australia have yielded some important information relating to past environmental conditions in the region. The third and fourth aim are essentially complimentary. The third was to examine the minor element composition of soda-straw stalactites as a proxy record for recent climate, and the fourth was to investigate the minor element composition of speleothems using continuous scanning and discrete ablation techniques. Several recent studies (Roberts *et al.*, 1998; Hellstrom, 1998) have shown the potential of laser ablation techniques to analyse the minor element composition of speleothems at very high resolution, in the order of tens of microns rather than millimetres, and to provide high resolution records of terrestrial palaeoclimate. In certain cases it is possible that sub-annual records may be resolved therefore potentially allowing comparison of speleothem records to instrumental records.

7.1.1. Speleothem Age Determination

Three different radiometric techniques were used to estimate the ages of speleothem samples, the $^{230}Th/^{234}U$ TIMS method, the excess ^{210}Pb technique, and the AMS radiocarbon technique. The first method was applied to speleothem samples from southeastern Australia and an age frequency histogram compiled (aim 1). The main assumption of the histogram method is that speleothem growth is wholly dependent on climate and not on any other factors. It is suggested that the dating of speleothem hiatuses may be a better method of identifying climate induced changes. The histogram results, consisting of 37 new TIMS uranium series

age estimates together with a number of other MS and αS age determinations from other studies, reveals some important clues on past moisture availability and the timing of glacial events in southeastern Australia especially during the last 50 ka. The timing of glacial maxima can also be inferred by the lack of speleothem growth. The age frequency results bear this out as there are two major periods in the last 200 ka where no speleothem growth occurs, from 150 to 125 ka and from 22 to 19 ka, suggesting that severe climatic conditions during the Penultimate Glacial may have been of much longer duration than during the Last Glacial.

Several technical problems with the other two dating methods has prevented any meaningful results from being obtained. The main difficulty with the excess ^{210}Pb technique has been not to pre-treat the samples by washing the inside and outside surfaces of the soda-straw stalactite with dilute acid prior to analysis thereby avoiding contamination by atmospheric radon plating out onto the exposed surfaces. There is also the problem of sample selection and the lack of knowledge of the factors controlling the sources and supply of the parent and daughter isotopes to the speleothem. The application of AMS radiocarbon dating was not entirely successful and is mainly due to restrictions in the number of samples that could be analysed. The main observation from the study is that the assumption of a linear growth rate may not be appropriate in accounting for the dead carbon proportion (dcp) in speleothem calcite. Major disturbances, such as fire or forestry activities, may have significant impacts on the soil organic matter (SOM) turnover and therefore the ^{14}C activity of speleothem calcite (for example Genty *et al.*, 1998). However, the experience gained from this study will help future work utilising these techniques.

7.1.2. Minor Elements in Speleothems

The application of laser ablation ICP-MS to speleothems (aim 4), namely soda-straw stalactites, stalagmites, and flowstones, has allowed investigation of the variations in their minor element composition encompassing three different temporal scales, interglacial/glacial (10^4–10^5 years), millenial (10^3–10^4 years), and secular ($<10^2$–10^3 years), at extremely high resolution. Four elements: magnesium (^{26}Mg), strontium (^{88}Sr), barium (^{138}Ba) and uranium (^{238}U) were selected for analysis as they were found in suitable concentrations for analysis and gave reproducible results from duplicate measurements. Nearly all samples showed high positive correlations between the Sr and Ba results suggesting that strontium and barium concentrations are controlled by the same environmental parameters at all temporal scales, this appears not to hold true for Mg and U. At the secular scale the elements seem to be responding to seasonal changes in the acidity of the seepage water, responding to changes in the PCO_2 and biological activity of the soil and vegetation above the cave. At the higher temporal scales several factors may be operating to produce discernible changes in the minor element composition of speleothems but the traces must be compared with other palaeoenvironmental records in order to narrow down the dominant factors (see Hellstrom, 1998 for an example).

Lateral variations in speleothem minor element composition have also been investigated by laser ablation ICP-MS and the results indicate that significant lateral variations can occur in stalagmites and flowstones due to the nature of their formation while soda-straw stalactites

show only very minor lateral differences. Further investigation is required on the lateral fluctuation of absolute concentrations.

The most significant results of the thesis have come from the study of the soda-straw stalactite, FC-SS5, which shows distinct cyclicity in its minor element content (aim 3). No other study using speleothems as an information source has demonstrated annual cyclicity in the minor element composition of speleothems along the entire length of the sample. The study also highlights the potential that LA-ICP-MS has in the analysis of minor elements in speleothems due to its relative speed and ease of sample preparation. A new method of dating was developed based on the autocorrelation of quasi-periodical minor element variations and the surface banding present on some soda-straw stalactites. Two chronologies were developed by two independent methods mentioned previously and they agreed to within 5%. Comparison of minor element results with instrumental climate data did not yield any significant correlation but this may be due to the climate stations for which data were available being located at some considerable distance from the cave in an area with a local relief of approximately 1,000 metres.

7.1.3. Stable Isotopes in Speleothems

Stable isotope profiles from three speleothems from southeastern Australia have yielded important palaeoenvironmental information particularly on regional differences in moisture availability and the timing of glacial events (essentially aim 2). These profiles were compared with several other palaeoenvironmental proxy records. While a certain degree of conformity exists between them, there are significant differences that may either be attributed to regional differences in moisture availability or to problems with the age-distance model of the proxy. Temporal control was provided by multiple high precision $^{230}Th/^{234}U$ age determinations.

The LT stalagmite isotope profile covers an interval of approximately 15 ka, a period equivalent to mid- to late- Oxygen Isotope Stage (OIS) 5. The LT stalagmite oxygen isotope profile broadly correlates with the variations in surface mean annual temperature at Vostok (Jouzel *et al.*, 1993) and a deep sea sediment core, RC11-120 (Martinson *et al.*, 1987). Overall the pattern is for a cooling trend for the first two-thirds of the record followed by rapid warming for the remainder, these trends are mirrored in the Vostok temperature record and also the sea-surface temperature record from RC11-120 (Martinson *et al.*, 1987). In the latter half of the LT $\delta^{18}O$ isotope record there are several isotopic "steps" of approximately 1 ka duration, it is difficult to tell whether they are related to local climatic events or to regional and/or global influences such as Dansgaard-Oeschger oscillations (Dansgaard *et al.*, 1993). In the LT stalagmite $\delta^{13}C$ results indicate that biological activity was greatly influenced by available moisture and temperature variations. The early part of the carbon isotope record corresponds to an insolation peak at approximately 94 ka and falling $\delta^{13}C$ values indicate that vegetation activity was decreasing as summer insolation was increasing indicating that available moisture was declining.

The depositional record for SC-S11 from Naracoorte, South Australia appears to be continuous and extends from approximately 185 to 157 ka, representing a period of approximately 28,000

years, a period equivalent to the earlier part of Marine Isotope Stage 6, the Penultimate Glacial stage, extending from approximately 128 ka to 195 ka (Bradley, 1985). The oxygen isotope record indicates that growth commenced under full glacial conditions but that rapid warming took place leading to a major interstadial between 178 and 162 ka with mean annual temperatures in the region similar to today. It is followed by rapid cooling until the record terminates at around 157 ka. Carbon isotope variations indicate that vegetation changes have also been dramatic. Interstadial conditions are interpreted to be associated with an active vegetation cover dominated by C3 plants as is the case today but probably with conditions of greater moisture availability as speleothem deposition was more abundant than as it has been during the Holocene (Ayliffe *et al.*, 1998). When the record is compared to the precessional cycle (Berger and Loutre, 1991), it is found that C3 vegetation flourished at a time when seasonality was increasing. C4 vegetation became dominant either at, or soon after, summer insolation values reached their maximum, a condition that would favour their dominance (Teeri and Stowe, 1976; Tieszen *et al.*, 1979). High moisture availability during the growing season favours both vegetation growth and speleothem deposition and appears to be strongly influenced by precessional cycles (Baker *et al.*, 1993a; Baker *et al.*, 1995; Goede, 1998).

The flowstone sample, JC-F1, from Jersey Cave, Yarrangobilly, New South Wales, has had three major periods of deposition and covers several key periods in the Late Pleistocence including OIS 2, 3, 5, and 6. Several more TIMS $^{230}Th/^{234}U$ age determinations are required to improve the correlation with the OIS 5 and 6 chronology but the OIS 2 and 3 period are very well constrained. The oxygen isotope results suggest that a major interstadial occurred during OIS 3 and that it was significantly wetter in the area than during the interstadials of OIS 5. Several studies of lake and marine cores from eastern and southeastern Australia have suggested that the opposite may have been true (for example Harle, 1997; Harle *et al.*, 1999). Since these records are poorly dated in comparison to the JC-F1 record their evidence remains equivocal. Differences between the sites may also reflect regional differences in moisture receipts but more investigation on other samples and sites is required to confirm this hypothesis. Carbon isotope variation in JC-F1 is believed to be related predominantly to vegetation activity, and, since biological response is closely related to moisture availability, summer insolation and temperature are key factors in determining this. The carbon isotope results of JC-F1 reflect sensitivity to insolation and temperature changes as higher $\delta^{13}C$ values, indicating increased biological activity and moisture availability, are associated with declining summer insolation values and *vice versa*.

7.2. Significance of the Research

Several aspects of this research project have used high-resolution analysis techniques to produce new and encouraging results which will aid future palaeoenvironmental investigations using speleothems, particularly in the study of minor elements in speleothem carbonate. It has demonstrated the potential of laser ablation ICP-MS to easily and quickly analyse the minor element composition of speleothem carbonate. An exciting development for future speleothems research is the next generation of ICP-MS which allow the analysis of the

isotopes of stable minor elements. The presence of annual banding of surface ridges and minor elements in soda-straw stalactites was confirmed by novel use of dendrochronological tools and laser-ablation ICP-MS. These results are highly significant as they indicate that it may be possible to use soda-straw stalactites to investigate very recent palaeoenvironmental change and to calibrate speleothem records against modern instrumental records. The age histogram results have expanded our understanding of past climate changes and how they have influenced the southeast Australian region. The numerous TIMS age estimates will add to the current speleothem age database but many more results are required. The stable isotope results of JC-F1, a flowstone from Jewel Cave, Yarrangobilly, show that this karst area has great potential for significantly more palaeoenvironmental research.

7.3. Suggestions for Future Speleothem Research

Several studies, including this one, have observed significant variations in the minor element composition of speleothem calcite. While a number of studies have successfully demonstrated that they are related to palaeoenvironmental changes, very few have looked at the contemporary context. Any future study of minor element variations should aim to somehow calibrate the present day signal by analysing several of the variables; such as surface, soil, and cave temperature, precipitation, evaporation; over a one to two year period, preferably longer if possible, and to compare these environmental variables to the minor element composition of contemporaneous calcite.

Further refinement of the excess ^{210}Pb and radiocarbon dating techniques as they are applied to speleothems is required. The main problem with the excess ^{210}Pb method applied to soda-straw stalactites is in isolating the original content from contamination by later deposition on inner and outer surfaces.

One avenue of speleothem research which has only recently begun to receive any attention is the stable isotope composition of various minor elements, for example strontium. It may be possible to gain valuable insights into past environmental change using the isotopic ratios of other elements such as magnesium or barium.

References

Adams, J., Maslin, M. and Thomas, E. 1999 Sudden climate transitions during the Quaternary. *Progress in Physical Geography*, 23(1), 1-36.

Aharon, P. and Chappell, J. 1986 Oxygen isotopes, sea level changes and temperature history of a coral reef environment in New Guinea over the last 10^5 years. *Palaeogeography, Palaeoclimatology, Palaeoecology*, 56, 337-379.

Allen, K.J. 1998 *A Dendroclimatological Investigation of Phyllocladus aspleniifolius (LABILL) HOOK. F.* Unpublished PhD thesis, School of Geography and Environmental Studies, University of Tasmania.

Allison, V.C. 1923 The growth of stalagmites and stalactites. *Journal of Geology*, 31, 106-125.

Atkinson, T.C., Harmon, R.S., Smart, P.L. and Waltham, A.C. 1978 Palaeoclimate and geomorphic implications of $^{230}Th/^{234}U$ dates on speleothems from Britain. *Nature*, 272, 24-28.

Augustinus, P.C., Short, S.A. and Heijnis, H. 1999 Uranium/Thorium dating of ferricretes from Mid- to Late Pleistocene glacial sediments, Western Tasmania, Australia. *Journal of Quaternary Science*, 12, 295-308.

Ayalon, A., Bar-Matthews, M. and Kaufman, A. 1999 Petrography, strontium, barium and uranium concentrations, and strontium and uranium isotope ratios in speleothems as palaeoclimatic proxies: Soreq Cave, Israel. *The Holocene*, 9, 715-722.

Ayliffe, L.K. and Veeh, H.H. 1988 Uranium-series dating of speleothems and bones from Victoria Cave, Naracoorte, South Australia. *Chemical Geology*, 72, 211-234.

Ayliffe, L.K., Marianelli, P.C., Moriarty, K.C., Wells, R.T., McCulloch, M.T., Mortimer, G.E. and Hellstrom, J.C. 1998 500 ka precipitation record from southeastern Australia: Evidence for interglacial relative aridity. *Geology*, 26, 147-150.

Baker, A. 1993 Speleothem growth rate and palaeoclimate. Unpublished PhD thesis, University of Bristol, England .

Baker, A., Smart, P.L. and Ford, D.C. 1993a North-west European palaeoclimate as indicated by growth frequency variations of secondary calcite deposits. *Palaeogeography, Palaeoclimatology, Palaeoecology*, 100, 291-301.

Baker, A., Smart, P.L., Edwards, R.L. and Richards, D.A. 1993b Annual growth banding in a cave stalagmite. *Nature*, 364, 518-520.

Baker, A. and Smart, P.L. 1995 Recent flowstone growth rates: Field measurements in comparison to theoretical predictions. *Chemical Geology*, 122, 121-128.

Baker A., Smart, P.L., Barnes, W.L. and Farrant, A.R. 1995a The Hekla 3 volcanic eruption recorded in a Scottish speleothem. *The Holocene*, 5, 336-342.

Baker, A., Smart, P.L. and Edwards, R.L. 1995b Paleoclimate implications of mass spectrometric dating of a British flowstone. *Geology*, 23, 309-312.

Baker, A., Barnes, W. L. and Smart, P. L. 1996a Speleothem luminescence intensity and spectral characteristics: Signal calibration and a record of palaeovegetation change. *Chemical Geology*, 130, 65-76.

Baker, A., Smart, P.L. and Edwards, R.L. 1996b Mass spectrometric dating of flowstones from Stump Cross Caverns and Lancaster Hole, Yorkshire: Palaeoclimate implications. *Journal of Quaternary Science*, 11, 107-114.

Baker, A., Barnes, W. L. and Smart, P. L. 1997a Stalagmite drip discharge and organic matter fluxes in Lower Cave, Bristol. *Hydrological Processes*, 11, 1541-1555.

Baker, A., Ito, E., Smart, P.L. and McEvan, R.F. 1997b Elevated and variable values of ^{13}C in speleothems in a British cave system. *Chemical Geology*, 136, 263-270.

Baker, A. and Barnes, W.L. 1998 Comparison of the luminescence properties of waters depositing flowstone and stalagmites at Lower Cave, Bristol. *Hydrological Processes*, 12, 1447-1459.

Baker, A., Genty, D. and Smart, P.L. 1998a High-resolution records of soil humification and paleoclimate change from variations in speleothem luminescence excitation and emission wavelengths. *Geology*, 26, 903-906.

Baker, A., Genty, D., Dreybrodt, W., Grapes, J. and Mockler, N.J. 1998b Testing theoretically predicted stalagmite growth rate with recent annually laminated samples: implications for past stalagmite deposition. *Geochimica et Cosmochimica Acta*, 62, 393-404.

Baker, A. and Genty, D. 1999 Fluorescence wavelength and intensity variations of cave waters. *Journal of Hydrology*, 217, 19-34.

Baker, A., Mockler, N.J. and Barnes, W.L. 1999a Fluorescence intensity variations of speleothem-forming groundwaters: Implications for paleoclimate reconstruction. *Water Resources Research*, 35, 407-413.

Baker, A., Proctor, C.J. and Barnes, W.L. 1999b Variations in stalagmite luminescence laminae structure at Poole's Cavern, England, AD1910-1996: calibration of a palaeoprecipitation proxy. *The Holocene*, 9, 683-688.

Baker, A., Caseldine, C.J., Gilmour, M.A., Charman, D., Proctor, C.J., Hawkesworth, C.J. and Phillips, N. 1999c. Stalagmite luminescence and peat humification records of palaeomoisture for the last 2500 years. *Earth and Planetary Science Letters*, 165, 157-162.

Banner, J.L. 1995 Application of the trace element and isotope geochemistry of strontium to studies of carbonate diagenesis. *Sedimentology*, 42, 805-824.

Banner, J.L., Musgrove, M.L., Asmerom, Y., Edwards, R.L. and Hoff, J.A. 1996 High-resolution temporal record of Holocene groundwater chemistry - Tracing links between climate and hydrology. *Geology*, 24, 1049-1053.

Bard, E., Hamelin, B., Fairbanks, R.G. and Zindler, A. 1990 Calibration of the ^{14}C timescale over the past 30,000 years using mass-spectrometric U-Th ages from Barbados coral. *Nature*, 345, 405-410.

Bard, E., Hamelin, B., Arnold, M., Montaggioni, L., Cabioch, G., Faure, G. and Rougerie, F. 1996 Deglacial sea-level record from Tahiti coral and the timing of global meltwater discharge. *Nature*, 382, 241-244.

Bard, E., Rostek, F. and Sonzogni, C. 1997 Interhemispheric synchrony of the last deglaciation inferred from alkenone palaeothermometry. *Nature*, 385, 707-710.

Bar-Matthews M., Matthews, A. and Ayalon, A. 1991, Environmental controls of speleothem mineralogy in a karstic dolomitic terrain (Soreq Cave, Israel). *Journal of Geology*, 99, 189-207.

Bar-Matthews, M., Ayalon, A., Matthews, A., Sass, E. and Halicz, L. 1996 Carbon and oxygen isotope study of the active water-carbonate system in a karstic Mediterranean cave: Implications for paleoclimate research in semiarid regions. *Geochimica et Cosmochimica Acta*, Vol. 60, 337-347.

Baskaran, M. and Iliffe, T.M. 1993 Age determination of recent cave deposit using excess ^{210}Pb - A new technique. *Geophysical Research Letters*, 20, 603-606.

Baskaran, M. and Krishnamurthy, R.V. 1993 Speleothems as proxy for the carbon isotope composition of atmospheric CO_2. *Geophysical Research Letters*, 20, 2905-2908.

Battey, M.H. 1981 *Mineralogy for Students*. Second edition, Longman, London, 355 p.

Bell, M. and Walker, M.J.C. 1992 *Late Quaternary Environmental Change: Physical and Human Perspectives*. Longman Scientific and Technical, Harlow, Essex, England, 273 p.

Bender, M., Sowers, T., Dickson, M., Orchardo, J., Grootes, P., Mayewski, P. and Meese, D. 1994 Climate teleconnections between Greenland and Antarctica throughout the last 100,000 years. *Nature*, 372, 663-666.

Benedetti, M.F., Van Riemsdijk, W.H., Koopal, L.K., Kinniburgh, D.G., Gooddy, D.C. and Milne, C.J. 1996 Metal ion binding by natural organic matter – from the model to the field. *Geochimica et Cosmochimica Acta*, 60, 2503-2513.

Benoit, G. and Hemond, H.F. 1991 Evidence for diffusive redistribution of ^{210}Pb in lake sediments. *Geochimica et Cosmochimica Acta*, 55, 543-554.

Berger, A. and Loutre, M.F. 1991 Insolation values for the last 10 million years. *Quaternary Science Reviews*, 10, 297-317.

Bird, M.I., Chivas, A.R. and Head, J. 1996 A latitudinal gradient in carbon turnover times in forest soils. *Nature*, 381, 143-146.

Bird, M.I., Ayliffe, L.K., Fifield, L.K., Turney, C.S.M., Cresswell, R.G.,Barrows, T.T. and David, B. 1999 Radiocarbon dating of "old" charcoal using a wet oxidation, stepped-combustion procedure. *Radiocarbon*, 41, 127-140.

Bischoff, J.L. and Fitzpatrick, J.A. 1991 U-series dating of impure carbonates; an isochron technique using total-sample dissolution. *Geochimica et Cosmochimica Acta*, 55, 543-554.

Bogli, A. 1980 *Karst hydrology and physical speleology*. (Translation of *Karsthydrographie und physische Spelaeologie*, translated by June C. Schmid), Springer, Berlin, 284 p.

Bond, G., Broecker, W., Johnsen, S., McManus, J., Labeyrie, L., Jouzel, J. and Bonani, G. 1993 Correlations between climate records from North Atlantic sediments and Greenland ice. *Nature*, 365, 143-147.

Bowen, R. 1988 *Isotopes in the Earth Sciences*. Elsevier, London, 647 p.

Bowen, R 1991 *Isotopes and Climates*. Elsevier, London, 483 p.

Bowler, J.M. 1982 Aridity in the Late Tertiary and Quaternary of Australia. In: Barker, W.R. and Greenslade, P.J.M. (eds) *Evolution of the Flora and Fauna of Arid Australia*. Peacock Publications, Adelaide, 35-45.

Bradley, R.S. 1985 *Quaternary Paleoclimatology: Methods of Paleoclimatic Reconstruction*. Chapman Hall, London, p. 472.

Broecker, W.S. and Denton, G.H. 1990 The role of ocean atmosphere reorganisations in glacial cycles. *Geochimica et Cosmochimica Acta*, 53, 2465-2501.

Broecker, W.S., Olson, E.A. and Orr, P.C. 1960 Radiocarbon measurements and annual rings in cave formations. *Nature*, 185, 93-94.

Brook, G.A., Burney, D.A. and Gowart, J.B. 1990 Desert paleoenvironmental data from cave speleothems with examples from the Chihuahuan Somali-Chalbi, and Kalahari deserts. *Palaeogeography, Palaeoclimatology, Palaeoecology*, 76, 311-329.

Buhmann, D. and Dreybrodt, W. 1985a The kinetics of calcite dissolution and precipitation in geologically relevant situations of karst areas: 1 open system. *Chemical Geology*, 48, 189-211.

Buhmann, D. and Dreybrodt, W. 1985b The kinetics of calcite dissolution and precipitation in geologically relevant situations of karst areas: 2 closed system. *Chemical Geology*, 53, 109-124.

Buhmann, D. and Dreybrodt. W. 1987 Calcite dissolution kinetics in the system H_2O-CO_2-$CaCO_3$ with the participation of foreign ions. *Chemical Geology*, 64, 89-102.

Burrett, C. and Goede, A. 1987 *Mole Creek – A Geological and Geomorphological Field Guide.* Geological Society of Australia (Tasmanian Division) Guidebook, 1, p. 21

Burton, E.A. and Walter, L.M. 1991 The effects of pCO_2 and temperature on magnesium incorporation in calcite in seawater and $MgCl_2$-$CaCl_2$ solutions. *Geochimica et Cosmochimica Acta*, 55, 777-785.

Butler, I.B. Nesbitt, R.W. 1999 Trace element distributions in the chalcopyrite wall of a black smoker chimney: insights from laser ablation inductively coupled plasma mass spectrometry (LA-ICP-MS). *Earth and Planetary Science Letters*, 167 335-345.

Cabrol, P. and Loundray, J. 1982 Climatic fluctuations influence the genesis and diagenesis of carbonate speleothems in southwestern France. *National Speleological Society Bulletin*, 44, 112-117.

Cerling, T.E., Quade, J., Wang, Y. and Bowman, J.R. 1989 Carbon isotopes in soils and palaeosols as ecology and palaeoecology indicators. *Nature*, 341, 138-139.

Chappell, J.M.A. and Shackleton, N.J. 1986 Oxygen isotopes and sealevel. *Nature*, 324, 137-140.

Chappell, J. 1991 Late Quaternary environmental changes in eastern and central Australia, and their climatic interpretation. *Quaternary Science Reviews*, 10, 377-390.

Chappell, J. 1996 Reconciliation of late Quaternary sea-levels derived from coral terraces at Huon Peninsula with deep sea oxygen isotope records. *Earth and Planetary Science Letters*, 141, 227-236.

Charles, C.D., Lynchstieglitz, J., Ninnemann, U.S. and Fairbanks, R.G. 1996 Climate connections between the hemisphere revealed by deep sea sediment core/ice core correlations. *Earth and Planetary Science Letters*, 142, 19-27.

Chen, J.H., Edwards, R.L. and Wasserburg, G.J. 1992 Mass spectrometry and applications to uranium-series disequilibrium. In: Ivanovich, M. and Harmon, R.S. (Eds) *Uranium-series Disequilibrium*, Oxford Science Publications, 174-206.

Clapperton, C.M. 1990 Quaternary glaciations in the Southern hemisphere: An overview. *Quaternary Science Reviews*, 9, 299-304.

Coles, G., Hunt, C.O. and Jenkinson, R.D.S. 1985 Robin Hood's Cave: palynology. In: Briggs, D.J., Gilbertson, D.D. and Jenkinson, R.D.S. (eds) *Peak District and Northern Dukeries Field Guide.* Quaternary Research Association, Cambridge, 174-178.

Colhoun, E.A. (Ed) 1988 *Cainozoic Vegetation of Tasmania.* Department of Geography, University of Newcastle, New South Wales, Australia, 151 p.

Colhoun, E.A. 1991 *Climate during the last glacial maximum in Australian and New Guinea.* Australian and New Zealand Geomorphology Group, Special Publication 2, .

Colhoun, E.A. and Hannan, D. 1990 Glaciation and Tasmania. In: Scanlon, A.P., Fish, G.J. and Yaxley, M.L. (Eds) *Behind the scenery.* Second edition, Department of Education and the Arts, Hobart, Tasmania, Australia, 163 p.

Colhoun, E.A. and Peterson, J.A. 1986 Quaternary landscape evolution and cryosphere: research progress from Sahul to Australia Antartica. *Australian Geological Studies*, 24, 145-167.

Coplen, T.B., Winograd, I.J., Landwehr, J.M. and Riggs, A.C. 1994 A 500,000-year stable carbon isotopic record from Devils Hole, Nevada. *Science*, 263, 361-365.

Costin, A.B., Gray, M., Totterdell, C.J. and Wimbush, D.J. 1979 *Kosciusko Alpine Flora.* CSIRO, Melbourne-Collins, Sydney, Australia, 408 p.

Craig, H. 1957 Isotopic standards for carbon and oxygen and correction factors for mass-spectrometric analysis of carbon dioxide. *Geochimica et Cosmochimica Acta*, 12, 113-149.

Craig, H. 1961 Isotopic variations in meteoric waters. *Science*, 133, 1702-1703.

Craig, H. 1965 The measurement of oxygen isotope paleotemperatures. In: Tongiorgi, E. (Ed) *Stable Isotopes in Oceanographic Studies and Paleotemperatures.* Consigleo Nationale delle Ricerche Laboratoriodi Geologia Nucleare, Piza, 3-24.

Crowley, T.J. 1994 Potential reconciliation of Devils Hole and deep-sea Pleistocene chronologies. *Paleoceanography*, 9, 1-5.

Crozaz, G., Picciotto, E. and DeBreuck, W. 1964 Antarctic snow chronology with ^{210}Pb. *Journal of Geophysical Research*, 69, 2597-2604.

Curl, R.L. 1972 Minimum diameter stalactites. *Bulletin of the National Speleological Society*, 34, 129–136.

Curl, R.L. 1973 Minimum diameter stalagmites. *Bulletin of the National Speleological Society*, 35, 1–9.

D'Costa, D.M. 1989 *Late Quaternary Vegetation and Environments from Lake Terang, Western Victoria.* Unpublished PhD Thesis, Monash University.

Dansgaard, W. 1964 Stable isotopes in precipitation. *Tellus*, 16, 436-468.

Dansgaard, W., Johnsen, S.J., Clausen, H.B., Dahljensen, D., Gundestrup, N.S., Hammer, C.U., Hvidberg, C.S., Steffensen, J.P., Sveinbjornsdottir, A.E., Jouzel, J. and Bond, G. 1993 Evidence for general instability of past climate from a 250 kyr ice core record. *Nature*, 364, 218-220.

Davies, J.L. 1967 Tasmanian landforms and Quaternary climates. In: Jennings, J.N. and Mabbutt, J.A. (Eds) *Landform Studies from Australia and New Guinea.* Australian National University Press, Canberra, Australia, 1-25.

Debenham, N.C. 1983 Reliability of thermoluminescence dating of stalagmitic calcite. *Nature*, 304, 154-156.

Debenham, N.C. and Aitken, M.J. 1984 Thermoluminescence dating of stalagmitic calcite. *Archaeometry*, 26, 155-170.

Dennis, P.F., Rowe, P.J. and Atkinson, T.C. 1996 Isotopic composition of palaeoprecipitation and palaeogroundwaters from speleothem fluid inclusions. In: Lauritzen, S.-E. (Ed) *Climate Change: The Karst Record.* Extended Abstracts, University of Bergen, Norway, Karst Waters Special Publication, 2, 20-22.

Derbyshire, E. 1971 A synoptic approach to the atmospheric circulation of the last glacial maximum in Southeastern Australia. *Palaeogeography, Palaeoclimatology, Palaeoecology*, 10, 103-124

Derbyshire, E. 1972 Pleistocene glaciation of Tamania: review and speculations. *Australian Geographical Studies*, 10, 79-94.

Desmarchelier, J.M. 1994 *An Isotopic Analysis of a Tasmanian Speleothem*. Unpublished Honours Thesis, School of Geography and Environmental Studies, University of Tasmania, Hobart, 129p.

Desmarchelier, J.M. and Goede, A. 1996 High resolution stable isotope analysis of a Tasmanian speleothem. *Papers and Proceedings of the Royal Society of Tasmania*, 130, 7-13.

Desmarchelier, J.M., Goede, A., Ayliffe, L.K., McCulloch, M.T. and Moriarty, K. 2000 Stable isotope record and its palaeoenvironmental interpretation for a late Middle Pleistocene speleothem from Victoria Fossil Cave, Naracoorte, South Australia. *Quaternary Science Reviews*, 19, 763-774.

Dettman, D. and Clohmann, K. 1995 Microsampling carbonates for stable isotope and minor element analysis: physical separation of samples on a 20 micrometer scale. *Journal of Sedimentary Research*, A65, 566-569.

Dickin, A.P. 1995 *Radiogenic Isotope Geology*. Cambridge University Press, p. 452.

Ding, Z.L., Liu, T.S., Rutter, N.W., Yu, Z.W., Guo, Z.T. and Zhu, R.X. 1995 Ice-volume forcing of east-Asian winter monsoon variations in the past 800,000 years. *Quaternary Research*, 44, 149-159.

Dodson, J.R. 1975 Vegetation history and water fluctuations at Lake Leake, southeastern South Australia. II. 50,000 to 10,000 B.P. *Australian Journal of Botany*, 23, 815-831.

Dodson, J.R. 1977 Late Quaternary palaeoecology of Wyrie Swamp, southeastern South Australia. *Quaternary Research*, 8, 97-144.

Dodson, J.R. 1998 Timing and response of vegetation change to Milankovitch forcing in temperate Australia and New Zealand. *Global and Planetary Change*, 18, 161-174.

Dorale, J.A., Gonzalez, L.A., Reagan, M.K., Pickett, D.A., Murrell, M.T. and Baker, R.G. 1992 A high-resolution record of Holocene climate change in speleothem calcite from Cold Water Cave, northeast Iowa. *Science*, 258, 1626-1630.

Dorale, J.A., Edwards, R.L., Ito, E. and Gonzalez, L.A. 1998 Climate and vegetation history of the midcontinent from 75 to 25 ka: A speleothem record from Crevice Cave, Missouri, USA. *Science*, 282, 1871-1874.

Dörr, H. and Münnich, K.O. 1989 Downward movement of soil organic matter and its influence on trace-element transport (^{210}Pb, ^{137}Cs). *Radiocarbon*, 30, 655-663.

Drake, J.J. 1980 The effect of soil activity on the chemistry of carbonate groundwater. *Water Resources Research*, 16, 381-386.

Drake, J.J. 1983 The effects of geomorphology and seasonality on the chemistry of carbonate groundwaters. *Journal of Hydrology*, 61, 223-226.

Drake, J.J. and Wigley, T.M.L. 1975 The effect of climate on the chemistry of carbonate groundwater. *Water Resources Research*, 11, 958-962.

Dreybrodt, W. 1980 Deposition of calcite from thin films of natural calcareous solutions and the growth of speleothems. *Chemical Geology*, 29, 89-105.

Dreybrodt, W. 1981 The kinetics of calcite precipitation from thin films of calcareous solutions and the growth of speleothems: Revisited. *Chemical Geology*, 32, 237-245.

Dreybrodt, W. 1988 *Processes in Karst Systems*. Springer-Verlag, Berlin, 288 p.

Dreybrodt, W. 1999 Chemical kinetics, speleothem growth and climate. *Boreas*, 28, 347-356.

Dreybrodt, W. and Buhmann, D. 1991 A mass transfer model for dissolution and precipitation of calcite from solutions in turbulent motion. *Chemical Geology*, 90, 107-122.

Dreybrodt, W., Buhmann, D., Michaelis, J. and Usdowski, E. 1992 Geochemically controlled calcite precipitation by CO_2 outgassing: Field measurements of precipitation rates to theoretical predictions. *Chemical Geology*, 97, 287-296.

Dreybrodt, W., Lauckner, J., Liu Zaihua., Svensson, U. and Buhmann, D. 1996. The kinetics of the reaction $CO_2 + H_2O - H^+ + HCO_3^-$ as one of the rate limiting steps for the dissolution of calcite in the system H_20-CO_2-$CaCO_3$. *Geochimica et Cosmochimica Acta*, 60, 3375-3381.

Dreybrodt, W., Eisenlohr, L., Madry, B. and Ringer, S. 1997. Precipitation kinetics of calcite in the system $CaCO_3 - H_2O - CO_2$: The conversion to CO_2 by the slow process $H^+ + HCO_3^- \rightarrow CO_2 + H_2O$ as a rate limiting step. *Geochimica et Cosmochimica Acta*, 61, 3897-3904.

Dulinski, M. and Rozanski, K. 1990 Formation of $^{13}C/^{12}C$ isotope ratios in speleothems: a semi-dynamic model. *Radiocarbon*, 32, 7-16.

Duplessy, J., Labeyrie, J., Lalou, C. and Nguyen, H.V. 1970 Continental climatic variations between 130,000 and 90,000 years BP. *Nature*, 226, 631-633.

Eberhard, R. 1994 *Inventory and Management of the Junee River Karst System.* Forestry Tasmania, Hobart, 125p.

Eberhard, R. 1996 *Inventory and Management of the Florentine Valley, Tasmania.* Forestry Tasmania, Hobart, 139p.

Edwards, R.L. and Gallup, C.D. 1993 Dating the Devils Hole calcite vein. *Science*, 259, 1626-.

Edwards, R.L., Chen, J.H. and Wasserburg, G.J. 1986 ^{238}U-^{234}U-^{230}Th-^{232}Th systematics and the precise measurement of time over the past 500,000 years. *Earth and Planetary Science Letters*, 81, 175-192.

Edwards, R.L., Chen, J.H. and Wasserburg, G.J. 1987 Precise timing of the last interglacial period from mass spectrometric determination of thorium-230 in corals. *Science*, 236, 1547-1553.

Eggins, S.M., Woodhead, J.D., Kinsley, L.P.J., Mortimer, G.E., Sylvester, P., McCulloch, M.T., Hergt, J.M. and Handler, M.R. 1997 A simple method for the precise determination of ≥ 40 trace elements in geological samples by ICP-MS using enriched isotope internal standardisation. *Chemical Geology*, 134, 311-326.

Eggins, S.M., Kinsley, L.P.J. and Shelley, J.M.G. 1998a Deposition and element fractionation processes during atmospheric pressure laser sampling for analysis by ICP-MS. *Applied Surface Science*, 129, 278-286.

Eggins S.M., Rudnick, R.L. and McDonough, W.F. 1998b The composition of peridotites and their minerals – A laser-ablation ICP-MS study. *Earth and Planetary Science Letters*, 154, 53-71.

Ehleringer, J.R. and Rundel, P.W. 1989 Stable isotopes: history, units and instrumentation. In: Rundel, P.W., Ehleringer, J.R. and Nagy, K.A. (Eds) *Stable Isotopes in Ecological Research*. Ecological Studies v68, Springer-Verlag, New York, 1-15.

Fairchild, I.J., Tooth, A.F., Huang, Y., Borsato, A., Frisia, S. and McDermott, F. 1996 Spatial and temporal variations in water and stalactite chemistry in currently active caves: a precursor to interpretations of past climate. In: Bottrell, S. (Ed) *Proceedings of the Fourth International Symposium on the Geochemistry of the Earth's Surface*. 4 p.

Falguères, C., Lumley, H. and Bischoff, J.L. 1992 U-series dates for stalagmitic flowstone E (Riss/Würm Interglaciation) at Grotte du Lazeret, Nice, France. *Quaternary Research*, 38, 227-233.

Fantadis, J. and Ehhalt, D.H. 1970 Variations of the carbon and oxygen isotopic composition in stalagmites and stalactites: evidence of non-equilibrium isotopic fractionation. *Earth and Planetary Science Letters*, 10, 136-144.

Faure, G. 1986 *Principles of Isotope Geology*. Second edition, New York, Wiley, 589 p.

Fisher, M.J., Gale, S.J., Heijnis, H. and Drysdale, R.N. 1996 Low latitude speleothems and paleoclimatic reconstruction. In: Lauritzen, S.E. (Ed.) *Climate Change: The Karst Record*. Karst Waters Institute Special Publication 2, Bergen, Norway, 26-29.

Folk, R.L. and Assereto, R. 1976 Comparative fabrics of length-slow and length-fast calcite and calcitized aragonite in a Holocene speleothem, Carlsbad Cavern, New-Mexico. *Journal of Sedimentary Petrology*, 46, 486-496.

Ford, D. and Williams, P. 1989. *Karst Geomorphology and Hydrology*. Unwin Hyman, London, 601 p.

Ford, D.C., Lundberg, J., Palmer, M.V., Dreybrodt, W. and Schwarcz, H.P. 1993 Uranium-series dating of the draining of an aquifer – the example of Wind Cave, Black hills, South Dakota. *Geological Society of America Bulletin*, 105, 241-250.

Franke, W.H. 1965. The theory behind stalagmite shapes. In: Ford, T.D. and Cullingford, C.H.D. (Eds) *The Science of Speleology*. Academic Press, London, 89–95.

Fuge, R., Palmer, T.J., Pearce, N.J.G. and Perkins, W.T. 1993 Minor and trace element chemistry of modern shells: a laser ablation inductively coupled plasma mass spectrometry study. *Applied Geochemistry*, Supplementry Issue No. 2, 111-116.

Fullagar, R.L.K., Price, D.M. and Head, L.M. 1996 Early human occupation of northern Australia: archaeology and thermoluminescence dating of Jinmium rock shelter, Northern Territory. *Antiquity*, 70, 751-773.

Gale, S.J. and Hunt, C.O. 1985 The stratigraphy of Kirkland Cave, an Upper Palaeolithic Site in Northern England. *Proceedings of the Prehistoric Society*, 51, 283-304.

Gale, S.J., Haworth, R.J. and Pisanu, P.C. 1995 The ^{210}Pb chronology of the Late Holocene deposition in an eastern Australian lake basin. *Quaternary Science Reviews*, 14, 395-408.

Galimov, E.M., Grinenko, V.A. and Gubkin, I.M. 1965 Effect of leaching under surface conditions on the isotopic composition of carbon in secondary calcite. Translated from *Geokhimiya*, 1, 115-117.

Galloway, R.W. 1963 Glaciation in the Snowy Mountains: a reappraisal. *Proceedings of the Linnean Society of NSW*, 88, 180-198.

Gascoyne, M. 1977 Trace element geochemistry of speleothems. *International Congress of Speleology*, 7, 205-207.

Gascoyne, M. 1978 Trace elements in calcite - The only cause of speleothem colour? *Bulletin of the National Speleological Society*, 40, p. 98-.

Gascoyne, M. 1982 Geochemistry of the actinides and their daughters. In: Ivanovich, M. and Harmon, R.S. (Eds) *Uranium Series Disequilibria: Applications to Environmental Problems.* Clarendon Press, Oxford, 33-55.

Gascoyne, M. 1983 Trace-element partition coefficients in the calcite-water system and their paleoclimatic significance in cave studies. *Journal of Hydrology*, 61, 213-222.

Gascoyne, M. 1985 Application of the $^{227}Th/^{230}Th$ method to dating Pleistocene carbonates and comparison with other dating methods. *Geochimica et Cosmochimica Acta*, 49, 1165-1171.

Gascoyne, M. 1992 Paleoclimate determination from cave calcite deposits. *Quaternary Science Reviews*, 11, 609-632.

Gascoyne, M. and Schwarcz, H.P. 1982 Carbonate and Sulphate Precipitates. In: Ivanovich, M. and Harmon, R.S. (Eds) *Uranium Series Disequilibria: Applications to Environmental Problems.* Clarendon Press, Oxford, 268-301.

Gascoyne, M. and Nelson, D.E. 1983. Growth mechanisms of recent speleothems from Castleguard Cave, Columbia Icefields, Alberta, Canada, inferred from a comparison of uranium–series and carbon–14 age data. *Journal of Arctic and Alpine Research*, 15, 537–542.

Gascoyne, M., Schwarcz, H.P. and Ford, D.C. 1978 Uranium series dating and stable isotope studies of speleothems: Part 1. theory and technique. *Transactions of the British Cave Research Association*, 5, 91-111.

Gascoyne, M., Benjamin, G.J., Ford, D.C. and Schwarcz, H.P., 1979 Sea-level lowering during the Illinoain glaciation: Evidence from a Bahama 'blue hole'. *Science*, 205, 806-808.

Gascoyne, M., Schwarcz, H.P. and Ford, D.C. 1980 A paleotemperature curve for the mid-Wisconsin in Vancouver Island. *Nature*, 285, 474-476.

Gascoyne, M., Ford, D.C. and Schwarcz, H.P. 1981 Late Pleistocene chronology and paleoclimate of Vancouver Island determined from cave deposits. *Canadian Journal of Earth Sciences*, 18, 1643-1652.

Gentilli, J. 1972 The Climates of Tasmania. In: Gentilli, J. *Australian Climate Patterns.* Thomas Nelson (Australia) Ltd, Melbourne, Australia, 248-249.

Genty, D. and Quinif, Y. 1996 Annually laminated sequences in the internal structure of some Belgian stalagmites - Importance for paleoclimatology. *Journal of Sedimentary Research*, 66, 275-288.

Genty, D. and Massault, M. 1997 Bomb C-14 recorded in laminated speleothems: Calculation of dead carbon proportion. *Radiocarbon*, 39, 33-48.

Genty, D. and Deflandre, G. 1998 Drip flow variations under a stalactite of the Père Noël cave (Belgium). Evidence of seasonal variations and air pressure constraints. *Journal of Hydrology*, 211, 208-232.

Genty, D. and Massault, M. 1999 Carbon transfer dynamics from bomb-^{14}C and $\delta^{13}C$ time series of a laminated stalagmite from SW France-Modelling and comparison with other stalagmite records. *Geochimica et Cosmochimica Acta*, 63, 1537-1548.

Genty, D., Vokal, B., Obelic, B. and Massault, M. 1998 Bomb ^{14}C time history recorded in two modern stalagmites-importance for soil organic matter dynamics and bomb ^{14}C distribution over continents. *Earth and Planetary Science Letters*, 160, 795-809.

Geyh, M.A. and Schleicher, H. 1990 *Absolute Age Determination: Physical and Chemical Dating Methods and Their Application.* Springer-Verlag, Berlin, p. 503.

Ghil, M. and Yiou, P. 1996 Spectral methods: What they can and cannot do for climatic time series. In: Anderson, D. and Willebrand, J. (Eds) *Decadal Climate Variability: Dynamics and Predictability.* Elsevier, Amsterdam, 445-482.

Gilbert, J.M. 1958 Forest succession in the Florentine Valley, Tasmania. *Papers and Proceedings of the Royal Society of Tasmania*, 93, 129-151.

Gill, R. (Ed) 1997 *Modern Analytical Geochemistry.* Longman, Harlow, England, 329 p.

Girard, C. and Albarede, F. 1996 Trace elements in conodont phosphates from the Frasnian/Famennian boundary. *Palaeogeography, Palaeoclimatology, Palaeoecology*, 126, 195-209.

Given, R.K. and Wilkinson, B.H. 1986 Kinetic control of morphology, composition and mineralogy of abiotic sedimentary carbonates. *Journal of Sedimentary Petrology*, 55, 109-119.

Goede, A. 1981 Variation in hardness of cave drips at two Tasmanian sites. *Helictite*, 19, 57-67.

Goede, A. 1991 Tasmanian speleothems: progress and prospects for palaeoenvironmental reconstructions. *Quaternary Australasia*, 9, 23-28.

Goede, A. 1994 Continuous early last glacial palaenvironmental record from a Tasmanian speleothem based on stable isotope and minor element varations. *Quaternary Science Reviews*, 13, 283-291.

Goede, A. 1998 *Quaternary Studies of Caves and Coasts.* PhD Thesis, School of Geography and Environmental Studies, University of Tasmania, Hobart, Vol 1, 330 p.

Goede, A. and Harmon, R.S. 1983 Radiometric dating of Tasmanian speleothems: Evidence of cave evolution and climatic change. *Journal of the Geological Society of Australia*, 30, 89-100.

Goede, A. and Hitchman, M.A. 1984 Late Quaternary climatic change-evidence from Tasmanian speleothem. In: Vogel, J.C. (Ed) *Late Cainozoic Palaeoclimates of the Southern Hemisphere.* Balkema, Rotterdam, 221-232.

Goede, A. and Vogel, J.C. 1991 Trace element variation and dating of a Late Pleistocene Tasmanian speleothem. *Palaeogeography, Palaeoclimatology, Palaeoecology*, 88, 121-131.

Goede, A., Green, D.C. and Harmon, R.S. 1982 Isotopic composition of precipitation, cave drips and actively forming speleothems at three Tasmania cave sites. *Helictite*, 20, 17-28.

Goede, A., Green, D.C. and Harmon, R.S. 1986 Late Pleistocene palaeotemperature record from a Tasmanian speleothem. *Australian Journal of Earth Sciences*, 33, 333-342.

Goede, A., Harmon, R.S. and Atkinson, T.C. 1990a. Pleistocene climatic change in Southern Australia and its effect on speleothem deposition in some Nullarbor caves. *Journal of Quaternary Science*, 5, 29-38.

Goede, A., Veeh, H.H. and Ayliffe, L.K. 1990b. Late Quaternary palaeotemperature records for two Tasmanian speleothems. *Australian Journal of Earth Sciences*, 37, pp.267-278.

Goede, A., McDermott, F., Hawkesworth, C., Webb, J. and Finlayson, B. 1996 Evidence of Younger Dryas and Neoglacial cooling in a Late Quaternary palaeotemperature record from a speleothem in eastern Victoria, Australia. *Journal of Quaternary Science*, 11, 1-7.

Goede, A., McCulloch, M., McDermott, F. and Hawkesworth, C. 1998 Aeolian contribution to strontium and strontium isotope variations in a Tasmanian speleothem. *Chemical Geology*, 149, 37-50.

Gonzalez, L.A. and Lohmann, K.C. 1988 Controls on the mineralogy and composition of spelean carbonates: Carlsbad Caverns, New Mexico. In: James, N.P. and Choquette, P.W. (Eds) *Paleokarst*. Springer-Verlag, New York, 81-101.

Gonzalez, L.A., Carpenter, S.J. and Lohmann, K.C. 1992 Inorganic calcite morphology: roles of fluid chemistry and fluid flow. *Journal of Sedimentary Petrology*, 62, 383-399.

Gordon, D., Smart, P.L., Ford, D.C., Andrews, J.N., Atkinson, T.C., Rowe, P.J. and Christopher, N.J. 1989 Dating of Late Pleistocene interglacial and interstadial periods in the United Kingdom from speleothem growth frequency. *Quaternary Research*, 31, 14-26.

Goudie, A. 1992 *Environmental Change*. Clarendon Press, Oxford, England, 329p.

Gray, J. 1981 The use of stable-isotope data in climate reconstruction. In: Wigley, T.M.L., Ingram, M.J. and Farmer, G. (Eds) *Climate and History: Studies in Past Climates and Their Impact on Man*. Cambridge University Press, Cambridge, 53-81.

Grimes, K.G. 1994 The South-East karst province of South Australia. *Environmental Geology* , 23, 134-148.

Grün, R., McCulloch, M.T., and Mortimer, G.E. 1999 Detailed mass spectrometric U-series analyses of two teeth from the archaeological site of Pech de l'Aze II: Implications for uranium migration and dating. *Journal of Archaeological Science*, 26, 1301-1310.

Guo, Z., Liu, T., Guiot, J., Wu, N., Lu, H., Han, J., Liu, J. and Gu, Z. 1996 High frequency pulses of East Asian monsoon climate in the last two glaciations: link with the North Atlantic. *Climate Dynamics*, 12, 701-709.

Halicz L., Bar-Matthews, M., Ayalon, A. and Kaufman A. 1997 Determination of low concentrations of U and Th in carbonate rocks using FI-ICP-MS. *Atomic Spectroscopy*, 18, 175-179.

Hannan, D.G. and Colhoun, E.A. 1987 Glacial stratigraphy of the Upper Mersey Valley. *Australian Geographical Studies*, 25, 36-46.

Harle, K.J. 1997 Late Quaternary vegetation and climate change in southeastern Australia: palynological evidence from marine core E55-6. *Palaeogeography, Palaeoclimatology, Palaeoecology*, 131, 465-483.

Harle, K.J., Kershaw, A.P. and Heijnis, H. 1999 The contributions of uranium/thorium and marine palynology to the dating of the Lake Wangoon pollen record, western plains of Victoria, Australia. *Quaternary International*, 57/58, 25-34.

Harmon, R.S. and Curl, R.L. 1978 Preliminary results on growth rate and paleoclimate studies of a stalagmite from Ogle Cave - New Mexico. *National Speleological Society Bulletin*, 40, 25-26.

Harmon, R.S. and Schwarcz, H.P. 1981 Changes in ^{2}H and ^{18}O enrichment of meteoric water and Pleistocene glaciation. *Nature*, 290, 125-128.

Harmon, R.S., Schwarcz, H.P. and Ford, D.C. 1978 Stable isotope geochemistry of speleothems and cave water from the Flint Ridge-Mammoth Cave system Kentucky: implications for terrestrial climate change during the period 230,000 to 100,000 years B.P. *Journal of Geology*, 86, 373-384.

Harmon, R.S., Schwarcz, H.P., Ford, D.C. and Koch, D.L. 1979 An isotopic paleotemperature record for Late Wisconsian time in Northeast Iowa. *Geology*, 7, 430-433.

Harmon, R.S., Land, L.S., Mitterer, R.M., Garrett, P., Schwarcz, H.P. and Larson, G.J. 1981 Bermuda sea level during the last interglacial. *Nature*, 289, 481-483.

Hartley, G. and Mucci, A. 1996 The influence of PCO_2 on the partitioning of magnesium in calcite overgrowths precipitated from artificial seawater at 25°C and 1 atm total pressure. *Geochimica et Cosmochimica Acta*, 60, 315-324.

Hays, J.D., Imbrie, J. and Shackleton, N.J. 1976 Variations in the earth's orbit: pacemaker of the ice ages. *Science*, 194, 1121-1132.

Heinrich, H. 1988 Origin and consequences of cyclic ice rafting in the northeast Adlantic Ocean during the past 130,000 years. *Quaternary Research*, 29, 142-152.

Hellstrom, J.C. 1998 *Late Quaternary Palaeoenvironmental Records from the Geochemistry of Speleothems, North-West Nelson, New Zealand.* Unpublished PhD Thesis, Research School of Earth Sciences, Australian National University, Canberra, 265p.

Hellstrom, J., McCulloch, M. and Stone, J. 1998 A detailed 31,000 year record of climate and vegetation changes, from the isotope geochemistry of two New Zealand speleothems. *Quaternary Research*, 50, 167-178.

Henderson, L.M. and Kracek, F.C. 1927 The fractional precipitation of barium and radium chromates. Quoted in: Morse, J.W. and Mackenzie, F.T. 1990 *Geochemistry of Sedimentary Carbonates.* Elsevier, Amsterdam, 707 p.

Hendy, C. and Wilson, A.T. 1968 Palaeoclimatic data from speleothem. *Nature*, 216, 48-51.

Hendy, C.H. 1971 The isotopic geochemistry of speleothems-I. The calculation of the effects of different modes of formation on the isotopic composition of speleothems and their applicability as paleoclimatic indicators. *Geochimica et Cosmochimica Acta*, 35, 801-824.

Hennig, G.J., Grün, R. and Brunnacker, K. 1983 Speleothems travertines and paleoclimates. *Quaternary Research*, 20, 1-29.

Hesse, P.P. 1994 The record of continental dust from Australia in Tasman Sea sediments. *Quaternary Science Reviews*, 13, 257-272.

Heusser, L.E. and Van de Geer, G. 1994 Direct correlation of terrestrial and marine paleoclimatic records from four glacial-interglacial cycles- DSDP Site 594, southwest Pacific. *Quaternary Science Reviews*, 13, 273-282.

Hill, C and Forti, P. 1997 *Cave Minerals of the World.* Second edition, National Speleological Society, Inc., Huntsville, Alabama, USA. 463 p.

Holland, H.D., Kirsipu, T.V., Huebner, J.S. and Oxburgh, U.M. 1964 On some aspect of the chemical evolution of cave waters. *Journal of Geology*, 72, 36-67.

Howson, M.R., Pethybridge, A.D. and House, W.A. 1987 Synthesis and distribution coefficient of low-magnesium calcites. *Chemical Geology*, 64, 79-87.

Ikeya, M. 1975 Dating a stalactite by electron paramagnetic resonance. *Nature*, 255, 48-50.

Ikeya, M. 1988 Dating and radiation dosimetry with electron spin resonance. *Magnetic Resonance Review*, 13, 91-134.

Imbrie, J. and Imbrie, K.P. 1979 *Ice Ages – Solving the Mystery.* Enslow, Short Hills, USA, 224 p.

Imbrie, J., Berger, A., Boyle, E.A., Clemens, S.C., Duffy, A., Howard, W.R., Kukla, G., Kutzbach, J., Martinson, D.G., Mcintyre, A., Mix, A.C., Molfino, B., Morley, J.J., Peterson, L.C., Pisias, N.G.. Prell, W.L., Raymo, M.E., Shackleton, N.J. and Toggweiler, J.R. 1992 On the structure and origin of major glacial cycles I. Linear responses to Milankovich forcing. *Paleoceanography*, 7, 701-738.

Imbrie, J., Berger, A., Boyle, E.A., Clemens, S.C., Duffy, A., Howard, W.R., Kukla, G., Kutzbach, J., Martinson, D.G., Mcintyre, A., Mix, A.C., Molfino, B., Morley, J.J., Peterson, L.C., Pisias, N.G.. Prell, W.L., Raymo, M.E., Shackleton, N.J. and Toggweiler, J.R. 1993b On the structure and origin of major glacial cycles II. 100,000 year cycle. *Paleoceanography*, 8, 699-735.

Imbrie, J., Mix, A.C. and Martinson, D.G. 1993a Milankovich theory viewed from Devil's Hole. *Nature*, 363, 531-533.

Inokuchi, H.; Morinaga, H. and Yaskawa, K. 1981 Preliminary report on paleomagnetism of cave deposit. *Journal of Geomagnetism and Geoelectricity*, 33, 325–327.

Ivanovich, 1982 Uranium Series Disequilibria applications in Geochronology. In: Ivanovich, M. and Harmon, R.S. (Eds) *Uranium Series Disequilibria: Applications to Environmental Problems.* Clarendon Press, Oxford, 56-78.

Ivanovich, M. and Harmon, R.S. (Eds) 1992 *Uranium-series Disequilibrium: Applications to Earth, Marine, and Environmental Sciences.* Clarendon Press, Oxford, 608 p.

Jackson, W.D. 1999 Palaeohistory of vegetation change: The last 2 million years. In: Reid, J.B., Hill, R.S., Brown, M.J. and Hovenden, M.J. (Eds) *Vegetation of Tasmania.* Australian Biological Resources Study, Flora of Australia Supplementary Series, no. 8, Commonwealth of Australia, 64-88.

Jouzel, J., Lorius, C., Petit, J.R., Genthon, C., Barkov, N.I., Kotlyakov, V.M. and Petrov, V.M. 1997 Vostok ice core: a continuous isotope temperature record over the last climatic cycle (160,000 years). *Nature*, 329, 403-407.

Jouzel, J., Barkov, N.I., Barnola, J.M., Bender, M., Chappellaz, J., Genthon, C., Kotlyakov, V.M., Lipenkov, V., Lorius, C., Petit, J.R., Raynaud, D., Raisbeck, G., Ritz, C., Sowers, T., Stievenard, M., Yiou, F. and Yiou, P. 1993 Extending the Vostok ice core record of palaeoclimate to the Penultimate Glacial period. *Nature*, 364, 407-412.

Kashiwaya, K., Atkinson, T.C. and Smart, P.L. 1991 Periodic variations in Late Pleistocene speleothem abundance in Britain. *Quaternary Research*, 35, 190-196.

Katz, A., Sass, E., Starinsky, A. and Holland, H.D. 1972 Strontium behaviour in the aragonite-calcite transformation: an experimental study at 40 - 90°C. *Geochimica et Cosmochimica Acta*, 36, 481-496.

Katz, J.L., Reick, M.R., Herzogg, E.R. and Parsiegla, K.I. 1993. Calcite growth inhibition by iron. *Langmuir*, 9, 1423-1430.

Kendall, A. C. and Broughton, P.L. 1978 Origin of fabrics in speleothems composed of columnar calcite crystals. *Journal of Sedimentary Petrology*, 48, 519-538.

Kendall, A. C. and Broughton, P.L. 1993 Columnar calcite speleothems: discussion. *Journal of Sedimentary Petrology*, 63, 550-552.

Kershaw, A.P. and Nanson, G.C. 1993 The last full glacial cycle in the Australian region. *Global and Planetary Change*, 7, 1-9.

Kershaw, A.P. D'Costa, D.M., McEwen Mason, J.R.C. and Wagstaff, B.E. 1991 Palynological evidence for Quaternary vegetation and environments of mainland and southeastern Australia. *Quaternary Science Reviews*, 10, 391-404.

Kiernan, K. 1983 Weathering evidence for an additional glacial stage in Tasmania. *Australian Geographical Studies*, 21, 197-220.

Kiernan, K. 1990 Weathering as an indicator of the age of Quaternary glacial deposits in Tasmania. *Australian Geographer*, 21, 1-17.

Kirkpatrick, J.B. (Ed) 1991 *Tasmanian Native Bush – A Management Handbook*. Tasmanian Environment Centre, Hobart, Tasmania, 352 p.

Koide, M., Soutar, A. and Goldberg, E.D. 1972 Marine geochronology with ^{210}Pb. *Earth and Planetary Science Letters*, 14, 442-446.

Kukla, G. 1987 Loess stratigraphy in Central China. *Quaternary Science Reviews*, 6, 191-219.

Labeyrie, L., Labracherie, M., Gorfti, N., Pichon, J.J., Vautravers, M., Arnold, M., Duplessy, J.C., Paterne, M. Michel, E., Duprat, J., Caralp, M. and Turon, J.L. 1996 Hydrographic changes of the Southern Ocean (southeast Indian sector) over the last 230 kyr. *Paleoceanography*, 11, 57-76.

Langmuir, D. 1971 The geochemistry of some carbonate groundwaters in central Pennsylvania. *Geochimica et Cosmochimica Acta*, 35, 1023-1045.

Langmuir, D. and Herman, J.S. 1980 The mobility of thorium in natural waters at low temperatures. *Geochimica et Cosmochimica Acta*, 44, 1753-1766.

Latham, A.G., Schwarcz, H.P. and Ford, D.C. 1979 Paleomagnetism of stalagmite deposit. *Nature*, 280, 383-385.

Latham, A.G., Schwarcz, H.P. and Ford, D.C. 1986 The paleomagnetism and U-Th dating of Mexican stalagmite - DAS2. *Earth and Planetary Science Letters*, 79, 195-207.

Latham, A.G., Schwarcz, H.P., Ford, D.C. and Pearce, G.W. 1982 The palaeomagnetism and U-dating of three Canadian speleothems: evidence for the westward drift, 5.4-2.1 ka BP. *Canadian Journal of Earth Science*, 19, 1985-1995.

Lau, K.M., Sui, C.H., Chou, M.D. and Tao, W.K. 1994. An inquiry into the cirrus-cloud thermostat effect for tropical sea surface temperature. *Geophysical Research Letters*, 21, 1157-1160.

Lauritzen, S.E. 1995 High-resolution paleotemperature proxy record for the Last Interglaciation based on Norwegian speleothems. *Quaternary Research*, 43, 133-146.

Lauritzen, S.E., Ford, D.C. and Schwarcz, H.P. 1986 Humic substances in speleothem matrix - Paleoclimatic significance. *Proceedings of the 9th International Speleology Congress Barcelona*, 2, 77-79.

Lauritzen, S.E., Lovlie, R., Moe, D. and Ostbye, E. 1990 Paleoclimate deduced from a multidisciplinary study of a half-million-year-old stalagmite from Rana, Northern Norway. *Quaternary Research*, 34, 306-316.

Lauritzen, S.E., Haugen, J.E., Lovlie, R. and Gilje-Nielsen, H. 1994 Geochronological potential of isoleucine epimerization in calcite speleothems. *Quaternary Research*, 41, 52-58.

Lea, D.W. and Martin, P.A. 1999 A rapid mass spectrometric method for the simultaneous analysis of barium, cadmium, and strontium in foraminifera shells. *Geochimica et Cosmochimica Acta*, 60, 3143-3149.

Lebron, I. and Suarez, D.L. 1998 Kinetics and mechanisms of precipitation of calcite as affected by pCO_2 and organic ligands at 25°C. *Geochimica et Cosmochimica Acta*, 62, 405-416.

Li, W.-X., Lundberg, J., Dickin, A.P., Ford, D.C., Schwarcz, H.P., McNutt, R. and Williams, D. 1989 High precision mass-spectrometric uranium-series dating of cave deposits and implication for palaeoclimate studies. *Nature*, 339, 334-336.

Linsley, B.K. 1996 Oxygen-isotope record of sea level and climate variations in the Sulu Sea over the past 150,000 years. *Nature*, 380, 234-237.

Linsley, B.K. and Dunbar, R.B. 1994 The late Pleistocene history of surface water $\delta^{13}C$ in the Sulu Sea-possible relationship to Pacific Deepwater $\delta^{13}C$ changes. *Paleoceanography*, 9, 317-340.

Liu, H.S. and Chao, B.F. 1998 Wavelet spectral analysis of the Earth's orbital variations and paleoclimatic cycles. *Journal of Atmospheric Sciences*, 55, 227-236.

Liu, T.S., Ding, Z.L. and Rutter, N. 1999 Comparison of Milankovitch periods between continental loess and deep sea records over the last 2.5 Ma. *Quaternary Science Reviews*, 18, 1205-1212.

Lorens, R.B. 1981 Sr, Cd, Mn and Co distribution coefficients in calcite as a function of calcite precipitation rate. *Geochimica et Cosmochimica Acta*, 45, 553-561.

Lorius, C., Jouzel, J., Ritz, C., Merlivat, L., Barkov, N.I., Korotkevich, Y.S. and Kotlyakov, V.M. 1985 A 150,000 climatic record from Antarctic ice. *Nature*, 316, 591-596.

Lowe, D, amd Newnham, R. 1999 Advances in Quaternary tephrostratigraphy and teprochronology in New Zealand. *Quaternary Australasia*, 17, 12-19.

Ludwig, K.R., Simmons, K.R., Szabo, B.J., Winograd, I.J., Landwehr, J.M., Riggs, A.C. and Hoffman, R.J. 1992 Mass spectrometric ^{230}Th-^{234}U-^{238}U dating of the Devils Hole calcite vein. *Science*, 256, 284-287.

Lundberg J. and Ford, D.C. 1994 Late Pleistocene sea level change in the Bahamas from mass spectrometric U-series dating of submerged speleothem. *Quaternary Science Reviews*, 13, 1-14.

Mackenzie, F.T., Bischoff, W.B., Bishop, F.C., Loijens, M., Schoonmaker, J. and Wollast, R. 1983 Magnesian calcites: low temperature occurrence, solubility and solid-solution behaviour. In: Reeder, R.J. (Ed) *Carbonates, Mineralogy and Chemistry*. BookCrafters, Chealsea, Michegan, USA, 97-144.

Mano, S. and Andreae, M.O. 1994 Emissions of methyl bromide from biomass burning. *Science*, 263, 1255-1257.

Marino, B.D., McElroy, M.B., Salawitch, R.J. and Spaulding, W.G. 1992 Glacial-to-interglacial variations in the carbon isotopic composition of atmospheric CO_2. *Nature*, 357, 461-466.

Marker, M.E. 1975 *The Lower Southeast of South Australia: A Karst Province*. Department of Geography and Environmental Studies, Occasional Paper 13, University of Witwatersrand, Johannesburg, South Africa, 38 p.

Markgraf, V., Dodson, J.R., Kershaw, A.P., McGlone, M.S. and Nicholls, N. 1992 Evolution of late Pleistocene and Holocene climates in the circum-South Pacific land areas. *Climate Dynamics*, 6, 193-211.

Martinson, D.F., Pisias, N.G., Imbrie, J., Moore, T.C. and Shackelton, N.J. 1987 Age dating and the orbital theory of ice ages: development of a high resolution 0 to 300,000-year chronostratigraphy. *Quaternary Science Reviews*, 27, 1-29.

Matthews, P.G. (Ed) 1985 *Australian Karst Index*. Australian Speleological Federation Inc., Melbourne, Australia.

McCulloch, M.T., Tudhope, A.W., Esat, T.M., Mortimer, G.E., Chappell, J., Pillans, B., Chivas, A.R. and Omura, A. 1999 Coral record of equatorial sea-surface temperatures during the penultimate deglaciation at Huon Peninsula. *Science*, 283, 202-204.

McGowran, B., Li, Q.Y., Cann, J., Padley, D., Mckirdy, D.M. and Shafik S. 1997 Biogeographic impact of the Leeuwin Current in southern Australia since the Late Middle Eocene. *Palaeogeography, Palaeoclimatology, Palaeoecology*, 136, 19-40.

McTainsh, G. 1989 Quaternary aeolian dust processes and sediments in the Australian region. *Quaternary Science Reviews*, 8, 235-253.

Miller, G.H., Magee, J.W. and Jull, A.J.T. 1997 Low-altitude glacial cooling in the Southern Hemisphere from amino-acid racemization in emu eggshells. *Nature*, 385, 241-244.

Moore, G.W. 1952 Speleothem: a new term. *National Speleological Society News*, 10, 2.

Moore, G.W. 1962 The growth of stalactites. *Bulletin of the National Speleological Society*, 24, 95- 106.

Morse, J.W. and Bender, M.L. 1990 Partition coefficients in calcite: Examination of factors influencing the validity of experimental results and their application to natural systems. *Chemical Geology*, 82, 265-277.

Morse J.W. and Mackenzie, F.T. 1990 Geochemistry of Sedimentary Carbonates. Elsevier, Amsterdam, 707 p.

Mucci, A. 1987 Influence of temperature on the composition of magnesian calcite overgrowths precipitated from seawater. *Geochimica et Cosmochimica Acta*, 51, 1977-1984.

Mucci, A. and Morse, J.W. 1983 The incorporation of Mg^{2+} and Sr^{2+} into calcite overgrowths: Influences of growth rate and solution composition. *Geochimica et Cosmochimica Acta*, 47, 217-233.

Mucci, A. and Morse, J.W. 1985 Auger spectroscopy determination of the surfacemist absorbed layer composition on aragonite, calcite, dolomite and magnesite in synthetic seawater. *American Journal of Science*, 285, 306-317.

Nanson, G.C., Price, D. and Short, S.A. 1992 Wetting and drying of Australia over the past 300 ka. *Geology*, 20, 791-794.

Nees, S. 1997 Late Quaternary palaeoceanography of the Tasman Sea: the benthic foraminiferal view. *Palaeogeography, Paleoclimatology, Palaeoecology*, 13, 365-389.

O'Neil, J.R. Adami, L.H. and Epstein, S. 1975 Revised value for the ^{18}O fractionation between CO_2 and H_2O at 25°C. *Journal Research U.S. Geological Survey*, 3, 623-624.

Okada, H. and Wells, P. 1997 Late Quaternary nannofossil indicators of climate change in two deep-sea cores associated with the Leeuwin Current off Western Australia. *Paleogeography, Paleoclimatology, Paleoecology*, 131, 413-432.

Oomori, T., Kaneshima, H., Maezato, T. 1987 Distribution coefficient of Mg^{2+} ions between calcite and solution at 10-50°C. *Marine Chemistry*, 20, 327-336.

Paquette, J. and Reeder, R.J. 1990 New type of compositional zoning in calcite: insights into crystal growth mechanisms. *Geology*, 18, 1244-1247.

Paquette, J. and Reeder, R.J. 1995 Relationship between surface structure, growth mechanism, and trace element incorporation in calcite. *Geochimica Cosmochimica Acta*, 59, 735-749.

Pazdur, A., Pazdur, M.F., Pawlyta, J., Gorny, A. and Olszewski, M. 1995 Paleoclimatic implications of radiocarbon dating of speleothems from the Cracow-Weilun upland, southern Poland. *Radiocarbon*, 37, 103-110.

Penney, C.L. 1983 Climate. In: Tyler, M.J., Turidale, C.R., King, J.K. and Holmes, J.W. (Eds) *Natural History of the South East*. Royal Society of South Australia Inc., Adelaide, 85-94.

Perkins, W.T. and Pearce, N.J.G. 1995 Mineral microanalysis by laser probe Inductively-Coupled Plasma Mass Spectrometry. In: Potts, P.J., Bowles, J.F.W., Reed, S.J.B. and Cave, M.R. (Eds) *Microprobe Techniques in the Earth Sciences*. Chapman and Hall, London, 291-325

Pilcher, J.R. 1991 Radiocarbon Dating. In: Smart, P.L. and Frances, P.D. (Eds) *Quaternary Dating Methods: A Users Guide*. Technical Guide 4, Quaternary Research Association, Cambridge, 16-36.

Pillans, B. 1991 New Zealand Quaternary stratigraphy: an overview. *Quaternary Science Reviews*, 10, 405-418.

Pingitore, N.E. Jr, and Eastman, M.P. 1986 The co-precipitation of Sr^{2+} with calcite at 25°C and 1 atm. *Geochimica et Cosmochimica Acta*, 50, 2195-2203.

Pittock, A.B. 1975 Climatic change and patterns of variation in Australian rainfall. *Search*, 6, 498-503.

Pittock, A.B., Frakes, L.A., Jessen, D., Peterson, J.A. and Zillman, J.W. (Eds) 1978 *Climatic Change and Variability: A Southern Perspective*. Cambridge University Press, Cambridge, 455 p.

Pitty, A.F. 1966 *An Approach to the Study of Karst Water*. University of Hull, Occasional Paper in Geography No. 5, 70 p.

Plummer, L.N., Wigley, T.N.L. and Parkhurst, D.L. 1978 The kinetics of calcite dissolution in CO_2 water systems at 5 to 60°C and 0.0 to 1.0 atm CO_2. *American Journal of Science*, 278, 179-216.

Quade, J., Cerling, T.E. and Bowman, J.R. 1989 Systematic variations in the carbon and oxygen isotope composition of pedogenic carbonate along elevation transects in the southern Great Basin, United States. *Geological Society of America Bulletin*, 101, 464-475.

Railsback, L.B., Brook, G.A., Chen, J., Kalin, R. and Fleisher, C.J. 1994 Environmental controls on the petrology of a late Holocene speleothem from Botswana with annual layers of aragonite and calcite. *Journal of Sedimentary Research*, A64, 147-155.

Ramanathan, V. and Collins, W. 1991 Thermodynamic regulation of ocean warming by cirrus clouds deduced from observations of the 1997 El Niño. *Nature*, 351, 27-32.

Ramseyer, K., Miano, T.M., Dorazio, V., Wildberger, A., Wagner, T. and Geister, J. 1997 Nature and origin of organic matter in carbonates from speleothems, marine cements, and coral skeletons. *Organic Geochemistry*, 26, 361-378.

Rasmussen, T.L., Van Weering, C.E. and Labeyrie, L. 1997 Climate instability, ice sheets and ocean dynamics at high northern latitudes during the last glacial period (58-10 ka BP). *Quaternary Science Reviews*, 16, 71-80.

Reddy, M.M. and Wang, K.K. 1980 Crystallisation of calcium carbonate in the presence of metal ions. I. Inhibition by magnesium ion at pH 8.8 and 25°C. *Journal of Crystal Growth*, 50, 470-480.

Reddy, M.M., Plummer, L.N. and Busenberg, E. 1981 Crystal growth of calcite from calcium bicarbonate solutions at constant PCO_2 and 25°C: a test of a calcite dissolution model. *Geochimica et Cosmochimica Acta*, 45, 1281-1289.

Reed, S.J.B. 1990 Recent developments in geochemical microanalysis. *Chemical Geology*, 83, 1-9.

Reed, S.J.B. 1995 Electron probe microanalysis. In: Potts, P.J., Bowles, J.F.W., Reed, S.J.B. and Cave, M.R. (Eds) *Microprobe Techniques in the Earth Sciences*. Chapman and Hall, London, 49-89.

Reeder, R.J. and Grams, J.C. 1987 Sector zoning in calcite cement crystals: Implications for trace element distributions in carbonates. *Geochimica et Cosmochimica Acta*, 51, 187-194.

Richards, D.A., Smart, P.L. and Edwards, R.L. 1994 Maximum sea levels for the last glacial period from U-series ages of submerged speleothems. *Nature*, 367, 357-360.

Roberts, M.S. 1997 *Trace elements in speleothem calcite: the potential for terrestrial palaeoclimate studies.* Unpublished PhD thesis, Department of Geography, University of Bristol, England, 185 p.

Roberts, M.S., Smart, P.L. and Baker A. 1998 Annual trace element variations in a Holocene speleothem. *Earth and Planetary Science Letters*, 154, 237-246.

Roberts, R., Bird, M., Olley, J., Galbraith, R., Lawson, E., Laslett, G., Yoshida, H., Jones, R., Fullagar, R., Jacobsen, G. and Hua, Q. 1998 Optical and radiocarbon dating at Jinmium rock shelter in Northern Australia. *Nature*, 393, 358-362.

Rollinson, H.R. 1993 *Using geochemical data: evaluation, presentation, interpretation*. Longman Scientific, Burnt Mill, Harlow, Essex, England, 352 p.

Rosholt, J.N. and Antal, P.S. 1962 Evaluation of the Pa^{231}/U-Th^{230}/U method for dating Pleistocene carbonate rocks. *USGS Professional Paper*, 450-E, 108-111.

Rowe, P.J. and Atkinson, T.C. 1985 Uranium-thorium dating results from Robin Hood's Cave. In Briggs, D.J., Gilbertson, D.D. and Jenkinson, R.D.S. (eds). *Peak District and Northern Dukeries Field Guide*, Quaternary Research Association, Cambridge, 196-203.

Rowe, P., Dennis, P., Atkinson, T., Lauritzen, S.-E. and Lundberg, J. 1998 A high resolution deuterium record from fluid inclusions in a late Holocene speleothem from southwest Britain. In: Marcolli, B. (Ed) *Past Global Climates and Their Significance for the Future*. IGBP PAGES, London, 88 p.

Santschi, P.H., Li, Y.H., Adler, D.M., Amdurer, M., Bell, J. and Nyffeler, U.P. 1983 The relative mobility of natural (Th, Pb, and Po) and fallout (Pu, Am, and Cs) radionuclides in the coastal marine environment: results from model ecosystems (MERL) and Narragansett Bay. *Geochimica et Cosmochimica Acta*, 47, 201-210.

Schotterer, U., Oldfield, F. and Frohich, D.W. 1996 *GNIP – Global Network for Isotopes in Precipitation*. Bern, Switzerland, 48 p.

Schrag, D.P., Hampt, G. and Murray, D.W. 1996 Pore fluid constraints on the temperature and oxygen isotopic composition of the glacial ocean. *Science*, 272, 1930-1932.

Schwarcz, H.P. 1980 Absolute age determination of archaeological sites by uranium-series dating of travertines. *Archaeometry*, 22, 3-24.

Schwarcz, H. 1986 Geochronology and Isotopic Geochemistry of Speleothems. In: Fritz, P. and Fontes, J.C. (Eds) *Handbook of Environmental Isotope Chemistry: Volume 2, The Terrestrial Environment, B*. Elsevier, New York, 271-303.

Schwarcz, H.P. and Yonge, C. 1983 Isotopic composition of a palaeowater as inferred from speleothem and its fluid inclusion. In: *Palaeoclimates and Palaeowaters: A Collection of Environmental Isotope Studies*. IAEA, Vienna, 115-133.

Schwarcz, H.P., Harmon, R.S., Thompson, P. and Ford, D.C. 1976 Stable isotope studies of fluid inclusions in speleothems and their palaeoclimatic significance. *Geochimica et Cosmochimica Acta*, 40, 657-665.

Shackleton, N.J. 1987 Oxygen isotopes, ice volume and sealevel. *Quaternary Science Reviews*, 6, 183-190.

Sharp, M., Tison, J-L. and Fierens, G. 1990 Geochemistry of subglacial calcites: implications for the hydrology of the basal water film. *Arctic and Alpine Research*, 22, 141-152.

Shaw, T.R. 1992 *History of Cave Science: The Exploration and Study of Limestone Caves to 1900.* Sydney Speleological Society, 2nd edition, 338 p.

Shaw, T.R. 1997 Historical Introduction. In Hill, C and Forti, P. (Eds) 1997 *Cave Minerals of the World.* Second edition, National Speleological Society, Inc., Huntsville, Alabama, USA., 27-43.

Shopov, Y.Y., Ford, D.C. and Scwarcz, H.P. 1994 Luminescent microbanding in speleothems: high-resolution chronology and paleoclimate. *Geology*, 22, 407-410.

Sinclair, D.J., Kinsley, L.P.J. and McCulloch, M.T. 1998 High resolution analysis of trace elements in corals by laser ablation ICP-MS. *Geochimica et Cosmochimica Acta*, 62, 1889-1901.

Singh, G and Geissler, E.A. 1985 Late Cainozoic history of vegetation, fire, lake levels, and climate at Lake George, New South Wales, Australia. *Philosophical Transactions of the Royal Society*, B311, 379-477.

Singh, G., Opdyke, N.D. and Bowler, J.M. 1981 Late Cainozoic stratigraphy, paleomagnetic chronology and vegetational history from Lake George, N.S.W. *Geological Society of Australia Journal*, 28, 435-452.

Smart, P.L. 1991 Uranium series dating. In: Smart, P.L. and Frances, P.D. (Eds) *Quaternary Dating Methods – A Users Guide.* Technical Guide No. 4, Quaternary Research Association, Cambridge, 45-83.

Smart, P.L. and Richards, D. 1992 Age estimates for the late Quaternary sea-stands. *Quaternary Science Reviews*, 11, 687-696.

Smart, P.L., Roberts, M.S., Baker, A. and Richards, D.R. 1996 Palaeoclimate determination from speleothems – a critical appraisal of the state of the art. In: Lauritzen, S.-E. (Ed) *Climate Change: The Karst Record.* Extended Abstracts, University of Bergen, Norway, Karst Waters Special Publication, 2, 157-159.

Stirling, C.h., Esat, T.M., McCulloch, M.T. and Lambeck, K. 1995 High-precision U-series dating of corals from Western Australia and implications for the timing and duration of the last interglacial. *Earth and Planetary Science Letters*, 135, 115-130.

Stuiver, M. and Reimer, P.J. 1993 Extended ^{14}C data base and revised Calib 3.0 ^{14}C age calibration program. *Radiocarbon*, 35, 215-230.

Stuiver, M., Reimer, P.J. and Braziunas, T.F. 1998 High-precision radiocarbon age calibration for terrestrial and marine samples. *Radiocarbon*, 40, 1127-1151.

Stumm, W., Sigg, L. and Sulzberger, B. 1992. *Chemistry of the Solid-Water Interface: Processes at the Mineral-Water and Particle-Water Interface in Natural Systems.* Wiley-Interscience, New York. 428 p.

Szabo, B.J. and Butzer, K.W. 1979 Uranium-series dating of lacustrine limestones from pan deposits and final Acheulian assemblage at Rooidam, Kimberley District, South Africa. *Quaternary Research*, 11, 257-260.

Talma, A.S. and Vogel, J.C. 1992 Late Quaternary paleotemperatures derived from a speleothem from Cango Caves, Cape Province, South Africa. *Quaternary Research*, 37, 203-213.

Tanahara, A., Taira, H., Yamakawa, K. and Takemura, M. 1997 Radon distribution and the ventilation of a limestone cave on Okinawa. *Geochemical Journal*, 31, 49-56.

Tanahara, A., Taira, H., Yamakawa, K. and Tsuha, A. 1998. Application of excess ^{210}Pb dating method to stalactites. *Geochemical Journal*, 32, 183-187.

Taylor, K.C., Lamorey, G.M., Doyle, G.A., Alley, R.B., Grootes, D.M. and Barlow, L.K. 1993 The "flickering switch" of late Pleistocene climate change. *Nature*, 361, 432-436.

Teeri, J.A. and Stowe, L.G. 1976 Climatic patterns and the distribution of C4 grasses in North America. *Oecologia*, 23, 1-12.

Tesoriero, A.J. and Pankow, J.F. 1996 Solid solution partitioning of Sr^{2+}, Ba^{2+}, and Cd^{2+} to calcite. *Geochimica et Cosmochimica Acta*, 60, 1053-1060.

Thompson, P., Schwarcz, H.P. and Ford, D.C. 1974 Continental Pleistocene climatic variations from speleothem age and isotopic data. *Science*, 184, 893-895.

Thompson, P., Schwarcz, H.P. and Ford, D.C. 1976 Stable isotope geochronology, geothermometry and geochronology of speleothems from West Virginia. *Geological Society of America Bulletin*, 87, 1730-1738.

Tieszen, L.L., Senyimba, M.M., Imbamba, S.K. and Troughton, J.H. 1979 The distribution of C3 and C4 grasses and carbon isotope discrimination along an altitudinal and moisture gradient in Kenya. *Oecologia*, 37, 337-350.

Toth, V.A. 1998 Spatial and temporal variations in the dissolved organic carbon concentrations in the vadose karst waters of Marengo Cave, Indiana. *Journal of Cave and Karst Studies*, 60, 167-171.

Vadillo, J.M., Vadillo, I., Carrasco, F. and Laserna, J.J. 1998 Spatial distribution profiles of Mg and Sr in speleothems using laser induced breakdown spectrometry. *Fresenius Journal of Analytical Chemistry*, 361, 119-123.

Wasson, R.J. 1986 Geomorphology and Quaternary history of the Australian continental dunefields. *Geographical Review of Japan*, Series B59; 1, 55-67.

Wells, P. and Hickey, J. 1999 Wet Sclerophyll, Mixed and Swamp Forest. In: Reid, J.B., Hill, R.S., Brown, M.J. and Hovenden, M.J. (Eds) *Vegetation of Tasmania*. Australian Biological Resources Study, Flora of Australia Supplementary Series, no. 8, Commonwealth of Australia, 224-243.

White, W.B., 1976. Cave minerals and speleothems. In: Ford, T.D. and Cullingford, C.H.D. (Eds) *The Science of Speleology*. Academic Press, London, 267-327.

White, W.B. 1981 Reflectance spectra and color in speleothems. *National Speleological Society Bulletin*, 43, 20-26.

White, W.B. 1986 Luminescence of cave deposits: a current appraisal. *National Speleological Society Bulletin*, 48, 40.

White, W.B. 1997 Color of Speleothems. In Hill, C and Forti, P. 1997. *Cave Minerals of the World*. Second edition, National Speleological Society, Inc., Huntsville, Alabama, USA., 239-244.

White, W.B. and Brennan, E.S. 1989 Luminescence of speleothems due to fulvic acid and other activators. *Proceedings of the 10th International Conference of Speleology*, 212-214.

Whitehead, N.E., Ditchburn, R.G., Williams, P.W. and McCabe, W.J. 1999 ^{231}Pa and ^{230}Th contamination at zero age: a possible limitation on U/Th series dating of speleothem material. *Chemical Geology*, 156, 359-366.

Wigley, T.M.L. amd Brown, M.C., 1977. The physics of caves. In: Ford, T.D. and Cullingford, C.H.D. (Eds) *The Science of Speleology*. Academic Press, London, 329-358.

Williams, M.A.J., Dunkerly, D.L., De Deckker, P., Kershaw, A.P. and Stokes, T. 1993 *Quaternnary Environments*. Arnold, London, 329 p.

Williams, P.W. 1983 The role of the subcutaneous zone in karst hydrology. *Journal of Hydrology*, 61, 45-67.

Williams, P.W., Marshall, A., Ford, D.C. and Jenkinson, A.V. 1999 Palaeoclimatic interpretation of stable isotope data from Holocene speleothems of the Waitomo district, North Island, New Zealand. *The Holocene*, 9, 649-657.

Winograd, I. J., Szabo B.J., Coplen, T.B. and Riggs, A.C. 1988 A 250,000-year climatic record from Great Basin Vein Calcite: Implications for Milankovitch theory. *Science*, 242, 1275-1280.

Winograd, I.J., Coplen, T.B., Landwehr, J.M., Riggs, A.C., Ludwig, K.R., Szabo, B.J., Kolesar, P.T. and Revesz, K.M. 1992 Continuous 500,000 year climate record from vein calcite in Devils Hole, Nevada. *Science*, 258, 255-260.

Wyborn, D., Owen, M. and Wyborn, L. 1990. *Geology of the Kosciuszko National Park* (1:250,000 scale map). Bureau of Mineral Resources, Canberra.

Yonge, C.J. 1981 Fluid inclusions in speleothems as palaeoclimate indicators. In: Beck, B.F. (Ed) *Proceedings of the 8th International Congress of Speleology*, National Speleology Society, Kentucky, 1, pp. 301-304.

Yonge, C.J. 1982 *Stable Isotope Studies of Water Extracted from Speleothems.* Unpublished PhD thesis, McMaster University, Hamilton, Ontario, 298 p.

Yonge, C.L., Ford, D.C., Gray, J. and Schwarcz, H.P. 1985 Stable isotope studies of cave seepage water. *Chemical Geology*, 58, 97-105.